UC Santa Barbara

UC Santa Barbara Electronic Theses and Dissertations

Title

Linking biological and physical processes to understand microbial diversity and nitrogen dynamics along the aquatic continuum

Permalink

https://escholarship.org/uc/item/1530x8dv

Author

Laperriere, Sarah Marie

Publication Date

2019

Peer reviewed|Thesis/dissertation

eScholarship.org Powered by the California Digital Library
University of California

UNIVERSITY OF CALIFORNIA

Santa Barbara

Linking biological and physical processes to understand microbial diversity and nitrogen dynamics along the aquatic continuum

A dissertation submitted in partial satisfaction of the

requirements for the degree Doctor of Philosophy

in Marine Science

by

Sarah Marie Laperriere

Committee in charge:

Professor Alyson E. Santoro, Chair

Professor Craig A. Carlson

Professor David L. Valentine

September 2019

The dissertation of Sarah Marie Laperriere is approved.

_____

Craig A. Carlson

_____

David L. Valentine

_____

Alyson E. Santoro, Committee Chair

September 2019

Linking biological and physical processes to understand microbial diversity and nitrogen dynamics along the aquatic continuum

Copyright © 2019

by

Sarah Marie Laperriere

ACKNOWLEDGEMENTS

I would like to first thank Alyson Santoro for her invaluable support, mentorship, and patience throughout the course of my degree. I would like to acknowledge my committee members for their expertise and time. I am extremely thankful to past and present members of the Santoro Laboratory for their advice and assistance. I would also like to extend my gratitude to everyone at Horn Point Laboratory who supported my research. Finally, I thank my friends and family for their continued support and encouragement.

VITA OF SARAH MARIE LAPERRIERE

September 2019

Education

Doctor of Philosophy in Marine Science, University of California, Santa Barbara (UCSB), September 2019 (expected)

Bachelor of Science in Biology, Providence College, Providence, RI, May 2011
Bachelor of Arts in Mathematics, Providence College, Providence, RI, May 2011

Research Experience

Graduate Research Assistant, UCSB/University of Maryland	2013 - present
Visiting Graduate Student, J. Craig Venter Institute, La Jolla, CA	Spring 2016
Antarctic Field Team Leader, Marine Biological Laboratory, Woods Hole, MA	2012 - 13
Staff Environmental Scientist, NewFields, Rockland, MA	2011 - 12
Research Assistant, Marine Biological Laboratory, Woods Hole, MA	Summers 2010 - 12

Teaching Experience

Teaching Assistant, UCSB	Fall 2017 & 2018, Winter 2019
Introductory Biology Lab II, Marine Microbiology	

Awards

Schmidt Family Foundation Research Mentorship Award	2019
Maryland Sea Grant Research Fellow	2014 - 16
Horn Point Laboratory Student Travel Award	2014
Horn Point Laboratory Graduate Fellowship	2013 - 14

Publications

Laperriere SM, Morando MB, Capone DG, Smith JM, Santoro AE. Nitrification and nitrous oxide dynamics in the Southern California Bight. In preparation.

Laperriere SM, Hilderbrand RH, Keller SR, Trott R, Santoro AE. Microbial indicators of watershed land use and headwater stream condition. In preparation.

Santoro AE, Kellom M, Laperriere SM. Contributions of single-cell genomics to our understanding of planktonic marine archaea. In press.

Laperriere SM, Nidzieko NJ, Fox RJ, Fisher AW, Santoro, AE. 2019. Observations of variable ammonia and nitrous oxidation oxide flux in a eutrophic estuary. Estuaries and Coasts, 42:33.

Wilson, ST et al. 2018. An intercomparison of oceanic methane and nitrous oxide measurements. Biogeosciences, 15.

ABSTRACT

Linking biological and physical processes to understand microbial diversity and nitrogen dynamics along the aquatic continuum

by

Sarah Marie Laperriere

This dissertation examines the effects of anthropogenic perturbation on microbial diversity and freshwater and marine nitrogen cycling, with a particular focus on nitrification and the production of the greenhouse gas nitrous oxide (N_2O).

In the first chapter, headwater stream microbial communities were characterized across a gradient of urban and agricultural land use using 16S rRNA gene amplicon sequencing and compared to traditional physiochemical and biotic indicators of stream health. Stream microbial diversity differed in watersheds with high agricultural, urban, and forested land uses, and community structure differed in streams classified in good, fair, poor, and very poor condition using benthic macroinvertebrate indicators of water quality. Along with changes in diversity, stream community respiration correlated with forest cover and negatively correlated with nutrients associated with anthropogenic influence. Additionally, N_2O concentrations negatively correlated with forested land use and positively correlated with dissolved inorganic nitrogen concentrations. The findings suggest stream microbial communities and ecosystem processes are impacted by watershed land use and can potentially assess ecosystem health.

The physical and biological controls on N_2O production in the eutrophic Chesapeake Bay were investigated in the second chapter using gas measurements (N_2O and N_2/Ar) and stable isotope tracer incubations. Nitrification rates were highest following wind events that mixed oxygenated surface water below the pycnocline into ammonium-rich bottom waters, resulting in the accumulation of nitrite (NO_2^-) and N_2O. During periods of weak vertical mixing, both N_2O concentrations and nitrification rates were lower, and lower oxygen (O_2) concentrations below the pycnocline allowed for N_2O consumption by denitrification. A three-layer box model provided estimates of N_2O production demonstrating the importance of both biological (production and consumption) and physical (advection and vertical exchange) processes in driving the observed large fluctuations in N_2O concentrations. The results demonstrate physical processes affect the net balance between N_2O production and consumption, making Chesapeake Bay a variable source and sink for N_2O.

The final chapter investigates the seasonal coupling of primary production and nitrification, and the relationship between these processes and N_2O production in the Southern California Bight (SCB). Over two seasonal upwelling cycles, nitrification rates fueled by ammonia and urea-derived N were measured using stable isotope tracer additions and N_2O concentrations were measured using gas chromatography. Nitrification rates were highest at the onset of upwelling and correlated with rates of primary production. Similar ammonia and urea-derived N oxidation rates suggest urea is a significant nitrogen source fueling nitrification in the SCB. Nitrification supplied a large proportion of phytoplankton nitrogen demand, demonstrating significant nitrogen remineralization within the euphotic zone. The SCB was always a source of N_2O to the atmosphere, which likely was advected into the system from the eastern tropical North Pacific. Together, the results suggest nitrification is an

important control on the amount of organic carbon available for export, and the coupling of nitrogen remineralization and primary production may export a smaller fraction of primary production out of the surface ocean, but physical transport dominates over local production of N_2O in the SCB.

TABLE OF CONTENTS

I. Introduction

Anthropogenic alteration of the nitrogen cycle through fertilizer production and the combustion of fossil fuels has more than doubled fixed nitrogen (N) inputs to terrestrial systems (Galloway et al. 2004). A portion of this N is transported along the land-sea aquatic continuum – freshwater, estuarine, and coastal waters, causing eutrophication in many coastal ecosystems around the world (Nixon 1995; Nixon et al. 1996; Vitousek et al. 1997). Microbial nitrogen cycling determines the fate of excess nitrogen once in aquatic ecosystems, having important implications for primary production and climate through the production of greenhouse gases (Capone et al. 2008). With increasing anthropogenic pressure, understanding how microbial communities respond to environmental stressors and the resulting impact on biogeochemical cycles is critical. This dissertation examines the effects of land use and nutrient pollution on microbial communities and nutrient transformations along the aquatic continuum, with a specific focus on estuarine and coastal nitrogen cycling.

Streams are the primary conduit of terrestrial derived nutrients to rivers and the coastal ocean (Vannote et al. 1980; Alexander et al. 2000; Peterson et al. 2001). Agricultural and urban land use modifies stream hydrographic flow, increases nutrient and agricultural contaminants, and alters biodiversity (Delong and Brusven 1998; Paul and Meyer 2001; Walsh et al. 2005; Figueiredo et al. 2010). Previous studies demonstrate the effects of urbanization on stream carbon and nitrogen processes, with particular focus on the retention and removal of nutrients (Hill et al. 2002; Groffman et al. 2004; Harbott and Grace 2005; Claessens et al. 2010). And widely used as biotic indicators, a great deal is known regarding the response of macro-organisms, such as macroinvertebrates and fish to land use (Whiting

and Clifford 1983; Delong and Brusven 1998; Hall et al. 2001; Walsh et al. 2001; Moore and Palmer 2005). The effects of watershed land use on stream microbial communities have also been previously demonstrated (Wang et al. 2011; Hosen et al. 2017; Qu et al. 2017; Roberto et al. 2018; Simonin et al. 2019). However, it is less clear how changes in microbial community composition relate to macroinvertebrate diversity and traditional biotic indices of stream health.

Urbanization alters the composition of stream microbes linked to key N metabolisms, potentially altering N loss from urban streams and the export of nitrogen to riverine and coastal systems (Perryman et al. 2008, 2011; Merbt et al. 2015). Nitrogen exists in several chemical forms with multiple reduction-oxidation states, and for this reason, microbes use N both for growth and energy. In marine systems, the most abundant N form is dinitrogen gas (N_2), followed by nitrate (NO_3^-) and dissolved organic nitrogen (DON), with particulate organic nitrogen (PON), ammonium (NH_4^+), nitrite (NO_2^-), and nitrous oxide (N_2O) making up the remaining inventory (Gruber 2008). Nitrification, the oxidation of ammonia (NH_3) to NO_2^- and subsequently to NO_3^- by nitrite- and ammonia-oxidizing microbes, is of particular importance because it links the most reduced and oxidized forms of nitrogen, controlling the availability of N for removal pathways.

Nitrification is considered the rate-limiting step in nitrogen removal in coastal systems (Herbert 1999). Nitrification supplies oxidized forms of N to the denitrification pathway, i.e. the reduction of NO_3^- to N_2, the major sink for fixed N. The balance between nitrogen fixation, i.e. the conversion of N_2 to NH_3 or organic compounds, and N loss from denitrification ultimately controls marine primary production, as N is often the limiting nutrient (Guildford and Hecky 2000; Howarth and Marino 2006). In the ocean, primary

production fueled by NO_3^- is considered new production and is related to the amount of organic carbon available for export out of the surface ocean (Dugdale and Goering 1967). Whereas, production fueled by recycled nutrients within the euphotic zone is considered regenerated production (Dugdale and Goering 1967). The original paradigm assumed nitrification was minimal in the euphotic zone, though it is now evident nitrification in the upper ocean is a source of NO_3^- for primary production (Dore and Karl 1996; Wankel et al. 2007; Yool et al. 2007; Santoro et al. 2013). However, the contribution of nitrification to phytoplankton N demand is poorly constrained.

As the preferred N source, phytoplankton and ammonia oxidizers compete for NH_4^+ in the photic zone, regulating rates of nitrification in the surface ocean (Ward 2005; Smith et al. 2014; Wan et al. 2018). Once nitrifiers are released from competition at the base of the euphotic zone, nitrification rates increase exponentially with depth (Ward et al. 1982; Dore and Karl 1996; Santoro et al. 2010, 2013; Smith et al. 2016). The main source of NH_4^+ in the ocean is the degradation of organic matter, for this reason it is logical to assume rates of ammonia oxidation are controlled by the flux NH_4^+ supplied by organic matter. Previous studies demonstrate ammonia oxidation rates increase in response to additions of NH_4^+ (Newell et al. 2013; Horak et al. 2013), though this relationship is not always observed (Shiozaki et al. 2016), suggesting different environmental factors limit nitrification, such as the availability of micronutrients (Amin et al. 2013; Shiozaki et al. 2016) and DON compounds (Damashek et al. 2019).

Dissolved organic nitrogen compounds make up a significant portion of the fixed nitrogen in the upper ocean, with similar euphotic zone concentrations to NO_3^- (Bronk 2002; Gruber 2008). One abundant component of the DON pool is urea (CH_4N_2O) (Glibert et al.

2006; Aluwihare and Meador 2008), which enters coastal systems from agricultural runoff (Glibert et al. 2006) and is excreted by fish, zooplankton, and microbes (Mayzaud 1973; Wright et al. 1995; Cho et al. 1996; Wood et al. 1998). It is widely known that phytoplankton utilize urea for growth (Mulholland and Lomas 2008), and recently, it has been demonstrated that ammonia-oxidizing archaea (AOA) are also capable of utilizing urea as an NH_3 source for ammonia oxidation (Qin et al. 2014; Bayer et al. 2016; Carini et al. 2018). Nitrification fueled by organic N substrates provides an additional link between inorganic and organic nitrogen pools in the ocean, however the contribution of urea-derived N to ammonia oxidation in marine systems is unclear.

Besides controlling N availability for primary production, nitrification and denitrification, also result in the production of the greenhouse gas N_2O. Ammonia-oxidizing bacteria (AOB) produce N_2O through the release of nitric oxide (NO) and hydroxylamine (NH_2OH) and enzymatically during nitrifier denitrification (Poth and Focht 1985; Kool et al. 2007; Zhu et al. 2013; Kozlowski et al. 2014; Zhu-Barker et al. 2015; Jones et al. 2015), and AOA produce N_2O in poorly understood pathways (Santoro et al. 2011; Kozlowski et al. 2016). Denitrification both produces and consumes N_2O as an obligate intermediate in the reduction of NO_3^- to N_2. Predicting N_2O production is difficult because N_2O is produced through multiple pathways and is strongly influenced by dissolved oxygen (DO) concentration.

Atmospheric emissions of N_2O are difficult to predict because of the complex way oxygen (O_2) influences its production. During ammonia oxidation, the yield of N_2O increases as O_2 concentrations decrease, as shown in both culture and in the environment (Goreau et al. 1980; Löscher et al. 2012; Qin et al. 2017). As O_2 concentrations decrease,

denitrification also produces N_2O, and yields increase as microbes become substrate limited and at elevated NO_3^- concentrations (Blackmer and Bremner 1978; Tiedje 1988; Dalsgaard et al. 2014). Denitrifying bacteria also consume N_2O below a threshold O_2 concentration, where it is used as a terminal electron acceptor. High N loading and low DO concentrations make coastal ecosystems potential hotspots for N_2O production (Arévalo-Martínez et al. 2015; Farías et al. 2015). However, coastal N_2O fluxes are poorly constrained and often not included in marine N_2O budgets (Bange et al. 1996; Buitenhuis et al. 2017). For this reason, higher temporal and spatial sampling is needed to better constrain N_2O emissions from coastal areas.

The focus of this work is to gain a better understanding of how anthropogenic perturbation affects microbial diversity and biogeochemical processes in aquatic systems, with a particular focus on nitrification and N_2O production in coastal systems. In addition to the three chapters presented here, I also participated in an international intercomparison of oceanic N_2O concentrations (Wilson et al. 2018; Appendix C), where batches of seawater and gas standards were used to improve analytical accuracy of N_2O measurements. Additionally, I participated in a research cruise aboard the *R/V* Falkor to the oxygen deficient zone in the Tropical Pacific to examine nitrogen cycling under low oxygen conditions, with a particular emphasis on the distribution of N_2O.

Chapter 1 explores the impact of land use modification on microbial diversity and ecosystem function. The objectives of this chapter were to determine how stream bacteria and archaea are distributed across gradients of watershed land use and stream condition, and to assess how changes in microbial community composition relate to benthic macroinvertebrate diversity and traditional indices of stream condition. Microbial diversity

was measured using 16S rRNA amplicon sequencing across 83 headwater streams within the Chesapeake Bay watershed in the state of Maryland, USA in spring and summer for two years. Measurements were collected in conjunction with stream physicochemical parameters and traditional invertebrate indicators of stream health. I further identified how changes in community structure influence stream function by relating microbial community composition to rates of microbial respiration and concentrations of N_2O.

Chapter 2 considers the fate of estuarine N_2O by examining how physical and biological processes in the eutrophic Chesapeake Bay estuary influence the temporal and spatial variability of N_2O production. During two, week-long, cruises in the mesohaline region of the Bay, the spatial and temporal variability of N_2O concentrations was examined using gas chromatography. To evaluate the relative roles of nitrification and denitrification as sources of N_2O in the water column, ammonia oxidation rates were measured using $^{15}NH_4^+$ tracer additions and denitrification was assessed using water column N_2/Ar ratios. Additionally, a control volume approach was used to estimate the relative importance of physical and biological processes in governing N_2O dynamics in the Bay.

Finally, Chapter 3 investigates the seasonal coupling of primary production and nitrogen remineralization in an upwelling system and determines how these processes relate to N_2O production. The work was conducted over two years at the San Pedro Ocean Time-series (SPOT) station in the Southern California Bight. Rates of ammonia and urea-N oxidation were measured using ^{15}N tracer additions to determine the contribution of nitrification to phytoplankton nitrogen demand in the upper ocean. Additionally, N_2O concentrations were measured monthly using gas chromatography to better constrain coastal N_2O fluxes.

References

Alexander, R. B., R. A. Smith, and G. E. Schwarz. 2000. Effect of stream channel size on the delivery of nitrogen to the Gulf of Mexico. Nature **403**: 758–761.

Aluwihare, L. I., and T. Meador. 2008. Chemical composition of marine dissolved organic nitrogen, p. 95–140. In E. J. Carpenter and D. G. Capone [eds.], Nitrogen in the marine environment. Academic Press.

Amin, S. A., J. W. Moffett, W. Martens-Habbena, and others. 2013. Copper requirements of the ammonia-oxidizing archaeon *Nitrosopumilus maritimus* SCM1 and implications for nitrification in the marine environment. Limnol. Oceanogr. **58**: 2037–2045.

Arévalo-Martínez, D. L., A. Kock, C. R. Löscher, R. A. Schmitz, and H. W. Bange. 2015. Massive nitrous oxide emissions from the tropical South Pacific Ocean. Nat. Geosci. **8**: 530–533.

Bange, H. W., S. Rapsomanikis, and M. O. Andreae. 1996. Nitrous oxide in coastal waters. Global Biogeochem. Cycles **10**: 197–207.

Bayer, B., J. Vojvoda, P. Offre, and others. 2016. Physiological and genomic characterization of two novel marine thaumarchaeal strains indicates niche differentiation. ISME J. **10**: 1051–1063.

Blackmer, A. M., and J. M. Bremner. 1978. Inhibitory effect of nitrate on reduction of N_2O to N_2 by soil microorganisms. Soil Biol. Biochem. **10**: 187–191.

Bronk, D. A. 2002. Dynamics of DON, p. 153–247. In D. A. Hansell and C. A. Carlson [eds.], Biogeochemistry of marine dissolved organic matter. Academic Press.

Buitenhuis, E. T., P. Suntharalingam, and C. Le Quéré. 2017. Constraints on global oceanic emissions of N_2O from observations and models. Biogeosci. Discuss. **15**: 2161–2175.

Capone, D. G., D. A. Bronk, M. R. Mulholland, and E. J. Carpenter. 2008. Nitrogen in the Marine Environment. Academic Press.

Carini, P., C. L. Dupont, and A. E. Santoro. 2018. Patterns of thaumarchaeal gene expression in culture and diverse marine environments. Environ. Microbiol. **20**: 2112–2124.

Cho, B. C., M. G. Park, J. H. Shim, and F. Azam. 1996. Significance of bacteria in urea dynamics in coastal surface waters. Mar. Ecol. Prog. Ser. **142**: 19–26.

Claessens, L., C. L. Tague, P. M. Groffman, and J. M. Melack. 2010. Longitudinal assessment of the effect of concentration on stream N uptake rates in an urbanizing watershed. Biogeochemistry **98**: 63–74.

Dalsgaard, T., F. J. Stewart, B. Thamdrup, L. De Brabandere, N. P. Revsbech, O. Ulloa, D. E. Canfield, and E. F. DeLong. 2014. Oxygen at nanomolar levels reversibly suppresses process rates and gene expression in anammox and denitrification in the oxygen minimum zone off northern Chile. MBio **5**: e01966.

Damashek, J., B. B. Tolar, Q. Liu, A. O. Okotie-Oyekan, N. J. Wallsgrove, B. N. Popp, and J. T. Hollibaugh. 2019. Microbial oxidation of nitrogen supplied as selected organic nitrogen compounds in the South Atlantic Bight. Limnol. Oceanogr. **64**: 982–995.

Delong, M. D., and M. A. Brusven. 1998. Macroinvertebrate Community Structure Along the Longitudinal Gradient of an Agriculturally Impacted Stream. Environ. Manage. **22**: 445–457.

Dore, J. E., and D. M. Karl. 1996. Nitrification in the euphotic zone as a source for nitrite, nitrate, and nitrous oxide at Station ALOHA. Limnol. Oceanogr. **41**: 1619–1628. doi:10.4319/lo.1996.41.8.1619

Dugdale, R. C., and J. J. Goering. 1967. Uptake of new and regenerated forms of nitrogen in primary productivity1. Limnol. Oceanogr. **12**: 196–206.

Farías, L., V. Besoain, and S. García-Loyola. 2015. Presence of nitrous oxide hotspots in the coastal upwelling area off central Chile: an analysis of temporal variability based on ten years of a biogeochemical time series. Environ. Res. Lett. **10**: 044017.

Figueiredo, R. O., D. Markewitz, E. A. Davidson, A. E. Schuler, O. dos S. Watrin, and P. de Souza Silva. 2010. Land-use effects on the chemical attributes of low-order streams in the eastern Amazon. J. Geophys. Res. **115**.

Galloway, J. N., F. J. Dentener, D. G. Capone, and others. 2004. Nitrogen cycles: past, present, and future. Biogeochemistry **70**: 153–226.

Glibert, P. M., J. Harrison, C. Heil, and S. Seitzinger. 2006. Escalating Worldwide use of urea – A global change contributing to coastal eutrophication. Biogeochemistry **77**: 441–463.

Goreau, T. J., W. A. Kaplan, S. C. Wofsy, M. B. McElroy, F. W. Valois, and S. W. Watson. 1980. Production of NO_2 and N_2O by nitrifying bacteria at reduced concentrations of oxygen. Appl. Environ. Microbiol. **40**: 526–532.

Groffman, P. M., N. L. Law, K. T. Belt, L. E. Band, and G. T. Fisher. 2004. Nitrogen fluxes and retention in urban watershed ecosystems. Ecosystems **7**: 393-403.

Gruber, N. 2008. The Marine Nitrogen Cycle, p. 1-50. In E. J. Carpenter and D. G. Capone [eds.], Nitrogen in the marine environment. Academic Press.

Guildford, S. J., and R. E. Hecky. 2000. Total nitrogen, total phosphorus, and nutrient limitation in lakes and oceans: Is there a common relationship? Limnol. Oceanogr. **45**: 1213–1223.

Hall, M. J., G. P. Closs, and R. H. Riley. 2001. Relationships between land use and stream invertebrate community structure in a South Island, New Zealand, coastal stream catchment. N. Z. J. Mar. Freshwater Res. **35**: 591–603.

Harbott, E. L., and M. R. Grace. 2005. Extracellular enzyme response to bioavailability of dissolved organic C in streams of varying catchment urbanization. J. North Am. Benthol. Soc. **24**: 588-601.

Herbert, R. 1999. Nitrogen cycling in coastal marine ecosystems. FEMS Microbiol. Rev. **23**: 563–590.

Hill, B. H., A. T. Herlihy, and P. R. Kaufmann. 2002. Benthic microbial respiration in Appalachian Mountain, Piedmont, and Coastal Plains streams of the eastern U.S.A. Freshw. Biolo. **47**: 185–194.

Horak, R. E. A., W. Qin, A. J. Schauer, E. V. Armbrust, A. E. Ingalls, J. W. Moffett, D. A. Stahl, and A. H. Devol. 2013. Ammonia oxidation kinetics and temperature sensitivity of a natural marine community dominated by Archaea. ISME J. **7**: 2023–2033.

Hosen, J. D., C. M. Febria, B. C. Crump, and M. A. Palmer. 2017. Watershed urbanization linked to differences in stream bacterial community composition. Front. Microbiol. **8**: 1452.

Howarth, R. W., and R. Marino. 2006. Nitrogen as the limiting nutrient for eutrophication in coastal marine ecosystems: Evolving views over three decades. Limnol. Oceanogr. **51**: 364–376.

Jones, L. C., B. Peters, J. S. Lezama Pacheco, K. L. Casciotti, and S. Fendorf. 2015. Stable isotopes and iron oxide mineral products as markers of chemodenitrification. Environ. Sci. Technol. **49**: 3444–3452.

Kool, D. M., N. Wrage, O. Oenema, J. Dolfing, and J. W. Van Groenigen. 2007. Oxygen exchange between (de)nitrification intermediates and H_2O and its implications for source determination of NO_3^- and N_2O: a review. Rapid Commun. Mass Spectrom. **21**: 3569–3578.

Kozlowski, J. A., J. Price, and L. Y. Stein. 2014. Revision of N_2O-Producing Pathways in the ammonia-oxidizing bacterium *Nitrosomonas europaea* ATCC 19718. Appl. Environ. Microbiol. **80**: 4930–4935.

Kozlowski, J. A., M. Stieglmeier, C. Schleper, M. G. Klotz, and L. Y. Stein. 2016. Pathways and key intermediates required for obligate aerobic ammonia-dependent chemolithotrophy in bacteria and Thaumarchaeota. ISME J. **10**: 1836–1845.

Löscher, C. R., A. Kock, M. Könneke, J. LaRoche, H. W. Bange, and R. A. Schmitz. 2012. Production of oceanic nitrous oxide by ammonia-oxidizing archaea. Biogeosciences **9**: 2419–2429.

Mayzaud, P. 1973. Respiration and nitrogen excretion of zooplankton. II. Studies of the metabolic characteristics of starved animals. Mar. Biol. **21**: 19–28.

Merbt, S. N., J.-C. Auguet, A. Blesa, E. Martí, and E. O. Casamayor. 2015. Wastewater treatment plant effluents change abundance and composition of ammonia-oxidizing microorganisms in mediterranean urban stream biofilms. Microb. Ecol. **69**: 66–74.

Moore, A. A., and M. A. Palmer. 2005. Invertebrate biodiversity in agricultural and urban headwater streams: implications for conservation and management. Ecol. Appl. **15**: 1169–1177.

Mulholland, M. R., and M. W. Lomas. 2008. Nitrogen Uptake and Assimilation, p. 303–384. In E. J. Carpenter and D. G. Capone [eds.], Nitrogen in the marine environment.

Academic Press.

Newell, S. E., S. E. Fawcett, and B. B. Ward. 2013. Depth distribution of ammonia oxidation rates and ammonia-oxidizer community composition in the Sargasso Sea. Limnol. Oceanogr. **58**: 1491–1500.

Nixon, S. W. 1995. Coastal marine eutrophication: A definition, social causes, and future concerns. Ophelia **41**: 199–219.

Nixon, S. W., J. W. Ammerman, L. P. Atkinson, and others. 1996. The fate of nitrogen and phosphorus at the land-sea margin of the North Atlantic Ocean. Biogeochemistry **35**: 141–180.

Paul, M. J., and J. L. Meyer. 2001. Streams in the urban landscape. Annu. Rev. Ecol. Syst. **32**: 333–365.

Perryman, S. E., G. N. Rees, and C. J. Walsh. 2008. Analysis of denitrifying communities in streams from an urban and non-urban catchment. Aquat. Ecol. **42**: 95–101.

Perryman, S. E., G. N. Rees, C. J. Walsh, and M. R. Grace. 2011. Urban stormwater runoff drives denitrifying community composition through changes in sediment texture and carbon content. Microb. Ecol. **61**: 932–940.

Peterson, B. J., W. M. Wollheim, P. J. Mulholland, and others. 2001. Control of nitrogen export from watersheds by headwater streams. Science **292**: 86–90.

Poth, M., and D. D. Focht. 1985. N Kinetic Analysis of N_2O production by *Nitrosomonas europaea*: an examination of nitrifier denitrification. Appl. Environ. Microbiol. **49**: 1134–1141.

Qin, W., S. A. Amin, W. Martens-Habbena, and others. 2014. Marine ammonia-oxidizing archaeal isolates display obligate mixotrophy and wide ecotypic variation. Proc. Natl.

Acad. Sci. U. S. A. **111**: 12504–12509.

Qin, W., K. A. Meinhardt, J. W. Moffett, A. H. Devol, E. Virginia Armbrust, A. E. Ingalls, and D. A. Stahl. 2017. Influence of oxygen availability on the activities of ammonia-oxidizing archaea. Environ. Microbiol. Rep. **9**: 250–256.

Qu, X., Z. Ren, H. Zhang, M. Zhang, Y. Zhang, X. Liu, and W. Peng. 2017. Influences of anthropogenic land use on microbial community structure and functional potentials of stream benthic biofilms. Sci. Rep. **7**: 15117.

Roberto, A. A., J. B. Van Gray, and L. G. Leff. 2018. Sediment bacteria in an urban stream: Spatiotemporal patterns in community composition. Water Res. **134**: 353–369.

Santoro, A. E., C. Buchwald, M. R. McIlvin, and K. L. Casciotti. 2011. Isotopic signature of N_2O produced by marine ammonia-oxidizing archaea. Science **333**: 1282–1285.

Santoro, A. E., K. L. Casciotti, and C. A. Francis. 2010. Activity, abundance and diversity of nitrifying archaea and bacteria in the central California Current. Environ. Microbiol. **12**: 1989–2006.

Santoro, A. E., C. M. Sakamoto, J. M. Smith, and others. 2013. Measurements of nitrite production and nitrite-producing organisms in and around the primary nitrite maximum in the central California Current. Biogeosci. Discuss. **10**: 5803–5840.

Shiozaki, T., M. Ijichi, K. Isobe, and others. 2016. Nitrification and its influence on biogeochemical cycles from the equatorial Pacific to the Arctic Ocean. ISME J. **10**: 2184–2197.

Simonin, M., K. A. Voss, B. A. Hassett, and others. 2019. In search of microbial indicator taxa: shifts in stream bacterial communities along an urbanization gradient. Environ. Microbiol.

Smith, J. M., F. P. Chavez, and C. A. Francis. 2014. Ammonium uptake by phytoplankton regulates nitrification in the sunlit ocean. PLoS One **9**: e108173.

Smith, J. M., J. Damashek, F. P. Chavez, and C. A. Francis. 2016. Factors influencing nitrification rates and the abundance and transcriptional activity of ammonia-oxidizing microorganisms in the dark northeast Pacific Ocean. Limnol. Oceanogr. **61**: 596–609.

Tiedje, J. M. 1988. Ecology of denitrification and dissimilatory nitrate reduction to ammonium, p. 179-244. In A. J. B. Zehnder [eds.], Biology of anaerobic microorganisms. John Wiley and Sons.

Vannote, R. L., G. Wayne Minshall, K. W. Cummins, J. R. Sedell, and C. E. Cushing. 1980. The River Continuum Concept. Can. J. Fish. Aquat. Sci. **37**: 130-137.

Vitousek, P. M., J. D. Aber, R. W. Howarth, G. E. Likens, P. A. Matson, D. W. Schindler, W. H. Schlesinger, and D. G. Tilman. 1997. Human alteration of the global nitrogen cycle: sources and consequences. Ecol. Appl. **7**: 737–750.

Walsh, C. J., A. H. Roy, J. W. Feminella, P. D. Cottingham, P. M. Groffman, and R. P. Morgan. 2005. The urban stream syndrome: current knowledge and the search for a cure. J. North Am. Benthol. Soc. **24**: 706-723.

Walsh, C. J., A. K. Sharpe, P. F. Breen, and J. A. Sonneman. 2001. Effects of urbanization on streams of the Melbourne region, Victoria, Australia. I. Benthic macroinvertebrate communities. Freshw. Biol. **46**: 535–551.

Wang, S.Y., E. B. Sudduth, M. D. Wallenstein, J. P. Wright, and E. S. Bernhardt. 2011. Watershed urbanization alters the composition and function of stream bacterial communities. PLoS One **6**: e22972.

Wankel, S. D., C. Kendall, J. Timothy Pennington, F. P. Chavez, and A. Paytan. 2007.

Nitrification in the euphotic zone as evidenced by nitrate dual isotopic composition: Observations from Monterey Bay, California. Global Biogeochem. Cycles **21**.

Wan, X. S., H.-X. Sheng, M. Dai, and others. 2018. Ambient nitrate switches the ammonium consumption pathway in the euphotic ocean. Nat. Commun. **9**: 915.

Ward, B. B. 2005. Temporal variability in nitrification rates and related biogeochemical factors in Monterey Bay, California, USA. Mar. Ecol. Prog. Ser. **292**: 97–109.

Ward, B. B., R. J. Olson, and M. J. Perry. 1982. Microbial nitrification rates in the primary nitrite maximum off southern California. Deep-Sea Res. A **29**: 247–255.

Whiting, E. R., and H. F. Clifford. 1983. Invertebrates and urban runoff in a small northern stream, Edmonton, Alberta, Canada. Hydrobiologia **102**: 73–80.

Wood, C. M., K. M. Gilmour, S. F. Perry, P. Part, and P. J. Walsh. 1998. Pulsatile urea excretion in gulf toadfish (Opsanus beta): evidence for activation of a specific facilitated diffusion transport system. J. Exp. Biol. **201**: 805–817.

Wright, P., A. Felskie, and P. Anderson. 1995. Induction of ornithine-urea cycle enzymes and nitrogen metabolism and excretion in rainbow trout (Oncorhynchus mykiss) during early life stages. J. Exp. Biol. **198**: 127–135.

Yool, A., A. P. Martin, C. Fernández, and D. R. Clark. 2007. The significance of nitrification for oceanic new production. Nature **447**: 999–1002.

Zhu-Barker, X., A. R. Cavazos, N. E. Ostrom, W. R. Horwath, and J. B. Glass. 2015. The importance of abiotic reactions for nitrous oxide production. Biogeochemistry **126**: 251–267.

Zhu, X., M. Burger, T. A. Doane, and W. R. Horwath. 2013. Ammonia oxidation pathways and nitrifier denitrification are significant sources of N_2O and NO under low oxygen

availability. Proc. Natl. Acad. Sci. U. S. A. **110**: 6328–6333.

II. Chapter I: Microbial indicators of watershed land use and headwater stream condition

Sarah M. Laperriere[a,b], Robert H. Hilderbrand[c], Stephen R. Keller[c,d], Regina Trott[c], Alyson E. Santoro[b]

[a]Horn Point Laboratory, University of Maryland Center for Environmental Science, Cambridge, Maryland, USA

[b]Department of Ecology, Evolution, and Marine Biology, University of California, Santa Barbara, California, USA

[c]Appalachian Laboratory, University of Maryland Center for Environmental Science, Frostburg, Maryland, USA

[d]Department of Plant Biology, University of Vermont, Burlington, Vermont, USA

Abstract

Anthropogenic activity impacts stream ecosystems resulting in a loss of diversity and ecosystem function, however, little is known about the response of aquatic microbial communities to changes in land use. Here, microbial communities were characterized across 83 headwater streams across a gradient of urban and agricultural land use using 16S rRNA gene amplicon sequencing and compared to a rich dataset of physicochemical variables and traditional benthic invertebrate indicators. Stream microbial diversity differed among watersheds with high agricultural, urban, and forested land uses, and community structure differed in streams classified in good, fair, poor, and very poor condition using benthic invertebrate indicators. Microbial community similarity decayed with geographic distance

across the study region, but not environmental distance. Important taxa involved in nitrogen and carbon cycling (Thaumarchaeota and Cyanobacteria) were identified as indicators of streams in good condition, while taxa often associated with high nutrients and polluted environments (Campylobacterales and Burkholderiales) were strong indicators of poor and very poor stream condition, and agricultural and urban land use. Stream community respiration rates streams ranged from 21.7 to 1,570 mg O_2 m^{-2} d^{-1} and 31.9 and 3,670 mg O_2 m^{-2} d^{-1} for water column and sediments, and rates correlated with nutrients associated with anthropogenic influence and microbial community structure. N_2O concentrations ranged from 0.22 µg L^{-1} to 4.41 µg L^{-1}; N_2O negatively correlated with forested land use, and positively correlated with dissolved inorganic nitrogen concentrations. Our findings suggest stream microbial communities are impacted by watershed land use and can potentially assess ecosystem health.

Importance

Stream ecosystems are frequently impacted by changes in watershed land use, resulting in altered hydrology, increased pollutant and nutrient loads, and habitat degradation. Macroinvertebrates and fish are strongly affected by changes in stream condition and are commonly used in biotic indices to assess ecosystem health. Similarly, microbes respond to environmental stressors, and changes in community composition alter key ecosystem processes. The response of microbes to habitat degradation and their role in global biogeochemical cycles provides an opportunity use microbes as a monitoring tool. Here, we identify stream microbes that respond to watershed urbanization and agricultural

development and demonstrate microbes can be used to assess stream condition and ecosystem functioning.

Introduction

Biodiversity is critical to ecosystem functioning and is threatened by anthropogenic activity (1). Understanding how microbes respond to environmental stressors is of particular importance, as they drive key biogeochemical cycles. Streams are examples of such ecosystems, where watershed modification decreases stream integrity and water quality (2–5), altering macroinvertebrate, fish, and microbial diversity (5-9). The use of macroinvertebrate and fish indices to assess stream condition is fundamental to stream ecology (10) and depends on known relationships between stream integrity and community structure (11-12). The Benthic Index of Biotic Integrity (B-IBI) is one such index, using the abundance and diversity of stream benthic macroinvertebrates to accurately distinguish degraded streams (12). Biotic indices are calibrated to specific regions, as the distribution of stream macroinvertebrates is controlled by a combination of dispersal limitation and local environmental conditions (13). A great deal is known about how larger organisms respond to environmental disturbance in streams, but the impact of environmental disturbance on the distribution of microbes is less clear.

Stream water microbial communities are strongly influenced by watershed land use (14-15). As with macroinvertebrates, dispersion and environmental selection control the spatial distribution of microbes along stream continuums (16). Dispersion, or advection of microbes from the surrounding landscape, can drive headwater stream community composition, and environmental sorting becomes increasingly more important downstream,

as stream residence time increases (16). Several studies demonstrate the effect of urbanization on stream microbial communities, showing watershed urbanization leads to shifts in bacterial communities (17–20). These changes in community composition are accompanied by changes in ecosystem function (17, 21).

Microbes mediate important stream ecosystem functions, controlling the movement of carbon (C) and nitrogen (N) through freshwater ecosystems. Previous studies demonstrate the effects of urbanization on stream nutrient transformations, such as N uptake (22), N retention (23), and C processing (24-25). Likewise, watershed urbanization alters the composition of microbes linked to key nutrient transformations, specifically the composition of ammonia-oxidizing (18,26) and denitrifying microbes (17-18, 27-28). These changes in community composition are linked to changes in denitrification potential, and therefore N loss, in urban streams (17). However, it is less clear how changes in microbial groups that cannot be clearly linked to specific metabolisms influence key ecosystem processes.

The objectives of this study were to determine how stream bacteria and archaea are distributed across gradients of watershed land use and stream condition, and to assess how changes in microbial community composition relate to benthic macroinvertebrate diversity and traditional indices of stream condition. We measured microbial diversity using 16S rRNA amplicon sequencing across 83 headwater streams within the Chesapeake Bay watershed in the state of Maryland, USA in spring and summer for two years. Measurements were collected in conjunction with stream physicochemical parameters and traditional invertebrate indicators of stream health. We further identified how changes in community structure influence stream function by relating microbial community composition to rates of microbial respiration and concentrations of the greenhouse gas nitrous oxide (N_2O).

Materials and Methods

Sample collection and physicochemistry

Stream sediment and water column samples were collected across three general geographic regions (coastal plains, highland, and piedmont) in Maryland during spring and summer of 2014 and 2015 (Fig. 1). In 2014, 83 headwater streams were sampled, and in 2015, 23 streams were resampled to assess temporal variability. Sampling sites were co-located with Maryland Biological Stream Survey (MBSS) sites -- a Maryland Department of Natural Resources (DNR) monitoring program that assesses the condition of wadeable streams via physicochemical and biological variables.

Water column samples for bacterial and archaeal diversity were collected in 500-mL sterile bottles and kept refrigerated until filtration. Samples were filtered on 0.22 μm pore size, 47 mm diameter polyethersulfone filters (MO BIO, Carlsbad, CA, USA) and stored at -80 °C. Sediment samples were collected using sterile 5 mL syringes by inserting the open plunger end of the syringe to a depth of 1 cm. Three cores were collected from each stream from within pools and stored in Whirl Pak bags at -80 °C until extraction.

Benthic invertebrate samples were collected to calculate a Benthic Index of Biotic Integrity (B-IBI) (29), which is a legal biocriterion in the state. Covariates used as predictors of stream quality in our analyses were provided by the Maryland DNR Monitoring and Non-tidal Assessment Division (https://dnr.maryland.gov/streams) and include watershed land use (urban, agricultural, and forested), substrate embeddedness, average thalweg depth, maximum depth, average stream width, average velocity, pH, specific conductance, acid neutralizing capacity (ANC), dissolved organic carbon (DOC), chloride (Cl^-), sulfate (SO_4^{2-}

), total nitrogen (TN), total phosphorus (TP), orthophosphate (PO_4^{3-}), ammonium (NH_4^+), nitrite (NO_2^-), nitrate (NO_3^-), magnesium (Mg), calcium (Ca), bromide (Br), zinc (Zn), and copper (Cu). Since a large proportion of MBSS sites are randomly selected within a specific set of subwatersheds for any given year, the environments captured by a given sampling year will be diverse, but not necessarily representative of the entire region.

Nitrous oxide concentrations

Nitrous oxide samples were collected from a subset (Table 1) of streams in summer 2014 and summer 2015. Samples were collected in triplicate in 160-mL glass serum vials by inserting silicon tubing to the bottom of the vial, then inverting and submerging the vial into the stream water with the other end of the tube venting to the atmosphere. Samples were preserved with 100 µL of a saturated mercuric chloride ($HgCl_2$) solution, sealed with grey butyl septa and aluminum crimp tops, and stored at room temperature until analysis.

Nitrous oxide concentrations were measured using a headspace equilibration method as described in (30). Each headspace was over-pressurized with an addition of 2.5 or 5 mL of ultra high purity (UHP) N_2 and equilibrated with the underlying stream water by gentle shaking at room temperature for at least 2 h. Subsamples from each headspace were analyzed using a SRI Greenhouse Gas Monitoring Gas Chromatograph (GC) equipped with an electron capture detector (ECD), dual HayeSep D packed columns, and a 1-mL sample loop (SRI Instruments, Torrance, California, USA). The carrier gas was UHP N_2 and the sample loop and column oven were heated to 60°C and 100°C, respectively. Two certified standards, 0.1 ppm and 1 ppm N_2O, from Matheson Tri-Gas were used for daily calibration. N_2O concentrations from the original stream sample were calculated according to Walter et al. 2006 (31), and the equilibrium N_2O concentration with the atmosphere at in situ

temperature was calculated using the Weiss and Price 1980 (32) solubility equations, using an atmospheric mole fraction of 328 ppb (33).

Community respiration rates

Sediment and water column respiration rates were measured in a subset of coastal plains streams (Table 2) using two O_2 consumption methods. In 2014, O_2 was measured using a membrane inlet mass spectrometer (MIMS) following Kana et al. 1994 (34), and in 2015, using a Fibox 3 fiber optic oxygen meter (PreSens, Regensburg, Germany). In 2014, water column incubations were conducted in 12-mL Exetainers (Labco, Lampeter, Wales, UK). For each stream, 9 water samples were collected by inserting a piece of tubing into the bottom of the vial and inverting and submerging the vial into the stream with the other end of the tube venting to the atmosphere. Three vials were sacrificially killed with a concentrated $HgCl_2$ solution at three time points, with the first time point immediately after collection and the remaining time points every 4 to 6 hours. Vials were transported in a dark cooler back to the laboratory, where they were incubated in the dark at in situ temperature for the remainder of the incubation. Sediment incubations were conducted in 160-mL serum vials with butyl septa and aluminum crimp tops. Modified from the above collection procedure, sediment was collected by inserting the plunger end of a sterile 30-mL syringe into the sediment and collecting 5 to 10 mL of sediment. The sediment was placed into each vial and topped with stream water.

In 2015, water column and sediment incubations were conducted in 60-mL glass biological demand (BOD) bottles with ground glass stoppers. Each BOD bottle contained a PSt3 oxygen sensor (PreSens, Regensburg, Germany). Five replicates were collected with one killed control from each stream using the methods described above. Once the bottles

were full, a thin layer of stream water was added to the top of each stopper to reduce gas exchange with the atmosphere. The bottles were stored in a cooler and transported back to the laboratory where they were incubated in the dark at in situ temperature. O_2 was measured using a Fibox 3 fiber optic oxygen meter (PreSens) every hour until the killed control bottle equilibrated, and thereafter, every 3 to 6 hours for up to 24 hours. All respiration rates were calculated using least square linear models with the function lm in the R package stats v. 3.5.0 (35). Rates in 2014 were calculated by fitting a model through all 9 data points, while rates from 2015 are the mean of models from each of the replicate bottles. Water column respiration rates were subtracted from sediment rates to isolate O_2 consumption in the sediments.

16S rRNA gene sequencing and processing

Water column and sediment DNA were extracted using a PowerSoil-HTP 96 well Soil DNA Isolation Kit (MO BIO, Carlsbad, CA, USA) with modifications. For water column samples, half of the filter was extracted, and filters were suspended in 925 µL of PowerSoil-HTP bead solution and 75 µL of solution C1 and vortexed for 10 minutes. Samples were digested with 20 µL of a 20 mg mL^{-1} Proteinase K solution for 30 minutes at 56 °C, and then centrifuged for 1 minute at 3000 x g. Sediment samples were also digested with Proteinase K, and additionally, samples were bead beaten at 20 Hz for 20 minutes on a Qiagen Tissuelyser. The PowerSoil-htp 96 well Soil DNA Isolation Kit protocol was followed for the remainder of the extractions.

16S rRNA gene amplicons were prepared using the standard Illumina protocol (Illumina, San Diego, CA, USA) with forward primer U515F and 806R. After amplicon PCR, the three sediment core samples from each site were pooled prior to PCR clean-up.

Following the second PCR clean-up, DNA was quantified using a Qubit dsDNA High Sensitivity Kit. Illumina MiSeq 2 x 150 bp (samples collected in 2014) and 2 x 250 bp (samples collected in 2015) sequencing was conducted at the University of Maryland Center for Environmental Science Institute of Marine and Environmental Technology.

Amplicon data were analyzed using the mothur software package v. 1.31.2 (36). The samples sequenced in 2014 did not have adequate read overlap to merge the reads, and for this reason, only the forward reads were used for all analyses. The mothur standard pipeline was followed with modifications (36). First, sequences with primer mismatches were removed and reads were trimmed using an average quality score cutoff of 35 over a 50 bp sliding window. Sequences were aligned with SILVA (v. 119) and classified using GreenGenes (v. 13.8.99). Sequences were binned based on taxonomy prior to clustering into operational taxonomic units (OTUs) at a 97% identity level.

Statistical analyses

All statistical analyses were computed in R (v. 3.5.0) (35). OTU richness, Shannon diversity, and Pielou's evenness were used to estimate microbial alpha diversity and were calculated using the R package phyloseq (v. 1.24.2) (37). Least square linear models and stepwise linear regression models for Shannon diversity and the physicochemical data were fit using lm in the stats package. All co-linear variables (Pearson's $|r| \geq 0.7$) were removed prior to stepwise linear regression analysis.

Beta diversity was quantified using Bray-Curtis dissimilarity and Sorensen index, and was calculated with singletons removed using vegdist in the vegan package (v. 2.5.2) (38). Correlations between community structure and the physicochemistry were calculated using the mantel function in vegan. Similarly, the relationships between community

structure, geographic distance, and environmental variables were examined using the mantel and partial.mantel functions in vegan. Community similarity was visualized using nonmetric multidimensional scaling (NMDS), which was calculated using metaMDS in the vegan package. Values for the exponent Z in the taxa-area relationship $S = cA^Z$, where A is area, S is the number of species, and c is a constant, were calculated using least square linear models of natural logarithm transformed Sorensen indices and geographic distance.

Correlations between taxa abundance and environmental data were quantified using Spearman correlations with the function associate in the microbiome package (v. 1.1.10013) (39). Adjusted p-values (p) were converted to z-scores and only correlations with a |z-score| $\geq$ 1.96. Indicator taxa, taxa both abundant and concentrated in a particular group, were found for highly urban (> 50%), agricultural (> 50%), and forested (> 90%) streams, as well as streams classified by B-IBI scores as good (B-IBI 4 - 5), fair (B-IBI 3 - 3.9), poor (B-IBI 2 - 2.9), and very poor (B-IBI 1 - 1.9) using multipatt in indicspecies (v.1.7.6) according to (40). An indicator was considered significant with an indicator statistic r > 0.5, specificity value A > 0.5, fidelity value B > 0.1, and a $p < 0.05$. We report the top three indicators for each substrate (water/sediment) in each land use and B-IBI group.

Data availability

Sequences are accessible from NCBI under BioProject accession number PRJNA545742.

Results

Higher microbial alpha diversity in spring

OTU richness differed according to substrate, ranging from 831 to 13,203 and 625 to 11,206 for water column and sediment samples, respectively, with water column OTU richness being significantly higher than sediment (paired Wilcoxon, $p < 0.001$). However, sediment Shannon diversity, 7.0 ± 0.4, was greater than water column diversity, 6.2 ± 1.3 (paired Wilcoxon, $p < 0.001$), as sediment communities were more even, 0.86 ± 0.04, than water column communities, 0.74 ± 0.14 (paired Wilcoxon, $p < 0.001$). Similarly, beta diversity (Bray-Curtis dissimilarity) differed by substrate (PERMANOVA, $R^2 = 0.11$, $p < 0.001$). Water column communities had more Actinobacteria, Bacteroidetes, and Proteobacteria; while, Acidobacteria, Planctomycetes, and Verrucomicrobia were more abundant in sediments (Fig. S1).

Interannually, there was no difference in alpha diversity between samples collected in 2014 and 2015, and collection year only explained a small fraction of the variance in beta diversity between water column and sediment communities (PERMANOVA, $R^2 = 0.01$, $p < 0.001$ and $R^2 = 0.02$, $p < 0.001$, respectively), with heterogeneous dispersion driving this difference (PERMDISP2, $p < 0.001$). Seasonally, Shannon diversity was greater in spring than in summer for water column and sediment samples (paired Wilcoxon, $p < 0.001$ and $p < 0.001$, respectively), a result of higher richness in spring (paired Wilcoxon, $p < 0.001$ and $p < 0.001$, respectively). Sediment samples were more even in summer (paired Wilcoxon, $p < 0.001$), while water column communities were more even in spring (paired Wilcoxon, $p = 0.005$). Additionally, there were seasonal changes in water column and sediment community

structure (PERMANOVA, $R^2 = 0.06$, $p < 0.001$ and $R^2 = 0.09$, $p < 0.001$, respectively), with Actinobacteria being more abundant in summer than in spring (Fig. S2).

Distance-decay relationships partially drive microbial diversity

Water column alpha diversity metrics differed across the three geographic regions, while sediment diversity remained constant (Fig. 2). Streams on the coastal plains had lower Shannon diversity than streams in the piedmont and highland regions (Dunn's Kruskal-Wallis, $p < 0.001$ and $p < 0.001$, respectively). This was driven by lower evenness in coastal plains streams compared to the other regions (Dunn's Kruskal-Wallis, $p < 0.001$ and $p < 0.001$, piedmont and highland, respectively), as there was no significant difference in the number of observed OTUs across the three regions. Regional differences in Bray-Curtis dissimilarity were observed in water column (PERMANOVA, $R^2 = 0.08$, $p < 0.001$; Fig. 3a) and sediment (PERMANOVA, $R^2 = 0.08$, $p < 0.001$; Fig. 3b) communities. Streams on the coastal plains had more Actinobacteria and fewer Acidobacteria than the other regions, while piedmont streams had more Proteobacteria and fewer Bacteroidetes (Fig. S3).

Partial Mantel tests detected correlations between water column and sediment Bray-Curtis dissimilarity and geographic distance ($\rho = 0.21$, $p = 0.001$ and $\rho = 0.18$, $p = 0.001$), and no significant relationship between Bray-Curtis dissimilarity and environmental distance ($\rho = 0.03$, $p = 0.2$ and $\rho = 0.07$, $p = 0.07$). Positive distance-decay relationships were observed between the natural logarithm transformed least squares linear regressions of water column and sediment community similarity (Sorensen index) and geographic distance. The absolute value of the regression coefficients (species-area z-values) for water column and sediment communities were 0.084 ($R^2 = 0.047$, $p < 0.001$) and 0.093 ($R^2 = 0.051$, $p < 0.001$; Fig. 4), for water and sediment communities, respectively.

Microbial diversity relates to stream physicochemistry

Stream physicochemistry varied by geographic region (Table S1), land use (Table S2), and stream condition (Table S3). N_2O concentrations ranged from 0.22 ± 0.00 μg L^{-1} to 4.41 ± 0.07 μg L^{-1} (58 to 1,217% saturated; Table 1), with no difference in N_2O concentration or saturation between individual streams sampled in 2014 and 2015 (paired T-Test, $p = 0.2$). N_2O negatively correlated with percent forest cover ($R^2 = 0.20$, $p = 0.01$), and positively correlated with TN ($R^2 = 0.54$, $p < 0.001$), NO_3^- ($R^2 = 0.51$, $p < 0.001$), NO_2^- ($R^2 = 0.41$, $p < 0.001$), NH_4^+ ($R^2 = 0.39$, $p < 0.001$), and Br ($R^2 = 0.30$, $p = 0.002$).

Respiration rates in coastal plains streams ranged from 21.7 to 1,573.2 mg O_2 m^{-2} d^{-1} and 31.9 and 3,667.9 mg O_2 m^{-2} d^{-1} for water column and sediments, respectively (Table 2). There was no significant difference in water column rates measured in streams in both 2014 and 2015 (paired t-test, $p = 0.9$), while sediment rates were higher in 2014 than in 2015 (paired t-test, $p = 0.04$). Water column respiration rates most strongly negatively correlated with specific conductance, Cl^-, Mg, and pH, and positively correlated with embeddedness, forest cover, and Shannon diversity (Table S4). Sediment respiration rates negatively correlated with Zn, TP, and PO_4^{3-} concentrations, and positively correlated with Br (Table S5). Water column and sediment microbial community structure correlated with respiration rates (Mantel, r = 0.37, $p = 0.004$ and r = 0.32, $p = 0.01$, respectively).

Water column Shannon diversity negatively correlated with several environmental variables, including embeddedness, Cu, DOC, TP, NO_2^-, and agricultural and urban land use, and positively correlated with forest cover and stream velocity (Table S6). The best fit stepwise multiple linear regression model to explaining 40% of the variance in water column Shannon diversity included pH, DOC, SO_4^{2-}, TP, forest cover, Mg, Cu, and thalweg depth.

Sediment diversity negatively correlated with DOC and embeddedness, and positively correlated with pH, NO_3^-, B-IBI, and TN (Table S7). A stepwise linear regression model explained 18% of the variation in sediment Shannon diversity, with pH, thalweg depth, Mg, and Br being the most significant predictors. Similarly, Bray-Curtis dissimilarity correlated with several environmental variables (Tables S8 and S9), including DOC, pH, embeddedness, and Zn. The measured physicochemical variables explained 11% and 14% of the variation in community structure according to constrained correspondence analysis in stream water and sediment communities, respectively.

Strong associations between taxon abundance and stream physicochemistry were observed when OTUs were grouped at the order level (Fig. 5). Methylococcales positively correlated with NH_4^+, DOC, Zn, and NO_3^-, and negatively correlated with forest cover (Fig. 5a). Actinomycetales positively correlated with embeddedness, TP, DOC and NO_2^-, and negatively correlated with forest cover. Pedosphaerales negatively correlated with ANC, urban cover, Cl^-, and pH. The strongest sediment associations were positive correlations between RB41 (Acidobacteria) and pH, velocity, and NO_3^-, and negative correlations with embeddedness, DOC, TP, and Zn (Fig. 5b).

Microbial communities vary according to watershed land use and stream condition

Stream water column alpha and beta diversity differed in watersheds with high agricultural, urban, and forested land use. Sediment community structure also differed according to land use, with no change in alpha diversity. Forested streams had higher water column Shannon diversity than agricultural (Kruskal-Wallis, $p = 0.001$) and urban (Kruskal-Wallis, $p < 0.001$) streams (Fig. 6). There was no difference in richness across watersheds dominated by different land uses, but forested streams were more even (Kruskal-Wallis, $p <$

0.001 and Kruskal-Wallis, $p = 0.001$, for agricultural and urban, respectively). Similarly, community structure differed in both water column (PERMANOVA, $R^2 = 0.12$, $p < 0.001$) and sediment communities (PERMANOVA, $R^2 = 0.07$, $p < 0.001$). Microbial indicator taxa were identified for streams in watersheds with high forested, agricultural, and urban land use (Table 3; Fig. 7). Forest indicators included Steroidobacter (Xanthomonadales), an unclassified Acidobacteria, and an unclassified Hyphomicrobiaceae (Rhizobiales). Strong agricultural indicators included Sulfurospirillum and Arcobacter, both Campylobacterales, and Prosthecobacter (Verrucomicrobiales). An unclassified Methylococcaceae (Methylococcales), Hydrogenophaga (Burkholderiales), and an unclassified Alcaligenaceae (Burkholderiales) were strong urban indicators.

Benthic macroinvertebrate Shannon diversity weakly correlated with water column and sediment microbial Shannon diversity ($R^2 = 0.03$, $p = 0.003$ and $R^2 = 0.02$, $p = 0.02$, respectively), and B-IBI scores correlated with sediment microbial Shannon diversity ($R^2 = 0.03$, $p = 0.008$). Additionally, benthic macroinvertebrate Bray-Curtis dissimilarities correlated with sediment and water column microbial Bray-Curtis dissimilarities (Mantel, $\rho = 0.34$, $p = 0.001$ and $\rho = 0.33$, $p = 0.001$, respectively), and B-IBI scores correlated with sediment (Mantel, $\rho = 0.11$, $p = 0.001$) and water column community structure (Mantel, $\rho = 0.084$, $p = 0.001$).

Microbial community structure differed in streams classified as in good, fair, poor, and very poor condition using the B-IBI (PERMANOVA, water column: $R^2 = 0.02$, $p = 0.007$, sediment: $R^2 = 0.03$, $p < 0.001$), and microbial indicator taxa were identified for streams in each condition (Table 4; Fig. 8). Indicators of good stream condition included Nitrosopumilus (Nitrosopumilales), an unclassified Chamaesiphonaceae (Synechococcales),

and Pseudanabaena (Pseudanabaeles), the latter two being Cyanobacteria. Indicators of poor stream condition included Novosphingobium (Sphingomonadales), Sulfurimonas (Campylobacterales), and Methylosinus (Rhizobiales). An unclassified Holophagaceae (Holophagales), Hydrogenophaga (Burkholderiales), and Thiobacillus (Hydrogenophilales) were indicators of very poor stream condition.

Discussion

The aims of this study were to understand how stream bacteria and archaea are distributed across gradients of watershed land use and water quality, to assess how changes in microbial community composition relate to benthic macroinvertebrate diversity, and to discern how these changes relate to stream ecosystem function. Microbial alpha diversity (Shannon diversity and OTU richness) was greatest in spring, when water flow through the landscape is greatest, and therefore when advection of microbes from the surrounding landscape is greatest to headwater streams. In contrast to marine systems (41-42), water column richness was greater than sediment richness likely due to the high interconnectivity between the water column and terrestrial soil environment, and the increased frequency of environmental and physical disturbances in the water column (43). Resuspension of stream sediment is an unlikely cause of the observed high water column richness, as water and sediment communities were distinct, sharing only 12 ± 4% (mean ± standard deviation) of OTUs. In agreement, previous studies demonstrate the influence of soil and local environmental conditions in structuring headwater stream communities (14-16).

Bacterial and archaeal diversity significantly differed across the geographic regions (Fig. 2,3), further demonstrating the influence of the surrounding landscape on headwater

stream communities. Lower alpha diversity in coastal plains streams (Fig. 2) was likely a result of regional alluvium composition. Sediments on the coastal plains of the eastern United States are composed of gravel, sand, silt, and clay (44), making streams more embedded, with streams having a higher percentage of larger particles surrounded by fine sediments (Table S1). Embeddedness was the environmental factor that most strongly negatively correlated with Shannon diversity (Table S6), and homogeneous fine sediments have been shown to have lower diversity than sites with riffles, shallow turbulent sections (45). Similarly, community structure varied across the geographic regions (Fig. 3), strongly correlating with DOC, pH, and embeddedness (Table S6 and S7), all of which significantly differentiate coastal plains streams from the other regions (Table S1). This finding is in agreement with previous studies, demonstrating the strong influence of DOC and pH on freshwater communities (16, 46, 47).

Distance-decay relationships were observed between water column and sediment community similarity and geographic distance (Fig. 4). These results, and the significant relationships between Bray-Curtis dissimilarity and spatial distance, suggest headwater stream microbes display geographic distribution patterns. Water column communities correlated more strongly with distance than sediment communities, perhaps because of dispersion of microbes from the local landscape directly into stream water. In contrast, sediment communities are likely more influenced by local stream environmental conditions due to increased residence times (16), integrating stream condition over longer periods of time. Microbial distance-decay relationships have been observed previously in streams (48, 49). Z-values obtained in this study (0.084 and 0.093) represent the rate at which species similarity decreases with increasing distance, and are similar to microbial values from soil,

salt marshes, and lakes (50–53), but lower than regional differences observed in salt marshes (54), suggesting different dispersal limitations across regional scales.

Indicator taxa were identified for streams in watersheds with high urban, agricultural, and forested land use (Table 3; Fig. 7). Many urban and agricultural indicators were taxa associated with high nutrient and low oxygen environments. The strongest urban indicators were taxa in the order Burkholderiales (Families Alcaligenaceae and Comamonadaceae), which correlated strongly with several anthropogenic nutrients (Fig. 5a). Comamonadaceae are often associated with high nutrient conditions, and are ubiquitous in many environments, including aquatic, soil, activated sludge, and wastewater (20, 55). Comamonadaceae have previously been associated with urban streams (20) and found to have the highest number of urban tolerant taxa (19). Sulfurospirillum and Arcobacter, both in the order Campylobacterales, were the strongest indicators of highly agricultural streams. Arcobacter are known to thrive in microaerobic and anaerobic conditions, such as surface water, groundwater, and livestock (56), and Sulfurospirillum are associated with microaerophilic polluted habits, commonly growing on arsenate or selenate using NO_3^- and sulfur compounds as electron acceptors (56, 57). In contrast, many indicators of forested watersheds are frequently associated with low nutrient environments, including an unclassified, potentially phototrophic, Acidobacteria, Hyphomicrobiaceae (Rhizobiales), and Steroidobacter (Nevskiales). Acidobacteria and Hyphomicrobiaceae, previously identified as indicators of forested streams (17-18), decrease in abundance with increasing watershed urbanization (19).

Both sediment community composition and water column communities correlated with the B-IBI, albeit to differing degrees. Similarly, Simonin et al. (2019) found stream

microbial community structure correlates with a macroinvertebrate biotic index in North Carolina, USA (19). Here, we provide further evidence stream microbial community structure changes according to stream condition. Nitrosopumilus (Phylum Thaumarchaeota) and two Cyanobacteria in the class Synechococcophycideae (Families Chamaesiphonaceae and Pseudanabaeceae) were indicators of streams in good condition (Table 4, Fig. 8) and play important roles in ecosystem C and N cycling. Thaumarchaeota are ammonia-oxidizing archaea found in many aquatic and terrestrial habitats (58–62) and are often associated with low nutrient environments (63). In this study, Cenarchaeales, another Thaumarchaeota order, negatively correlated with several anthropogenic nutrients (Fig. 5a). Many genera in the Chamaesiphonaceae family are characteristic of low nutrient environments, and some Pseudanabaeceae species are associated with oligotrophic waters reviewed in Mateo et al. 2015 (64). An unclassified Oscillatoriophycideae (Phylum Cyanobacteria) was an indicator of urban streams, Oscillatoriophycideae are often described as a pollution tolerant cyanobacteria (64). Additionally, indicators of poor and very poor stream condition (Table 4, Fig. 8), Sulfurimonas (Campylobacterales), Novosphingobium (Sphingomonadales), Holophagaceae (Holophagales), and Hydrogenophaga (Burkholderiales), are commonly associated with anaerobic, reducing, and contaminated environments (65-67). Roberto et al (2018) found Sphingomonadaceae, a family of Sphingomonadales, to be more abundant at urban sites, and hypothesized their dominance was a result of contamination from wastewater treatment effluent or a response to stormwater runoff (20).

Water column respiration from streams on the coastal plains positively correlated with forest cover and negatively correlated with urban cover (Fig. S4), implying stream ecosystem function, measured by C removal, is altered by watershed land use. Urbanized

streams have decreased organic matter retention and processing (68), and respiration is reported as a good indicator of stream ecosystem health (69). Benthic respiration rates (0.0785 ± 0.0740 g O_2 m^{-2} d^{-1}) were lower than rates previously reported from streams on the coastal plains of the Eastern USA (0.40 ± 0.05 g O_2 m^{-2} d^{-1}) (25,70). Water column respiration rates negatively correlated with several physicochemical variables (Table S4), including conductivity, Cl^-, ANC, Mg, pH, Ca, and embeddedness. ANC, Cl^-, and pH, all signatures of anthropogenic influence, were found to previously correlate with benthic stream respiration across the highland, piedmont, and coastal plains regions of the eastern United States (25). Sediment respiration rates strongly negatively correlated with Zn (Table S5), a common urban pollutant (71-74), which was significantly higher in urban streams, providing further evidence that in-stream respiration is altered by watershed modification.

Anthropogenic N inputs and watershed modification increase stream N_2O, as is evident by elevated N_2O in coastal plains streams with high concentrations of NO_3^- and the negative correlation between N_2O and forest cover. N_2O production is known to vary by land use, with higher production in streams in agricultural and urban basins (75). N_2O concentrations measured in this study, 0.22 to 4.41 μg L^{-1} (58 to 1,217% saturated), are similar to values reported from headwater streams in the midwestern United States, 0.84 to 4.34 μg L^{-1} (45 to 1,358% saturated) (76). N_2O production is elevated in streams with high NO_3^- indirectly due to high rates of denitrification rather than an increased N_2O yield relative to N_2 (75). In this study, N_2O was stable on a yearly time frame, there was no significant difference in N_2O concentrations between streams sampled in 2014 and 2015, likely because there was no significant difference in NO_3^- concentration between years.

Here, we demonstrate headwater stream microbial communities respond to gradients in land use and stream condition, and these differences are reflected in ecosystem processes, such as microbial C and N transformations. Regional differences in stream microbial communities and the observed distance-decay relationship are further evidence that stream communities are seeded from the surrounding landscape, and likely reflect local environmental conditions. Across geographic regions, stream communities correlated with a macroinvertebrate biotic index of stream condition and indicator taxa were identified for urban, agricultural, and forested land use, some of which have been identified as indicators of forested and urban watersheds in other geographic regions (18-19). Our results suggest certain microbes respond to stress similarly across ecosystems, making them potential candidate taxa for stream monitoring programs. Culturing these indicators could provide a better understanding of the physiology of these taxa and will provide a better understanding of how stream ecosystem function responds to changes in land use.

Acknowledgements

We thank Jason Cessna for conducting much of the field sampling. This work was supported by funds from Maryland Sea Grant (R/EH-16) to AES, SRK, and RHH. SML was supported by a Maryland Sea Grant Research Fellowship and the Interdepartmental Graduate Program in Marine Science at the University of California, Santa Barbara. AES and SML were also supported by United States National Science Foundation award OCE-1437310. The authors declare no conflict of interest.

Figures and tables

Table 1

Nitrous oxide concentrations (± standard deviation) and percent saturation relative to equilibrium at in situ temperature.

	2014		2015	
Stream site	**N_2O, µg L^{-1}**	**% saturation**	**N_2O, µg L^{-1}**	**% saturation**
CORS102	1.16	289.6	1.06 ± 0.03	302.3
LMON302	0.87 ± 0.01	223.7		
LOCR102	1.68 ± 0.32	536.9	1.16 ± 0.04	353.0
MATT104	0.55 ± 0.01	139.8		
MATT115	1.17 ± 0.03	286.0		
MATT320	0.55 ± 0.00	152.4		
NASS108	0.22 ± 0.00	58.4	0.48 ± 0.04	120.0
NASS302	1.33 ± 0.01	394.0	0.74 ± 0.01	197.1
PAXL294	0.55 ± 0.01	142.1	0.65 ± 0.03	168.2
SEAS109	1.1 ± 0.03	262.8		
SEAS111	1.41 ± 0.01	384.9		
UMON134	0.55 ± 0.04	139.2		
UMON299	2.88 ± 0.10	711.4		
UPCK102	1.65 ± 0.01	398.3	1.11 ± 0.05	286.9
UPCK113	1.28 ± 0.00	316.4		
UPCR208S			0.76 ± 0.03	178.8
WIRH215	4.26 ± 0.15	1217.4		
WIRH220	4.41 ± 0.07	1115.7	4.13 ± 0.12	1039.8

Table 2

Rates of water column and sediment respiration (mg O_2 m^{-2} d^{-1}; ± standard deviation) from streams on the coastal plains.

	2014		2015	
Stream site	Water column	Sediment	Water column	Sediment
CORS102	148.8	1563.7	181.9 ± 51.7	204.7 ± 68.8
LOCR102	246.0	3220.3	267.3 ± 79.6	31.9 ± 9.9
LOWI104	221.7	2441.1		
MATT104	95.0	128.7		
MATT115	52.6	394.2		
MATT320	23.8	1897.1		
NASS108	348.5	716.5		
NASS302	1573.2	3667.9	248.2 ± 31.8	96.3± 19.6
PAXL294	45.3	235.7	264.2 ± 49.9	498.2 ± 123.4
SEAS109	21.7	264.2		
SEAS111	35.9			
UPCK102	314.3			
UPCK113	112.3		77.2 ± 8.0	98.2 ± 18.8
UPCK208	79.0	889.1	67.3 ± 12.5	97.7 ± 18.8
WIRH215	56.5	1124.4		
WIRH220	77.0	1593.4	1029.3 ± 633.9	357.6 ± 233.4

Table 3

Microbial OTUs indicative of streams in highly forested (> 90%), agricultural (> 50%), and urban (> 50%) watersheds. A is the mean relative abundance of the OTU in each group compared to all groups. B is the relative frequency of each OTU belonging to each group.

Group	Substrate	Taxonomy (Domain/Phylum/Class/Order/Family/Genus)	Indicator r	p-value	A	B
Agriculture	sediment	Bacteria/Verrucomicrobia/Verrucomicrobiae/Verrucomicrobiales/ Verrucomicrobiaceae/Prosthecobacter	0.88	0.002	0.77	1.00
Agriculture	sediment	Bacteria/Proteobacteria/Deltaproteobacteria/BPC076/unclassified/ unclassified	0.87	0.001	0.76	1.00
Agriculture	sediment	Bacteria/Firmicutes/Bacilli/Bacillales/Bacillaceae/Bacillus	0.86	0.001	0.75	1.00
Agriculture	water	Bacteria/Proteobacteria/Epsilonproteobacteria/Campylobacterales/ Campylobacteraceae/Sulfurospirillum	0.96	0.00	0.93	1.00
Agriculture	water	Bacteria/Proteobacteria/Epsilonproteobacteria/Campylobacterales/ Campylobacteraceae/Arcobacter	0.89	0.00	0.80	1.00
Agriculture	water	Bacteria/Bacteroidetes/Bacteroidia/Bacteroidales/Prevotellaceae/ Prevotella	0.87	0.00	0.76	1.00
Forest	sediment	Bacteria/Acidobacteria/Chloracidobacteria/RB41/unclassified/ unclassified	0.82	0.002	0.80	0.85
Forest	sediment	Bacteria/FCPU426/unclassified/unclassified/unclassified/unclassified	0.81	0.001	0.69	0.96
Forest	sediment	Bacteria/Proteobacteria/Alphaproteobacteria/Rhizobiales/ Hyphomicrobiaceae/unclassified	0.81	0.001	0.65	1.00
Forest	water	Bacteria/Proteobacteria/Gammaproteobacteria/Nevskiales/ Sinobacteraceae/Steroidobacter	0.83	0.00	0.72	0.96

Table 3. Continued

Group	Substrate	Taxonomy (Domain/Phylum/Class/Order/Family/Genus)	Indicator r	p-value	A	B
Forest	water	Bacteria/Actinobacteria/Acidimicrobiia/Acidimicrobiales/unclassified/ unclassified	0.81	0.00	0.85	0.77
Forest	water	Bacteria/Verrucomicrobia/Spartobacteria/Chthoniobacterales/ Chthoniobacteraceae/DA101	0.80	0.00	0.64	1.00
Urban	sediment	Bacteria/Proteobacteria/Gammaproteobacteria/PYR10d3/unclassified/ unclassified	0.68	0.002	0.83	0.56
Urban	sediment	Bacteria/Cyanobacteria/Oscillatoriophycideae/unclassified/ unclassified/unclassified	0.60	0.012	0.73	0.50
Urban	sediment	Bacteria/Bacteroidetes/Saprospirae/Saprospirales/Chitinophagaceae/ Niastella	0.60	0.004	0.83	0.44
Urban	water	Bacteria/Proteobacteria/Betaproteobacteria/Burkholderiales/ Comamonadaceae/Hydrogenophaga	0.91	0.00	0.82	1.00
Urban	water	Bacteria/Proteobacteria/Betaproteobacteria/Burkholderiales/ Alcaligenaceae/unclassified	0.82	0.00	0.78	0.88
Urban	water	Bacteria/Proteobacteria/Gammaproteobacteria/Methylococcales/ Methylococcaceae/unclassified	0.82	0.00	0.72	0.94

Table 4

Microbial OTUs indicative of stream condition according to the Benthic Index of Biotic Integrity (BIBI). A is the mean relative abundance of the OTU in each group compared to all groups. B is the relative frequency of each OTU belonging to each group.

Group	Substrate	Taxonomy (Domain/Phylum/Class/Order/Family/Genus)	Indicator r	p-value	A	B
Good	sediment	Archaea/Thaumarchaeota/Thaumarchaeota/ Nitrosopumilales/Nitrosopumilaceae/Nitrosopumilus	0.65	0.02	0.50	0.83
Good	sediment	Bacteria/Cyanobacteria/Synechococcophycideae/ Pseudanabaeles/Pseudanabaeceae/Pseudanabaena	0.57	0.05	0.62	0.52
Good	water	Bacteria/Cyanobacteria/Synechococcophycideae/ Synechococcales/Chamaesiphonaceae/unclassified	0.63	0.03	0.56	0.70
Poor	sediment	Bacteria/Proteobacteria/Alphaproteobacteria/Rhizobiales/ Methylocystaceae/Methylosinus	0.67	0.01	0.50	0.89
Poor	sediment	Bacteria/Proteobacteria/Deltaproteobacteria/ Syntrophobacterales/Syntrophaceae/Desulfobacca	0.67	0.04	0.51	0.87
Poor	sediment	Bacteria/Chloroflexi/Dehalococcoidetes/Dehalococcoidales/ Dehalococcoidaceae/unclassified	0.58	0.04	0.50	0.66
Poor	water	Bacteria/Proteobacteria/Alphaproteobacteria/ Sphingomonadales/Sphingomonadaceae/Novosphingobium	0.73	0.01	0.53	1.00
Poor	water	Bacteria/Proteobacteria/Epsilonproteobacteria/ Campylobacterales/Helicobacteraceae/Sulfurimonas	0.72	0.01	0.54	0.95
Very poor	sediment	Bacteria/Acidobacteria/Holophagae/Holophagales/ Holophagaceae/unclassified	0.77	0.05	0.59	1.00
Very poor	sediment	Bacteria/WPS2/unclassified/unclassified/unclassified/ unclassified	0.73	0.02	0.58	0.92

Table 4. Continued

Group	Substrate	Taxonomy (Domain/Phylum/Class/Order/Family/Genus)	Indicator r	p-value	A	B
Very poor	sediment	Bacteria/Proteobacteria/Gammaproteobacteria/PYR10d3/ unclassified/unclassified	0.66	0.00	0.80	0.54
Very poor	water	Bacteria/Proteobacteria/Betaproteobacteria/Burkholderiales/ Comamonadaceae/Hydrogenophaga	0.76	0.02	0.75	0.77
Very poor	water	Bacteria/Proteobacteria/Gammaproteobacteria/34P16/ unclassified/unclassified	0.65	0.00	0.80	0.54
Very poor	water	Bacteria/Proteobacteria/Betaproteobacteria/ Hydrogenophilales/Hydrogenophilaceae/Thiobacillus	0.64	0.00	0.60	0.69

Figure 1. Map of Maryland, USA indicating headwater stream sampling locations. Symbol color indicates the geographic region.

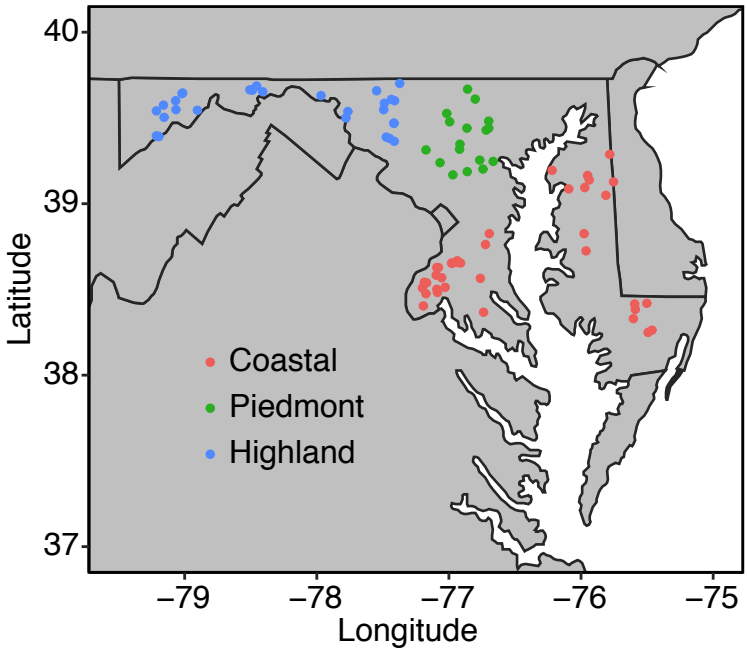

Figure 2. Alpha diversity metrics for water column (a, c, e) and sediment samples (b, d, f) in spring (white) and summer (grey) when grouped by geographic region. Dunn's test: *$p < 0.05$, **$p < 0.01$, ***$p < 0.001$, seasonal below and regional above.

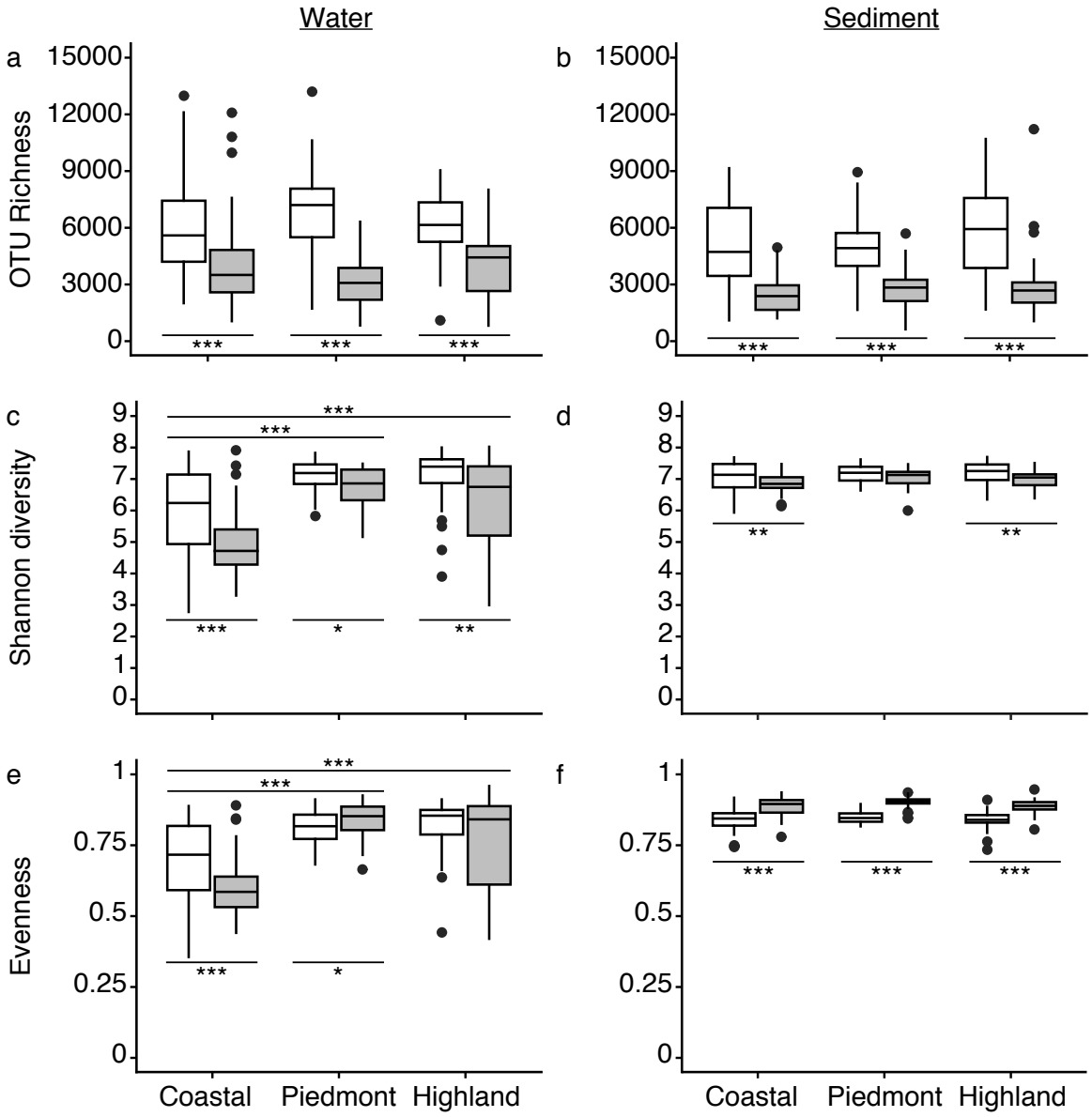

Figure 3. Non-metric multidimensional scaling (NMDS) plots of Bray-Curtis distances for all water column (a) (PERMANOVA, region: $R^2 = 0.08$, $p < 0.001$, season: $R^2 = 0.06$, $p < 0.001$) and sediment (b) (PERMANOVA, region: $R^2 = 0.08$, $p < 0.001$, season: $R^2 = 0.09$, $p < 0.001$) samples, symbol color indicates geographic region and symbol shape denotes season.

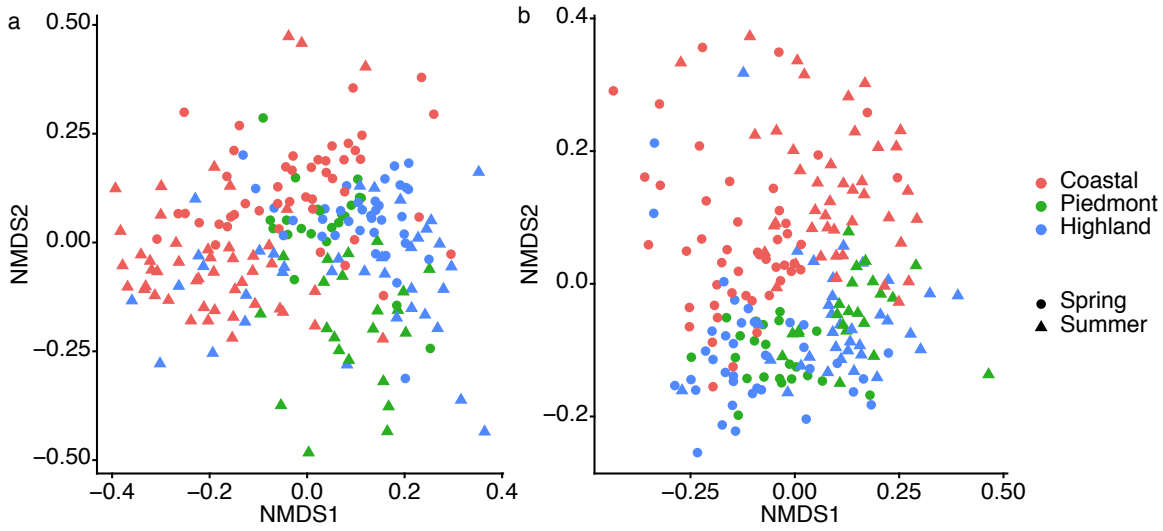

Figure 4. Relationship between microbial community composition (Sorensen index) and geographic distance for water column (a) and sediment (b) samples. Model fitting is least squares linear regression.

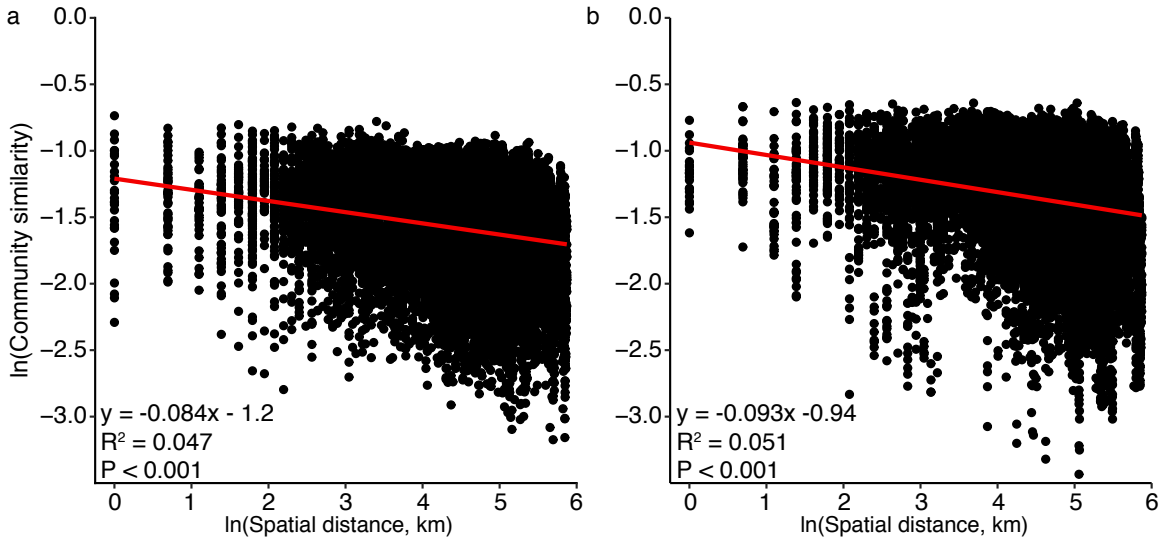

Figure 5. Correlations between the most abundant water column (a) and sediment (b) taxa at the order level and environmental variables. Color indicates the associated z-score. Correlations with an |z-score| < 1.96 are not shown and '+' symbols denote |z-scores| > 3.

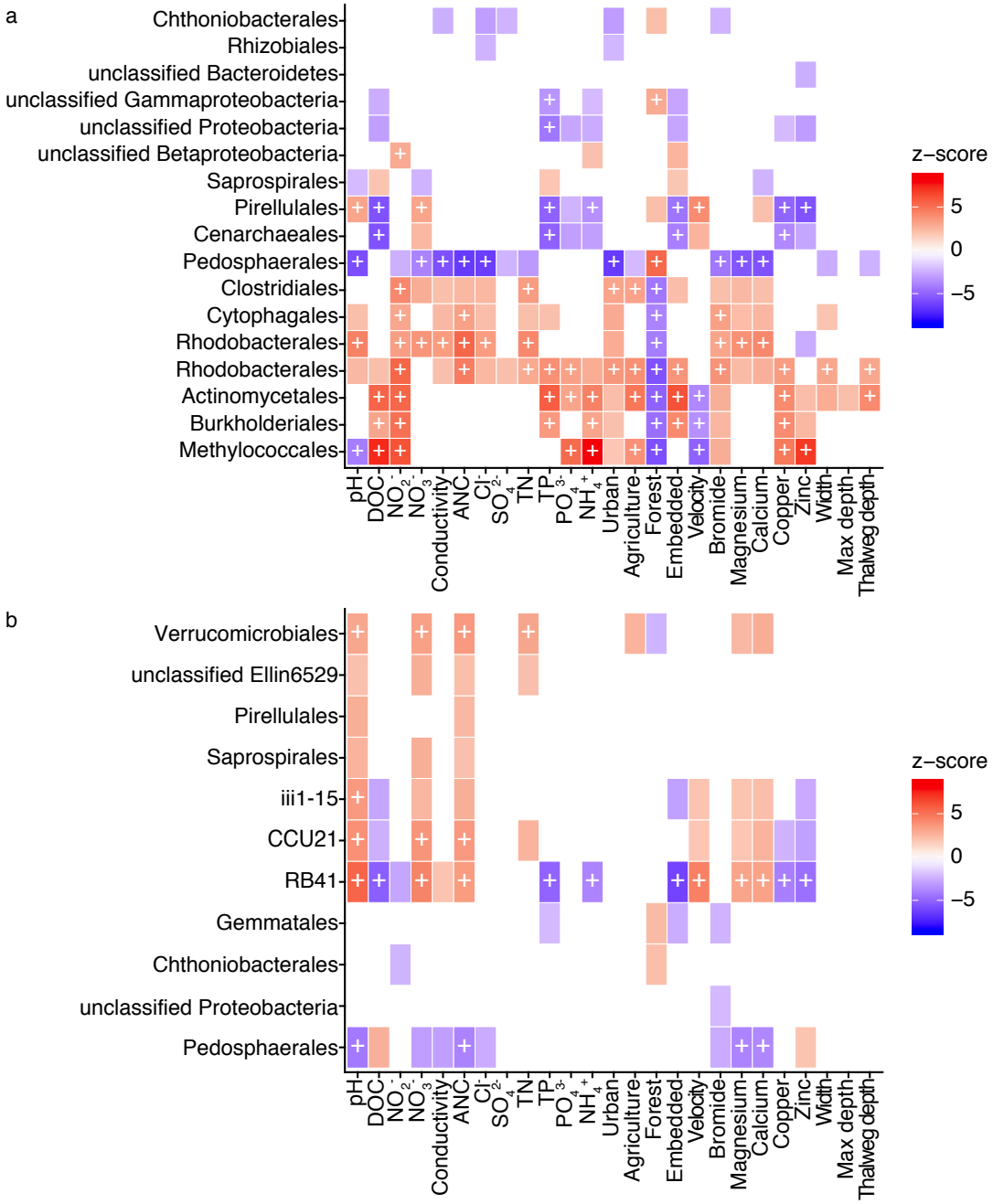

Figure 6. Alpha diversity metrics for water column (a, c, e) and sediment samples (b, d, f) in spring (white) and summer (grey) from streams in watersheds with highly forested (> 90%), agricultural (> 50%), and urban (> 50%) land use. Dunn's test: *$p < 0.05$, **$p < 0.01$, ***$p < 0.001$, seasonal below and land use above.

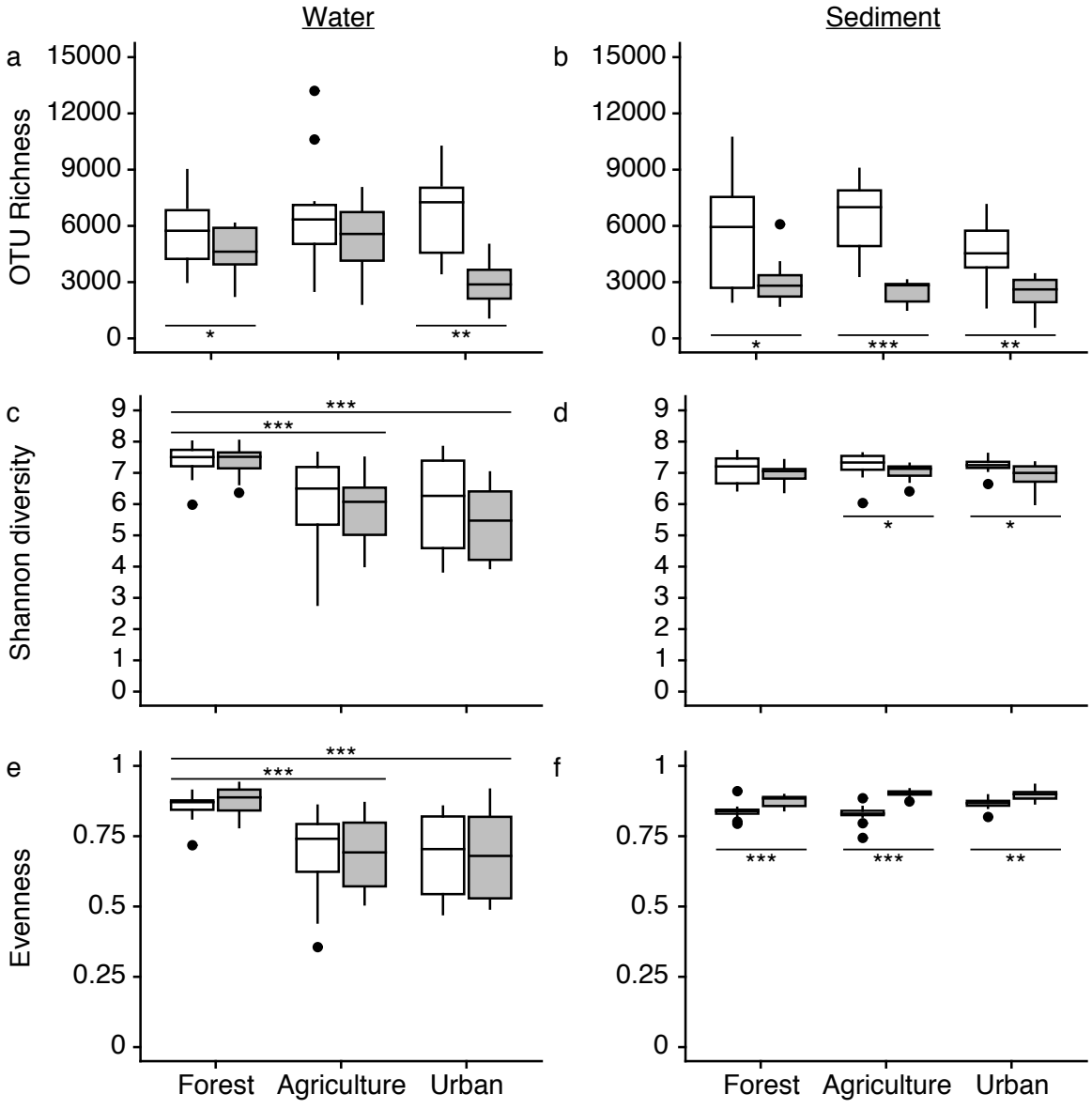

Figure 7. Water column and sediment microbial indicators of streams in highly forested (> 90%; a, b), agricultural (> 50%; c, d), and urban (> 50%; e, f) watersheds. The lowest classified taxonomic rank is provided for each indicator.

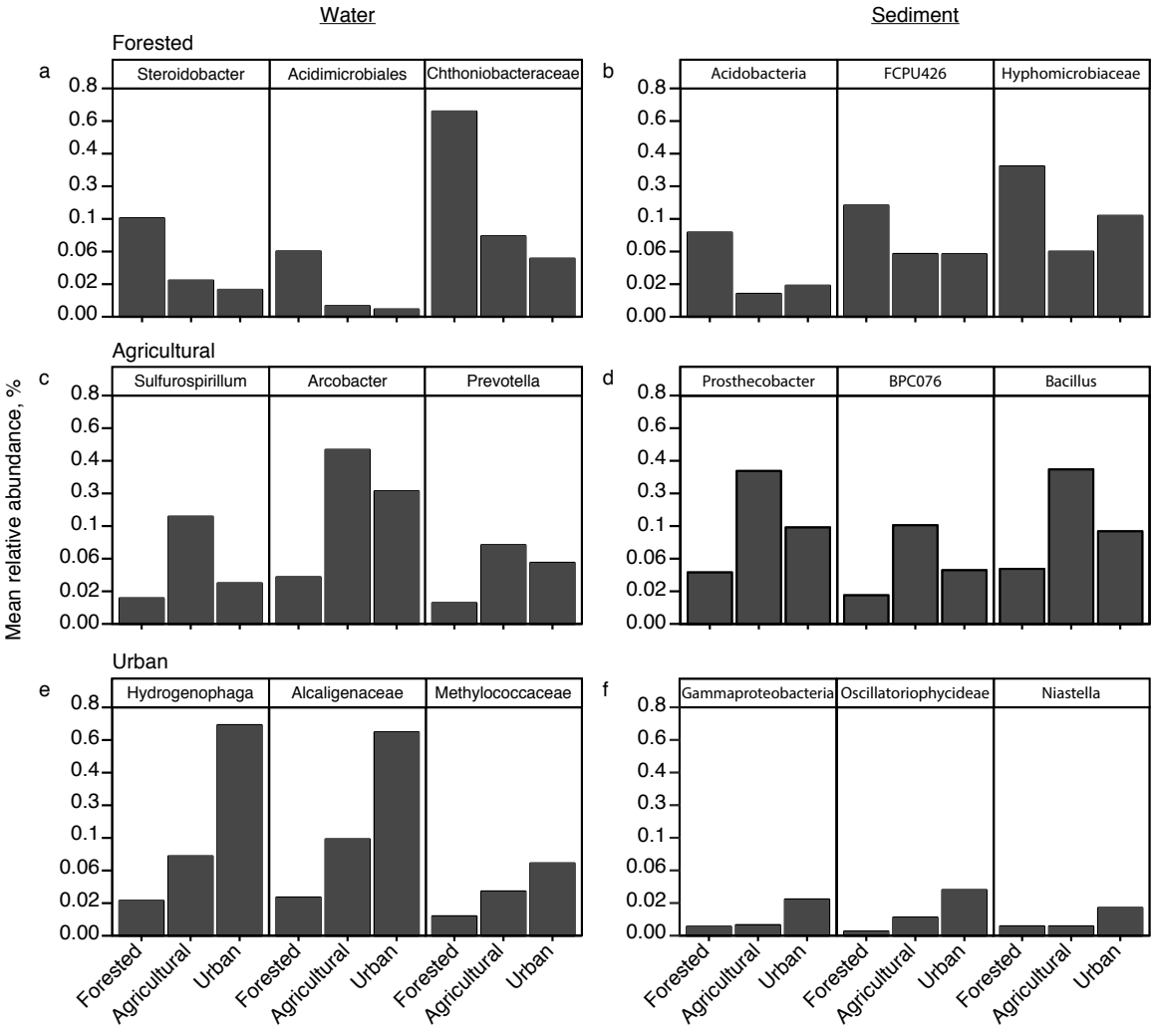

Figure 8. Stream water column and sediment microbial indicators of streams in good (a, b), poor (c, d), and very poor (e, f) condition according to the B-IBI. The lowest classified taxonomic rank is provided for each indicator.

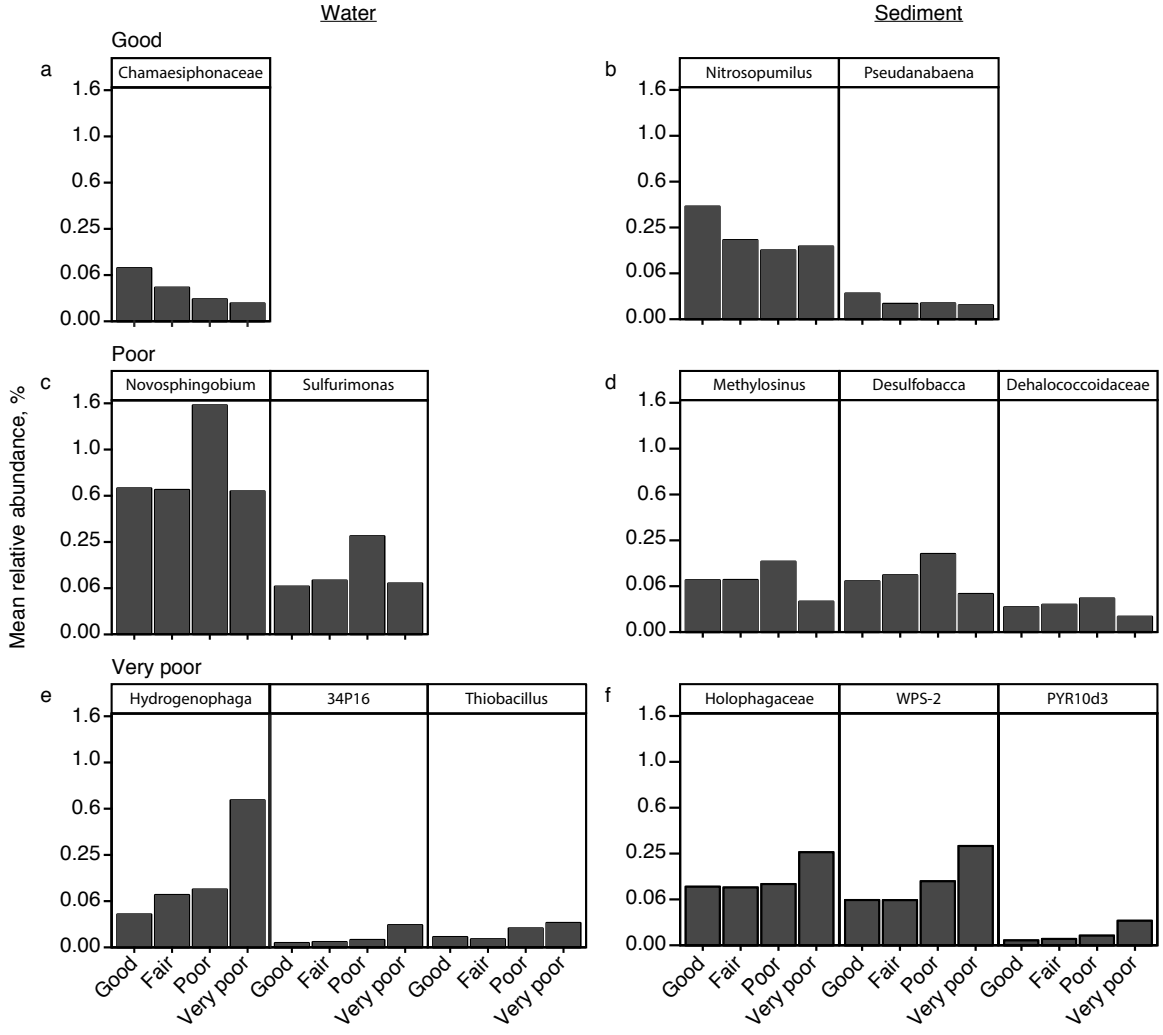

References

1. Tilman D. 1997. The influence of functional diversity and composition on ecosystem processes. Science 277: 1300-1302.
2. Delong MD, Brusven MA. 1998. Macroinvertebrate community structure along the longitudinal gradient of an agriculturally impacted stream. Environ Manage 22:445–457.
3. Young RG, Huryn AD. 1999. Effects of land use on stream metabolism and organic matter turnover. Ecol Appl 9:1359-1376.
4. Meyer JL, Paul MJ, Keith Taulbee W. 2005. Stream ecosystem function in urbanizing landscapes. J North Am Benthol Soc 24:602-612.
5. Moore AA, Palmer MA. 2005. Invertebrate biodiversity in agricultural and urban headwater streams: implications for conservation and management. Ecol Appl 15:1169-1177.
6. Whiting ER, Clifford HF. 1983. Invertebrates and urban runoff in a small northern stream, Edmonton, Alberta, Canada. Hydrobiologia 102:73-80.
7. Lenat DR, Kent Crawford J. 1994. Effects of land use on water quality and aquatic biota of three North Carolina Piedmont streams. Hydrobiologia 294:185-199.
8. Walsh CJ, Sharpe AK, Breen PF, Sonneman JA. 2001. Effects of urbanization on streams of the Melbourne region, Victoria, Australia. I. Benthic macroinvertebrate communities. Freshw Biol 46:535-551.
9. Hall MJ, Closs GP, Riley RH. 2001. Relationships between land use and stream invertebrate community structure in a South Island, New Zealand, coastal stream

catchment. NZ J Mar Freshwater Res 35:591-603.

10. Bonada N, Prat N, Resh VH, Statzner B. 2006. Developments in aquatic insect biomonitoring: a comparative analysis of recent approaches. Annu Rev Entomol 51:495–523.
11. Southerland MT, Rogers GM, Kline MJ, Morgan RP, Boward DM, Kazyak PF, Klauda RJ, Stranko SA. 2007. Improving biological indicators to better assess the condition of streams. Ecol Indic 7:751-767.
12. Weisberg SB, Ananda Ranasinghe J, Dauer DM, Schaffner LC, Diaz RJ, Frithsen JB. 1997. An estuarine benthic index of biotic integrity (B-IBI) for Chesapeake Bay. Estuaries 20:149.
13. Campbell RE, McIntosh AR. 2013. Do isolation and local habitat jointly limit the structure of stream invertebrate assemblages? Freshw Biol 58:128-141.
14. Crump BC, Amaral-Zettler LA, Kling GW. 2012. Microbial diversity in arctic freshwaters is structured by inoculation of microbes from soils. ISME J 6:1629–1639.
15. Crump BC, Adams HE, Hobbie JE, Kling GW. 2007. Biogeography of bacterioplankton in lakes and streams of an Arctic tundra catchment. Ecology 88:1365–1378.
16. Niño-García JP, Ruiz-González C, Del Giorgio PA. 2016. Interactions between hydrology and water chemistry shape bacterioplankton biogeography across boreal freshwater networks. ISME J 10:1755–1766.
17. Wang S-Y, Sudduth EB, Wallenstein MD, Wright JP, Bernhardt ES. 2011. Watershed urbanization alters the composition and function of stream bacterial communities. PLoS

One 6:e22972.

18. Hosen JD, Febria CM, Crump BC, Palmer MA. 2017. Watershed urbanization linked to differences in stream bacterial community composition. Front Microbiol 8:1452.
19. Simonin M, Voss KA, Hassett BA, Rocca JD, Wang SY, Bier RL, Violin CR, Wright JP, Bernhardt ES. 2019. In search of microbial indicator taxa: shifts in stream bacterial communities along an urbanization gradient. Environ Microbiol.
20. Roberto AA, Van Gray JB, Leff LG. 2018. Sediment bacteria in an urban stream: Spatiotemporal patterns in community composition. Water Res 134:353-369.
21. Qu X, Ren Z, Zhang H, Zhang M, Zhang Y, Liu X, Peng W. 2017. Influences of anthropogenic land use on microbial community structure and functional potentials of stream benthic biofilms. Sci Rep 7:15117.
22. Claessens L, Tague CL, Groffman PM, Melack JM. 2010. Longitudinal assessment of the effect of concentration on stream N uptake rates in an urbanizing watershed. Biogeochemistry 98:63–74.
23. Groffman PM, Law NL, Belt KT, Band LE, Fisher GT. 2004. Nitrogen fluxes and retention in urban watershed ecosystems. Ecosystems 7:393–403.
24. Harbott EL, Grace MR. 2005. Extracellular enzyme response to bioavailability of dissolved organic C in streams of varying catchment urbanization. J North Am Benthol Soc 24:588–601.
25. Hill BH, Herlihy AT, Kaufmann PR. 2002. Benthic microbial respiration in Appalachian Mountain, Piedmont, and Coastal Plains streams of the eastern U.S.A. Freshw Biol 47:185-194.

26. Merbt SN, Auguet J-C, Blesa A, Martí E, Casamayor EO. 2015. Wastewater treatment plant effluents change abundance and composition of ammonia-oxidizing microorganisms in Mediterranean urban stream biofilms. Microb Ecol 69:66–74.
27. Perryman SE, Rees GN, Walsh CJ. 2008. Analysis of denitrifying communities in streams from an urban and non-urban catchment. Aquat Ecol 42:95–101.
28. Perryman SE, Rees GN, Walsh CJ, Grace MR. 2011. Urban stormwater runoff drives denitrifying community composition through changes in sediment texture and carbon content. Microb Ecol 61:932–940.
29. Southerland MG, Kline RM, Morgan R, Boward D, Kazyak P, Stranko S. 2005. Development of new fish and benthic macroinvertebrate indices of biotic integrity for Maryland streams. Report to Monitoring and Non-Tidal Assessment Division, Maryland Department of Natural Resources, Annapolis, MD.
30. Laperriere SM, Nidzieko NJ, Fox RJ, Fisher AW, Santoro AE. 2019. observations of variable ammonia oxidation and nitrous oxide flux in a eutrophic estuary. Estuaries Coast 42:33-44.
31. Walter S, Bange HW, Breitenbach U, Wallace DWR. 2006. Nitrous oxide in the North Atlantic Ocean. Biogeosciences 3:993-1022.
32. Weiss RF, Price BA. 1980. Nitrous oxide solubility in water and seawater. Mar Chem 8:347-359.
33. National Oceanic and Atmospheric Administration. 2019. Halocarbons & Other Atmospheric Trace Species Group (HATS). https://www.esrl.noaa.gov/gmd/hats/data.html

34. Kana TM, Darkangelo C, Duane. Hunt M, Oldham JB, Bennett GE, Cornwell JC. 1994. Membrane inlet mass spectrometer for rapid high-precision determination of N_2, O_2, and Ar in environmental water samples. Anal Chem 66:4166-4170.
35. R Core Team. 2013. R: A language and environment for statistical computing. R Foundation for Statistical Computing, Vienna, Austria. http://www.R-project.org/
36. Kozich JJ, Westcott SL, Baxter NT, Highlander SK, Schloss PD. 2013. Development of a dual-index sequencing strategy and curation pipeline for analyzing amplicon sequence data on the MiSeq Illumina sequencing platform. Appl Environ Microbiol 79:5112–5120.
37. McMurdie PJ, Holmes S. 2013. phyloseq: An R package for reproducible interactive analysis and graphics of microbiome census data. PLoS One 8:e61217.
38. Oksanen JF, Blanchet G, Friendly M, Kindt R, Legendre P, McGlinn D, Minchin PR, O'Hara RB, Simpson GL, Solymos P, Stevens MHH, Szoecs E, Wagner H. 2019. vegan: Community Ecology Package. R package version 2.5-5. https://CRAN.R-project.org/package=vegan
39. Lahti L, Shetty S, Blake T, Salojarvi J. microbiome R package. http://microbiome.github.io
40. Dufrene M, Legendre P. 1997. Species assemblages and indicator species: the need for a flexible asymmetrical approach. Ecol Monogr 67:345-366.
41. Zinger L, Amaral-Zettler LA, Fuhrman JA, Horner-Devine MC, Huse SM, Welch DBM, Martiny JBH, Sogin M, Boetius A, Ramette A. 2011. Global patterns of bacterial beta-diversity in seafloor and seawater ecosystems. PLoS One 6:e24570.

42. Feng BW, Li XR, Wang JH, Hu ZY, Meng H, Xiang LY, Quan ZX. 2009. Bacterial diversity of water and sediment in the Changjiang estuary and coastal area of the East China Sea. FEMS Microbiol Ecol 70:80–92.
43. Robinson JV, Sandgren CD. 1983. The effect of temporal environmental heterogeneity on community structure: a replicated experimental study. Oecologia 57:98–102.
44. Ator SW, Denver JM, Krantz DE, Newell WL, Martucci SK. 2005. A surficial hydrogeologic framework for the Mid-Atlantic Coastal Plain. US Geological Survey.
45. Rees GN, Watson GO, Baldwin DS, Mitchell AM. 2006. Variability in sediment microbial communities in a semipermanent stream: impact of drought. J North Am Benthol Soc 25:370-378.
46. Fierer N, Morse JL, Berthrong ST, Bernhardt ES, Jackson RB. 2007. Environmental controls on the landscape-scale biogeography of stream bacterial communities. Ecology 88:2162–2173.
47. Hullar MAJ, Kaplan LA, Stahl DA. 2006. Recurring seasonal dynamics of microbial communities in stream habitats. Appl Environ Microbiol 72:713–722.
48. Lear G, Lau K, Perchec A, Buckley HL, Case BS, Neale M, Fierer N, Leff JW, Handley KM, Lewis G. 2017. Following Rapoport's Rule: the geographic range and genome size of bacterial taxa decline at warmer latitudes. Environ Microbiol 8:3152-3162.
49. Lear G, Washington V, Neale M, Case B, Buckley H, Lewis G. 2013. The biogeography of stream bacteria. Glob Ecol Biogeogr 22:544-554.
50. Barreto DP, Conrad R, Klose M, Claus P, Enrich-Prast A. 2014. Distance-decay and taxa-area relationships for bacteria, archaea and methanogenic archaea in a tropical lake

sediment. PLoS One 9:e110128.

51. Horner-Devine MC, Claire Horner-Devine M, Lage M, Hughes JB, Bohannan BJM. 2004. A taxa–area relationship for bacteria. Nature 432:750.
52. Green JL, Holmes AJ, Westoby M, Oliver I, Briscoe D, Dangerfield M, Gillings M, Beattie AJ. 2004. Spatial scaling of microbial eukaryote diversity. Nature 432:747–750.
53. Fierer N, Jackson RB. 2006. The diversity and biogeography of soil bacterial communities. Proc Natl Acad Sci U S A 103:626-631.
54. Martiny JBH, Eisen JA, Penn K, Allison SD, Horner-Devine MC. 2011. Drivers of bacterial beta-diversity depend on spatial scale. Proc Natl Acad Sci U S A 108:7850–7854.
55. Willems A. 2014. The Family Comamonadaceae, p 777-851. In, The Prokaryotes: Alphaproteobacteria and Betaproteobacteria. Springer, Berlin, Heidelberg.
56. Lastovica AJ, On SL, Zhang L. 2014. The Family Campylobacteraceae, p 307-335. In, The Prokaryotes: Deltaproteobacteria and Epsilonproteobacteria. Springer, Berlin, Heidelberg.
57. Goris T, Diekert G. 2016. The genus Sulfurospirillum, p 209-234. In, Organohalide-respiring bacteria. Springer, Berlin, Heidelberg.
58. Francis CA, Roberts KJ, Beman JM, Santoro AE, Oakley BB. 2005. Ubiquity and diversity of ammonia-oxidizing archaea in water columns and sediments of the ocean. Proc Natl Acad Sci U S A 102:14683–14688.
59. Karner MB, DeLong EF, Karl DM. 2001. Archaeal dominance in the mesopelagic zone of the Pacific Ocean. Nature 409:507–510.

60. Wuchter C, Abbas B, Coolen MJL, Herfort L, van Bleijswijk J, Timmers P, Strous M, Teira E, Herndl GJ, Middelburg JJ, Schouten S, Sinninghe Damsté JS. 2006. Archaeal nitrification in the ocean. Proc Natl Acad Sci U S A 103:12317–12322.
61. Leininger S, Urich T, Schloter M, Schwark L, Qi J, Nicol GW, Prosser JI, Schuster SC, Schleper C. 2006. Archaea predominate among ammonia-oxidizing prokaryotes in soils. Nature 442:806-809.
62. Stempfhuber B, Engel M, Fischer D, Neskovic-Prit G, Wubet T, Schöning I, Gubry-Rangin C, Kublik S, Schloter-Hai B, Rattei T, Welzl G, Nicol GW, Schrumpf M, Buscot F, Prosser JI, Schloter M. 2015. pH as a driver for ammonia-oxidizing archaea in forest soils. Microb Ecol 69:879–883.
63. Martens-Habbena W, Berube PM, Urakawa H, de la Torre JR, Stahl DA. 2009. Ammonia oxidation kinetics determine niche separation of nitrifying Archaea and Bacteria. Nature 461:976–979.
64. Mateo P, Leganés F, Perona E, Loza V, Fernández-Piñas F. 2015. Cyanobacteria as bioindicators and bioreporters of environmental analysis in aquatic ecosystems. Biodivers Conserv 24:909-948.
65. Han Y, Perner M. 2015. The globally widespread genus Sulfurimonas: versatile energy metabolisms and adaptations to redox clines. Front Microbiol 6:989.
66. Glaeser SP, Kämpfer P. 2014. The Family Sphingomonadaceae, p 641-707. In, The Prokaryotes: Alphaproteobacteria and Betaproteobacteria. Springer, Berlin, Heidelberg.
67. Fukunaga Y, Ichikawa N. 2014. The Class Holophagaceae, p 683-687. In, The Prokaryotes: Other Major Lineages of Bacteria and the Archaea. Springer, Berlin,

Heidelberg.

68. O'Driscoll M, Clinton S, Jefferson A, Manda A, McMillan S. 2010. Urbanization effects on watershed hydrology and in-stream processes in the Southern United States. Water 2:605-648.
69. Fellows CS, Clapcott JE, Udy JW, Bunn SE, Harch BD, Smith M J, Davies PM. 2006. Benthic metabolism as an indicator of stream ecosystem health. Hydrobiologia 572:71-87.
70. Hill BH, Hall RK, Husby P, Herlihy AT, Dunne M. 2000. Interregional comparisons of sediment microbial respiration in streams. Freshw Biol 44:213-222.
71. Councell TB, Duckenfield KU, Landa ER, Callender E. 2004. Tire-wear particles as a source of zinc to the environment. Environ Sci Technol 38:4206–4214.
72. Paul MJ, Meyer JL. 2001. Streams in the Urban Landscape. Annu R Ecol Syst 32:333-365.
73. Lettenmaier DP, Hooper ER, Wagoner C, Faris KB. 1991. Trends in stream quality in the continental United States, 1978-1987. Water Resour Res 27:327-339.
74. Wilber WG, Hunter JV. 2007. The impact of urbanization on the distribution of heavy metals in bottom sediments of the Saddle River 1. J Am Water Resour Assoc 15:790-800.
75. Beaulieu JJ, Tank JL, Hamilton SK, Wollheim WM, Hall RO Jr, Mulholland PJ, Peterson BJ, Ashkenas LR, Cooper LW, Dahm CN, Dodds WK, Grimm NB, Johnson SL, McDowell WH, Poole GC, Valett HM, Arango CP, Bernot MJ, Burgin AJ, Crenshaw CL, Helton AM, Johnson LT, O'Brien JM, Potter JD, Sheibley RW, Sobota

DJ, Thomas SM. 2011. Nitrous oxide emission from denitrification in stream and river networks. Proc Natl Acad Sci U S A 108:214–219.

76. Beaulieu JJ, Arango CP, Hamilton SK, Tank JL. 2007. The production and emission of nitrous oxide from headwater streams in the Midwestern United States. Glob Chang Biol 14:878-894.

III. Chapter II: Observations of variable ammonia oxidation and nitrous oxide flux in a eutrophic estuary

Sarah M. Laperriere[1,2], Nicholas J. Nidzieko[1,3], Rebecca J. Fox[1*], Alexander W. Fisher[1,3], Alyson E. Santoro[1,2]

[1]Horn Point Laboratory, University of Maryland Center for Environmental Science, Cambridge, Maryland, USA

[2]Department of Ecology, Evolution, and Marine Biology, University of California, Santa Barbara, California, USA

[3]Department of Geography, University of California, Santa Barbara, California, USA

*present address: Department of Environmental Science and Studies, Washington College, Chestertown, Maryland, USA

Estuaries Coast 2019 42:(1), 33-44. doi:10.1007/s12237-018-0441-4

Abstract

Accurate global forecasting of marine nitrous oxide (N_2O) emissions requires a better understanding of atmospheric N_2O fluxes from coastal systems, particularly the mechanisms controlling the net balance between N_2O production and consumption. The objective of this study was to examine how physical and biological processes in the eutrophic Chesapeake Bay estuary influence the temporal and spatial variability of N_2O using a combination of gas measurements (N_2O and N_2:Ar) and stable isotope tracer

incubations. Observed concentrations of N_2O varied considerably in both space and time with the highest concentrations (up to 20.9 nM) across the pycnocline. Ammonia oxidation rates ranged from 14.3 to 108.9 nM h^{-1} and were highest following wind events that mixed oxygenated surface water below the pycnocline into ammonium-rich bottom waters, resulting in nitrite (NO_2^-) accumulations of up to 13 μM. During periods of weak vertical mixing, both N_2O concentrations and ammonia oxidation rates were lower, while lower O_2 concentrations also allowed N_2O consumption during denitrification. A three-layer box model provided estimates of N_2O production at the surface and across the pycnocline of 4 μmol m^{-2} d^{-1} and 21 μmol m^{-2} d^{-1}, respectively, and an estimate of N_2O consumption below the pycnocline of approximately -3 μmol m^{-2} d^{-1}. Our results demonstrate that physical processes affect the net balance between N_2O production and consumption, making Chesapeake Bay a variable source and sink for N_2O.

Introduction

Nitrous oxide (N_2O) is a potent greenhouse gas and stratospheric ozone-depleting agent (Ravishankara et al. 2009), and its atmospheric concentration (329 ppb; National Oceanic and Atmospheric Administration 2018) has increased by 20% since pre-industrial time (IPCC 2013). Atmospheric emissions of N_2O are predicted to increase with continued perturbation of the nitrogen (N) cycle, especially from coastal ecosystems (Bange 2000; Naqvi et al. 2010) as N loading increases and oxygen (O_2) concentrations decrease (Seitzinger and Kroeze 1998; Diaz and Rosenberg 2008; Codispoti 2010; Naqvi et al. 2010). But, recent projections of oceanic N_2O emissions also suggest a decrease in emissions due to

increased vertical stratification and reduced primary production and export of organic matter (Martinez-Rey et al. 2015; Battaglia and Joos 2018). The current magnitude of the N_2O flux to the atmosphere from coastal and estuarine systems is poorly constrained and not included in most estimates of marine N_2O flux (Bange et al. 1996; Buitenhuis et al. 2017). These fluxes are difficult to predict due to the complex way that oxygen influences N_2O production from multiple microbial metabolisms.

Nitrous oxide is produced during the first step of nitrification (ammonia oxidation) and is both produced and consumed during denitrification. N_2O is generated as a by-product during ammonia oxidation by poorly understood pathways (Poth and Focht 1985; Frame and Casciotti 2010; Santoro et al. 2011; Kozlowski et al. 2016). Denitrification both produces and consumes N_2O under low oxygen conditions, where N_2O is an obligate intermediate in the stepwise reduction of nitrate (NO_3^-) to N_2 gas. The N_2O yield (N_2O-N:NO_2^-) during ammonia oxidation increases considerably as O_2 concentrations decrease (Goreau et al. 1980; Löscher et al. 2012; Qin et al. 2017); the N_2O:N_2 yield from denitrification increases when organisms become stressed or exposed to O_2 (Tiedje 1988; Dalsgaard et al. 2014) and at elevated NO_3^- concentrations (Blackmer and Bremner 1978), up to a threshold O_2 concentration when N_2O is used as a terminal electron acceptor.

Nitrification is often credited as the dominant N_2O production pathway in estuaries (De Wilde and De Bie 2000; de Bie et al. 2002; Barnes and Upstill-Goddard 2011; Kim et al. 2013; Lin et al. 2016). N_2O concentrations are highly variable in these ecosystems, however, and are often related to rates of organic matter remineralization (Barnes and Upstill-Goddard 2011; Kim et al. 2013), oxygen concentration (De Wilde and De Bie 2000;

De Bie et al. 2002), and ammonium (NH_4^+) concentration (Barnes and Upstill-Goddard 2011). Surprisingly, few studies of N_2O dynamics have been made in the Chesapeake Bay, even though it is the largest estuary in the United States and has seasonal changes in both NH_4^+ and O_2 concentrations (Testa et al. 2018).

The Chesapeake Bay is a eutrophic estuary with a typical two-layer estuarine circulation pattern (Pritchard 1952). Strong vertical stratification in summer leads to severe O_2 depletion in deeper waters below the pycnocline (Kemp et al. 2005; Murphy et al. 2011; Testa et al. 2014). The resulting sharp oxygen gradient produces a strong redox gradient across the pycnocline, where highly reducing bottom waters accumulate phosphate (PO_4^{3-}) and NH_4^+ (Lee et al. 2015). The resupply of oxygen below the pycnocline in summer is largely controlled by wind-driven mixing across shallow shoals and advection of the oxygenated water up-Bay (Scully 2016). Wind events in fall erode the stronger summertime stratification, triggering moments of high ammonia oxidation in the Chesapeake Bay (Horrigan et al. 1990) and, potentially, increased N_2O production, as oxygen is mixed below the pycnocline.

Although few studies have measured N_2O in the main channel of Chesapeake Bay, studies in sub-estuaries suggest multiple N_2O production mechanisms. The primary source of N_2O in the York River was reported to be water column nitrification (McCarthy et al. 1984), while sediment denitrification was found to be the main source of N_2O in the Potomac River estuary (McElroy et al. 1978). There is evidence that denitrification in Chesapeake Bay also acts as a sink for N_2O in summer when dissolved oxygen (DO) concentrations decrease in bottom waters (Elkins et al. 1978).

The objectives of this study were to examine how physical processes in the Chesapeake Bay influence the temporal and spatial variability of N_2O and determine the fate of N_2O produced in the Bay during stratified summer conditions. We examined both spatial and temporal variability of N_2O concentrations in the Chesapeake Bay during two week-long sampling cruises in the mesohaline region of the Bay. To evaluate the relative roles of nitrification and denitrification as sources of N_2O in the water column, ammonia oxidation rates were measured using $^{15}NH_4^+$ tracer additions and denitrification was assessed using water column N_2:Ar ratios. N_2O concentrations were measured using gas chromatography, and a control volume approach was used to estimate the relative importance of physical and biological processes in governing N_2O dynamics.

Methods

Study site and sample collection

Samples were collected between 25-31 August 2013 and 13-17 September 2013 during two cruises aboard the R/V *Hugh R. Sharp* (HRS1316 & HRS1317). Nine stations were sampled in the mesohaline region of the Chesapeake Bay between the Choptank and Patuxent rivers (Fig. 1). The sampling grid was 21 km in the along-channel direction and 6 km in the across-channel direction. At each station, hydrographic profiles were conducted and samples for nutrients and N_2O concentration were collected. During both cruises, the central station M2 (38.47°N, 76.39°W) was chosen for higher frequency temporal sampling and ammonia oxidation rate measurements.

Water samples were collected using a 12 x 10 L Niskin bottle rosette sampler equipped with a conductivity, temperature, and pressure instrument package (SBE9, Sea-Bird Electronics, Bellevue, Washington, U.S.A.) and a sensor for dissolved oxygen (SBE43, Sea-Bird). Samples for nitrite (NO_2^-) and nitrite plus nitrate ($NO_2^- + NO_3^-$) concentration analyses were 0.2 μm filtered into 20 mL HDPE scintillation vials and frozen at -20°C until analysis. Samples were analyzed using standard colorimetric methods at the Horn Point Laboratory Analytical Services Laboratory. Ammonium was measured at sea using the o-phthaldialdehyde-based fluorometric method (Holmes et al. 1999). Wind data for all calculations were obtained from a buoy deployed at station M2 as part of a project investigating the role of wind in estuarine dynamics (Scully et al. 2015; Scully et al. 2016; Fisher et al. 2017; Fisher et al. 2018).

Dissolved gas samples for N_2O and N_2:Ar analyses were collected at all stations, with higher frequency collection at station M2. N_2O samples were collected in duplicate in 160 mL serum vials and N_2:Ar samples were collected in triplicate in 12 mL exetainers directly from the Niskin bottles using a small piece of tubing. The tubing was placed at the bottom of each container and water overflowed by approximately five volumes. The samples were preserved using 100 μL or 20 μL of a saturated mercuric chloride solution for N_2O and N_2:Ar, respectively. The serum vials were sealed using butyl septa and aluminum crimp tops, and both sample types were stored at room temperature, which was cooler than sampling temperature, until analysis.

Ammonia oxidation rates

Rates of ammonia oxidation were measured at station M2 twice per cruise at three or four depths. Water for ammonia oxidation rate incubations was collected directly from the rosette into 250 mL polycarbonate bottles. Bottles from each depth were spiked with $^{15}NH_4^+$ at 10% of the ambient ammonium concentration in duplicate along with one no addition control. Bottles were incubated in the dark at in situ temperature for 12 h. Subsamples were collected from each bottle at 0, 6, and 12 h, and filtered into 20 mL scintillation vials and frozen at -20°C until analysis.

Samples were prepared for $\delta^{15}NO_{2+3}^-$ analysis via the denitrifier method (Sigman et al. 2001) and the resulting N_2O headspaces were analyzed by isotope ratio mass spectrometry at the University of California Davis Stable Isotope Facility or the Central Appalachians Stable Isotope Facility at the University of Maryland Center for Environmental Science. Ammonia oxidation rates were calculated following previously described methods (Dugdale and Goering 1967; Damashek et al. 2016). Initial atom percent (atm%) enrichment in the starting NH_4^+ pool was calculated based on the measured in situ NH_4^+ concentration and the amount of 99 atm% ^{15}N labeled NH_4^+ added. Rates were not corrected for potential isotope dilution of the ^{15}N label from newly remineralized NH_4^+.

Dissolved gas concentrations

N_2O concentrations were measured using a headspace equilibration method. A 30 mL ultra-high purity N_2 headspace was added to each sample using a syringe with a vent needle inserted in the septa to drain sample water. Each headspace was over-pressurized with an additional 2.5 mL of N_2 to avoid atmospheric contamination upon headspace sample

removal. The headspace was equilibrated with the underlying seawater by gentle shaking at room temperature for at least 2 hours. From each headspace, a 2.5 mL subsample was injected into a 1 mL sample loop and analyzed on a Shimadzu GC-14B Gas Chromatograph (GC) equipped with a Porapak-Q packed column and an electron capture detector (ECD) (Elkins 1980). Differing from Elkins (1980), Ultra High Purity N_2 was used as the carrier gas and the column oven was kept at 32°C. The method was calibrated daily with two certified standards, 0.1 and 1 ppm N_2O, obtained from Matheson Tri-Gas. N_2O concentrations (C_{N_2O}) from the original seawater samples were calculated using the follow equation (Walter et al. 2006):

$$C_{N_2O} = \frac{(F\ x\ P\ V_w + \frac{x\ P}{R\ T}\ V_h)}{V_w}$$

where F includes corrections for all non-ideality effects and a water vapor saturated water-gas interphase (Weiss and Price 1980), x is the dry gas mole fraction of N_2O in the headspace, P is atmospheric pressure, V_w is the water volume, V_h is the headspace volume, R is the gas constant (L atm K^{-1} mol^{-1}), and T is the equilibration temperature (K).

N_2:Ar was measured on a membrane inlet mass spectrometer (MIMS) equipped with a flow-through capillary membrane inlet (Bay Instruments, Easton, Maryland) following Kana et al. (1994). Bottom water at 24.5°C from station M2 was used as standard water for all samples, and the solubility of N_2 and Ar were calculated according to Weiss (1970).

Nitrous oxide flux calculations

The air-water flux of N_2O was calculated as $F = k\,(C_{N_2O} - C_{eq})$, where k is the gas transfer velocity, C_{N_2O} is the surface N_2O concentration and C_{eq} is the equilibrium N_2O concentration with the atmosphere calculated using the Weiss and Price (1980) solubility equations. The gas transfer velocity was calculated according to Ho et al. (2006) using a 3-day prior average of the observed 10 m neutral wind speed at M2. Bulk transfer functions, COARE 3.0 (Fairall et al. 2003), were used to adjust measured wind conditions at 3 m to 10 m neutral conditions by accounting for near-surface thermal stability that can affect vertical turbulent transport within the atmospheric boundary layer. Values of k were corrected for N_2O at in situ temperature and salinity using $k = k^*(Sc/600)^{-0.5}$ (Wanninkhof 1992), where k^* is normalized to the molecular Schmidt number for CO_2 in freshwater at 20°C and Sc is the molecular Schmidt number for N_2O calculated after Wanninkhof (1992).

Data deposition

Dissolved gas concentrations, nutrient concentrations, and ammonia oxidation rate data have been deposited in the United States National Science Foundation Biological & Chemical Oceanography Data Management Office repository (bco-dmo.org) in association with project 'AmoA Archaea.'

Results

Hydrography and nutrient distributions

The August cruise was preceded by a brief 20 knot wind event on 23 August (Fig. S1a), and during the cruise, southerly winds between 25-27 August transported a high salinity, high dissolved oxygen (DO), and high NO_2^- water mass from south of station M2 northward up the Bay (Fig. S1a, Fig. 2a,c,e,g). During the second cruise, a 20 knot wind event on 14 September drove the deepening of the pycnocline on 15 September (Fig. S1b, Fig. 2a). Despite wind events, the main channel stations (S2, M2, and N2) remained highly stratified during both cruises (Fig. 2a-h). Representative data from M2 shows the strong stratification in both salinity and DO concentration (Fig. 2a-d). Average bottom water DO concentrations decreased from August to September from 27.4 ± 13.1 μM to 2.5 ± 0.2 μM, respectively, along with a deepening of the oxycline from 7.5 ± 2.1 m in August to 13.2 ± 1.9 m in September (Fig. 2c,d).

Dissolved inorganic nitrogen concentrations also varied between cruises. In August, water column NO_3^- concentrations were lower than NO_2^- concentrations (Fig. 2e-h). Mid-water column NO_3^- maxima were present 27-30 August, as the water mass moving northward transported bottom water with low NO_3^- and high NO_2^- concentrations up the Bay. NO_2^- concentrations were highest in August, reaching 13 μM in bottom waters (Fig. 2g). By the September cruise, most of the NO_2^- had disappeared and NO_3^- began to accumulate in bottom waters (Fig. 2f,h). Generally, NH_4^+ concentrations were low at the surface and increased with depth below the pycnocline. NH_4^+ concentrations at M2 also

increased from August to September, reaching concentrations of 5.6 μM in bottom waters (Fig. 3a,b).

Ammonia oxidation rates

Ammonia oxidation rates ranged from 14.3 ± 1.4 nM h^{-1} to 108.9 ± 7.2 nM h^{-1} across all depths during both the August and September cruises (Fig. 3a,b). In August, the highest ammonia oxidation rates were in bottom waters below the pycnocline, with the highest rate on 25 August at 25 m (Fig. 3a). The average ammonia oxidation rate decreased from 25 to 27 August, with average rates of 83.6 ± 34.5 nM h^{-1} and 15.2 ± 0.5 nM h^{-1}, respectively. In September, rates were highest at the top of the pycnocline and decreased with depth, with rates of ammonia oxidation reaching 44.3 ± 0.9 nM h^{-1} (Fig. 3b). No measured physical or chemical variable correlated with rates of ammonia oxidation.

Nitrous oxide dynamics

Samples for N_2O concentration were collected daily at station M2 during each cruise to examine higher resolution temporal changes (Fig. 4a,b). Generally, N_2O concentrations reached a mid-water column maximum coincident with the pycnocline (Fig. 4a,b). Maximum N_2O concentrations were greater in August than in September, with average concentrations of 17.4 ± 3.2 nM and 11.9 ± 1.8 nM, respectively. The highest N_2O concentration (20.9 ± 0.1 nM, 287% of saturation) measured during both cruises was collected at station M2 from 12 m on 27 August (Fig. 4a). In contrast, on 13 Sept, N_2O was undersaturated below the pycnocline with a minimum bottom water concentration of 6.4 ± 0.3 nM (88% of saturation; Fig. 4b). On all but one occasion, our observations indicate that

the main stem of Chesapeake Bay was a source of N_2O to the atmosphere (Fig. S2). Atmospheric fluxes over the two cruises ranged from 0.02 ± 0.02 to 4.3 ± 0.4 μmol m^{-2} d^{-1}, with the greatest atmospheric flux at station M2 on 28 August.

To examine the spatial variation in N_2O concentration, on 13 September the three main channel stations (S2, M2, and N2) were sampled (Fig. 5a-c) and on 15 September all nine stations were sampled (Fig. S3). On 13 Sept, bottom water N_2O concentrations were below saturation at all stations with bottom water N_2O concentrations of 7.0 ± 0.1 nM, 6.5 ± 0.3 nM, and 2.9 ± 0.2 nM at stations S2, M2, and N2, respectively. Station M2 had the highest N_2O concentration, 14.9 ± 0.4 nM, at the pycnocline. Surface N_2O concentrations were similar across the three stations ranging 121-129% of saturation.

On 15 September, N_2O concentrations were higher than on 13 Sept. All concentrations below the pycnocline were above saturation (Fig. S3), with bottom N_2O concentrations of 13.8 ± 0.2 nM, 10.3 ± 0.1 nM, and 11.0 ± 0.2 nM at stations S2, M2, and N2, respectively. Surface concentrations decreased from station S2 to N2, 11.3 ± 0.1 nM, 9.8 ± 0.8, and 8.0 ± 0.3 nM at stations S2, M2 and N2, respectively, ranging from 148% of saturation at S2 to 105% of saturation at N2. N_2O was well-mixed at the shallow lateral flank stations (N1, N3, M1, M3, S1, and S3) with an average concentration of 9.8 ± 0.3 nM.

N_2:Ar distribution

N_2:Ar ratios were measured daily at station M2 and at a lesser frequency at other stations. N_2:Ar profiles from 13 and 15 September are presented as representative data from the September cruise (Fig. 6a,b). N_2:Ar ratios below the pycnocline at the main channel stations were always above the expected ratio based on equilibrium with the atmosphere

(Fig. 6a,b). N_2:Ar increased at depth across the pycnocline, with maxima in the water column or close to the sediments. Average N_2:Ar ratios below the oxycline were higher on 13 Sept than 15 Sept, with average N_2:Ar ratios at M2 of 38.51 ± 0.04 and 38.35 ± 0.002 and at N2 of 38.63 ± 0.05 and 38.31 ± 0.02, respectively (Students' T-test, p=0.001 and $p<0.001$, respectively). There was no significant difference between average bottom water N_2:Ar ratios at station S2 between 13 and 15 Sept. N_2:Ar ratios increased in bottom waters moving north on 13 Sept, but this pattern was not present on 15 Sept.

Nitrous oxide yield

The ratio of excess N_2O to apparent oxygen utilization (ΔN_2O/AOU) is an estimate of the N_2O yield from organic matter decomposition, where $\Delta N_2O = N_2O_{water} - N_2O_{air}$ and apparent oxygen utilization, $AOU = O_{2air} - O_{2water}$, where N_2O_{air} and O_{2air} are the air-equilibrated concentrations. In August, the ΔN_2O/AOU at station M2 increased under high AOU (low DO concentrations; Fig. 7a). Above an AOU of 198 μM (~32 μM O_2), the slope of the least squares regression fit of ΔN_2O versus AOU from all samples from station M2 yielded a slope of 0.2 nM μM^{-1}, 10 times greater than below 198 μM, 0.02 nM μM^{-1} (breakpoint analysis, Davies' test for change of slope, $p<0.001$). In September, below 194 μM (~39 μM O_2), the ΔN_2O/AOU was 0.03 nM μM^{-1}, while the ΔN_2O/AOU value above 194 μM was negative, with a slope of -0.2 nM μM^{-1} (breakpoint analysis, Davies' test for change of slope, $p<0.001$; Fig. 7b).

Discussion

There is a close coupling between physical dynamics and nitrogen biogeochemistry in estuaries, and the data presented here illustrate the specific effects of wind-driven mixing on ammonia oxidation and N_2O production. Measured ammonia oxidation rates were highest following a 20-knot wind event prior to the August cruise (23 August; Fig. S1a). High winds likely increased vertical mixing and transported oxygenated surface waters across the pycnocline to NH_4^+-rich bottom waters. Following the event, NH_4^+ rapidly decreased and NO_2^- accumulated (Fig. 2g). Wind-driven oxidation events in the Chesapeake Bay are episodic and short-lived collapsing rapidly following the event once O_2 mixed below the pycnocline is consumed. Along with the rates reported here, previous studies have also measured high rates of ammonia oxidation following wind events fueled by the oxygenation of reduced species below the pycnocline (Horrigan et al. 1990). These results are contrary to the suppression of ammonia oxidation and N_2O production by sudden increases in O_2 observed in the Bedford Basin during mixing events (Punshon and Moore 2004).

The rates of measured ammonia oxidation (~340 to 2,600 nM d^{-1}) are in the range of rates found in many other estuaries, which span orders of magnitude (reviewed by Damashek et al. 2016). The rates reported here from the Chesapeake Bay are higher than those reported in San Francisco Bay, the Baltic Sea, and some rates from Naragansett Bay, 7-310 nM d^{-1}, 1-280 nM d^{-1}, and 0-20 nM d^{-1}, respectively (Enoksson 1986; Hietanen et al. 2012; Damashek et al. 2016; Heiss and Fulweiler 2016), but are lower than maximum ammonium oxidation rates in the Scheldt estuary (153,600 nM d^{-1}; De Wilde and De Bie

2000), Naragansett Bay (11,200 nM d^{-1}; Berounsky and Nixon 1993), and previous measurements in Chesapeake Bay (83,064 nM d^{-1}; Horrigan et al. 1990). Nitrification rates are often positively correlated with suspended organic matter and NH_4^+ concentration in eutrophic estuaries, while in oligotrophic estuaries, high nitrification rates are associated with rapid NH_4^+ regeneration (Damashek et al. 2016). In Chesapeake Bay, we observed a spatial separation between high ammonia oxidation rates and high NH_4^+ concentrations, likely due to poor ventilation of bottom waters and low oxygen concentrations limiting ammonia oxidation. Upon oxygenation of bottom waters, NH_4^+ is quickly oxidized creating nitrification "hot moments" in the Bay that accumulate NO_2^- and N_2O.

Pulses of dissolved oxygen delivered across the pycnocline, governed by winds during summer stratified conditions in the Chesapeake Bay, control rates of ammonia oxidation and therefore N_2O production. Transport of oxygenated water across the pycnocline into reducing conditions stimulates moments of high ammonia oxidation and N_2O production (Fig. 2c, 3a, & 4d). These events result in an accumulation of NO_2^- (Fig. 2g) caused by a decoupling of ammonia oxidation and nitrite oxidation, a common pattern in many estuaries in late summer and early fall (Horrigan et al. 1990; Schaefer and Hollibaugh 2017). This decoupling may affect N_2O production, as elevated NO_2^- concentrations may further increase N_2O yields from nitrification (Dong et al. 2002; Frame and Casciotti 2010; Santoro et al. 2011).

The highest N_2O concentrations are found at or near the pycnocline and in bottom waters after oxygenating events (Fig. 4). Collectively, our results suggest that ammonia oxidation is the primary N_2O production mechanism in Chesapeake Bay during the summer

months and that N_2O concentrations are strongly controlled by vertical mixing of O_2 across the pycnocline. Measured N_2O concentrations may be influenced both by water column production and by transport of N_2O to the main stem from wetlands or the shallow lateral flanks of the Bay, where N_2O may be produced via coupled nitrification-denitrification in the sediments. While transport from the lateral flanks is possible, the fact that water column concentrations at the main stem stations were greater than the concentrations on either lateral flank indicates that production in bottom waters, and not lateral advection, is the source of N_2O measured in the main stem. Although denitrification can also be a source of water column N_2O, the timing of increased N_2O production following oxygenating events and elevated rates of ammonia oxidation at depth suggest that nitrification was likely the dominant mechanism during our study.

Strong gradients in dissolved O_2 result in a correlation between N_2O excess (ΔN_2O) and AOU in all but the lowest O_2 waters (Fig. 7). The N_2O-N yield per mole of NH_4^+ oxidized was calculated using the relationship between ΔN_2O and AOU measured in the Chesapeake Bay and a nutrient remineralization O_2:N ratio equal to 10.6 (Anderson and Sarmiento 1994), though additional N loading to estuaries may cause deviations from this O:N stoichiometry (Lipschultz et al. 1986). N_2O yields ranged from 0.03 to 0.4%, with a higher yield under low oxygen conditions. Our field-calculated yields are on the low end of measured yields from cultures of ammonia oxidizing bacteria (AOB; Goreau et al. 1980) and yields measured previously in the Chesapeake Bay (0.2 to 0.7%; McCarthy et al. 1984), but higher than maximum yields measured from ammonia-oxidizing archaea (AOA) grown in culture (Santoro et al. 2011; Löscher et al. 2012; Qin et al. 2017) and in the open ocean (Ji

et al. 2015; Trimmer et al. 2016). The negative linear relationship between ΔN_2O and AOU at low O_2 during the September cruise indicates N_2O consumption via denitrification (Fig. 7b).

Nitrous oxide was consumed in bottom waters during the September cruise, when low O_2 concentrations supported denitrification in the bottom water and/or sediments. Daily profiles show N_2:Ar ratios increasing across the pycnocline to maximum values in bottom waters (Fig. 6) as a result of N_2 production by either denitrification or anammox (Rich et al. 2008). As found previously, N_2:Ar ratios below the pycnocline were higher than expected based on equilibrium with the atmosphere and, on 13 September, increased in the bottom layer as water moved north up the Bay (Kana et al. 2006). N_2:Ar ratios were highest on 13 September, when N_2O was undersaturated in bottom waters, supporting a water column denitrification N_2O sink, not a source. This signal was quickly eroded and concentrations were above saturation the following day. A wind event on 14 September, with winds reaching ~20 knots, likely caused vertical mixing of oxygenated water and slowed bottom water denitrification, and therefore N_2O consumption.

Rapid changes in the coupling between N_2O production and consumption in bottom waters may make the Chesapeake Bay both a variable source and sink of N_2O. However, atmospheric fluxes of N_2O from Chesapeake Bay during late summer and early fall ranged 0.02 to 4.3 μmol m^{-2} d^{-1}, making the Bay a source of N_2O to the atmosphere. Consumption of N_2O was constrained to bottom waters, which do not directly interact with the atmosphere. Most studies indicate estuaries are a source of atmospheric N_2O via numerous production mechanisms, with few studies showing estuaries act as a sink for atmospheric

N_2O (De Wilde and De Bie 2000; Gonçalves et al. 2010; Reading et al. 2017; Yevenes et al. 2017). Here, the Chesapeake Bay is a transient sink for N_2O below the pycnocline when stratification is strong enough to support bottom water denitrification, however the bottom layer has limited interaction with the atmosphere. This likely occurs farther north in the Bay, such as at station N2, where oxygen concentrations are lowest, and stratification is not easily eroded by southerly winds (Scully 2016).

The observed changes in N_2O concentration observed here reflect the influence of advection of water from other regions of the Bay into the study area. To gain further insight into the interplay between biological and physical processes at controlling the observed day-to-day changes in N_2O concentration, we estimated the order of magnitude for terms in an N_2O mass balance for the mid-Bay region to better constrain N_2O sources and sinks. We consider the water column at station M2 and define a simplified three-layer system in which the middle layer (at the pycnocline) is a source of N_2O; the sources and sinks for the surface and bottom layers are determined by difference as the residual from the physical terms (Supplemental Material). The relevant transport processes are: in the surface layer, horizontal advective fluxes and vertical turbulent fluxes, both with the middle layer below and across the air-water interface; in the middle layer, only vertical turbulent fluxes; and in the bottom, along-channel advective fluxes and vertical turbulent fluxes with the middle layer. From this analysis, we conclude that the bottom layer (comprising both the bottom waters and the sediments) was a sink for N_2O of approximately -3 μmol m^{-2} d^{-1}, consistent with measured water column N_2:Ar ratios and measurements of estuarine sediment N_2O consumption in other estuaries (Foster and Fulweiler 2016). Both the middle and surface

layers were sources of N_2O with fluxes of 21 μmol m^{-2} d^{-1} and 4 μmol m^{-2} d^{-1}, respectively. High rates of N_2O production are estimated at the pycnocline where vertical mixing of oxygenated water alleviates O_2 limitation in the reducing NH_4^+-rich bottom waters. The main conclusion from the mass balance exercise is that, for a given station, both biological and physical transport processes are equally capable of contributing to local changes in concentration; this implies that biological processes within Chesapeake Bay are both spatially and temporally heterogeneous. Maximum N_2O production rates estimated using this approach are higher than previous rates measured in the Chesapeake Bay (McCarthy et al. 1984). Thus, by accounting for physical processes, this approach allowed us to quantify the magnitude of the biological denitrification sink independent of bottle incubations.

The fate of N_2O in the Chesapeake Bay is governed by vertical mixing across the pycnocline where it can either be released to the atmosphere or trapped and consumed in bottom waters with re-stratification of the water column. Physical dynamics, particularly wind induced mixing, control the net balance between N_2O production and consumption. Future work should focus on this tight coupling, which makes N_2O concentrations extremely heterogeneous in coastal systems and complicates the ability to accurately predict N_2O emissions. The transient nature of wind events calls for higher resolution temporal sampling to capture pulses of N_2O production.

Acknowledgements

We thank the captain and crew of the R/V Hugh R. Sharp and Chief Scientist Michael Roman for allowing our participation on the cruises, which were funded by United

States National Science Foundation (NSF) award OCE-1259691. We thank W. Boicourt and M. Scully for providing current velocity and wind data for the sampling area. We are grateful to James Pierson, Wen-Cheng Liu, Catherine Fitzgerald, and Hannah McFadden for sampling assistance at sea. We thank Todd Kana for valuable advice on the MIMS data and Jeff Cornwell, Larry Sanford, and the members of SCOR working group #143 for discussions. This work was supported by funds from the NSF to A.E.S. (OCE-1260006 and OCE-1437310) and startup funds from the University of Maryland Center for Environmental Science. S.M.L. was supported by a Horn Point Laboratory graduate student fellowship, a Maryland SeaGrant graduate fellowship, and the Interdepartmental Graduate Program in Marine Science at UCSB. N.J.N. was supported by NSF (OCE-1259691 and OCE-1334398). A.W.F. was supported by NSF OCE-1061609 awarded to W. Boicourt, L. Sanford, and Ming Li and a Horn Point Laboratory graduate student fellowship. R.J.F. was supported by NSF grants OCE-1260006, DEB-091918 and DEB-1252923. The authors declare no conflict of interest.

Figures

Figure 1. Map of the study site with an inset map of the Chesapeake Bay. Black circles indicate station locations and grey lines indicate bathymetry (10 m contour interval).

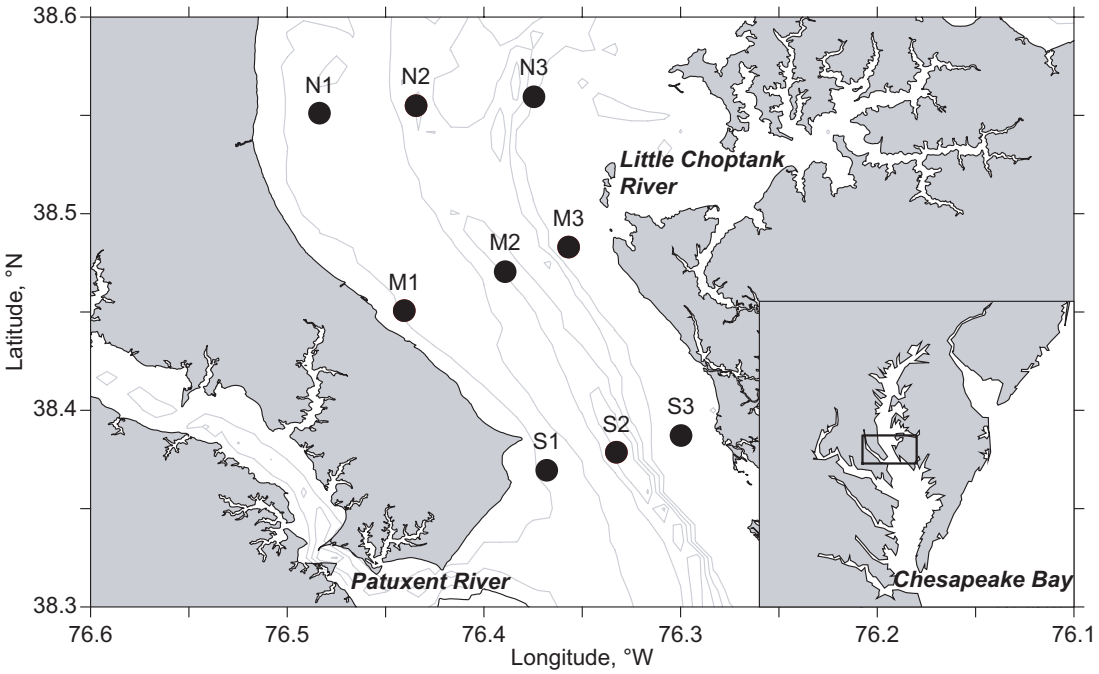

Figure 2. Salinity (a,b), oxygen (c,d), nitrate (e,f), and nitrite (g,h) at station M2 in the mesohaline region of the Chesapeake Bay on 25-31 August 2013 (a,c,e,g) and 13-17 September 2013 (b,d,f,h). Black circles indicate where discrete samples were collected.

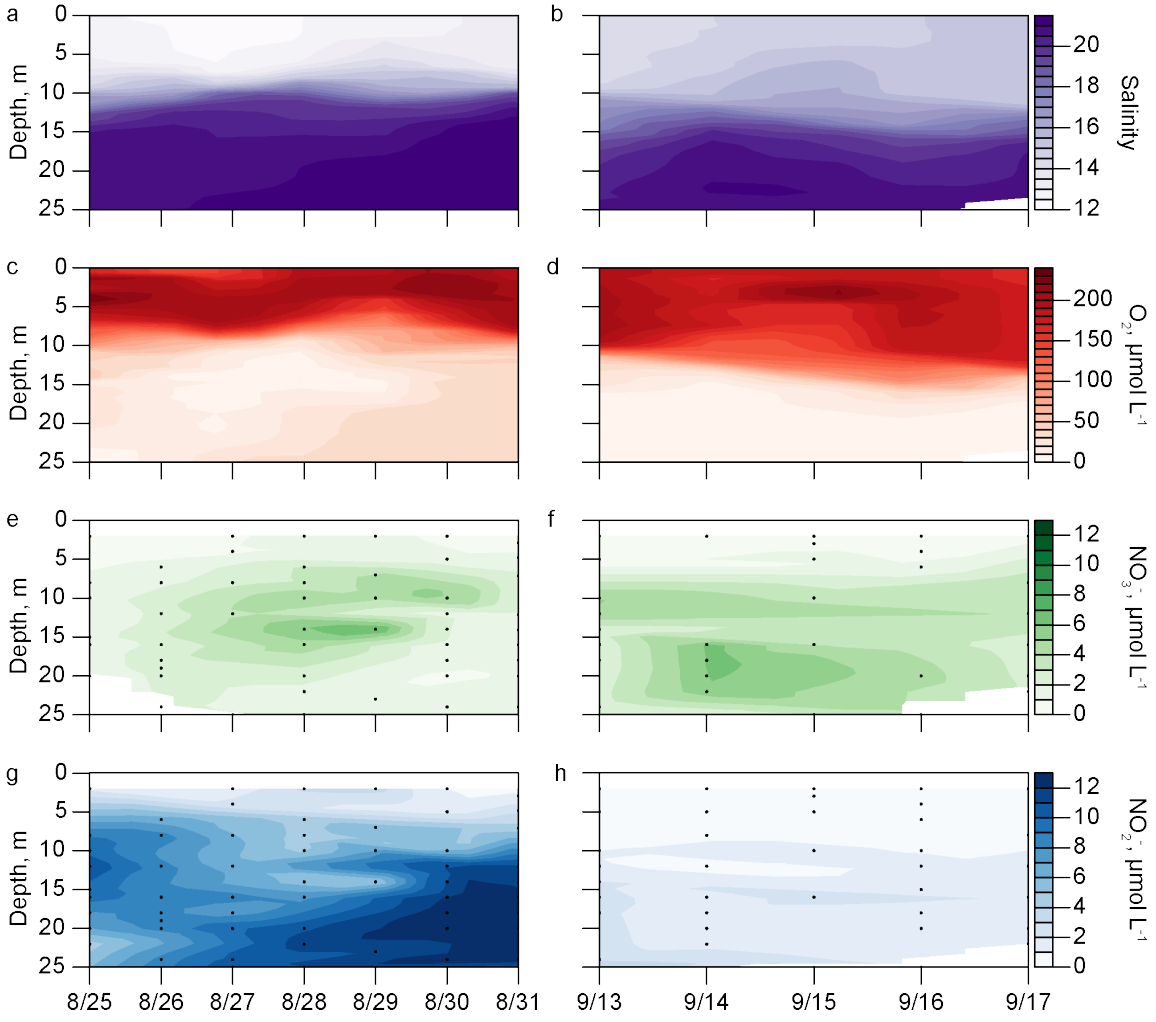

Figure 3. Depth profiles of NH_4^+ concentration (circles) and ammonia oxidation rates (squares) at station M2 on 25 August (closed symbols) and 27 August (open symbols) 2013 (a); 14 September (closed symbols) and 16 September (open symbols) 2013 (b). Error bars indicate the standard deviation between duplicate samples and are not shown in cases where the error bars are smaller than the symbol.

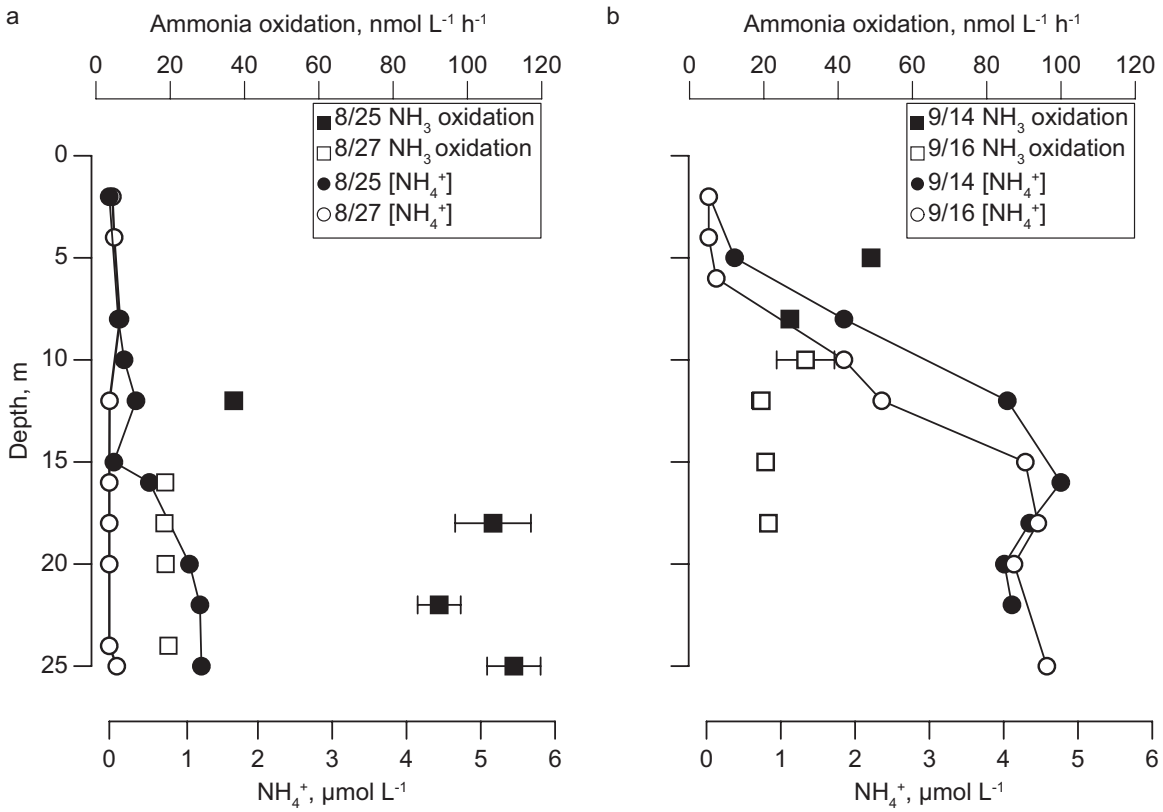

Figure 4. Average nitrous oxide (N_2O) concentrations at station M2 25-31 August 2013 (a) and 13-17 September 2013 (b). Black circles indicate where discrete samples were collected.

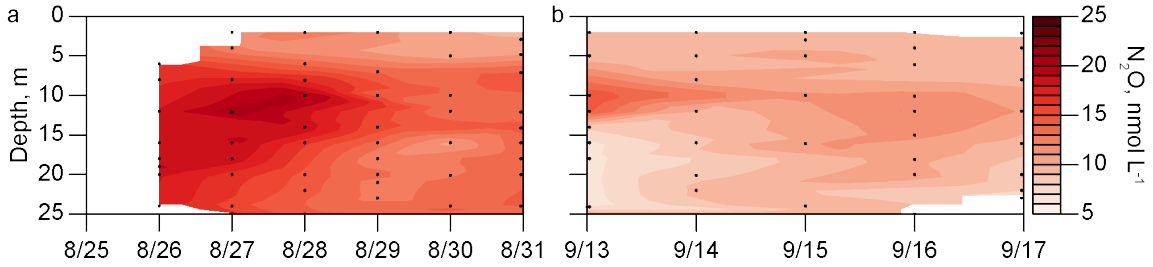

Figure 5. Depth profiles of nitrous oxide (N_2O) (circles), salinity (dashed line), and dissolved oxygen (solid line) at stations N2 (a), M2 (b), and S2 (c) on 13 September 2013. Solid circles indicate oversaturation of N_2O with respect to equilibrium with the atmosphere, and open circles indicate undersaturation. Error bars indicate the standard deviation of duplicate samples and are not shown in cases where the error bars are smaller than the symbol.

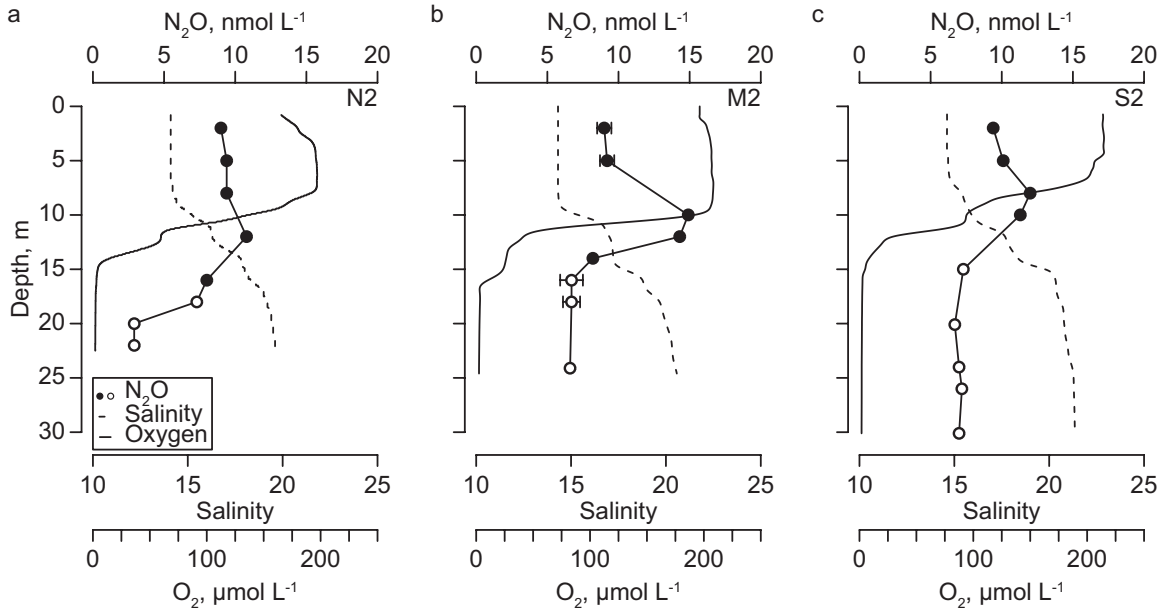

Figure 6. Depth profiles of N_2:Ar at stations S2 (triangles), M2 (squares), and N2 (circles) on 13 (a) and 15 (b) September 2013. Solid symbols indicate N_2:Ar ratios above those expected from air-equilibrated values and open symbols indicate ratios below expected values. Error bars indicate the standard deviation of triplicate samples and are not shown in cases where the error bars are smaller than the symbol.

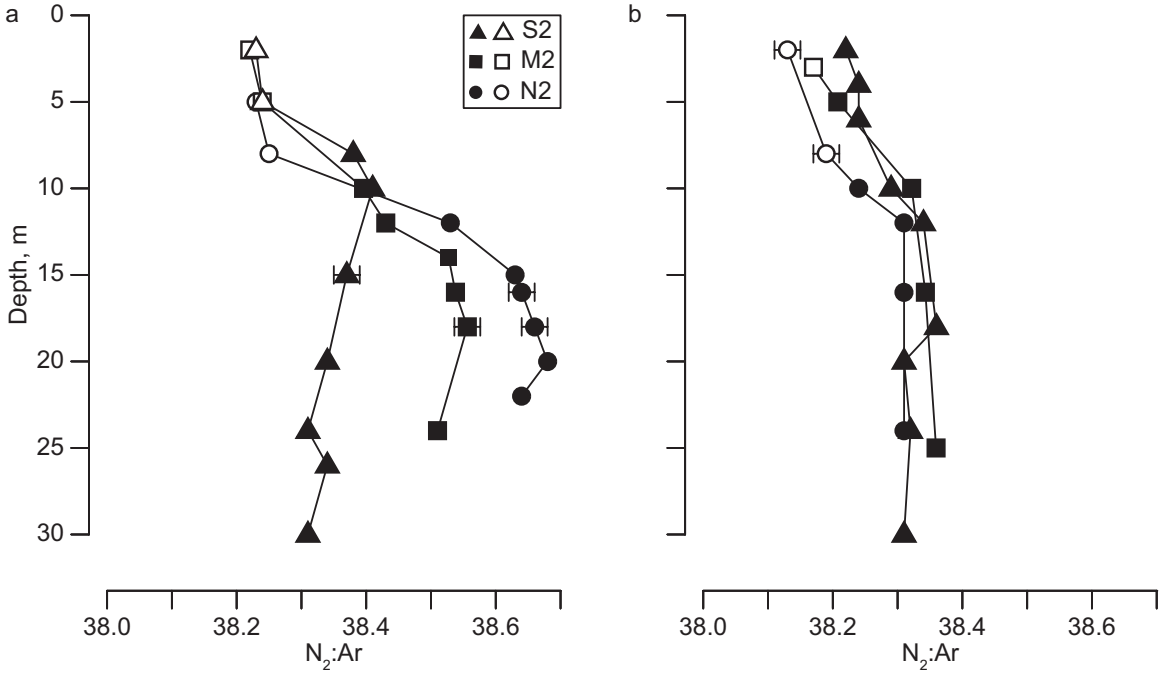

Figure 7. Relationships between ΔN_2O and AOU at station M2 from all depths from August 2013 (a) and September 2013 (b). Least squares regression fits of ΔN_2O versus AOU yielded slopes of 0.02 nM μM^{-1} (SE = 0.004) and 0.2 nM μM^{-1} (SE = 0.04) in August (a) and 0.03 nM μM^{-1} (SE = 0.007) and -0.2 nM μM^{-1} (SE = 0.04) in September (b). Slopes were significantly different according to breakpoint regression analysis and Davies' test (p<0.001). Error bars indicate the standard deviation of duplicate samples.

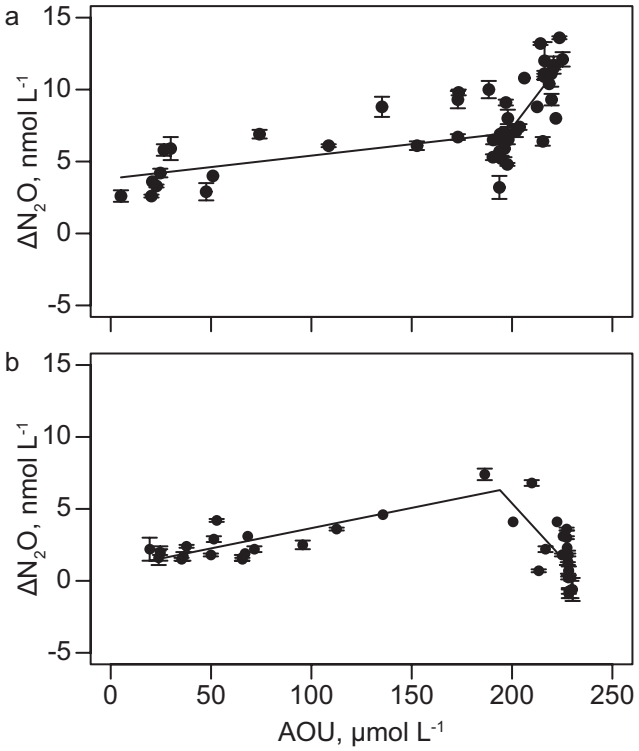

References

Anderson, Laurence A., and Jorge L. Sarmiento. 1994. Redfield ratios of remineralization determined by nutrient data analysis. *Global Biogeochemical Cycles* 8: 65–80. doi:10.1029/93GB03318.

Bange, Hermann W. 2000. It's not a gas. *Nature* 408: 301–302. doi:10.1038/35042656.

Bange, Hermann W., Spyridon Rapsomanikis, and Meinrat O. Andreae. 1996. Nitrous oxide in coastal waters. *Global Biogeochemical Cycles* 10: 197–207. doi:10.1029/95GB03834.

Barnes, J., and R. C. Upstill-Goddard. 2011. N_2O seasonal distributions and air-sea exchange in UK estuaries: Implications for the tropospheric N_2O source from European coastal waters. *Journal of Geophysical Research* 116: G01006. doi:10.1029/2009JG001156.

Battaglia, G., and F. Joos. 2018. Marine N_2O Emissions From Nitrification and Denitrification Constrained by Modern Observations and Projected in Multimillennial Global Warming Simulations. *Global Biogeochemical Cycles* 32: 92–121. doi:10.1002/2017GB005671.

Berounsky, Veronica M., and Scott W. Nixon. 1993. Rates of Nitrification Along an Estuarine Gradient in Narragansett Bay. *Estuaries and Coasts* 16: 718–730. doi:10.2307/1352430.

De Bie, M. J. M., J. J. Middelburg, Mathieu Starink, and H. J. Laanbroek. 2002. Factors controlling nitrous oxide at the microbial community and estuarine scale. *Marine Ecology Progress Series* 240: 1–9. doi:10.3354/meps240001.

Blackmer, A. M., and J. M. Bremner. 1978. Inhibitory effect of nitrate on reduction of N_2O to N_2 by soil microorganisms. *Soil Biology and Biochemistry* 10: 187–191. doi:10.1016/0038-0717(78)90095-0.

Buitenhuis, T. Erik, Parvadha Suntharalingam, and Corinne Le Quéré. 2017. Constraints on global oceanic emissions of N_2O from observations and models. *Biogeosciences Discussions* 1–23. doi:10.5194/bg-2017-193.

Codispoti, Louis A. 2010. Interesting Times for Marine N_2O. *Science* 327: 1339–1340. doi:10.1126/science.1184945.

Dalsgaard, Tage, Frank J. Stewart, Bo Thamdrup, Loreto De Brabandere, Niels Peter Revsbech, Osvaldo Ulloa, Don E. Canfield, and Edward F. DeLong. 2014. Oxygen at Nanomolar Levels Reversibly Suppresses Process Rates and Gene Expression in Anammox and Denitrification in the Oxygen Minimum Zone off Northern Chile. *mBio* 5: e01966-14. doi:10.1128/mBio.01966-14.

Damashek, Julian, Karen L. Casciotti, and Christopher A. Francis. 2016. Variable Nitrification Rates Across Environmental Gradients in Turbid, Nutrient-Rich Estuary Waters of San Francisco Bay. *Estuaries and Coasts* 39: 1050–1071. doi:10.1007/s12237-016-0071-7.

Diaz, R. J., and R. Rosenberg. 2008. Spreading Dead Zones and Consequences for Marine Ecosystems. *Science* 321: 926–929. doi:10.1126/science.1156401.

Dong, Liang F., David B. Nedwell, Graham J. C. Underwood, Daniel C. O. Thornton, and Iman Rusmana. 2002. Nitrous Oxide Formation in the Colne Estuary, England: the Central Role of Nitrite. *Applied and Environmental Microbiology* 68: 1240–1249.

doi:10.1128/AEM.68.3.1240-1249.2002.

Dugdale, R. C., and J. J. Goering. 1967. Uptake of new and regenerated forms of nitrogen in primary productivity. *Limnology and Oceanography* 12: 196–206. doi:10.4319/lo.1967.12.2.0196.

Elkins, James W. 1980. Determination of dissolved nitrous oxide in aquatic systems by gas chromatography using electron-capture detection and multiple phase equilibration. *Analytical Chemistry* 52: 263–267. doi:10.1021/ac50052a011.

Elkins, James W., Steven C. Wofsy, Michael B. McElroy, Charles E. Kolb, and Warren A. Kaplan. 1978. Aquatic sources and sinks for nitrous oxide. *Nature* 275: 602–606. doi:10.1038/275602a0.

Enoksson, Viveka. 1986. Nitrification rates in the baltic sea: comparison of three isotope techniques. *Applied and Environmental Microbiology* 51: 244–50.

Fairall, C. W., E. F. Bradley, J. E. Hare, A. A. Grachev, and J. B. Edson. 2003. Bulk Parameterization of Air–Sea Fluxes: Updates and Verification for the COARE Algorithm. *Journal of Climate* 16: 571–591. doi:10.1175/1520-0442(2003)016<0571:BPOASF>2.0.CO;2.

Fisher, Alexander W., Lawrence P. Sanford, and Malcolm E. Scully. 2018. Wind-Wave Effects on Estuarine Turbulence: a comparison of observations and second-moment closure predictions. *Journal of Physical Oceanography* JPO-D-17-0133.1. doi:10.1175/JPO-D-17-0133.1.

Fisher, Alexander W., Lawrence P. Sanford, Malcolm E. Scully, and Steven E. Suttles. 2017. Surface Wave Effects on the Translation of Wind Stress across the Air–Sea

Interface in a Fetch-Limited, Coastal Embayment. *Journal of Physical Oceanography* 47: 1921–1939. doi:10.1175/JPO-D-16-0146.1.

Foster, Sarah Q., and Robinson W. Fulweiler. 2016. Sediment Nitrous Oxide Fluxes Are Dominated by Uptake in a Temperate Estuary. *Frontiers in Marine Science* 3: 1–13. doi:10.3389/fmars.2016.00040.

Frame, C. H., and K. L. Casciotti. 2010. Biogeochemical controls and isotopic signatures of nitrous oxide production by a marine ammonia-oxidizing bacterium. *Biogeosciences* 7: 2695–2709. doi:10.5194/bg-7-2695-2010.

Gonçalves, Célia, Maria José Brogueira, and Maria Filomena Camões. 2010. Seasonal and tidal influence on the variability of nitrous oxide in the Tagus estuary, Portugal. *Scientia Marina* 74S1: 57–66. doi:10.3989/scimar.2010.74s1057.

Goreau, T. J., W. A. Kaplan, S. C. Wofsy, M. B. McElroy, F. W. Valois, and S. W. Watson. 1980. Production of NO_2^- and N_2O by nitrifying bacteria at reduced concentrations of oxygen. *Applied and Environmental Microbiology* 40: 526–532.

Heiss, Elise M., and Robinson W. Fulweiler. 2016. Coastal water column ammonium and nitrite oxidation are decoupled in summer. *Estuarine, Coastal and Shelf Science* 178: 110–119. doi:10.1016/j.ecss.2016.06.002.

Hietanen, Susanna, Helena Jäntti, Christo Buizert, Klaus Jürgens, Matthias Labrenz, Maren Voss, and Jorma Kuparinen. 2012. Hypoxia and nitrogen processing in the Baltic Sea water column. *Limnology and Oceanography* 57: 325–337. doi:10.4319/lo.2012.57.1.0325.

Ho, David T., Cliff S. Law, Murray J. Smith, Peter Schlosser, Mike Harvey, and Peter Hill.

2006. Measurements of air-sea gas exchange at high wind speeds in the Southern Ocean: Implications for global parameterizations. *Geophysical Research Letters* 33: L16611. doi:10.1029/2006GL026817.

Holmes, Robert M., Alain Aminot, Roger Kérouel, Bethanie A. Hooker, and Bruce J. Peterson. 1999. A simple and precise method for measuring ammonium in marine and freshwater ecosystems. *Canadian Journal of Fisheries and Aquatic Sciences* 56: 1801–1808. doi:10.1139/cjfas-56-10-1801.

Horrigan, S. G., J. P. Montoya, J. L. Nevins, J. J. McCarthy, H. Ducklow, R, Goericke, and T. Malone. 1990. Nitrogenous nutrient transformations in the spring and fall in the Chesapeake Bay. *Estuarine, Coastal and Shelf Science* 30: 369–391. doi:10.1016/0272-7714(90)90004-B.

Intergovernmental Panel on Climate Change, ed. 2013. *Climate Change 2013 - The Physical Science Basis*. Cambridge: Cambridge University Press. doi:10.1017/CBO9781107415324.

Ji, Qixing, Andrew R. Babbin, Amal Jayakumar, Sergey Oleynik, and Bess B. Ward. 2015. Nitrous oxide production by nitrification and denitrification in the Eastern Tropical South Pacific oxygen minimum zone. *Geophysical Research Letters* 42: 10,755-10,764. doi:10.1002/2015GL066853.

Kana, Todd M., Jeffrey C. Cornwell, and Liejun Zhong. 2006. Determination of denitrification in the Chesapeake Bay from measurements of N_2 accumulation in bottom water. *Estuaries and Coasts* 29: 222–231. doi:10.1007/BF02781991.

Kana, Todd M., Christina Darkangelo, M. Duane Hunt, James B. Oldham, George E.

Bennett, and Jeffrey C. Cornwell. 1994. Membrane Inlet Mass Spectrometer for Rapid High-Precision Determination of N_2, O_2, and Ar in Environmental Water Samples. *Analytical Chemistry* 66: 4166–4170. doi:10.1021/ac00095a009.

Kemp, W. M., W. R. Boynton, J. E. Adolf, D. F. Boesch, W. C. Boicourt, G. Brush, J. C. Cornwell, et al. 2005. Eutrophication of Chesapeake Bay: historical trends and ecological interactions. *Marine Ecology Progress Series* 303: 1–29. doi:10.3354/meps303001.

Kim, Dong-Gill, Guillermo Hernandez-Ramirez, and Donna Giltrap. 2013. Linear and nonlinear dependency of direct nitrous oxide emissions on fertilizer nitrogen input: A meta-analysis. *Agriculture, Ecosystems & Environment* 168: 53–65. doi:10.1016/j.agee.2012.02.021.

Kozlowski, Jessica A., Michaela Stieglmeier, Christa Schleper, Martin G. Klotz, and Lisa Y. Stein. 2016. Pathways and key intermediates required for obligate aerobic ammonia-dependent chemolithotrophy in bacteria and Thaumarchaeota. *The ISME Journal* 10: 1836–1845. doi:10.1038/ismej.2016.2.

Lee, Dong Y., Michael S. Owens, Byron C. Crump, and Jeffrey C. Cornwell. 2015. Elevated microbial CO_2 production and fixation in the oxic/anoxic interface of estuarine water columns during seasonal anoxia. *Estuarine, Coastal and Shelf Science* 164: 65–76. doi:10.1016/j.ecss.2015.07.015.

Lin, Hua, Minhan Dai, Shuh-Ji Kao, Lifang Wang, Elliott Roberts, Jin-Yu Terence Yang, Tao Huang, and Biyan He. 2016. Spatiotemporal variability of nitrous oxide in a large eutrophic estuarine system: The Pearl River Estuary, China. *Marine Chemistry* 182:

14–24. doi:10.1016/j.marchem.2016.03.005.

Lipschultz, Fredric, Steven C. Wofsy, and Lewis E. Fox. 1986. Nitrogen metabolism of the eutrophic Delaware River ecosystem1. *Limnology and Oceanography* 31: 701–716. doi:10.4319/lo.1986.31.4.0701.

Löscher, C. R., A. Kock, M. Könneke, J. LaRoche, H. W. Bange, and R. A. Schmitz. 2012. Production of oceanic nitrous oxide by ammonia-oxidizing archaea. *Biogeosciences* 9: 2419–2429. doi:10.5194/bg-9-2419-2012.

Martinez-Rey, J., L. Bopp, M. Gehlen, A. Tagliabue, and N. Gruber. 2015. Projections of oceanic N_2O emissions in the 21st century using the IPSL Earth system model. *Biogeosciences* 12: 4133–4148. doi:10.5194/bg-12-4133-2015.

McCarthy, James J., Warren Kaplan, and John L. Nevins. 1984. Chesapeake Bay nutrient and plankton dynamics. 2. Sources and sinks of nitrite1. *Limnology and Oceanography* 29: 84–98. doi:10.4319/lo.1984.29.1.0084.

McElroy, M. B., J. W. Elkins, S. C. Wofsy, C. E. Kolb, A. P. Durán, and W. A. Kaplan. 1978. Production and release of N_2O from the Potomac Estuary[1]. *Limnology and Oceanography* 23: 1168–1182. doi:10.4319/lo.1978.23.6.1168.

Murphy, Rebecca R., W. Michael Kemp, and William P. Ball. 2011. Long-Term Trends in Chesapeake Bay Seasonal Hypoxia, Stratification, and Nutrient Loading. *Estuaries and Coasts* 34: 1293–1309. doi:10.1007/s12237-011-9413-7.

Naqvi, S. W. A., H. W. Bange, L. Farías, P. M. S. Monteiro, M. I. Scranton, and J. Zhang. 2010. Marine hypoxia/anoxia as a source of CH_4 and N_2O. *Biogeosciences* 7: 2159–2190. doi:10.5194/bg-7-2159-2010.

National Oceanic and Atmospheric Administration. 2018. Halocarbons & Other Atmospheric Trace Species Group (HATS). https://www.esrl.noaa.gov/gmd/hats. Accessed April 2018.

Poth, Mark, and Dennis D. Focht. 1985. ^{15}N Kinetic Analysis of N_2O Production by Nitrosomonas europaea: an Examination of Nitrifier Denitrification. *Applied and environmental microbiology* 49: 1134–41.

Pritchard, D. W. 1952. Salinity distribution and circulation in the Chesapeake Bay estuarine system. *Journal of Marine Research* 11: 106-123.

Punshon, Stephen, and Robert M, Moore. 2004. Nitrous oxide production and consumption in a eutrophic coastal embayment. *Marine Chemistry* 91: 37–51. doi:10.1016/j.marchem.2004.04.003.

Qin, Wei, Kelley A. Meinhardt, James W. Moffett, Allan H. Devol, E. Virginia Armbrust, Anitra E. Ingalls, and David A. Stahl. 2017. Influence of oxygen availability on the activities of ammonia-oxidizing archaea. *Environmental Microbiology Reports* 9: 250–256. doi:10.1111/1758-2229.12525.

Ravishankara, A. R., J. S. Daniel, and R. W. Portmann. 2009. Nitrous Oxide (N_2O): The Dominant Ozone-Depleting Substance Emitted in the 21st Century. *Science* 326: 123–125. doi:10.1126/science.1176985.

Reading, Michael J., Isaac R. Santos, Damien T. Maher, Luke C. Jeffrey, and Douglas R. Tait. 2017. Shifting nitrous oxide source/sink behaviour in a subtropical estuary revealed by automated time series observations. *Estuarine, Coastal and Shelf Science* 194: 66–76. doi:10.1016/j.ecss.2017.05.017.

Rich, Jeremy J., Olivia R. Dale, Bongkeun Song, and Bess B. Ward. 2008. Anaerobic Ammonium Oxidation (Anammox) in Chesapeake Bay Sediments. *Microbial Ecology* 55: 311–320. doi:10.1007/s00248-007-9277-3.

Santoro, Alyson E., C. Buchwald, M. R. McIlvin, and K. L. Casciotti. 2011. Isotopic Signature of N_2O Produced by Marine Ammonia-Oxidizing Archaea. *Science* 333: 1282–1285. doi:10.1126/science.1208239.

Schaefer, Sylvia C., and James T. Hollibaugh. 2017. Temperature Decouples Ammonium and Nitrite Oxidation in Coastal Waters. *Environmental Science & Technology* 51: 3157–3164. doi:10.1021/acs.est.6b03483.

Scully, Malcolm E. 2016. Mixing of dissolved oxygen in Chesapeake Bay driven by the interaction between wind-driven circulation and estuarine bathymetry. *Journal of Geophysical Research: Oceans* 121: 5639–5654. doi:10.1002/2016JC011924.

Scully, Malcolm E., Alexander W. Fisher, Steven E. Suttles, Lawrence P. Sanford, and William C. Boicourt. 2015. Characterization and Modulation of Langmuir Circulation in Chesapeake Bay. *Journal of Physical Oceanography* 45: 2621–2639. doi:10.1175/JPO-D-14-0239.1.

Scully, Malcolm E., John H. Trowbridge, and Alexander W. Fisher. 2016. Observations of the Transfer of Energy and Momentum to the Oceanic Surface Boundary Layer beneath Breaking Waves. *Journal of Physical Oceanography* 46: 1823–1837. doi:10.1175/JPO-D-15-0165.1.

Seitzinger, Sybil P., and Carolien Kroeze. 1998. Global distribution of nitrous oxide production and N inputs in freshwater and coastal marine ecosystems. *Global*

Biogeochemical Cycles 12: 93–113. doi:10.1029/97GB03657.

Sigman, D. M., K. L. Casciotti, M. Andreani, C. Barford, M. Galanter, and J. K. Böhlke. 2001. A Bacterial Method for the Nitrogen Isotopic Analysis of Nitrate in Seawater and Freshwater. *Analytical Chemistry* 73: 4145–4153. doi:10.1021/ac010088e.

Testa, Jeremy M., Yun Li, Younjoo J. Lee, Ming Li, Damian C. Brady, Dominic M. Di Toro, W. Michael Kemp, and James J. Fitzpatrick. 2014. Quantifying the effects of nutrient loading on dissolved O_2 cycling and hypoxia in Chesapeake Bay using a coupled hydrodynamic–biogeochemical model. *Journal of Marine Systems* 139: 139–158. doi:10.1016/j.jmarsys.2014.05.018.

Testa, Jeremy M., Rebecca R. Murphy, Damian C. Brady, and William M. Kemp. 2018. Nutrient- and Climate-Induced Shifts in the Phenology of Linked Biogeochemical Cycles in a Temperate Estuary. *Frontiers in Marine Science* 5: 1–15. doi:10.3389/fmars.2018.00114.

Tiedje, J. M. 1988. Ecology of denitrification and dissimilatory nitrate reduction to ammonium. In *Environmental Microbiology of Anaerobes*, ed. J. B. Zehnder, 179–244. New York: John Wiley and Sons.

Trimmer, Mark, Panagiota-Myrsini Chronopoulou, Susanna T. Maanoja, Robert C. Upstill-Goddard, Vassilis Kitidis, and Kevin J. Purdy. 2016. Nitrous oxide as a function of oxygen and archaeal gene abundance in the North Pacific. *Nature Communications* 7: 13451. doi:10.1038/ncomms13451.

Walter, S., H. W. Bange, U. Breitenbach, and D. W. R. Wallace. 2006. Nitrous oxide in the North Atlantic Ocean. *Biogeosciences* 3: 607–619. doi:10.5194/bg-3-607-2006.

Wanninkhof, Rik. 1992. Relationship Between Wind Speed and Gas Exchange. *Journal of Geophysical Research* 97: 7373–7382. doi:10.1029/92JC00188.

Weiss, R. F., and B. A. Price. 1980. Nitrous oxide solubility in water and seawater. *Marine Chemistry* 8: 347–359. doi:10.1016/0304-4203(80)90024-9.

De Wilde, Hein P. J., and Monique J. M. De Bie. 2000. Nitrous oxide in the Schelde estuary: production by nitrification and emission to the atmosphere. *Marine Chemistry* 69: 203–216. doi:10.1016/S0304-4203(99)00106-1.

Yevenes, Mariela A., Estrella Bello, Sandra Sanhueza-Guevara, and Laura Farías. 2017. Spatial Distribution of Nitrous Oxide (N_2O) in the Reloncaví Estuary–Sound and Adjacent Sea (41°–43° S), Chilean Patagonia. *Estuaries and Coasts* 40: 807–821. doi:10.1007/s12237-016-0184-z.

IV. Chapter III: Nitrification and nitrous oxide dynamics in the Southern California Bight

Sarah M. Laperriere[1,2], Michael Morando[3], Douglas G. Capone[3], Troy Gunderson[3], Jason M. Smith[4], Alyson E. Santoro[2*]

[1]Horn Point Laboratory, University of Maryland Center for Environmental Science, Cambridge, Maryland, USA

[2]Department of Ecology, Evolution, and Marine Biology, University of California, Santa Barbara, California, USA

[3]Marine and Environmental Biology, University of Southern California, Los Angeles, CA, USA

[4]Marine Science Institute, University of California, Santa Barbara, California, USA

Abstract

Nitrogen remineralization plays an important role in controlling the amount of organic carbon available for export to the deep ocean, yet the controls on nitrification in the upper ocean are poorly constrained. This study examines how seasonal cycles in primary production influence rates of nitrification fueled both by ammonia and urea-derived N, and how these processes relate to the production of the greenhouse gas nitrous oxide (N_2O) using monthly rate measurements from the San Pedro Ocean Time-series (SPOT) station. Results indicate that rates of nitrification were highest at the onset of upwelling and were correlated with depth-integrated primary production in the lower euphotic zone. Similar

ammonia and urea-derived N oxidation rates suggest urea is a significant nitrogen source fueling nitrification, particularly below the euphotic zone. Nitrification supplied a large proportion of phytoplankton nitrogen demand in the lower euphotic zone, implying significant regenerated production within the euphotic zone. The Southern California Bight was always a source of N_2O to the atmosphere, which likely was advected into the system from the eastern tropical North Pacific and ventilated to the atmosphere during upwelling. Together, the results suggest the coupling of nitrogen remineralization and primary production in the upper ocean have important implications for the amount of organic carbon available for export out of the surface ocean, but that transport may dominate over local production in explaining local N_2O dynamics.

Introduction

Coastal upwelling regions are the most biologically productive oceanic ecosystems (Chavez and Messié 2009), accounting for a large fraction of carbon export to the deep ocean (Buesseler 1998; Jacob et al. 2011). Primary production, CO_2 fixation by phytoplankton, is fueled by a combination of new (supplied from outside the euphotic zone) and regenerated (remineralized within the euphotic zone) nutrients (Dugdale and Goering 1967). The amount of primary production available for export out of the euphotic zone is controlled by a combination of phytoplankton (Buesseler 1998; Boyd and Newton 1999) and zooplankton (Michaels and Silver 1988; Dagg et al. 2014; Cavan et al. 2015) community composition and rates of organic matter remineralization (Buesseler et al. 2007; Moigne et al. 2016). Nitrification, the oxidation of ammonia (NH_3) to nitrite (NO_2^-) and subsequently to nitrate (NO_3^-) by ammonia- and nitrite-oxidizing microbes, regulates the form of nitrogen

(N) available to fuel primary production (Yool et al. 2007; Santoro et al. 2010), and may influence nitrogen-based estimates of the fraction of carbon available for export to the deep ocean (Eppley and Peterson 1979).

Organic matter export efficiency, the fraction of primary production leaving the euphotic zone, is controlled by the balance between autotrophic and heterotrophic growth (Eppley and Peterson 1979; Falkowski et al. 1998, 2003). In much of the open ocean, export efficiencies are low, suggesting a tight coupling between primary production and organic matter remineralization in the upper ocean (Buesseler 1998; Emerson 2014; Henson et al. 2019). During periods of low export efficiency, when the coupling between organic matter remineralization and primary production is strongest, nitrification in the euphotic zone likely supports a larger fraction of the phytoplankton N demand compared to periods of high export efficiency. High export efficiencies are often observed when productivity and remineralization are decoupled in response to episodic pulses of upwelled nutrients (Buesseler 1998; Lipschultz et al. 2002; Dunne et al. 2007) and at the start of spring phytoplankton blooms (Buesseler 1998; Jacob et al. 2011; Henson et al. 2019). A recent study suggests nitrification supports a larger proportion of phytoplankton N demand as nitrifying microorganisms are released from competition for ammonium (NH_4^+) with phytoplankton moving from the surface to the base of the euphotic zone, and nitrification is largely controlled by ambient NO_3^- concentration (Wan et al. 2018). Despite the important implications for understanding the controls on carbon export, the circumstances under which nitrification contributes to phytoplankton N demand remain unclear.

Similar to vertical patterns of organic matter flux, nitrification rates follow a power law distribution with depth in the ocean. Generally, nitrification rates are low in the upper euphotic zone, increase exponentially with depth towards the base of the euphotic zone, and decrease rapidly thereafter (Ward et al. 1982; Dore and Karl 1996; Santoro et al. 2010, 2013; Smith et al. 2016). This pattern suggests organic matter flux controls rates of nitrification, though few studies have directly examined this relationship with contemporaneous measurements of both processes (Santoro et al. 2017). It is logical to assume organic matter flux regulates nitrification rates, as NH_3, long considered the sole substrate for ammonia-oxidizing microorganisms, is produced during the degradation of organic matter. Recent studies, however, indicate dissolved organic N compounds, such as urea, are additional substrates for ammonia-oxidizing archaea (Qin et al. 2014; Bayer et al. 2016; Carini et al. 2018) and widely used in marine environments (Shi et al. 2011; Alonso-Sáez et al. 2012; Pedneault et al. 2014; Tolar et al. 2016; Santoro et al. 2017; Carini et al. 2018). Together, these findings suggest the availability of dissolved organic N compounds provides an additional regulation on nitrification, however, it is unclear what proportion of nitrification is fueled by urea relative to NH_3, and the contribution of urea-derived N to regenerated production in the upper ocean (Morando and Capone 2018).

Besides controlling N availability for primary production, the activity of ammonia oxidizing microorganisms also contributes to the production of the greenhouse gas nitrous oxide (N_2O) (Poth and Focht 1985; Kool et al. 2011; Santoro et al. 2011; Zhu et al. 2013; Kozlowski et al. 2014, 2016). N_2O yield is elevated under low oxygen (O_2) conditions (Goreau et al. 1980; Löscher et al. 2012; Qin et al. 2017), often observed in highly

productive upwelling systems, a result of elevated rates of organic matter remineralization and sluggish circulation (Diaz and Rosenberg 2008). For this reason, and the ventilation of deep N_2O-enriched water during upwelling (Nevison et al. 1995; Seitzinger et al. 2000; Lueker et al. 2003), these systems are considered 'hotspots' of N_2O emissions to the atmosphere (Nevison et al. 1995, 2004; Bange et al. 1996; Arévalo-Martínez et al. 2015; Farías et al. 2015). N_2O emission estimates from coastal upwelling regions are poorly constrained in global N_2O budgets (Bange et al. 1996; Buitenhuis et al. 2017), partly due to the high temporal and spatial heterogeneity in N_2O production.

The objectives of this study were to investigate the seasonal coupling of primary production and N remineralization in an upwelling system, and to determine how these processes relate to N_2O production. This work was carried out over two seasonal upwelling cycles at the San Pedro Ocean Time-series (SPOT) station in the Southern California Bight (SCB) (Fig. 1). We measured ammonia and urea-derived N oxidation rates using ^{15}N tracer additions in relation to primary production and measured N_2O concentrations using gas chromatography monthly for two years. Typical of many upwelling systems, the SCB exhibits seasonality in primary production (Munro et al. 2013; Haskell et al. 2017), and previous studies report seasonal trends in export efficiency (Munro et al. 2013; Haskell et al. 2017). This seasonality is accompanied by changes in microbial community composition (Brown et al. 2005; Fuhrman et al. 2006; Chow et al. 2013; Kim et al. 2014; Cram et al. 2015; Connell et al. 2017), including elevated abundances of ammonia-oxidizing archaea and clades of abundant heterotrophic bacteria SAR11 and SAR86 during seasonal transitions (Beman et al. 2011b). Unlike previous studies at SPOT which provide rich context, this

study examines the relationship between primary production and nitrification and ties these rates to N_2O dynamics over a two year time series.

Methods

Study site and sample collection

SPOT is located in the Pacific Ocean 16 km off the coast of California, USA in San Pedro Basin between Los Angeles and Catalina Island (Fig. 1). In San Pedro Basin, the upper 250 - 300 m of the water column is characterized by the southward flow of northern sourced waters in the California Current (CC), which branches and turns poleward in the SCB forming the Southern California Countercurrent (SCC) and the Southern California Eddy (SCE) (Hickey 1998). Below 250 m, the California Under Current (CUC), originating in the eastern tropical North Pacific (ETNP), flows poleward with maximum influence from 100 m to deeper than 400 m (Lynn and Simpson 1987, 1990; Bograd et al. 2019). Additionally, water circulation is restricted by a sill in San Pedro Basin at ~740 m.

Samples were collected on monthly cruises between September 2014 and August 2016 aboard the R/V *Yellowfin*. Hydrographic data and water samples were collected during the first year using a 12 x 12 L Niskin bottle rosette equipped with a conductivity, temperature, and density (CTD) instrument package (SBE 9plus, Sea-Bird Electronics, Bellevue, Washington, USA), including dissolved oxygen (SBE 43) and photosynthetically available radiation (PAR, LI-COR, Biospherical Instruments Inc., San Diego, California, USA) sensors. Due to CTD failure, samples during the second year were collected primarily using manually triggered Go-Flo bottles and depths were chosen using a profiling natural

fluorometer (PNF) system as well as secchi disk. The PNF was used in year one in tandem with the original PAR sensor ensuring consistency. Nutrient and incubation samples were collected from separate CTD casts than N_2O samples. Upwelling intensity was obtained from the National Oceanic and Atmospheric Administration's (NOAA's) Pacific Fisheries Environmental Laboratory (https://www.pfeg.noaa.gov/).

Water for nutrient samples was collected directly from the rosette and frozen at -20 °C until analysis, with the exception of NH_4^+ which was always analyzed within 4 h. Samples for urea concentration were collected in triplicate and filtered using 0.22 µm PES Sterivex filters (MilliporeSigma, Burlington, Massachusetts, USA) prior to freezing. Nitrite plus nitrate (NOx^-) and phosphate (PO_4^{3-}) samples were analyzed in triplicate at the Marine Science Institute Analytical Laboratory at the University of California, Santa Barbara. Concentrations of urea and NH_4^+ were measured using previously described methods (Price and Harrison 1987; Goeyens et al. 1998; Holmes et al. 1999), with detection limits of 25 nmol L^{-1} (precision of 10 nmol L^{-1}) and 31 nmol L^{-1} for urea and NH_4^+, respectively. Chlorophyll-a (Chl *a*) was measured in triplicate by filtering whole seawater onto GF/F filters using previously described methods (Holm-Hansen and Riemann 1978).

Samples for particulate organic carbon (POC) and nitrogen (PON) concentration were collected by filtering 2 L whole seawater onto GF/F filters and analyzed using a Perkin Elmer 2400II elemental analyzer. Primary production was also assessed in these samples by quantifying the rates of CO_2 fixation via $H^{13}CO_3$ uptake. Quadruplicate samples were collected and amended to a final concentration of ~25 μmol L^{-1} of $H^{13}CO_3$. A single bottle was filtered immediately after isotope addition to establish a T_0 atom% ^{13}C of the particulate

carbon for each depth. The remaining triplicate replicate bottles were placed in circulating temperature-controlled incubators at ambient temperature and shaded by different mesh size combinations of aluminet screening to simulate ambient light intensity. Incubations were carried out for ~24 h. All samples were filtered onto precombusted (~5 h at 400 ˚C) 25 mm GF/F filters (Whatman, Maidstone, VT, United States), dried, and stored until analysis on an IsoPrime continuous flow isotope ratio mass spectrometer.

Nitrification rates

During the first year, rates of ammonia and urea-derived N oxidation were measured at the 1% surface irradiance depth and 100 m, and during the second year at 75 m, 1% surface irradiance depth, 100 m, and 150 m. All incubations were conducted in triplicate with one unamended control in 500-mL or 1-L polycarbonate bottles. Seawater was collected directly from the rosette and spiked with 30 nmol L^{-1} to 50 nmol L^{-1} $^{15}NH_4^+$ or $^{15}N_2$-urea (≥ 98 atom percent ^{15}N, Cambridge Isotope Laboratories, Tewksbury, MA, United States) and incubated for 24 h at in situ temperature and light. Depths below the euphotic zone were incubated in a temperature-controlled cooler and 1% surface irradiance samples were incubated in temperature-controlled rooftop incubators using natural sunlight mesh to approximate 1% of surface irradiance, as described above. Subsamples were collected at approximately 0, 8, and 24 h, with the exception of incubations from the 1% light level depth, which were subsampled at approximately 0, 8, 16, and 24 h intervals, and 0.2 μm syringe filtered into 60-mL HDPE bottles and stored at -20 °C until analysis. In addition, in March 2015, a kinetics experiment was conducted at the 1% surface irradiance depth, where

triplicate incubations were spiked with 15, 30, 75, 125, and 250 nmol L^{-1} $^{15}NH_4^+$ or $^{15}N_2$-urea.

From the subsamples, $\delta^{15}N_{NOx-}$ was measured from 10 nmol or 20 nmol of NO_x using the denitrifier method (Sigman et al. 2001; McIlvin and Casciotti 2011) using an isotope ratio mass spectrometer at the Marine Science Institute Analytical Laboratory at the University of California, Santa Barbara. $\delta^{15}N_{NOx-}$ values were calibrated using USGS32, USGS34, and USGS35 isotope references. Rates of ammonia and urea-derived N oxidation were calculated using previously described methods (Dugdale and Goering 1967; Damashek et al. 2016) using linear least squares fitting to determine the rate of NO_x^- production. Here, all urea-derived N oxidation rates are reported in terms of urea-derived N and the method cannot distinguish if the rate of urea-derived N oxidation is from urea degradation and subsequent N oxidation by the same or different organisms.

Nitrous oxide and atmospheric fluxes

Dissolved N_2O samples were collected directly from the rosette into 160-mL serum vials, single samples were collected with the exception of surface samples where five replicates were collected. Vials were filled using silicon tubing by placing the tubing at the bottom of the vials and allowing water to overflow by approximately 5 volumes. Samples were preserved with 200 μL of a saturated mercuric chloride solution and sealed with gray butyl septa (Thermo Scientific, Waltham, MA, United States, #200-932) and aluminum crimp tops. Samples were stored at room temperature until analysis.

N_2O concentrations were measured using a headspace equilibration method modified from Laperriere et al. (2019). A 30-mL ultra-high purity N_2 headspace was introduced to each sample using a 30-mL syringe with a second empty 30-mL syringe inserted into the septum to collect displaced sample water. Each headspace was overpressured with 10 mL of ultra high purity N_2 to minimize atmospheric contamination. Samples were analyzed on a SRI Greenhouse Gas Monitoring Gas Chromatograph (GC) equipped with an electron capture detector (ECD), dual HayeSep D packed columns, and a 1-mL sample loop (SRI Instruments, Torrance, California, USA). Ultra-high purity N_2 gas was used as the carrier with the sample loop kept at 60 °C and the column oven kept at 100 °C. Two certified standards, 0.1 ppm and 1 ppm N_2O, from Matheson Tri-Gas were used for daily calibration. N_2O concentrations from the original seawater sample were calculated according to Walter et al. (2006).

Nitrous oxide air-sea fluxes were calculated using gas transfer velocities calculated after Ho et al. (2006) using 16-day prior 10 m wind speeds and were corrected for in situ temperature and salinity after (Wanninkhof 1992). Wind data were obtained from the NOAA's National Data Buoy Center (NDBC) from Station 46025 Santa Monica Basin (33.761 °N 119.049 °W). Wind speed was converted to the wind speed at 10 m using bulk transfer functions (COARE 3.0; Fairall et al. 2003). Equilibrium N_2O concentrations were calculated using the Weiss and Price (1980) solubility equations with an atmospheric mole fraction of 328 ppb (www.esrl.noaa.gov/gmd/hats/).

Data deposition

Nitrous oxide concentrations, nutrient concentrations, and ammonia and urea-derived N oxidation rate data have been deposited in the United States National Science Foundation Biological and Chemical Oceanography Data Management Office repository (bco-dmo.org) in association with project number 516643.

Results

Hydrography and nutrients

Sampling at SPOT spanned two annual upwelling cycles, with upwelling initiating in February and peaking in early summer in both years (Fig. 2a; Table 1). Upwelling was evident in sea surface temperatures (SSTs), which varied between 16.3 and 23.1 °C (Table 1) and negatively correlated with surface [Chl *a*] (Pearson, r = -0.53, $p < 0.01$, n = 21). Depth-integrated primary production to the 1% surface irradiance depth varied between 1.7 and 27.6 mmol C m^{-2} d^{-1} and the highest values were observed just prior to the onset of upwelling (Table 1). Several shallow (18 to 23 m) [Chl *a*] maxima were observed reaching 2.6 ± 0.9 μg L^{-1} (mean ± standard deviation) near the onset of upwelling (Fig. 2b).

The nutricline shoaled during upwelling periods, seen in the vertical distribution of NO_3^- and PO_4^{3-} (Fig. 2c,d). [PON] and [POC] varied between 0.1 ± 0.03 μmol L^{-1} and 1.5 ± 0.07 μmol L^{-1} and 1.2 ± 0.08 μmol L^{-1} and 14.3 ± 3.5 μmol L^{-1}, respectively (Fig. 3a,b). PON and POC maxima occurred during periods of high [Chl *a*] and were lowest in fall. Ammonium concentration displayed typical vertical distribution patterns, with maxima (0.3 to 0.5 μmol L^{-1}) occurring at the base of the euphotic zone (Fig. 3c). Urea concentrations

varied between 0.04 and 0.7 ± 0.3 μmol L^{-1}, with no observable patterns in depth or time (Fig. 3d).

Nitrification rates

Ammonia oxidation rates ranged from 0.02 ± 0.01 to 35.9 ± 4.2 nmol N L^{-1} d^{-1} and urea-derived N oxidation rates ranged from 0.01 ± 0.01 to 25.3 ± 4.2 nmol N L^{-1} d^{-1} (Fig. 4). There was no difference in either ammonia or urea-derived N oxidation with depth (ANOVA, $p = 0.5$ and $p = 0.7$, respectively), but ammonia and urea-derived N oxidation rates were correlated with each other (Pearson, $r = 0.55$, $p < 0.001$, $n = 56$). The fraction of ammonia oxidation to total N oxidation (NH_4^+ + urea-derived N oxidation) was greater at the 1% light level depth (0.82 ± 0.11) compared to 100 m (0.49 ± 0.23; paired t-test, $p < 0.001$), and the fraction of urea-derived N oxidation was greater at 100 m (0.51 ± 0.23) than at the 1% light level depth (0.18 ± 0.11; paired t-test, $p < 0.001$). Ammonia and urea-derived N oxidation rates at the 1% surface irradiance depth did not respond to increasing additions of ^{15}N-labeled substrate from 15 to 250 nmol L^{-1} (Fig. 5). Rates of urea-derived N oxidation most strongly correlated with [O_2] (Pearson, $r = -0.56$, $p < 0.01$, $n = 23$) and [urea] (Pearson, $r = 0.42$, $p < 0.001$, $n = 56$) (Table 2), while ammonia oxidation rates did not correlate with any of the measured environmental variables. Depth-integrated ammonia and urea-derived N oxidation to 100 m correlated with depth-integrated primary production to the same depth (Pearson, $r = 0.52$, $p = 0.01$, $n = 20$ and $r = 0.46$, $p = 0.03$, $n = 20$, respectively).

The proportion of phytoplankton N demand supported by ammonia and urea-derived N oxidation in the lower euphotic zone was calculated using depth-integrated oxidation rates

and primary production between the 10% and the 1% light level depths (Table 1) and a C:N of 6.6 (Redfield 1958). Ammonia and urea-derived N oxidation supplied 0 - 47% and 0 - 26% of N demand (Fig. 6), respectively, with values reaching up to 47% for ammonia oxidation and 26% for urea-derived N oxidation in October 2015. The fraction of N supplied by ammonia and urea-derived N oxidation correlated with the 1% light level depth (Pearson, $r = 0.71$, $p < 0.001$, $n = 18$ and $r = 0.76$, $p < 0.001$, $n = 15$, respectively).

Nitrous oxide concentrations

Nitrous oxide concentrations varied from 9.4 to 67.2 nmol L^{-1} (93 - 553% saturated; Fig. 7). Generally, N_2O concentrations were low at the surface, increased to maxima around 500 - 750 m, and decreased again towards the seafloor. Maximum N_2O concentrations coincided with O_2 concentrations between ~8 and 30 μmol O_2 L^{-1} (Fig. 8a) and were associated with a low temperature (< 10 °C) and high salinity (> 34) water mass (Fig. 8b). Surface waters were always oversaturated with N_2O (111 to 215%) and atmospheric fluxes ranged between 1.8 ± 0.9 and 9.2 ± 5.3 μmol m^{-2} d^{-1}.

Discussion

The aim of this study was to understand how seasonal patterns in primary production influence rates of nitrification, and how these processes relate to N_2O dynamics in an upwelling system. Nitrification rates measured here (Fig. 4) are consistent with rates previously measured in the SCB (Beman et al. 2011a), elsewhere in the CC system (Ward et al. 1982; Ward 2005; Santoro et al. 2010; Smith et al. 2014, 2016), and are comparable to

rates measured in the open and coastal ocean (Clark et al. 2008; Beman et al. 2012; Newell et al. 2013; Santoro et al. 2017; Tolar et al. 2017; Liu et al. 2018; Damashek et al. 2019). Ammonia and urea-derived N oxidation rates were highest at 75 m, which was always deeper than the 1% surface irradiance depth, and rates decreased with depth thereafter (Fig. 4). Similar to previous observations, nitrification followed a power law distribution with maximum rates at the base of the euphotic zone (Newell et al. 2011; Smith et al. 2016; Santoro et al. 2017).

Depth-integrated nitrification correlated with depth-integrated primary production (Table 1), demonstrating a relationship between biomass and N remineralization in the upper ocean. This is consistent with previous studies observing positive correlations between nitrification and primary production (Beman et al. 2012; Shiozaki et al. 2016) and depth-integrated Chl *a* (Santoro et al. 2017). It is logical to assume nitrification is controlled by the supply of NH_4^+ from the degradation of organic matter as they are tightly coupled, but nitrification rates did not increase with additions of NH_4^+ or urea in this study (Fig. 5). A previous study reports a similar lack of response to NH_4^+ additions (Shiozaki et al. 2016), while other investigations of ammonia oxidation kinetics report increased rates of ammonia oxidation in response to added NH_4^+ (Newell et al. 2013; Horak et al. 2013). These differences in kinetic responses could be explained by different ammonia oxidizing populations, or potentially by differences in rates of NH_4^+ production at different sites, which would have the effect of diluting the added $^{15}NH_4^+$ to differing degrees. Our data suggest the standing stock of ammonia oxidizers at SPOT was set by NH_4^+ supply, but that they were not NH_4^+ limited. None of the environmental variables measured in this study

explained patterns in nitrification (Table 2). Together, our data suggest nitrification may be controlled by the availability of micronutrients (Amin et al. 2013; Shiozaki et al. 2016) or by top-down factors such as grazing or viral lysis (Zakem et al. 2018).

Maximum nitrification rates in the upper mesopelagic (Fig. 4) coincided with the onset of upwelling, when carbon export efficiencies are expected to be highest in response to pulses of upwelled nutrients (Buesseler 1998; Jacob et al. 2011; Haskell et al. 2017). Previously at SPOT, the lowest export efficiencies were observed in fall, with efficiencies increasing through winter and peaking in late February/early March at the onset of upwelling (Haskell et al. 2017). Consistent with these findings, in this study, nitrification supplied the highest proportion of phytoplankton N demand in fall (Fig. 6), suggesting regenerated production is of greater importance during weak upwelling when new production is expected to be at a minimum. Primary production off southern California is controlled by NO_3^- input into the euphotic zone and is inversely related to the depth of the nitracline (Eppley et al. 1979). Upwelling shoals the nitracline and increases the fraction of new production to total production (new and regenerated production), conversely, during weak upwelling, the nitracline deepens and the fraction of regenerated production increases (Eppley et al. 1979). In agreement, the fraction of phytoplankton N demand supplied by nitrification in this study correlated with the 1% surface irradiance depth, suggesting regenerated N is a more significant source of N fueling primary production when the depth of the euphotic zone increases.

In contrast, in 2016, the proportion of N supplied by nitrification increased through the beginning of spring upwelling (Fig. 6). Data from 2016 are consistent with the

hypothesis proposed by Haskell et al. (2017), who suggested the proportion of regenerated N relative to new N fueling primary production increases through spring as respiration in the euphotic zone increases and export efficiencies decrease. At the onset of upwelling, autotrophic and heterotrophic growth are likely not in equilibrium, and as upwelling precedes, growth likely approaches equilibrium, and regenerated production increases and export efficiencies decrease. The lack of congruity from year to year could be attributed to a warm SST anomaly (known as the Blob), which persisted from early 2014 through 2015 (Zaba and Rudnick 2016). This period was associated with weakened advection of colder waters from north to south, and was marked by increased stratification and lower Chl *a* concentrations (Cavole et al. 2016; Zaba and Rudnick 2016). Our data suggest nitrification in the euphotic zone supports a significant proportion of primary production, especially when new production and export efficiencies are expected to be low.

The importance of organic N substrates, particularly urea, in fueling nitrification is increasingly acknowledged (Santoro et al. 2017; Tolar et al. 2017; Damashek et al. 2019). There is evidence that in addition to indirect urea utilization, the abiotic and biotic breakdown of urea to NH_3, ammonia-oxidizing archaea also directly utilize urea (Kitzinger et al. 2019), however, little is known about the differential use of N substrates in nitrification. Our data suggest the proportion of ammonia and urea-derived N oxidation to total nitrification varies with depth, implying differential substrate utilization during nitrification in and below the euphotic zone. At the 1% irradiance depth, NH_4^+ fueled a larger fraction of total N oxidation, whereas at 100 m, there was no significant difference. These results indicate NH_4^+ may contribute more to primary production in the euphotic

zone, while urea-derived NO_3^- likely only impacts primary production once vertically advected into the euphotic zone during upwelling. It has been hypothesized that the oxidation of urea-derived N is of greater importance in oligotrophic waters (Damashek et al. 2019), suggesting urea utilization may be more significant under low substrate concentrations. Rates of urea-derived N oxidation were similar to ammonia oxidation and may be an important substrate fueling nitrification in the mesopelagic.

Nitrification in the upper ocean is considered a significant source of N_2O to the atmosphere (Dore et al. 1998; Zamora and Oschlies 2014). Here, maximum N_2O concentrations were observed well below the euphotic zone (Fig. 7), at depths where nitrification is expected to be minimal. Depth profiles of N_2O are consistent with previous observations in the central CC (Santoro et al. 2010) and Santa Monica Basin (Lueker 2004; Townsend-Small et al. 2014), and the atmospheric fluxes calculated here (1.8 to 9.2 μmol m^{-2} d^{-1}; Table 1) are similar to those previously observed in the CC system (1.8 to 6.9 μmol m^{-2} d^{-1} ; Lueker 2004; Nevison et al. 2004; Townsend-Small et al. 2014). N_2O fluxes from San Pedro Basin were slightly higher than fluxes measured in the oligotrophic Pacific (0.3 to 5.2 μmol m^{-2} d^{-1}; Dore et al. 1998; Popp et al. 2002) and lower than fluxes from other upwelling regions, including the Peruvian-Chilean upwelling system (27 to 260 μmol m^{-2} d^{-1}; Farías et al. 2009, 2015; Arévalo-Martínez et al. 2015) and the Arabian Sea (40 to 268 μmol m^{-2} d^{-1}; Naqvi et al. 2000).

Emission of subsurface-produced N_2O to the atmosphere requires a mechanism for water to mix towards the surface; upwelling provides a mechanism where N_2O produced below the mixed layer is ventilated to the atmosphere (Lueker et al. 2003; Nevison et al.

2004, 2011; Wittke et al. 2010). In San Pedro Basin, sea-air N_2O fluxes (Table 1) did not correlate with upwelling intensity, however, surface N_2O concentrations negatively correlated with SST (Pearson, r = -0.51, p = 0.01, n = 21), suggesting N_2O is transported into the mixed layer during upwelling. This is in agreement with a previous study, which reported increased surface N_2O oversaturation with decreasing SSTs in response to upwelling (Nevison et al. 2004). Here, piston velocity did not correlate with upwelling intensity or SST, as calculations only consider wind magnitude and not direction. This likely explains why N_2O fluxes did not directly correlate with upwelling intensity. Previous studies report a link between elevated N_2O production and primary production (Wittke et al. 2010; Nevison et al. 2011; Arévalo-Martínez et al. 2015; Farías et al. 2015), but this was not the case in San Pedro Basin where atmospheric fluxes did not correlate with primary production or Chl *a* concentration. The monthly sampling frequency may have missed higher frequency temporal fluctuations in primary production and N_2O production likely lags pulses in primary production. Alternatively, local N_2O production at SPOT is minimal and much of the N_2O is advected into San Pedro Basin from outside the system.

The main source of N_2O is likely advection into the system from the oxygen deficient zone in the ETNP, evidenced by a low O_2, low temperature, and high salinity water mass enriched in N_2O (Fig. 8). The transition between northern sourced surface waters (CC, SCC, and SCE) and southern sourced bottom waters (CUC) in the SCB typically occurs along the σ_θ = 26.5 kg m^{-3} isopycnal (Lynn and Simpson 1987; Bograd et al. 2019), consistent with the mixing of low- and high-N_2O containing water masses in this study (Fig. 8b). Maximum N_2O concentrations were observed at 500 m, slightly deeper than waters

predicted to have maximum CUC influence (Bograd et al. 2019). Though, the lack of sampling resolution in this study between 250 and 500 m makes it possible that the true N_2O maximum of the CUC was missed. Previous studies demonstrate the transport of denitrification influenced water from the ETNP through the CC system (Altabet et al. 1999; Castro et al. 2001; Sigman et al. 2005; Townsend-Small et al. 2014), with $\delta^{15}NO_3^-$ values showing maximum NO_3^- deficits in the CUC between 400 - 1000 m (Castro et al. 2001). Local water column and sediment N_2O production in San Pedro Basin via denitrification is likely minimal, as O_2 concentrations at 500 m were too high (~12 to 32 μM), and previously measured benthic N_2O fluxes (-0.2 and -1.2 μmol m^{-2} d^{-1}) in the SCB indicate sediments are a sink for N_2O (Townsend-Small et al. 2014). Denitrification in the ETNP is the likely source of the midwater column N_2O maxima observed in this study, as described in Santa Monica Basin (Townsend-Small et al. 2014).

A decoupling between primary production and organic matter remineralization in the upper ocean is thought to drive high organic carbon export efficiencies (Buesseler 1998; Henson et al. 2019). Our data lend support to this hypothesis, showing nitrification supplied a lower proportion of phytoplankton N demand at the initiation of upwelling, when primary production and organic matter remineralization are most likely to decouple in response to nutrient pulses. When primary production and organic matter remineralization are likely coupled, as upwelling progresses and during periods of weak upwelling, nitrification supplied a higher proportion of phytoplankton N demand. The relationship between primary production, nitrification, and N_2O production is less clear, however it is apparent physical forcing controls N_2O dynamics in San Pedro Basin. The bulk of N_2O emitted to the

atmosphere is likely advected into the system from the ETNP and ventilated to the surface during upwelling. With the predicted expansion and shoaling of oxygen deficient zones (Naqvi et al. 2010; Codispoti 2010), the CC system may become an increasing source of N_2O to the atmosphere. To increase our understanding of carbon export to the deep ocean and its impact on N_2O production, simultaneous measurements of primary production, export efficiency, and nitrification are needed.

Acknowledgements

We thank numerous contributors including Yubin Raut, Sebastian Krause, Thomas Lankiewicz, Briette Shea, Matthew Rawls, and Andrew McCarthy. Matthew Kellom is thanked for assistance editing the manuscript. We are thankful to the USC Wrigley Institute for Environmental Studies for supporting the cruises and the captain and crew of the *R/V* Yellowfin. This work was supported by the United States National Science Foundation award OCE-1437310. S.M.L was supported by a Maryland Sea Grant Research Fellowship and the Interdepartmental Graduate Program in Marine Science at the University of California, Santa Barbara. The authors declare no conflict of interest.

Figures and tables

Table 1

Summary of hydrographic parameters at San Pedro Ocean Time-series (SPOT) between September 2014 and August 2016. Depth-integrated values are integrated between the 10% and 1% surface irradiance depths.

Date	Upwelling intensity (m^3 s^{-1} 100 m coastline^{-1})	SST (°C)	Surface [Chl *a*] (μg L^{-1})	Depth at 1% surface irradiance (m)	[NO_x^-] at 1% surface irradiance (μmol L^{-1})	Depth-integrated [chl *a*] (mg m^{-2})	Depth-integrated primary production (mmol m^{-2} d^{-1})	Depth-integrated ammonia oxidation rate (μmol m^{-2} d^{-1})	Depth-integrated urea-derived N oxidation rate (μmol m^{-2} d^{-1})	N_2O atmospheric flux (μmol m^{-2} d^{-1})
9/10/2014	143	22.9	0.2	56	4.2	19.6	8.0	0.3	0.0	5.1 ± 2.2
10/1/2014	51	21.5	0.3	62	5.8	33.1	4.0	24.8		6.5 ± 3.4
11/12/2014	20	19.7	0.5	56	2.8	44.0	6.7	93.9	23.2	5.1 ± 3.1
12/8/2014	2	18.6	0.4	53	3.6	29.6	4.7	140.6	45.0	2.6 ± 1.6
1/15/2015	-1	16.8	0.4	56	0.7	56.4	5.0			3.2 ± 2.1
2/18/2015	39	16.4	1.2	36	5.7	47.7	22.2	236.3	102.4	2.4 ± 1.2
3/12/2015	72	17.2	0.4	51	3.8	29.1	4.0	19.6	11.3	2.2 ± 1.2
4/22/2015	168	16.9	0.3	30	0.9	13.4	8.1			9.1 ± 5.3
5/20/2015	212	17.6	0.3	45	11.8	25.7	13.2	47.3	20.3	6.4 ± 3.2
6/17/2015	269	18.9	0.3	35	7.4	12.0	7.0	12.0	0.8	1.8 ± 1.0

Table 1. Continued

Date	Upwelling intensity ($m^3\ s^{-1}$ 100 m coastline^{-1})	SST (°C)	Surface [Chl *a*] ($\mu g\ L^{-1}$)	Depth at 1% surface irradiance (m)	[NO_x^-] at 1% surface irradiance ($\mu mol\ L^{-1}$)	Depth-integrated [chl *a*] ($mg\ m^{-2}$)	Depth-integrated primary production ($mmol\ m^{-2}\ d^{-1}$)	Depth-integrated ammonia oxidation rate ($\mu mol\ m^{-2}\ d^{-1}$)	Depth-integrated urea-derived N oxidation rate ($\mu mol\ m^{-2}\ d^{-1}$)	N_2O atmospheric flux ($\mu mol\ m^{-2}\ d^{-1}$)
7/14/2015	178	20.2	0.2	47	4.0	24.8	3.7	7.6		2.5 ± 1.2
8/5/2015	229	22.0	0.4	52	1.5	36.4	6.5	6.4	2.1	1.8 ± 0.8
9/9/2015	95	22.4		45	1.0	45.2	9.2	1.4		1.9 ± 1.0
10/20/2015	74	23.1	0.3	92	8.8	56.4	1.7	117.2	65.9	2.4 ± 1.1
11/18/2015	39	18.9	0.4							3.4 ± 2.2
12/16/2015	76	17.5	1.3	33	0.7	28.5				2.6 ± 1.7
1/16/2016	13	16.3	1.1	31	0.4	48.6	10.9	3.2	0.8	5.6 ± 3.5
2/10/2016	38	16.3	0.3	45	1.7	24.8	27.6	143.9	9.5	2.4 ± 2.4
3/16/2016	163	17.5	1.0	34	3.7	24.4	17.8	201.6	20.7	
4/13/2016	165	17.8	0.5	41	14.5	37.5	3.7	65.5	15.3	5.2 ± 4.2
5/18/2016	218	19.2	0.4	49	15.4	30.6	18.9	156.3	21.3	3.4 ± 1.6
6/15/2016	248	17.4	0.6	53	19.3	71.8	10.0	130.2	43.4	2.9 ± 1.5
7/12/2016	271	21.8	0.3	54	12.1	35.5	9.2	40.3	5.2	1.8 ± 0.9
8/10/2016	253	22.1	0.2	68	17.0	27.1	15.8	273.0	56.0	2.2 ± 0.97

Upwelling intensity was obtained from the National Oceanic and Atmospheric Administration's Pacific Fisheries Environmental Laboratory.
SST, sea surface temperature; Chl *a*, chlorophyll *a*; NOx, nitrate + nitrite.

Table 2

Pearson correlations (*r*) between ammonia and urea-derived N oxidation rates and environmental variables. Bold values indicate a *p* < 0.05.

	NH_4^+ oxidation		Urea-derived N oxidation	
	r	*p*	*r*	*p*
Oxygen	0.00	1.00	**-0.56**	**0.00**
Urea	-0.18	0.18	**0.42**	**0.00**
PON	-0.16	0.33	**-0.38**	**0.02**
POC	-0.16	0.31	**-0.36**	**0.02**
NH_4^+	-0.21	0.11	**-0.28**	**0.03**
Temperature	0.25	0.11	-0.21	0.19
Pressure	-0.25	0.05	0.05	0.69
Salinity	-0.21	0.22	0.10	0.58
PO_4^{3-}	-0.10	0.44	0.12	0.38
Chl *a*	0.04	0.86	0.13	0.59
NO_3^-	-0.07	0.61	0.19	0.15
σ_θ	-0.28	0.09	0.19	0.26

Figure 1. Map of the location of San Pedro Ocean Time-series (SPOT) with an inset of California, USA. Lines indicate bathymetry, with 50 m, 200 m, 500 m, and 1000 m contours.

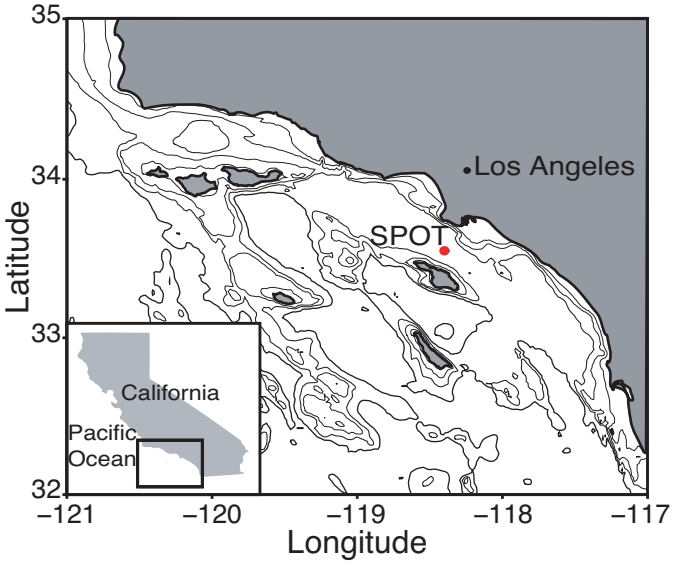

Figure 2. Upwelling intensity (a), chlorophyll *a* concentrations (b), nitrate + nitrite (c), and phosphate (d) at SPOT between September 2014 and August 2016. Upwelling intensity was obtained from the National Oceanic and Atmospheric Administration's Pacific Fisheries Environmental Laboratory.

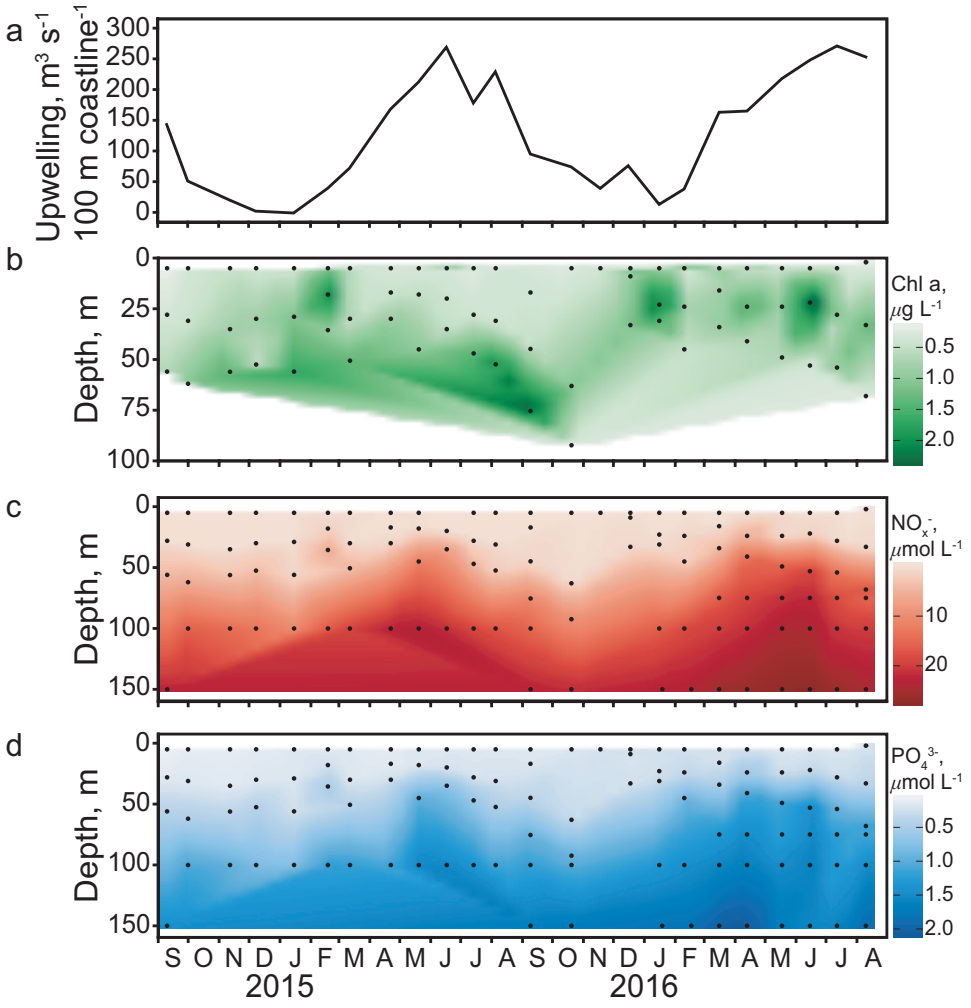

Figure 3. Time series of particulate organic nitrogen (a), particulate organic carbon (b), ammonium (c), and urea (d) at SPOT between September 2014 and August 2016. Black circles indicate where discrete samples were collected.

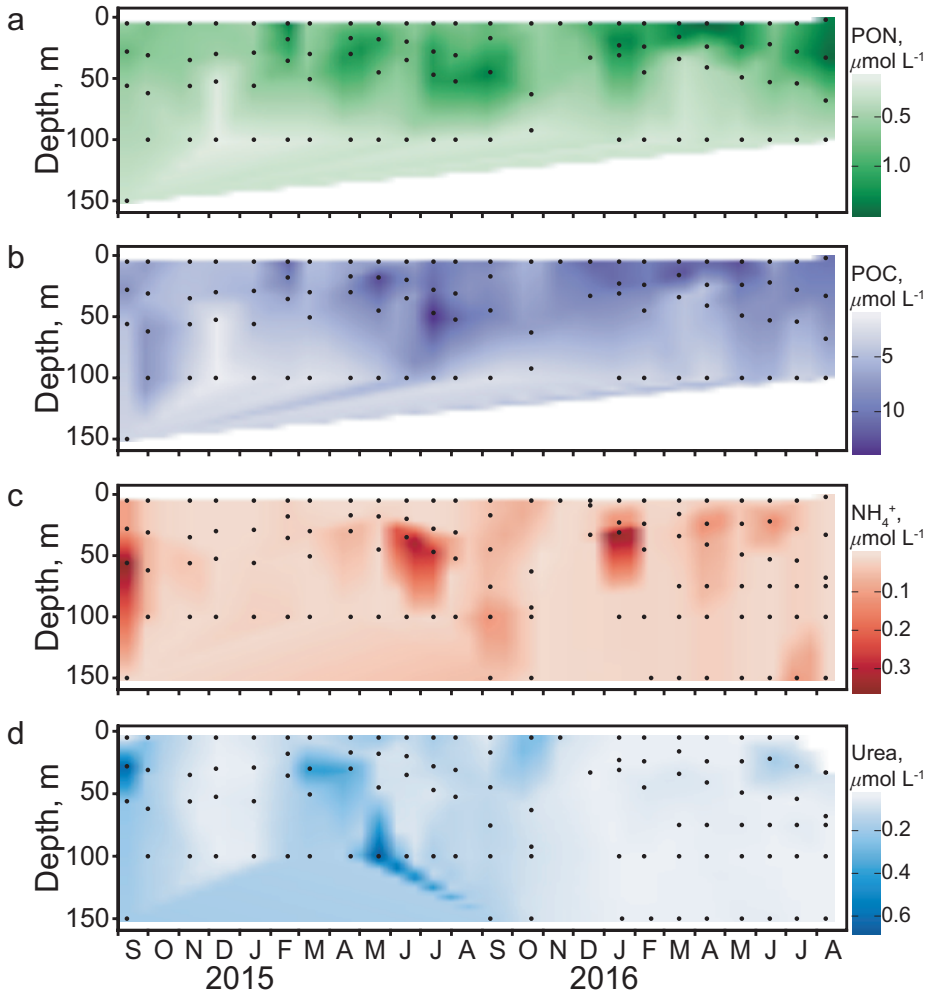

Figure 4. Ammonia (red) and urea-derived N (black) oxidation rates at the 1% surface irradiance depth (a) 75 m (b), 100 m (c), 150 (d) at SPOT between September 2014 and August 2016. Error bars indicate the standard deviation of triplicate samples.

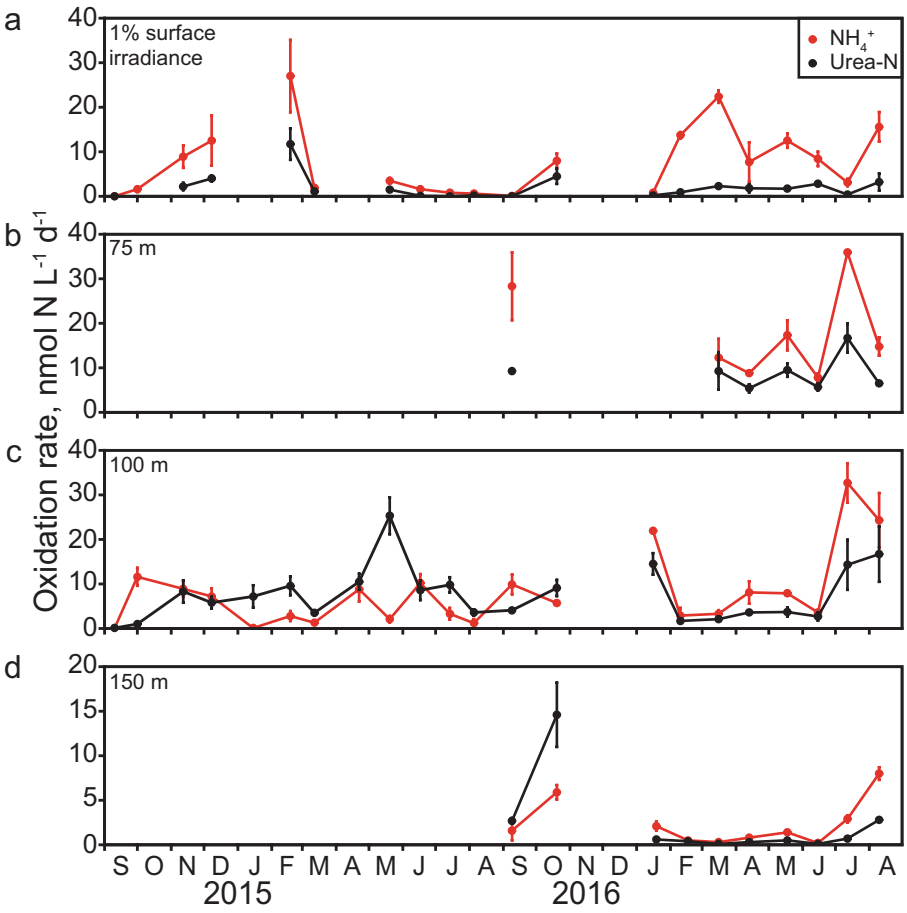

Figure 5. Ammonia (red) and urea-derived N (black) oxidation rates at the 1% surface irradiance depth at SPOT in March 2015. The horizontal axis represents substrate concentration (^{15}N addition + ambient concentration).

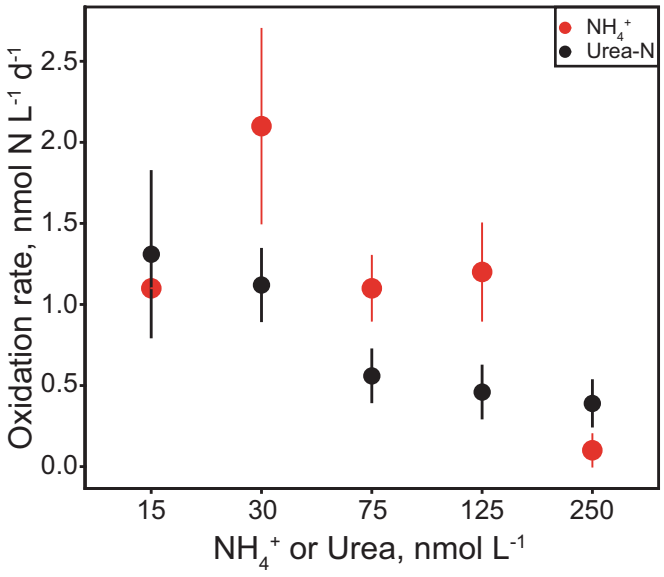

Figure 6. The percent of phytoplankton N demand supplied by ammonia oxidation (red) and urea-derived N oxidation (black) (a) and upwelling intensity (b) at SPOT between September 2014 and August 2016.

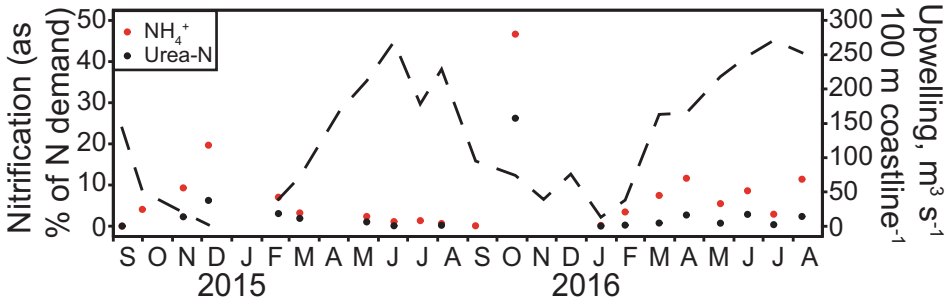

Figure 7. A time series of nitrous oxide concentration at SPOT between September 2014 and August 2016. Black circles indicate where discrete samples were collected.

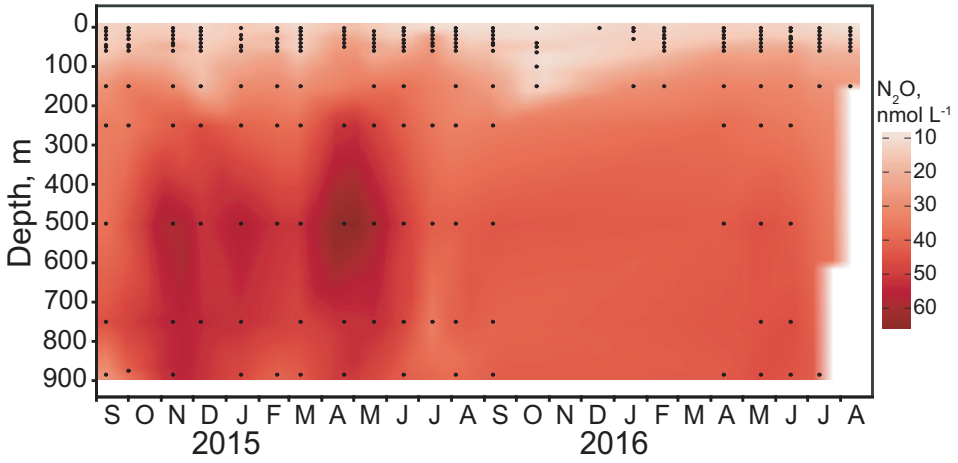

Figure 8. The relationships between nitrous oxide and oxygen concentrations between Sept 2014 to Sept 2015 (a) and potential temperature and salinity colored according to nitrous oxide concentration between Sept 2014 to Aug 2016 (b) at SPOT, where σ_θ isopycnals are depicted by the solid lines.

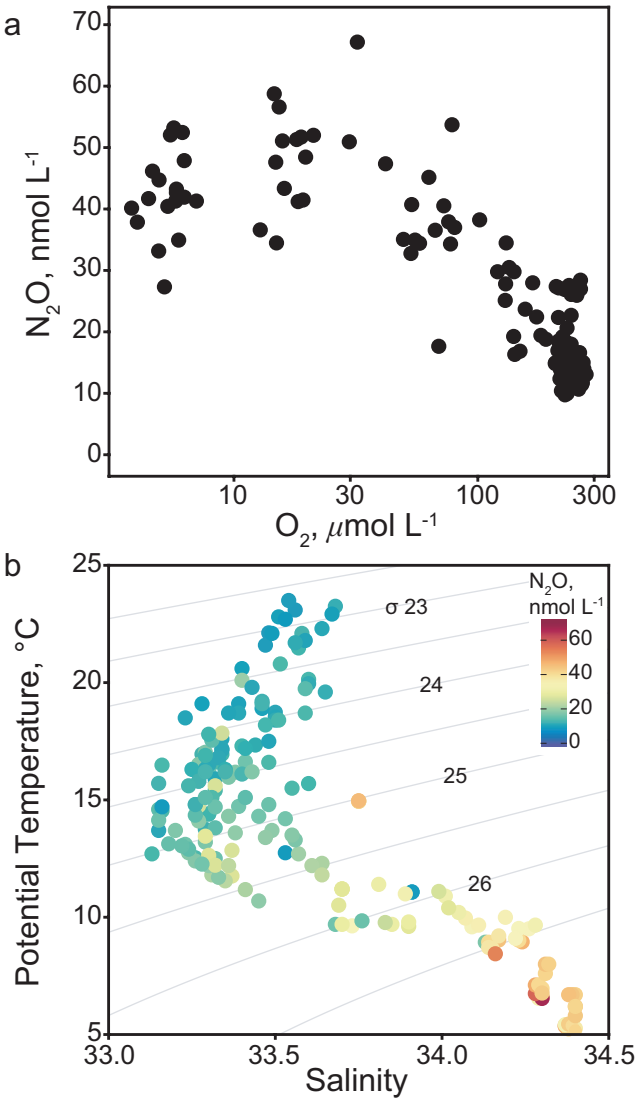

References

Alonso-Sáez, L., A. S. Waller, D. R. Mende, and others. 2012. Role for urea in nitrification by polar marine Archaea. Proc. Natl. Acad. Sci. USA **109**: 17989–17994. doi: 10.1073/pnas.1201914109

Altabet, M. A., C. Pilskaln, R. Thunell, C. Pride, D. Sigman, F. Chavez, and R. Francois. 1999. The nitrogen isotope biogeochemistry of sinking particles from the margin of the Eastern North Pacific. Deep-Sea Res. I **46**: 655–679. doi:10.1016/s0967-0637(98)00084-3

Amin, S. A., J. W. Moffett, W. Martens-Habbena, and others. 2013. Copper requirements of the ammonia-oxidizing archaeon *Nitrosopumilus maritimus* SCM1 and implications for nitrification in the marine environment. Limnol. Oceanogr. **58**: 2037–2045. doi:10.4319/lo.2013.58.6.2037

Arévalo-Martínez, D. L., A. Kock, C. R. Löscher, R. A. Schmitz, and H. W. Bange. 2015. Massive nitrous oxide emissions from the tropical South Pacific Ocean. Nat. Geosci. **8**: 530–533. doi:10.1038/ngeo2469

Bange, H. W., S. Rapsomanikis, and M. O. Andreae. 1996. Nitrous oxide in coastal waters. Global Biogeochem. Cycles **10**: 197–207. doi:10.1029/95gb03834

Bayer, B., J. Vojvoda, P. Offre, and others. 2016. Physiological and genomic characterization of two novel marine thaumarchaeal strains indicates niche differentiation. ISME J. **10**: 1051–1063. doi: 10.1038/ismej.2015.200

Beman, J. M., C. E. Chow, A. L. King, and others. 2011a. Global declines in oceanic

nitrification rates as a consequence of ocean acidification. Proc. Natl. Acad. Sci USA **108**: 208–213. doi:10.1073/pnas.1011053108

Beman, J. M., B. N. Popp, and S. E. Alford. 2012. Quantification of ammonia oxidation rates and ammonia-oxidizing archaea and bacteria at high resolution in the Gulf of California and eastern tropical North Pacific Ocean. Limnol. Oceanogr. **57**: 711–726. doi:10.4319/lo.2012.57.3.0711

Beman, J. M., J. A. Steele, and J. A. Fuhrman. 2011b. Co-occurrence patterns for abundant marine archaeal and bacterial lineages in the deep chlorophyll maximum of coastal California. ISME J. **5**: 1077–1085. doi:10.1038/ismej.2010.204

Bograd, S. J., I. D. Schroeder, and M. G. Jacox. 2019. A water mass history of the Southern California current system. Geophys. Res. Lett. doi:10.1029/2019gl082685

Boyd, P. W., and P. P. Newton. 1999. Does planktonic community structure determine downward particulate organic carbon flux in different oceanic provinces? Deep-Sea Res. I **46**: 63–91. doi:10.1016/s0967-0637(98)00066-1

Brown, M. V., M. S. Schwalbach, I. Hewson, and J. A. Fuhrman. 2005. Coupling 16S-ITS rDNA clone libraries and automated ribosomal intergenic spacer analysis to show marine microbial diversity: development and application to a time series. Environ. Microbiol. **7**: 1466–1479. doi: 10.1111/j.1462-2920.2005.00835.x

Buesseler, K. O. 1998. The decoupling of production and particulate export in the surface ocean. Global Biogeochem. Cycles **12**: 297–310. doi:10.1029/97gb03366

Buesseler, K. O., C. H. Lamborg, P. W. Boyd, and others. 2007. Revisiting carbon flux

through the ocean's twilight zone. Science **316**: 567–570. doi: 10.1126/science.1137959

Buitenhuis, E. T., P. Suntharalingam, and C. Le Quéré. 2017. Constraints on global oceanic emissions of N_2O from observations and models. Biogeosciences **15**: 2161–2175. doi:10.5194/bg-2017-193

Carini, P., C. L. Dupont, and A. E. Santoro. 2018. Patterns of thaumarchaeal gene expression in culture and diverse marine environments. Environ. Microbiol. **20**: 2112–2124. doi: 10.1111/1462-2920.14107

Castro, C. G., F. P. Chavez, and C. A. Collins. 2001. Role of the California Undercurrent in the export of denitrified waters from the eastern tropical North Pacific. Global Biogeochem. Cycles **15**: 819–830. doi:10.1029/2000gb001324

Cavan, E. L., F. A. C. Le Moigne, A. J. Poulton, G. A. Tarling, P. Ward, C. J. Daniels, G. M. Fragoso, and R. J. Sanders. 2015. Attenuation of particulate organic carbon flux in the Scotia Sea, Southern Ocean, is controlled by zooplankton fecal pellets. Geophys. Res. Lett. **42**: 821–830. doi:10.1002/2014gl062744

Cavole, L., A. Demko, R. Diner, and others. 2016. Biological impacts of the 2013–2015 warm-water anomaly in the Northeast Pacific: Winners, losers, and the future. Oceanography **29**: 273–285. doi: 10.5670/oceanog.2016.32

Chavez, F. P., and M. Messié. 2009. A comparison of eastern boundary upwelling ecosystems. Prog. Oceanogr. **83**: 80–96. doi:10.1016/j.pocean.2009.07.032

Chow, C.E. T., R. Sachdeva, J. A. Cram, J. A. Steele, D. M. Needham, A. Patel, A. E. Parada, and J. A. Fuhrman. 2013. Temporal variability and coherence of euphotic zone

bacterial communities over a decade in the Southern California Bight. ISME J. **7**: 2259–2273. doi:10.1038/ismej.2013.122

Clark, D. R., A. P. Rees, and I. Joint. 2008. Ammonium regeneration and nitrification rates in the oligotrophic Atlantic Ocean: Implications for new production estimates. Limnol. Oceanogr. **53**: 52–62. doi:10.4319/lo.2008.53.1.0052

Codispoti, L. A. 2010. Interesting times for marine N_2O. Science **327**: 1339–1340. doi: 10.1126/science.1184945

Connell, P. E., V. Campbell, A. G. Gellene, S. K. Hu, and D. A. Caron. 2017. Planktonic food web structure at a coastal time-series site: II. Spatiotemporal variability of microbial trophic activities. Deep-Sea Res. I **121**: 210–223. doi:10.1016/j.dsr.2017.01.007

Cram, J. A., C. E. T. Chow, R. Sachdeva, D. M. Needham, A. E. Parada, J. A. Steele, and J. A. Fuhrman. 2015. Seasonal and interannual variability of the marine bacterioplankton community throughout the water column over ten years. ISME J. **9**: 563–580. doi: 10.1038/ismej.2014.153

Dagg, M. J., G. A. Jackson, and D. M. Checkley. 2014. The distribution and vertical flux of fecal pellets from large zooplankton in Monterey bay and coastal California. Deep-Sea Res. I **94**: 72–86. doi:10.1016/j.dsr.2014.09.001

Damashek, J., K. L. Casciotti, and C. A. Francis. 2016. Variable nitrification rates across environmental gradients in turbid, nutrient-rich estuary waters of San Francisco Bay. Estuaries Coast **39**: 1050–1071. doi:10.1007/s12237-016-0071-7

Damashek, J., B. B. Tolar, Q. Liu, A. O. Okotie-Oyekan, N. J. Wallsgrove, B. N. Popp, and J. T. Hollibaugh. 2019. Microbial oxidation of nitrogen supplied as selected organic nitrogen compounds in the South Atlantic Bight. Limnol. Oceanogr. **64**: 982–995. doi:10.1002/lno.11089

Diaz, R. J., and R. Rosenberg. 2008. Spreading dead zones and consequences for marine ecosystems. Science **321**: 926–929. doi: 10.1126/science.1156401

Dore, J. E., and D. M. Karl. 1996. Nitrification in the euphotic zone as a source for nitrite, nitrate, and nitrous oxide at Station ALOHA. Limnol. Oceanogr. **41**: 1619–1628. doi:10.4319/lo.1996.41.8.1619

Dore, J. E., B. N. Popp, D. M. Karl, and F. J. Sansone. 1998. A large source of atmospheric nitrous oxide from subtropical North Pacific surface waters. Nature **396**: 63–66. doi:10.1038/23921

Dugdale, R. C., and J. J. Goering. 1967. Uptake of new and regenerated forms of nitrogen in primary productivity[1]. Limnol. Oceanogr. **12**: 196–206. doi:10.4319/lo.1967.12.2.0196

Dunne, J. P., J. L. Sarmiento, and A. Gnanadesikan. 2007. A synthesis of global particle export from the surface ocean and cycling through the ocean interior and on the seafloor. Global Biogeochem. Cycles **21**. doi:10.1029/2006gb002907

Emerson, S. 2014. Annual net community production and the biological carbon flux in the ocean. Global Biogeochem. Cycles **28**: 14–28. doi:10.1002/2013gb004680

Eppley, R. W., and B. J. Peterson. 1979. Particulate organic matter flux and planktonic new production in the deep ocean. Nature **282**: 677–680. doi:10.1038/282677a0

Eppley, R. W., E. H. Renger, and W. G. Harrison. 1979. Nitrate and phytoplankton production in southern California coastal waters. Limnol. Oceanogr. **24**: 483-494. doi: 10.4319/lo.1979.24.3.0483

Fairall, C. W., E. F. Bradley, J. E. Hare, A. A. Grachev, and J. B. Edson. 2003. Bulk parameterization of air–sea Fluxes: Updates and verification for the COARE algorithm. J. Clim. **16**: 571–591. doi:2.0.co;2">10.1175/1520-0442(2003)016<0571:bpoasf>2.0.co;2

Falkowski, P. G., R. T. Barber, and V. Smetacek. 1998. Biogeochemical controls and feedbacks on ocean primary production. Science **281**: 200–207. doi: 10.1126/science.281.5374.200

Falkowski, P. G., E. A. Laws, R. T. Barber, and J. W. Murray. 2003. Phytoplankton and their role in primary, new, and export production, p. 99–121. In Ocean Biogeochemistry. Springer.

Farías, L., V. Besoain, and S. García-Loyola. 2015. Presence of nitrous oxide hotspots in the coastal upwelling area off central Chile: an analysis of temporal variability based on ten years of a biogeochemical time series. Environ. Res. Lett. **10**: 044017. doi:10.1088/1748-9326/10/4/044017

Farías, L., M. Castro-González, M. Cornejo, J. Charpentier, J. Faúndez, N. Boontanon, and N. Yoshida. 2009. Denitrification and nitrous oxide cycling within the upper oxycline of the eastern tropical South Pacific oxygen minimum zone. Limnol. Oceanogr. **54**: 132–144. doi:10.4319/lo.2009.54.1.0132

Fuhrman, J. A., I. Hewson, M. S. Schwalbach, J. A. Steele, M. V. Brown, and S. Naeem. 2006. Annually reoccurring bacterial communities are predictable from ocean conditions. Proc. Natl. Acad. Sci. USA. **103**: 13104–13109. doi: 10.1073/pnas.0602399103

Goeyens, L., N. Kindermans, M. Abu Yusuf, and M. Elskens. 1998. A room temperature procedure for the manual determination of urea in seawater. Estuar. Coast. Shelf Sci. **47**: 415–418. doi:10.1006/ecss.1998.0357

Goreau, T. J., W. A. Kaplan, S. C. Wofsy, M. B. McElroy, F. W. Valois, and S. W. Watson. 1980. Production of NO_2^- and N_2O by nitrifying bacteria at reduced concentrations of oxygen. Appl. Environ. Microbiol. **40**: 526–532.

Haskell, W. Z., M. G. Prokopenko, D. E. Hammond, R. H. R. Stanley, and Z. O. Sandwith. 2017. Annual cyclicity in export efficiency in the inner Southern California Bight. Global Biogeochem. Cycles. **31**: 357-376. doi:10.1002/2016gb005561

Henson, S., F. Le Moigne, and S. Giering. 2019. Drivers of carbon export efficiency in the global ocean. Global Biogeochem. Cycles. doi:10.1029/2018gb006158

Hickey, B. M. 1998. Coastal oceanography of western North America from the tip of Baja California to Vancouver Island, p. 345–393. In A. R. Robinson and K. H. Brink [eds.], The Sea 11. Harvard University Press.

Ho, D. T., C. S. Law, M. J. Smith, P. Schlosser, M. Harvey, and P. Hill. 2006. Measurements of air-sea gas exchange at high wind speeds in the Southern Ocean: Implications for global parameterizations. Geophys. Res. Lett. **33**.

doi:10.1029/2006gl026817

Holmes, R. M., A. Aminot, R. Kerouel, B. A. Hooker, and B. J. Peterson. 1999. A simple and precise method for measuring ammonium in marine and freshwater ecosystems. Can. J. Fish. Aquat. Sci. **56**:1801-1808. doi: 10.1139/f99-128

Holm-Hansen, O., and B. Riemann. 1978. Chlorophyll a determination: Improvements in methodology. Oikos 3**0**: 438. doi:10.2307/3543338

Horak, R. E. A., W. Qin, A. J. Schauer, E. V. Armbrust, A. E. Ingalls, J. W. Moffett, D. A. Stahl, and A. H. Devol. 2013. Ammonia oxidation kinetics and temperature sensitivity of a natural marine community dominated by Archaea. ISME J. **7**: 2023–2033. doi: 10.1038/ismej.2013.75

Jacob, B., G. Daneri, R. A. Quiñones, and M. Sobarzo. 2011. Community metabolism, phytoplankton size -structure and heterotrophic prokaryote production in a highly productive upwelling zone off northern Chile. Mar. Ecol. Prog. Ser. **430**: 23–34. doi:10.3354/meps09074

Kim, D. Y., P. D. Countway, A. C. Jones, A. Schnetzer, W. Yamashita, C. Tung, and D. A. Caron. 2014. Monthly to interannual variability of microbial eukaryote assemblages at four depths in the eastern North Pacific. ISME J. **8**: 515–530. doi: 10.1038/ismej.2013.173

Kitzinger, K., C. C. Padilla, H. K. Marchant, and others. 2019. Cyanate and urea are substrates for nitrification by Thaumarchaeota in the marine environment. Nat. Microbiol. **4**: 234–243. doi: 10.1038/s41564-018-0316-2

Kool, D. M., J. Dolfing, N. Wrage, and J. W. Van Groenigen. 2011. Nitrifier denitrification as a distinct and significant source of nitrous oxide from soil. Soil Biol. Biochem. **43**: 174–178. doi:10.1016/j.soilbio.2010.09.030

Kozlowski, J. A., J. Price, and L. Y. Stein. 2014. Revision of N_2O-producing pathways in the ammonia-oxidizing bacterium *Nitrosomonas europaea* ATCC 19718. Appl. Environ. Microbiol. **80**: 4930–4935. doi:10.1128/AEM.01061-14

Kozlowski, J. A., M. Stieglmeier, C. Schleper, M. G. Klotz, and L. Y. Stein. 2016. Pathways and key intermediates required for obligate aerobic ammonia-dependent chemolithotrophy in bacteria and Thaumarchaeota. ISME J. **10**: 1836–1845. doi:10.1038/ismej.2016.2

Laperriere, S. M., N. J. Nidzieko, R. J. Fox, A. W. Fisher, and A. E. Santoro. 2019. Observations of variable ammonia oxidation and nitrous oxide flux in a eutrophic estuary. Estuaries Coast **42**: 33–44. doi: 10.1007/s12237-018-0441-4

Lipschultz, F., N. R. Bates, C. A. Carlson, and D. A. Hansell. 2002. New production in the Sargasso Sea: History and current status. Global Biogeochem. Cycles **16**: 1–1. doi:10.1029/2000gb001319

Liu, Q., B. B. Tolar, M. J. Ross, J. B. Cheek, C. M. Sweeney, N. J. Wallsgrove, B. N. Popp, and J. T. Hollibaugh. 2018. Light and temperature control the seasonal distribution of thaumarchaeota in the South Atlantic bight. ISME J. **12**: 1473–1485. doi: 10.1038/s41396-018-0066-4

Löscher, C. R., A. Kock, M. Könneke, J. LaRoche, H. W. Bange, and R. A. Schmitz. 2012.

Production of oceanic nitrous oxide by ammonia-oxidizing archaea. Biogeosciences **9**: 2419–2429. doi:10.5194/bg-9-2419-2012

Lueker, T. J. 2004. Coastal upwelling fluxes of O_2, N_2O, and CO_2 assessed from continuous atmospheric observations at Trinidad, California. Biogeosciences **1**: 101–111. doi:10.5194/bg-1-101-2004

Lueker, T. J., S. J. Walker, M. K. Vollmer, R. F. Keeling, C. D. Nevison, R. F. Weiss, and H. E. Garcia. 2003. Coastal upwelling air-sea fluxes revealed in atmospheric observations of O_2/N_2, CO_2 and N_2O. Geophys. Res. Lett. **30**. doi:10.1029/2002gl016615

Lynn, R. J., and J. J. Simpson. 1987. The California Current system: The seasonal variability of its physical characteristics. J. Geophys. Res. **92**: 12947. doi:10.1029/jc092ic12p12947

Lynn, R. J., and J. J. Simpson. 1990. The flow of the undercurrent over the continental borderland off southern California. . J. Geophys. Res. **95**: 12995. doi:10.1029/jc095ic08p12995

McIlvin, M. R., and K. L. Casciotti. 2011. Technical updates to the bacterial method for nitrate isotopic analyses. Anal. Chem. **83**: 1850–1856. doi: 10.1021/ac1028984

Michaels, A. F., and M. W. Silver. 1988. Primary production, sinking fluxes and the microbial food web. Deep Sea Res. A **35**: 473–490. doi:10.1016/0198-0149(88)90126-4

Moigne, F. A. C. L., F. A. C. Le Moigne, S. A. Henson, and others. 2016. What causes the inverse relationship between primary production and export efficiency in the Southern

Ocean? Geophys. Res. Lett. **43**: 4457–4466. doi:10.1002/2016gl068480

Morando, M., and D. G. Capone. 2018. Direct utilization of organic nitrogen by phytoplankton and its role in nitrogen cycling within the Southern California Bight. Front. Microbiol. **9**: 2118. doi:10.3389/fmicb.2018.02118

Munro, D. R., P. D. Quay, L. W. Juranek, and R. Goericke. 2013. Biological production rates off the Southern California coast estimated from triple O_2 isotopes and O_2:Ar gas ratios. Limnol. Oceanogr. **58**: 1312–1328. doi:10.4319/lo.2013.58.4.1312

Naqvi, S. W. A., H. W. Bange, L. Farías, P. M. S. Monteiro, M. I. Scranton, and J. Zhang. 2010. Marine hypoxia/anoxia as a source of CH_4 and N_2O. Biogeosciences **7**: 2159–2190. doi:10.5194/bg-7-2159-2010

Naqvi, S. W. A., D. A. Jayakumar, P. V. Narvekar, H. Naik, V V S, W. D'Souza, S. Joseph, and M. D. George. 2000. Increased marine production of N_2O due to intensifying anoxia on the Indian continental shelf. Nature **408**: 346–349. doi:10.1038/35042551

Nevison, C. D., E. Dlugokencky, G. Dutton, and others. 2011. Exploring causes of interannual variability in the seasonal cycles of tropospheric nitrous oxide. Atmos. Chem. Phys. **11**: 3713–3730. doi:10.5194/acp-11-3713-2011

Nevison, C. D., T. J. Lueker, and R. F. Weiss. 2004. Quantifying the nitrous oxide source from coastal upwelling. Global Biogeochem. Cycles **18**. doi:10.1029/2003gb002110

Nevison, C. D., R. F. Weiss, and D. J. Erickson. 1995. Global oceanic emissions of nitrous oxide. J. Geophys. Res. **100**: 15809. doi:10.1029/95jc00684

Newell, S. E., A. R. Babbin, A. Jayakumar, and B. B. Ward. 2011. Ammonia oxidation rates

and nitrification in the Arabian Sea. Global Biogeochem. Cycles **25**. doi:10.1029/2010gb003940

Newell, S. E., S. E. Fawcett, and B. B. Ward. 2013. Depth distribution of ammonia oxidation rates and ammonia-oxidizer community composition in the Sargasso Sea. Limnol. Oceanogr. **58**: 1491–1500. doi:10.4319/lo.2013.58.4.1491

Pedneault, E., P. E. Galand, M. Potvin, J.É. Tremblay, and C. Lovejoy. 2014. Archaeal amoA and ureC genes and their transcriptional activity in the Arctic Ocean. Sci. Rep. **4**: 4661. doi: 10.1038/srep04661

Popp, B. N., M. B. Westley, S. Toyoda, and others. 2002. Nitrogen and oxygen isotopomeric constraints on the origins and sea-to-air flux of N_2O in the oligotrophic subtropical North Pacific gyre. Global Biogeochem. Cycles **16**: 12–11. doi:10.1029/2001gb001806

Poth, M., and D. D. Focht. 1985. N kinetic analysis of n_2o production by *Nitrosomonas europaea*: an examination of nitrifier denitrification. Appl. Environ. Microbiol. **49**: 1134–1141.

Price, N. M., and P. J. Harrison. 1987. Comparison of methods for the analysis of dissolved urea in seawater. Mar. Biol. **94**: 307–317. doi:10.1007/bf00392945

Qin, W., S. A. Amin, W. Martens-Habbena, and others. 2014. Marine ammonia-oxidizing archaeal isolates display obligate mixotrophy and wide ecotypic variation. Proc. Natl. Acad. Sci. USA **111**: 12504–12509. doi:10.1073/pnas.1324115111

Qin, W., K. A. Meinhardt, J. W. Moffett, A. H. Devol, E. Virginia Armbrust, A. E. Ingalls, and D. A. Stahl. 2017. Influence of oxygen availability on the activities of ammonia-

oxidizing archaea. Environ. Microbiol. Rep. **9**: 250–256. doi: 10.1111/1758-2229.12525

Redfield, A. C. 1958. The biological control of chemical factors in the environment. Am. Sci. **46**: 230A-221.

Santoro, A. E., C. Buchwald, M. R. McIlvin, and K. L. Casciotti. 2011. Isotopic signature of N_2O produced by marine ammonia-oxidizing archaea. Science **333**: 1282–1285. doi:10.1126/science.1208239

Santoro, A. E., K. L. Casciotti, and C. A. Francis. 2010. Activity, abundance and diversity of nitrifying archaea and bacteria in the central California Current. Environ. Microbiol. **12**: 1989–2006. doi:10.1111/j.1462-2920.2010.02205.x

Santoro, A. E., M. A. Saito, T. J. Goepfert, C. H. Lamborg, C. L. Dupont, and G. R. DiTullio. 2017. Thaumarchaeal ecotype distributions across the equatorial Pacific Ocean and their potential roles in nitrification and sinking flux attenuation. Limnol. Oceanogr. **62**: 1984–2003. doi:10.1002/lno.10547

Santoro, A. E., C. M. Sakamoto, J. M. Smith, and others. 2013. Measurements of nitrite production in and around the primary nitrite maximum in the central California Current. Biogeosciences **10**: 7395–7410. doi:10.5194/bg-10-7395-2013

Seitzinger, S. P., C. Kroeze, and R. V. Styles. 2000. Global distribution of N_2O emissions from aquatic systems: natural emissions and anthropogenic effects. Chemosphere Global Change Sci. **2**: 267–279. doi:10.1016/s1465-9972(00)00015-5

Shiozaki, T., M. Ijichi, K. Isobe, and others. 2016. Nitrification and its influence on biogeochemical cycles from the equatorial Pacific to the Arctic Ocean. ISME J. **10**:

2184–2197. doi:10.1038/ismej.2016.18

Shi, Y., G. W. Tyson, J. M. Eppley, and E. F. DeLong. 2011. Integrated metatranscriptomic and metagenomic analyses of stratified microbial assemblages in the open ocean. ISME J. **5**: 999–1013. doi:10.1038/ismej.2010.189

Sigman, D. M., K. L. Casciotti, M. Andreani, C. Barford, M. Galanter, and J. K. Böhlke. 2001. A bacterial method for the nitrogen isotopic analysis of nitrate in seawater and freshwater. Anal. Chem. **73**: 4145–4153. doi:10.1021/ac010088e

Sigman, D. M., J. Granger, P. J. DiFiore, M. M. Lehmann, R. Ho, G. Cane, and A. van Geen. 2005. Coupled nitrogen and oxygen isotope measurements of nitrate along the eastern North Pacific margin. Global Biogeochem. Cycles **19**. doi:10.1029/2005gb002458

Smith, J. M., F. P. Chavez, and C. A. Francis. 2014. Ammonium uptake by phytoplankton regulates nitrification in the sunlit ocean. PLoS ONE **9**: e108173. doi:10.1371/journal.pone.0108173

Smith, J. M., J. Damashek, F. P. Chavez, and C. A. Francis. 2016. Factors influencing nitrification rates and the abundance and transcriptional activity of ammonia-oxidizing microorganisms in the dark northeast Pacific Ocean. Limnol. Oceanogr. **61**: 596–609. doi:10.1002/lno.10235

Tolar, B. B., M. J. Ross, N. J. Wallsgrove, Q. Liu, L. I. Aluwihare, B. N. Popp, and J. T. Hollibaugh. 2016. Contribution of ammonia oxidation to chemoautotrophy in Antarctic coastal waters. ISME J. **10**: 2605–2619. doi:10.1038/ismej.2016.61

Tolar, B. B., N. J. Wallsgrove, B. N. Popp, and J. T. Hollibaugh. 2017. Oxidation of urea-derived nitrogen by thaumarchaeota-dominated marine nitrifying communities. Environ. Microbiol. **19**: 4838–4850. doi: 10.1111/1462-2920.13457

Townsend-Small, A., M. G. Prokopenko, and W. M. Berelson. 2014. Nitrous oxide cycling in the water column and sediments of the oxygen minimum zone, eastern subtropical North Pacific, Southern California, and Northern Mexico (23°N-34°N). J. Geophys. Res. Oceans **119**: 3158–3170. doi:10.1002/2013jc009580

Walter, S., H. W. Bange, U. Breitenbach, and D. W. R. Wallace. 2006. Nitrous oxide in the North Atlantic Ocean. Biogeosciences **3**: 607–619. doi:10.5194/bg-3-607-2006

Wanninkhof, R. 1992. Relationship between wind speed and gas exchange over the ocean. J. Geophys. Res. **97**: 7373. doi:10.1029/92jc00188

Wan, X. S., H.X. Sheng, M. Dai, and others. 2018. Ambient nitrate switches the ammonium consumption pathway in the euphotic ocean. Nat. Commun. **9**: 915. doi: 10.1038/s41467-018-03363-0

Ward, B. B. 2005. Temporal variability in nitrification rates and related biogeochemical factors in Monterey Bay, California, USA. Mar. Ecol. Prog. Ser. **292**: 97–109. doi:10.3354/meps292097

Ward, B. B., R. J. Olson, and M. J. Perry. 1982. Microbial nitrification rates in the primary nitrite maximum off southern California. Deep-Sea Res. A **29**: 247–255. doi:10.1016/0198-0149(82)90112-1

Weiss, R. F., and B. A. Price. 1980. Nitrous oxide solubility in water and seawater. Mar.

Chem. **8**: 347–359. doi:10.1016/0304-4203(80)90024-9

Wittke, F., A. Kock, and H. W. Bange. 2010. Nitrous oxide emissions from the upwelling area off Mauritania (NW Africa). Geophys. Res. Lett. **37**. doi:10.1029/2010gl042442

Yool, A., A. P. Martin, C. Fernández, and D. R. Clark. 2007. The significance of nitrification for oceanic new production. Nature **447**: 999–1002. doi:10.1038/nature05885

Zaba, K. D., and D. L. Rudnick. 2016. The 2014-2015 warming anomaly in the Southern California Current System observed by underwater gliders. Geophys. Res. Lett. **43**: 1241–1248. doi:10.1002/2015gl067550

Zakem, E. J., A. Al-Haj, M. J. Church, and others. 2018. Ecological control of nitrite in the upper ocean. Nat. Commun. 9: 1206. doi: 10.1038/s41467-018-03553-w

Zamora, L. M., and A. Oschlies. 2014. Surface nitrification: A major uncertainty in marine N_2O emissions. Geophys. Res. Lett. **41**: 4247–4253. doi:10.1002/2014gl060556

Zhu, X., M. Burger, T. A. Doane, and W. R. Horwath. 2013. Ammonia oxidation pathways and nitrifier denitrification are significant sources of N_2O and NO under low oxygen availability. Proc. Natl. Acad. Sci. USA **110**: 6328–6333. doi: 10.1073/pnas.1219993110

V. Conclusions and future directions

The data presented here contributes to a better understanding of the effects of anthropogenic activity on microbial diversity and nitrogen cycling in aquatic systems. Chapter I reveals the influence of land use on headwater stream microbial diversity and ecosystem function. Stream microbial diversity correlated with a traditional benthic macroinvertebrate index of stream integrity, and similar to macroinvertebrates, microbial diversity was influenced by watershed land use and stream condition. These results indicate microbes can be used by stream monitoring programs, along with traditional biotic and physicochemical indices, to assess stream condition. Taxa linked to key nitrogen and carbon metabolisms (Thaumarchaeota and Cyanobacteria) were more abundant and pervasive in streams in good condition, suggesting key ecosystem processes, i.e. carbon and nitrogen cycling, are affected by land use. Along gradients of land use, shifts in microbial diversity were accompanied by changes in community respiration and the production of the greenhouse gas nitrous oxide (N_2O), having important implications for climate. Together, these results demonstrate land use modification alters stream microbial diversity and these changes are accompanied by changes in biogeochemical processes. Future work should focus on developing a diagnostic tool of stream condition using microbes, similar to existing macroinvertebrate and fish indices. A better understanding of the physiology of key microbial indicator taxa will help link diversity with function and help to better predict the response of stream ecosystems to continued anthropogenic pressure.

The results of Chapter II demonstrate the impact of physical processes on nitrogen biogeochemistry in the eutrophic Chesapeake Bay, specifically the effects of wind-driven mixing on nitrification and N_2O production. Spatial separation was observed in the water column between high nitrification rates and high ammonium concentrations, a result of strong vertical stratification and low oxygen concentrations, suggesting ammonia oxidation is limited by oxygen in bottom waters of the Bay. Wind events oxygenated bottom waters and created "hot moments" of nitrification and N_2O production, relieving ammonia oxidizers of oxygen limitation. During periods of weak mixing, N_2O was consumed in bottom waters by denitrification and bottom waters were a sink for N_2O. Additionally, a box model indicated advection is a significant factor explaining the high temporal and spatial variability in N_2O concentrations observed in the Bay. Collectively, the results suggest a balance between biological (production and consumption) and physical (advection and vertical exchange) processes drive large fluctuations in N_2O concentrations making Chesapeake a variable source and sink of N_2O. Efforts should be taken to better constrain models of N_2O production in coastal systems. Integrating physical models with what is known about ammonia oxidizers and denitrifiers, specifically rates of growth and nitrogen transformations, will help better constrain estimates of N_2O emissions.

Finally, Chapter III demonstrates the importance of nitrification in the upper ocean as a source of nitrate for primary production. Depth-integrated nitrification correlated with depth-integrated primary production demonstrating a relationship between biomass and nitrogen remineralization in the upper ocean. Though, rates did not respond to additions of

ammonium or urea, implying nitrification was not limited by nitrogen substrate, but rather a micronutrient associated with increased primary production. Rates of urea-derived N oxidation were similar to ammonia oxidation rates, demonstrating urea is an important substrate fueling nitrification, providing an additional link between the organic matter pool and nitrification in the ocean. The data support the hypothesis that a decoupling between primary production and organic matter remineralization leads to high organic carbon export efficiencies, the fraction of primary production leaving the euphotic zone, out of the surface ocean. The relationship between primary production and N_2O is less clear, but it is evident the Southern California Bight is a source of N_2O to the atmosphere and a majority of the N_2O emitted likely originates in the eastern tropical North Pacific. A better understanding of water mass transport from the eastern tropical North Pacific through the Southern California Bight will better constrain coastal N_2O fluxes. Future studies should simultaneously measure primary production, carbon export, and nitrification to better inform our quantitative understanding of the controls on carbon export efficiency, which will improve predictions of carbon sequestration in the ocean.

This dissertation provides insights into the controls on microbial diversity and nitrogen transformations in aquatic systems. Directly linking watershed land use with microbial diversity and community respiration provides insight into the response of stream ecosystems to environmental perturbation and demonstrates the potential of using microbial diversity to monitor stream condition. Data presented here affirm the importance of nitrification in controlling surface ocean primary production and directly links the

degradation of organic matter to nitrification in observations of urea-derived N oxidation. Further, these studies demonstrate the importance of physical processes, specifically wind-driven mixing and advection in regulating microbial nitrogen transformations and the distribution of nitrogen compounds in coastal systems.

Appendix

A. Chapter I Supplemental Materials

Figure S1. The mean relative abundance (%) of the most abundant phyla grouped by substrate from all spring and summer samples collected in 2014 and 2015. Relative abundance values refer to the percentage each phylum contributes to all phyla in each sample.

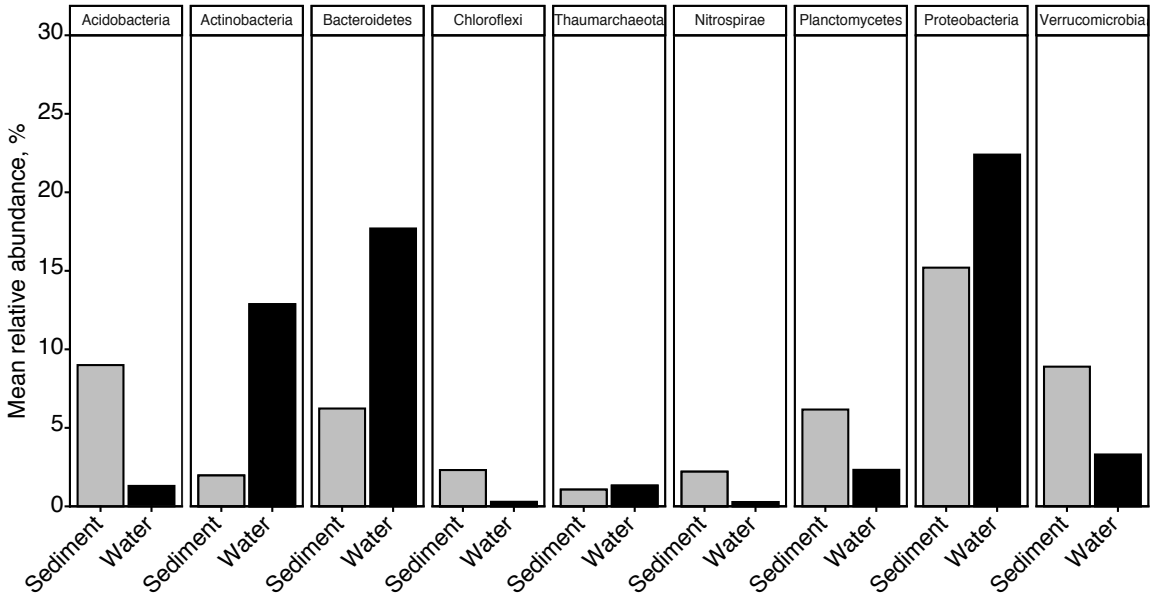

Figure S2. The mean relative abundance (%) of the most abundant phyla from all water (a) and sediment (b) samples from 2014 and 2015 grouped by season. Relative abundance values refer to the percentage each phylum contributes to all phyla in each sample.

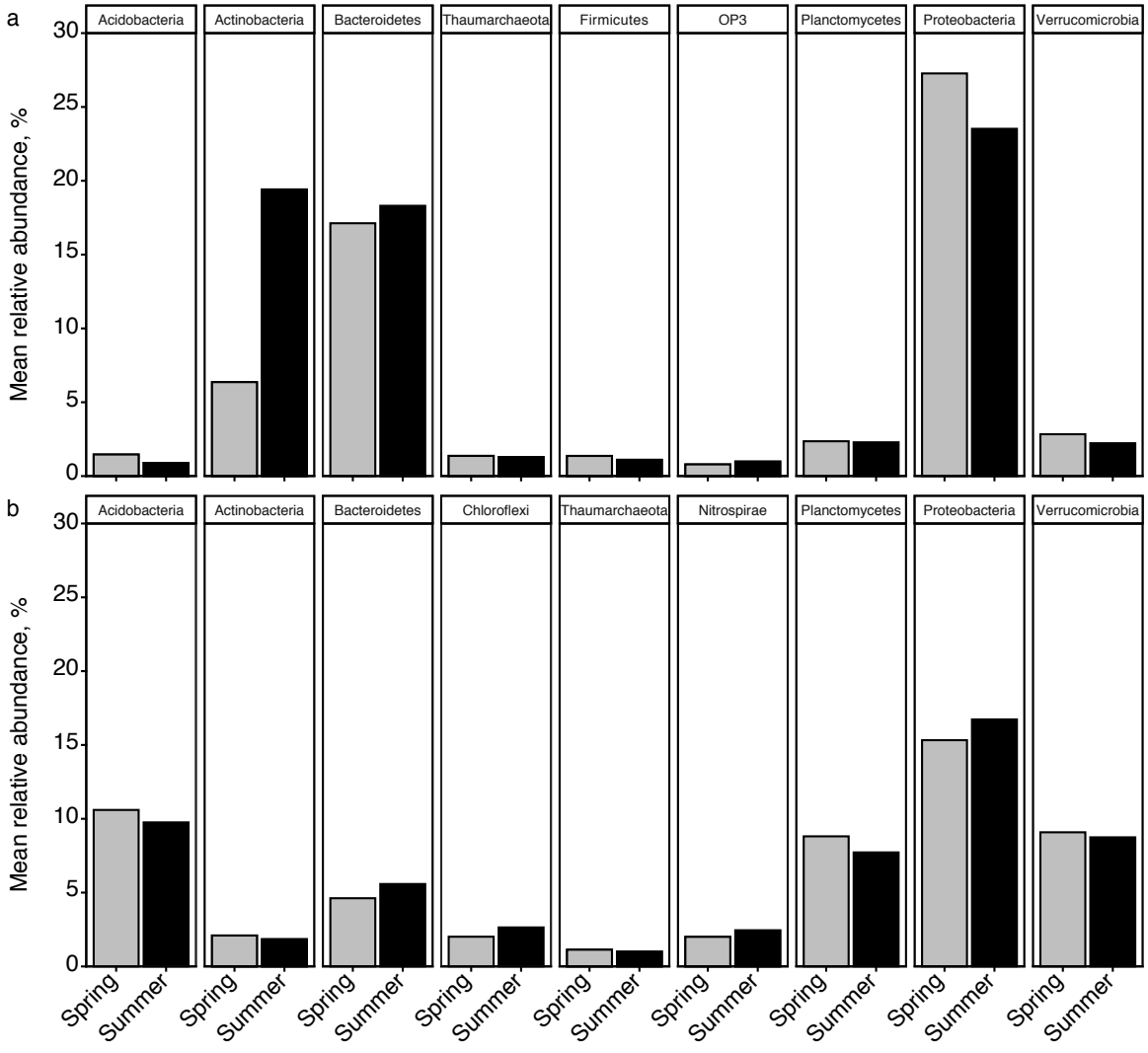

Figure S3. The mean relative abundance (%) of the most abundant phyla from all water (a) and sediment (b) samples from 2014 and 2015 grouped by geographic region. Relative abundance values refer to the percentage each phylum contributes to all phyla in each sample.

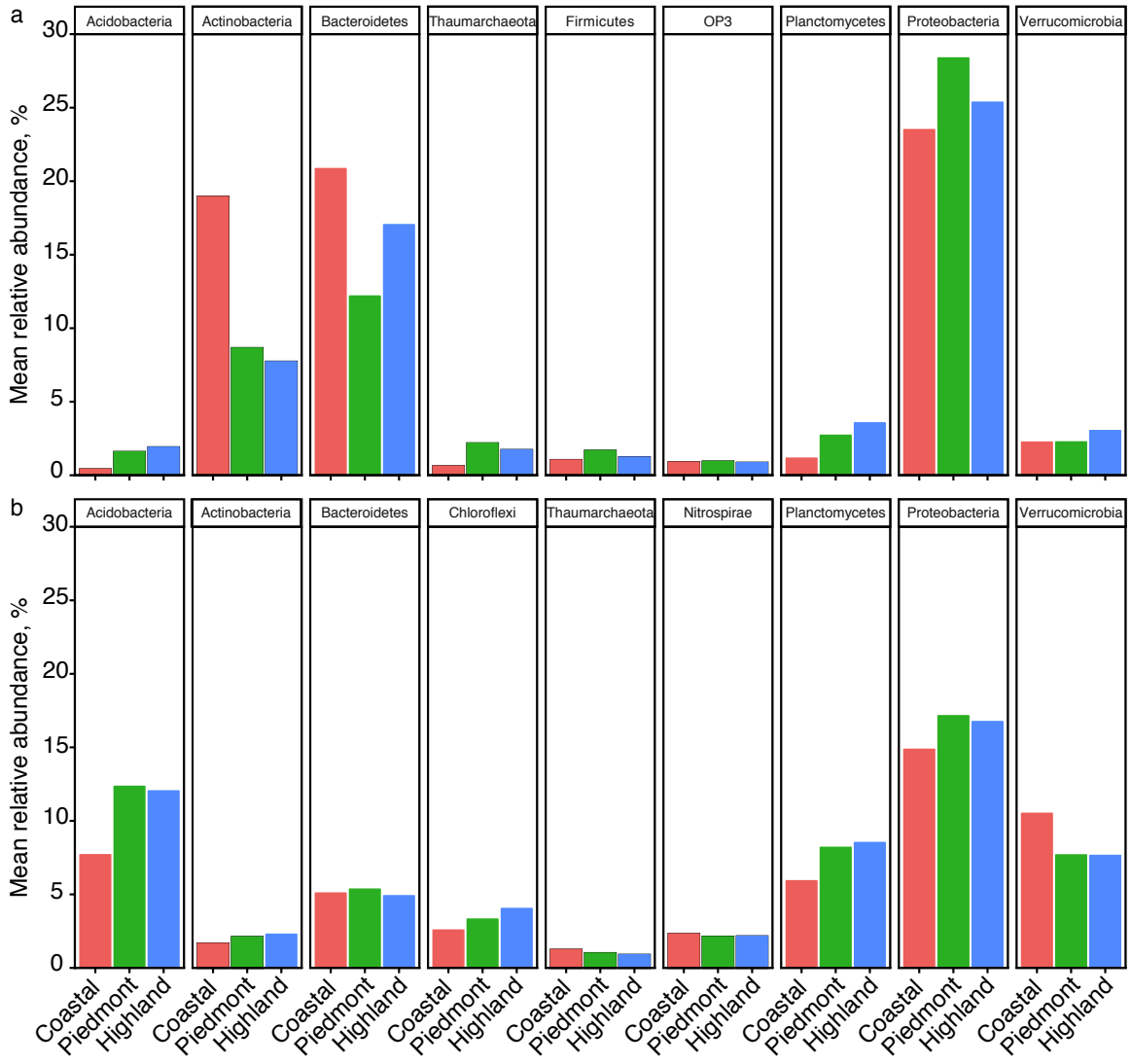

Table S1

Stream physicochemistry by geographic region of Maryland, USA. Values represent mean ± standard deviation.

	Coastal	Piedmont	Highland
Conductivity, µmho cm^{-1}	123.4 ± 73.0^{b}	589.2 ± 729.9^{a}	232.5 ± 265^{b}
ANC, µeq L^{-1}	198.2 ± 187.3^{b}	728.2 ± 602.7^{a}	492.2 ± 650.5^{a}
pH	6.4 ± 0.7^{b}	7.3 ± 0.5^{a}	7.3 ± 0.7^{a}
DOC, mg L^{-1}	8.7 ± 6.5^{a}	1.1 ± 0.5^{b}	1.3 ± 0.4^{b}
Cl-, mg L^{-1}	19.1 ± 15.0^{b}	129.1 ± 163.1^{a}	24.2 ± 29.9^{b}
SO_4^{2-}, mg L^{-1}	10.2 ± 5.3^{a}	9.1 ± 9.4^{a}	34.5 ± 89.1^{a}
TN, mg L^{-1}	1.4 ± 1.8^{b}	2.8 ± 1.5^{a}	1.1 ± 1.2^{b}
TP, µg L^{-1}	47.6 ± 49.4^{a}	10.9 ± 5^{b}	9.5 ± 4.8^{b}
PO_4^{3-}, µg L^{-1}	13.1 ± 27.2^{a}	4.4 ± 1.4^{a}	3.9 ± 2.3^{a}
NH_3, µg L^{-1}	44.3 ± 91.6^{a}	8.0 ± 8.2^{a}	11.3 ± 21.3^{a}
NO_2^{-}, µg L^{-1}	5.9 ± 7.7^{a}	4.2 ± 3.8^{a}	2.8 ± 3.8^{a}
NO_3^{-}, mg L^{-1}	0.9 ± 1.6^{b}	2.7 ± 1.6^{a}	1.0 ± 1.2^{b}
Br, ng L^{-1}	21.3 ± 21.2^{a}	34.7 ± 31.5^{a}	26 ± 69.9^{a}
Mg, µg L^{-1}	2.3 ± 1.5^{b}	7.0 ± 3.8^{a}	4.8 ± 5.0^{a}
Ca, µg L^{-1}	6.4 ± 5.1^{b}	20.5 ± 16.8^{a}	16.9 ± 21.3^{a}
Cu, µg L^{-1}	1.6 ± 0.9^{a}	0.7 ± 0.8^{b}	0.8 ± 0.6^{b}
Zn, µg L^{-1}	11.3 ± 4.6^{a}	4.7 ± 7.8^{a}	9.5 ± 30.8^{a}
Embeddedness, %	79.7 ± 22.2^{a}	37.0 ± 15.2^{b}	19.0 ± 22.4^{c}
Maximum depth, cm	66.3 ± 25.8^{a}	64.8 ± 22.2^{a}	62.0 ± 29.1^{a}
Average width, m	4.4 ± 3.4^{a}	3.9 ± 2.1^{a}	5.3 ± 4.2^{a}
Average thalweg depth, cm	30.8 ± 18^{a}	22.6 ± 8.0^{a}	27.1 ± 16^{a}
Average velocity, mm s^{-1}	77.7 ± 79.1^{b}	151.1 ± 73.1^{ab}	228.2 ± 175.3^{a}
B-IBI	3.6 ± 1.0^{a}	3.5 ± 1.0^{a}	3.5 ± 0.9^{a}
Urban, %	13.4 ± 18.2^{b}	29.0 ± 26.4^{a}	8.3 ± 10.0^{b}
Agriculture, %	21.5 ± 19.1a^{b}	25.6 ± 25.9^{a}	12.3 ± 15.9^{b}
Forest, %	58.1 ± 19.9^{c}	43.3 ± 20.9^{b}	78.2 ± 24.8^{a}

Values marked with a differing letter are significantly different according to Tukey's HSD test with a $P \leq 0.05$.

Table S2

Stream physicochemistry grouped by streams in watersheds with high forested (> 90%), agricultural (> 50%), and urban land use (> 50%). Values represent mean ± standard deviation.

	Forest	Agriculture	Urban
Conductivity, µmho cm^{-1}	82.8 ± 47.2^{b}	258.6 ± 147.5^{b}	1096.2 ± 1044.1^{a}
ANC, µeq L^{-1}	271.7 ± 193.1^{b}	485.6 ± 190.6^{b}	1100.4 ± 790.1^{a}
pH	7.1 ± 0.7^{a}	7.3 ± 0.4^{a}	7.4 ± 0.5^{a}
DOC, mg L^{-1}	1.4 ± 0.5^{a}	3.3 ± 2.7^{a}	4.5 ± 4.7^{a}
Cl-, mg L^{-1}	9.5 ± 10.6^{b}	30.7 ± 11.5^{b}	245 ± 224.4^{a}
SO_4^{2-}, mg L^{-1}	7.8 ± 3^{a}	13.7 ± 9.2^{a}	17.2 ± 12^{a}
TN, mg L^{-1}	0.5 ± 0.3^{b}	4.8 ± 1.1^{a}	1.0 ± 0.5^{b}
TP, µg L^{-1}	9.8 ± 5.2^{a}	59.4 ± 91.4^{a}	25.9 ± 15.2^{a}
PO_4^{3-}, µg L^{-1}	4.2 ± 3.2^{a}	27.4 ± 57.7^{a}	5.3 ± 2.6^{a}
NH_3, µg L^{-1}	3.2 ± 0.8^{a}	51.8 ± 97.8^{a}	16.7 ± 14.6^{a}
NO_2^{-}, µg L^{-1}	1.2 ± 0.2^{b}	11.3 ± 8.8^{a}	6.1 ± 5.2^{ab}
NO_3^{-}, mg L^{-1}	0.5 ± 0.3^{b}	4.4 ± 1.0^{a}	0.7 ± 0.6^{b}
Br, ng L^{-1}	9.4 ± 5.3^{b}	22.1 ± 5^{b}	64.3 ± 39.4^{a}
Mg, µg L^{-1}	2.3 ± 1.2^{b}	6.0 ± 1.8^{a}	8.4 ± 6.4^{a}
Ca, µg L^{-1}	5.8 ± 4.2^{b}	23.1 ± 26.8^{ab}	30.6 ± 24.9^{a}
Cu, µg L^{-1}	0.9 ± 0.6^{b}	1.3 ± 1.1^{ab}	1.9 ± 1.1^{a}
Zn, µg L^{-1}	1.7 ± 1.3^{b}	5.3 ± 4.2^{b}	14.7 ± 10.8^{a}
Embeddedness, %	7.3 ± 3.9^{b}	62.8 ± 29.6^{a}	49.4 ± 22.4^{a}
Maximum depth, cm	57.4 ± 21.5^{a}	62.2 ± 37.3^{a}	80.3 ± 28.3^{a}
Average width, m	4.1 ± 1.4^{a}	3.7 ± 2.0^{a}	4.3 ± 1.7^{a}
Average thalweg depth, cm	21.6 ± 6.5^{a}	25.3 ± 10.2^{a}	25.2 ± 10.7^{a}
Average velocity, mm s^{-1}	291.7 ± 172.1^{a}	188.6 ± 171.0^{ab}	76.6 ± 46.1^{b}
B-IBI	3.6 ± 1.1^{a}	3.1 ± 1.0^{a}	2.9 ± 1.2^{a}
Urban, %	2.9 ± 2.3^{c}	10.0 ± 5.1^{b}	72.1 ± 11.4^{a}
Agriculture, %	1.6 ± 2.2^{b}	65.7 ± 5.5^{a}	1.5 ± 1.7^{b}
Forest, %	95.3 ± 3.8^{a}	23.1 ± 6.7^{b}	25.0 ± 9.4^{b}

Values marked with a differing letter are significantly different according to Tukey's HSD test with a $p \leq 0.05$.

Table S3

Stream physicochemistry grouped by stream condition according to the Benthic Index of Biotic Integrity (B-IBI). Values represent mean ± standard deviation.

	Good	Fair	Poor	Very poor
Conductivity, µmho cm^{-1}	156.8 ± 120.4^{b}	235.5 ± 241.1^{b}	355.0 ± 462.2^{b}	812.9 ± 1167.8^{a}
ANC, µeq L^{-1}	258.9 ± 213.1^{ab}	418.9 ± 403.2^{ab}	663.6 ± 870.2^{a}	712.1 ± 877.6^{a}
pH	7.0 ± 0.5^{a}	6.9 ± 0.8^{a}	6.7 ± 1.2^{a}	6.6 ± 1.4^{a}
DOC, mg L^{-1}	3.4 ± 3.4^{b}	5.0 ± 5.3^{ab}	7.9 ± 9.4^{a}	4.8 ± 7.0^{ab}
Cl-, mg L^{-1}	24.4 ± 22.8^{b}	34.7 ± 43.6^{b}	69.4 ± 109.8^{ab}	159.6 ± 255.3^{a}
SO_4^{2-}, mg L^{-1}	16.4 ± 46^{a}	23.6 ± 76.9^{a}	12.7 ± 7.2^{a}	15.5 ± 14.6^{a}
TN, mg L^{-1}	1.3 ± 1.5^{a}	2.1 ± 1.9^{a}	1.8 ± 1.8^{a}	1.3 ± 1.6^{a}
TP, µg L^{-1}	21.5 ± 16.5^{a}	33.2 ± 58.7^{a}	36.7 ± 44.9^{a}	22.9 ± 27.4^{a}
PO_4^{3-}, µg L^{-1}	6.2 ± 4.8^{a}	13.1 ± 35.2^{a}	8.0 ± 6.1^{a}	3.7 ± 2.9^{a}
NH_3, µg L^{-1}	25.6 ± 81.4^{a}	30.8 ± 63.8^{a}	21.8 ± 19.5^{a}	19.7 ± 17.6^{a}
NO_2^{-}, µg L^{-1}	3.6 ± 6.4^{a}	4.9 ± 6.2^{a}	5.8 ± 4.4^{a}	6.2 ± 7.0^{a}
NO_3^{-}, mg L^{-1}	1.1 ± 1.4^{a}	1.8 ± 1.8^{a}	1.5 ± 1.9^{a}	1.0 ± 1.5^{a}
Br, ng L^{-1}	24.4 ± 56.8^{a}	21.2 ± 13^{a}	31.7 ± 39.0^{a}	37.5 ± 43.7^{a}
Mg, µg L^{-1}	3.1 ± 2.4^{a}	4.8 ± 4.2^{a}	5.1 ± 5.1^{a}	6.0 ± 5.8^{a}
Ca, µg L^{-1}	8.4 ± 6.6^{b}	12.2 ± 10.4^{b}	18.1 ± 20^{ab}	32.0 ± 39.1^{a}
Cu, µg L^{-1}	1.0 ± 0.8^{ab}	1.1 ± 0.8^{ab}	1.7 ± 1.1^{a}	1.7 ± 1.0^{a}
Zn, µg L^{-1}	7.4 ± 14.0^{a}	11.9 ± 27.9^{a}	9.2 ± 6.7^{a}	12.3 ± 11.9^{a}
Embeddedness, %	43.5 ± 33.5^{a}	48.4 ± 34.7^{a}	67.1 ± 30.9^{a}	42.5 ± 42.0^{a}
Maximum depth, cm	72.4 ± 26.7^{a}	51.3 ± 18^{ab}	59.3 ± 21.1^{ab}	74.0 ± 40.7^{a}
Average width, m	5.1 ± 4.0^{a}	4.1 ± 3.2^{a}	4.4 ± 2.5^{a}	3.2 ± 1.2^{a}
Average thalweg depth, cm	30.4 ± 18.6^{a}	23.5 ± 8.5^{a}	27.9 ± 17.0^{a}	23.9 ± 10.1^{a}
Average velocity, mm s^{-1}	157.8 ± 131.5^{a}	119.9 ± 144.8^{a}	131 ± 116.7^{a}	234.6 ± 193.0^{a}
B-IBI	4.4 ± 0.3^{a}	3.3 ± 0.3^{b}	2.4 ± 0.2^{c}	1.5 ± 0.1^{d}
Urban, %	11.5 ± 13.9^{a}	13.5 ± 15.3^{a}	21.0 ± 24.3^{a}	30.1 ± 40.8^{a}
Agriculture, %	15.9 ± 17.1^{a}	23.9 ± 22.2^{a}	23.4 ± 22.4^{a}	12.2 ± 24.0^{a}
Forest, %	68.0 ± 22.3^{a}	58.6 ± 23.3^{a}	53.0 ± 27.2^{a}	55.3 ± 41.4^{a}

Values marked with a differing letter are significantly different according to Tukey's HSD test with a $p \leq 0.05$.

Table S4

Spearman's rank correlations of water column respiration rates and physicochemical variables.

	Rho (ρ)	p-value
Conductivity, µmho cm^{-1}	-0.634	0.001
Cl^-, mg L^{-1}	-0.611	0.002
Mg, µg L^{-1}	-0.573	0.004
pH	-0.570	0.005
Ca, µg L^{-1}	-0.537	0.009
Embeddedness, %	0.504	0.014
ANC, µeq L^{-1}	-0.491	0.018
Br, ng L^{-1}	-0.473	0.024
Forest, %	0.467	0.025
Urban, %	-0.467	0.025
PO_4^{3-}, µg L^{-1}	-0.461	0.027
SO_4^{2-}, mg L^{-1}	-0.461	0.028
Shannon diversity	0.458	0.029
NO_3^-, mg L^{-1}	-0.346	0.106
TP, µg L^{-1}	-0.320	0.136
Maximum depth, cm	0.291	0.178
Average thalweg depth, cm	0.289	0.181
DOC, mg L^{-1}	0.270	0.212
N_2O saturation, %	0.210	0.349
Agriculture, %	-0.147	0.502
NO_2^-, µg L^{-1}	-0.146	0.505
B-IBI	-0.116	0.598
NH_3, µg L^{-1}	-0.109	0.620
N_2O, nmol L^{-1}	0.107	0.634
Zn, µg L^{-1}	0.083	0.706
TN, mg L^{-1}	-0.068	0.757
Average width, m	-0.046	0.834
Cu, µg L^{-1}	0.039	0.862
Average velocity, mm s^{-1}	-0.004	0.984

Table S5

Spearman's rank correlations of sediment respiration rates and physicochemical variables.

	Rho (ρ)	p-value
Zn, µg L^{-1}	-0.605	0.007
TP, µg L^{-1}	-0.496	0.032
PO_4^{3-}, µg L^{-1}	-0.464	0.046
Br, ng L^{-1}	0.467	0.046
Average thalweg depth, cm	0.409	0.083
Average width, m	0.347	0.145
DOC, mg L^{-1}	-0.314	0.190
Shannon diversity	-0.305	0.203
N_2O, nmol L^{-1}	0.282	0.288
Cl^-, mg L^{-1}	0.254	0.292
Urban, %	0.251	0.301
N_2O saturation, %	0.250	0.349
Mg, µg L^{-1}	0.200	0.410
Conductivity, µmho cm^{-1}	0.200	0.411
Maximum depth, cm	0.194	0.425
Embeddedness, %	-0.185	0.448
pH	0.181	0.459
NO_3^-, mg L^{-1}	0.128	0.600
NO_2^-, µg L^{-1}	0.125	0.611
ANC, µeq L^{-1}	0.116	0.636
Forest, %	-0.094	0.702
Cu, µg L^{-1}	-0.086	0.726
Agriculture, %	-0.082	0.739
B-IBI	0.069	0.780
Ca, µg L^{-1}	0.068	0.781
NH_3, µg L^{-1}	-0.047	0.847
SO_4^{2-}, mg L^{-1}	0.047	0.848
TN, mg L^{-1}	-0.040	0.871
Average velocity, mm s^{-1}	0.000	1.000

Table S6

Linear least squares regression models of water column Shannon diversity and stream physicochemical variables.

	Slope	Std. error	t-value	p-value	R^2
Embeddedness, %	-0.018	0.002	-7.46	0.000	0.213
Cu, µg L^{-1}	-0.554	0.098	-5.63	0.000	0.133
Average thalweg depth, cm	-0.031	0.006	-5.45	0.000	0.124
DOC, mg L^{-1}	-0.082	0.016	-5.26	0.000	0.117
TP, µg L^{-1}	-11.573	2.346	-4.93	0.000	0.104
Forest, %	0.017	0.004	4.96	0.000	0.101
Average velocity, mm s^{-1}	2.864	0.664	4.32	0.000	0.080
NO_2^-, µg L^{-1}	-63.226	15.265	-4.14	0.000	0.074
Agriculture, %	-0.015	0.005	-3.40	0.001	0.048
Average width, m	-0.084	0.026	-3.18	0.002	0.043
PO_4^{3-}, µg L^{-1}	-13.148	4.956	-2.65	0.009	0.029
Maximum depth, cm	-0.010	0.004	-2.65	0.009	0.029
NH_3, µg L^{-1}	-3.437	1.440	-2.39	0.018	0.023
Urban, %	-0.010	0.005	-1.99	0.048	0.014
B-IBI	0.154	0.095	1.61	0.108	0.008
Cl^-, mg L^{-1}	0.001	0.001	1.35	0.179	0.004
TN, mg L^{-1}	-0.075	0.056	-1.34	0.182	0.004
Conductivity, µmho cm^{-1}	0.000	0.000	1.09	0.276	0.001
Mg, µg L^{-1}	0.025	0.025	1.02	0.309	0.000
SO_4^{2-}, mg L^{-1}	0.002	0.002	0.91	0.366	-0.001
Br, ng L^{-1}	-1.703	2.166	-0.79	0.433	-0.002
pH	0.092	0.120	0.77	0.445	-0.002
Ca, µg L^{-1}	-0.004	0.006	-0.68	0.500	-0.003
ANC, µeq L^{-1}	0.000	0.000	-0.59	0.556	-0.003
Zn, µg L^{-1}	-0.002	0.005	-0.37	0.711	-0.004
NO_3^-, mg L^{-1}	-0.014	0.058	-0.25	0.805	-0.005

Table S7

Linear least squares regression models of sediment Shannon diversity and stream physicochemical variables.

	Slope	Std. error	t-value	p-value	R^2
pH	0.156	0.032	4.81	0.000	0.101
DOC, mg L^{-1}	-0.020	0.005	-4.50	0.000	0.089
NO_3^-, mg L^{-1}	0.043	0.016	2.66	0.009	0.030
B-IBI	0.071	0.027	2.66	0.008	0.029
Embeddedness, %	-0.002	0.001	-2.49	0.013	0.026
TN, mg L^{-1}	0.037	0.016	2.34	0.020	0.022
Agriculture, %	0.003	0.001	1.94	0.054	0.013
Zn, µg L^{-1}	-0.002	0.002	-1.63	0.105	0.008
Average thalweg depth, cm	-0.003	0.002	-1.57	0.118	0.007
Forest, %	-0.002	0.001	-1.52	0.129	0.006
NH_3, µg L^{-1}	0.622	0.413	1.51	0.134	0.006
ANC, µeq L^{-1}	0.000	0.000	1.48	0.141	0.006
Cu, µg L^{-1}	-0.043	0.030	-1.43	0.154	0.005
Br, ng L^{-1}	-0.870	0.611	-1.42	0.156	0.005
Average velocity, mm s^{-1}	0.242	0.200	1.21	0.227	0.002
NO_2^-, µg L^{-1}	5.432	4.534	1.20	0.232	0.002
SO_4^{2-}, mg L^{-1}	-0.001	0.001	-1.19	0.235	0.002
Ca, µg L^{-1}	0.002	0.002	1.04	0.301	0.000
Urban, %	0.001	0.001	0.72	0.471	-0.002
Average width, m	-0.005	0.008	-0.57	0.572	-0.003
PO_4^{3-}, µg L^{-1}	0.538	1.435	0.37	0.708	-0.004
TP, µg L-$^{-1}$	-0.253	0.708	-0.36	0.721	-0.004
Conductivity, µmho cm^{-1}	0.000	0.000	0.12	0.904	-0.005
Maximum depth, cm	0.000	0.001	0.12	0.906	-0.005
Cl^-, mg L^{-1}	0.000	0.000	0.10	0.924	-0.005
Mg, µg L^{-1}	0.000	0.007	0.02	0.984	-0.005

Table S8

Mantel tests using Spearman's rank correlation of water column Bray-Curtis dissimilarities and physicochemical variables.

	Rho (ρ)	p-value
DOC, mg L^{-1}	0.294	0.001
pH	0.255	0.001
Embeddedness, %	0.241	0.001
Zn, µg L^{-1}	0.230	0.001
TP, µg L^{-1}	0.156	0.001
Cu, µg L^{-1}	0.134	0.001
NH_3, µg L^{-1}	0.115	0.001
Br, ng L^{-1}	0.106	0.002
Forest, %	0.104	0.001
Mg, µg L^{-1}	0.095	0.003
B-IBI	0.084	0.001
Ca, µg L^{-1}	0.073	0.023
Average thalweg depth, cm	0.070	0.020
ANC, µeq L^{-1}	0.068	0.032
NO_2^-, µg L^{-1}	0.063	0.053
Conductivity, µmho cm^{-1}	0.050	0.079
Average velocity, mm s^{-1}	0.048	0.057
SO_4^{2-}, mg L^{-1}	0.040	0.109
NO_3^-, mg L^{-1}	0.033	0.159
Urban, %	0.031	0.187
PO_4^{3-}, µg L^{-1}	0.027	0.215
Cl^-, mg L^{-1}	0.019	0.274
Average width, m	0.017	0.290
Agriculture, %	0.011	0.305
Maximum depth, cm	0.006	0.394
TN, mg L^{-1}	-0.011	0.604

Table S9

Mantel tests using Spearman's rank correlation of sediment Bray-Curtis dissimilarities and physicochemical variables.

	Rho (ρ)	p-value
pH	0.388	0.001
DOC, mg L^{-1}	0.301	0.001
Embeddedness, %	0.222	0.001
Zn, µg L^{-1}	0.192	0.001
Average thalweg depth, cm	0.125	0.001
ANC, µeq L^{-1}	0.123	0.001
TP, µg L^{-1}	0.122	0.001
Cu, µg L^{-1}	0.113	0.001
B-IBI	0.111	0.001
Mg, µg L^{-1}	0.11	0.001
Ca, µg L^{-1}	0.102	0.004
Average width, m	0.072	0.016
Forest, %	0.059	0.004
NO_3^-, mg L^{-1}	0.054	0.06
NO_2^-, µg L^{-1}	0.053	0.074
Conductivity, µmho cm^{-1}	0.05	0.092
NH_3, µg L^{-1}	0.05	0.099
PO_4^{3-}, µg L^{-1}	0.04	0.127
Average velocity, mm s^{-1}	0.03	0.185
Agriculture, %	0.026	0.184
SO_4^{2-}, mg L^{-1}	0.015	0.311
TN, mg L^{-1}	0.014	0.319
Br, ng L^{-1}	0.014	0.361
Maximum depth, cm	0.007	0.41
Cl^-, mg L^{-1}	0.004	0.43
Urban, %	0.002	0.457

B. Chapter II Supplemental Materials

Methods

Nitrous oxide mass balance

We used a box model to constrain an N_2O mass balance of the study area. The water column at station M2 was divided into three layers (surface, middle, and bottom): the surface and bottom layers have thicknesses on the order of 10 m and 15 m, respectively; the middle later is thin, on the order of 1 m. Non-conservative advection-diffusion equations describe the evolution of N_2O in a given layer, though not all terms are retained. In the following analysis, we estimate all of the terms from measurements except for the source/sink terms, which we obtain as the residual sum of the estimated terms. This exercise provides insight into the relative roles of physical and biological processes (on the right hand side of the following equations) in the context of observed changes in N_2O concentration (on the left hand side).

The surface layer includes horizontal transport (advection by currents) and vertical turbulent fluxes, both from the layer below and across the sea surface:

$$(1)\quad \underbrace{\mathrm{H}\frac{\partial \mathrm{C}}{\partial \mathrm{t}}}_{\substack{change\ in\\ storage}} = \underbrace{-\mathrm{uH}\frac{\partial \mathrm{C}}{\partial \mathrm{x}}}_{\substack{along-channel\\ advection}} - \underbrace{\mathrm{vH}\frac{\partial \mathrm{C}}{\partial \mathrm{y}}}_{\substack{lateral\\ advection}} - \underbrace{A_z \frac{\partial \mathrm{C}}{\partial \mathrm{z}}\Big|_{z_{sm}}}_{\substack{vertical\ exchange\ with\\ middle\ layer}} - \underbrace{\mathrm{k}\left(\mathrm{C}-\mathrm{C_{eq}}\right)}_{\substack{air-sea\\ exchange}} + \underbrace{S_S}_{source/sink}.$$

We assume in the middle layer that there is a steady-state balance in which the production of N_2O is mixed vertically to the surface and bottom layers, across the interfaces at z_{sm} and z_{mb}, respectively:

$$(2)\ 0 = \underbrace{A_z \frac{\partial C}{\partial z}\Big|_{z_{sm}}}_{\substack{vertical\ exchange\ with\ surface\ layer}} - \underbrace{A_z \frac{\partial C}{\partial z}\Big|_{z_{mb}}}_{\substack{vertical\ exchange\ with\ bottom\ layer}} + \underbrace{S_m}_{\substack{N_2O\ production}} .$$

Finally, the equation that describes the bottom layer includes only along-channel advection (there is no transport directly from the shoals to the deep channel) and turbulent mixing from above. In the absence of sediment porewater concentration data, the benthic flux is lumped into the source/sink term, S_b:

$$(3)\ \underbrace{H\frac{\partial C}{\partial t}}_{\substack{change\ in\ storage}} = \underbrace{-uH\frac{\partial C}{\partial x}}_{\substack{along-channel\ advection}} + \underbrace{A_z \frac{\partial C}{\partial z}\Big|_{z_{mb}}}_{\substack{vertical\ exchange\ with\ middle\ layer}} + \underbrace{S_b}_{\substack{source/sink}} .$$

The notation is: x, y, and z are the along-channel, lateral, and vertical coordinates, positive up-estuary, towards the western shore, and up, respectively; C is the concentration of N_2O; u and v are along-channel and lateral velocities, respectively; H is a layer thickness; A_z is the turbulent diffusivity at the interface between layers; k is the air-sea piston velocity; C_{eq} is the equilibrium concentration. Note that, to reduce notation, all of the terms are

assumed to be layer-specific (that is, u in equation 1 is not the same as u in equation 3), with exception of the diffusive flux terms that couple the equations. The units in the above equations are mass (of N_2O) per area per time.

We estimate the order of magnitude of terms in the above equations from 13 Sept to 15 Sept with the goal of examining whether there is net N_2O consumption or production in the surface and bottom layers and to gain insight into the relative magnitude of biological and physical processes, in light of the large changes in N_2O concentration observed through time. Terms are estimated using a finite difference approximation based on observations (Fig. S4). The concentration gradients are estimated from direct measurements of N_2O, summarized in Table S1. The velocity data are taken from a bottom-mounted current profiler deployed concurrently with the cruise at station M2 (Fig. S5); the details of the deployment of that profiler are identical to those described in Xie et al. 2017 (note that M2 in our study is located at MB in the reference). Finally, estimates of vertical diffusivity are derived from detailed turbulence measurements made close to M2 immediately following the cruise. A turbulence tower instrumented with a vertical array of 6 acoustic doppler velocimeters (ADVs) was deployed at M2 between September 18 – October 29, 2013 as part of a separate project evaluating the role of wind in physical forcing in Chesapeake Bay. That deployment measured vertical profiles of eddy viscosity from direct observations of mean shear and Reynolds stresses (Fisher et al. 2018); we use these eddy viscosity measurements to estimate vertical turbulent diffusivity of dissolved N_2O as a function of wind speed (Fig. S6).

We begin in the middle layer and assess the apparent rate of N_2O production based on observed concentration gradients and turbulent diffusivity (Fig. S4). On 13 Sept, there is a mid-water column peak in N_2O that decreases by 15 Sept, indicating that the pycnocline is a source of N_2O that is mixed into the surface and bottom layers. We used the 13 Sept and N_2O measurements at M2 to estimate the upward and downward concentration gradients, as illustrated in Fig. S4. These are multiplied against the vertical diffusivity: the three-day prior average wind speed was ~3 m s^{-1}, which results in a diffusivity of 10 m^2 d^{-1} in the surface layer and 7 m^2 d^{-1} in the bottom layer. The vertical turbulent flux from the middle layer to the surface layer is O(10 μmol m^{-2} d^{-1}) . The flux of N_2O from the middle layer to the bottom layer is O(11 μmol m^{-2} d^{-1}). Thus, the total source of N_2O within the pycnocline is O(11 μmol m^{-2} d^{-1}), for the one-meter thick layer assumed here, this equated to a source of 21 μmol m^{-3} d^{-1}.

In the surface layer (Fig. S4), the N_2O concentration increased by 1 nM from 13 Sept to 15 Sept; the change in storage term is O(5 μmol m^{-2} d^{-1}), roughly half the vertical flux from the middle layer. The along-channel gradient was -2 nM, decreasing from S2 to N2 over 20 km, with subtidal along-channel advection on the order of -9 cm s^{-1} (mean surface currents flowing seaward, Fig. S5); the along-channel advection term is O(-8 μmol m^{-2} d^{-1}). There was no significant lateral gradient from M3 to M1 and so the lateral advection term is negligible. The reported surface flux values are O(-1 μmol m^{-2} d^{-1}). Combining these, the residual is O(4 μmol m^{-2} d^{-1}), indicating a source of N_2O; for the ten-meter thick layer assumed here, this equates to a source of 0.4 μmol m^{-3} d^{-1}. Note that this value combines

both the error from the order-of-magnitude scaling used to estimate these terms, measurement error, and the true biological signal. It is worth nothing that one of the most sensitive parameters here is the vertical mixing term, as the vertical gradient varies by a factor of two from 13 Sept to 15 Sept. If we were to average in the weaker vertical gradient on 15 Sept, the residual term in the surface layer becomes larger.

In the bottom layer (Fig. S4), the N_2O concentration change was much larger than in the surface, changing by 5 nM from 13 Sept to 15 Sept; this term is O(30 μmol m^{-2} d^{-1}). The along-channel gradient was similar to the surface, -3 nM, decreasing from S2 to N2 over 20 km, but with much larger subtidal along-channel velocities that were ~10 cm s^{-1} (landward, Fig. S5); the along-channel advection term is O(22 μmol m^{-2} d^{-1}). We neglect any lateral transport from the shoals to the deep channel. Vertical mixing from the middle layer provides a source of N_2O that is O(11 μmol m^{-2} d^{-1}). Combining these, the residual is O(-3 μmol m^{-2} d^{-1}); for the 15 m-thick layer assumed here, this equates to a sink: -0.2 μmol m^{-3} d^{-1}. As above, note that this value includes the errors previously noted, as well as the biological processes in both the bottom portion of the water column and the sediments. In the absence of sediment porewater concentrations, the best we can conclude is that, combined, the lower water column and benthic community are collectively a sink of N_2O; the large increase in N_2O concentration is primarily driven by the advection of N_2O-rich waters from the southern portion of the Bay.

Figure S1. Wind speed and direction at NOAA's Gooses Reef buoy (38.56°N, 76.41°W) on 18-31 August 2013 (a) and 6-17 September 2013 (b). Vectors are in the direction the wind is blowing towards. The cruise periods are indicated by the dashed lines.

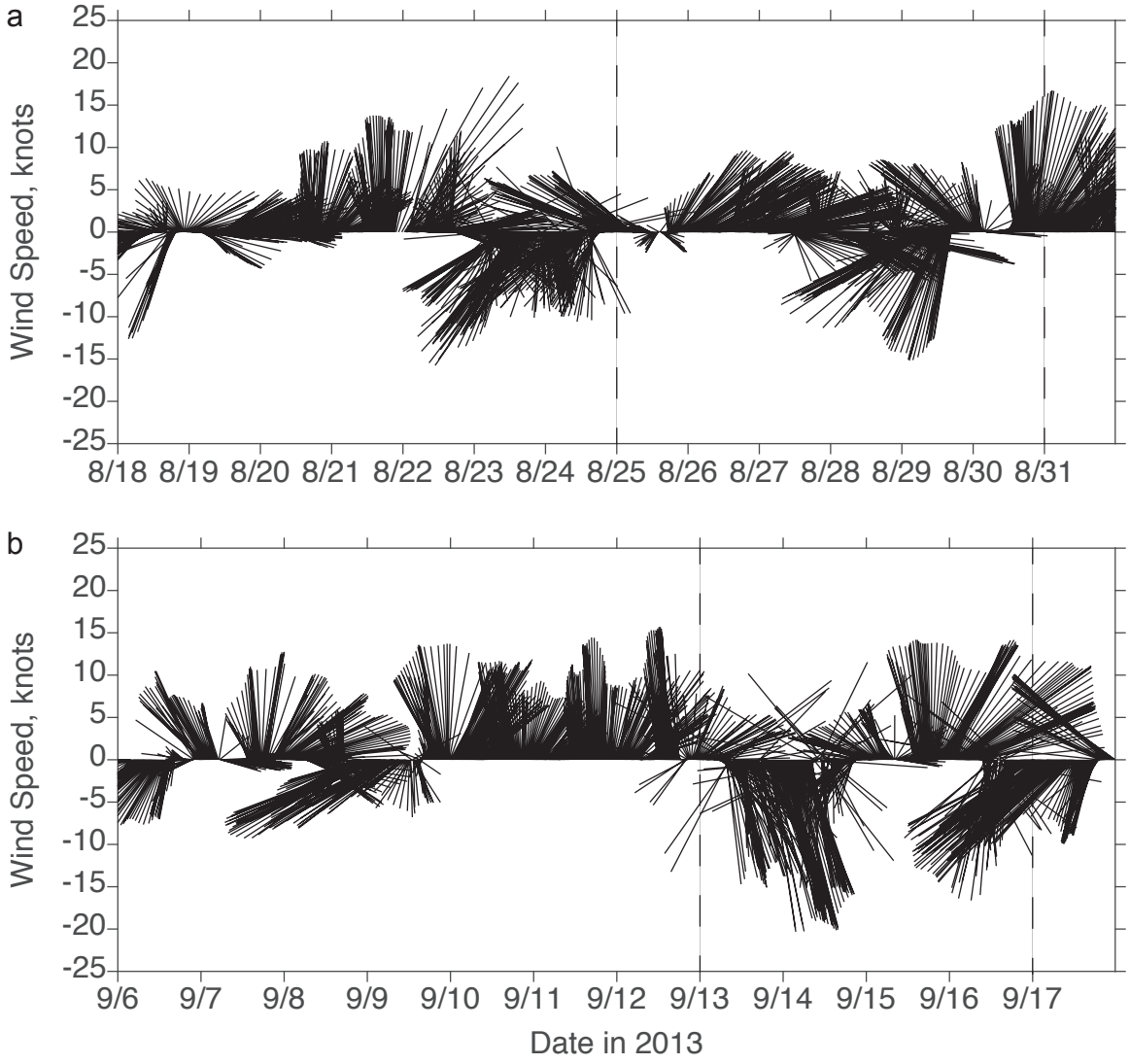

Figure S2. Nitrous oxide atmospheric fluxes at station M2 in August 2013 (a) and September 2013 (b). Calculated from surface N_2O supersaturation and the wind-speed parameterized gas exchange formulation of Ho et al. 2006. Error bars indicate the total uncertainty and are not shown in cases where the error bars are smaller than the symbol.

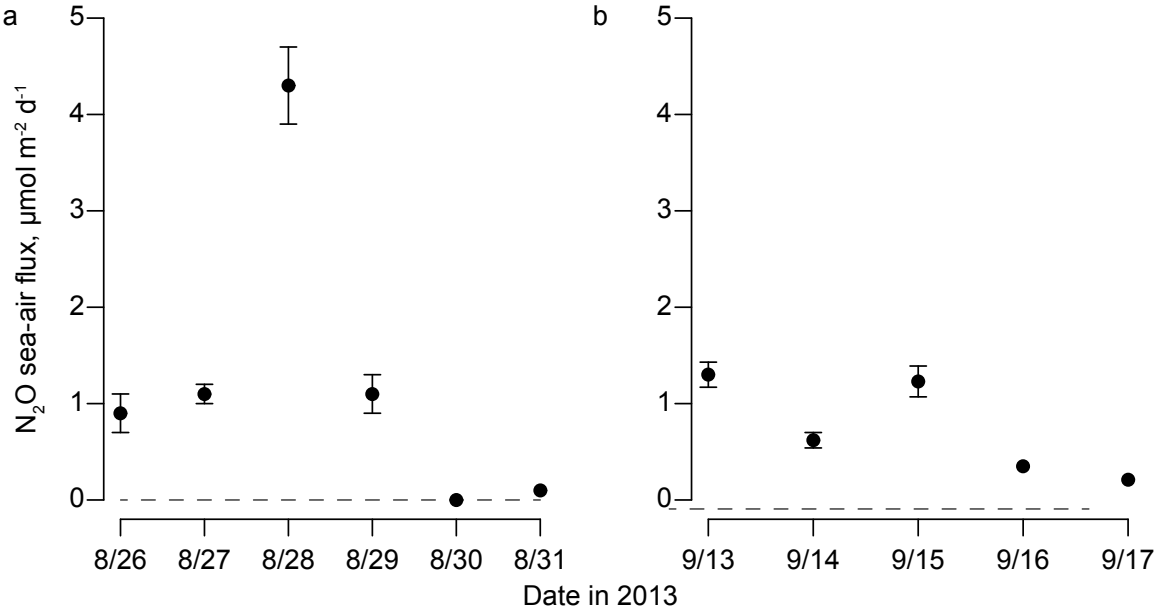

Figure S3. Depth profiles of nitrous oxide (N_2O) (circles), salinity (dashed line), and oxygen concentrations (solid line) at all nine stations on 15 September 2013. Solid circles indicate oversaturation of N_2O with respect to equilibrium with the atmosphere, and open circles indicate undersaturation. Error bars indicate the standard deviation of duplicate samples and are not shown in cases where the error bars are smaller than the symbol.

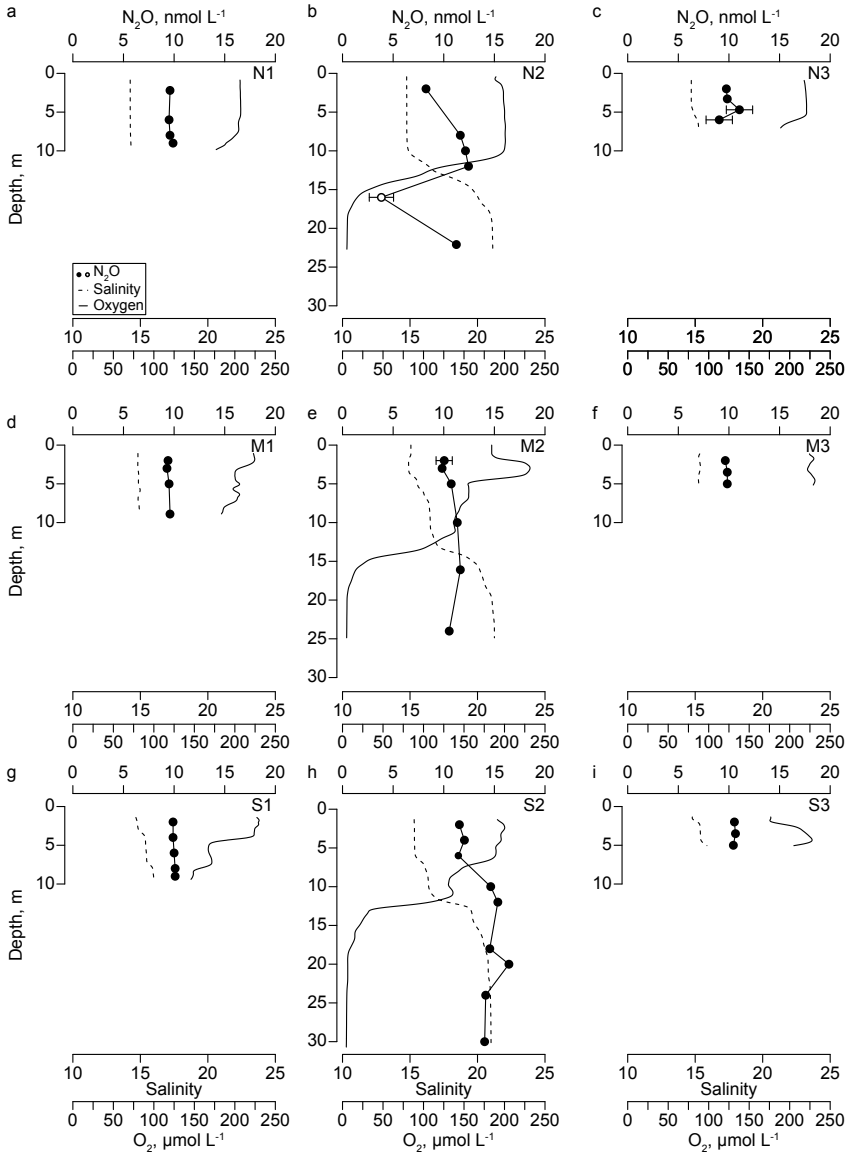

Figure S4. Summary of box model calculations. Profile at left shows representative vertical profile of N_2O (red) and density (blue, as density minus 1000 kg/m^3) from station M2 on 9/13/2013. We conceptualize this water column into surface and bottom layers separated by a thin middle layer. Within the middle layer, N_2O production is balanced by the vertical turbulent transport to the surface and bottom layers. The governing equations for each of the layers is shown in the first column. The values used to estimate the size of each term is shown in the middle column, with some unit conversions omitted for space considerations. The result of the equation is shown at right, indicating a source of N_2O in the upper water column and a small sink in the lower water column and/or sediments. See the supplemental text for further details.

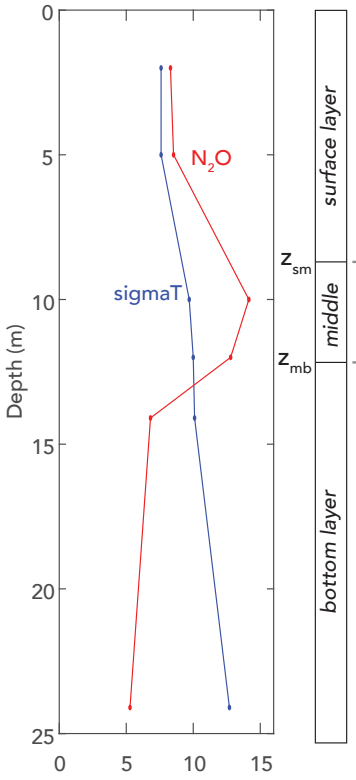

equation	*evaluated as (unit conversion omitted)*	*result in μmol/m²/day*
$H\frac{\partial c}{\partial t} =$	(10 m) $\frac{(1\ \text{nM})}{(2\ \text{days})} =$	5 =
$-uH\frac{\partial c}{\partial x}$	– (-7 cm/s)(10 m) $\frac{(-2\ \text{nM})}{(20\ \text{km})}$	-8
$-k(c - c_{eq})$	– (3 m/h)(8 nM - 7.7 nM)	-1
$-A_z\frac{\partial c}{\partial z}\Big\|_{z_{sm}}$	– (10 m²/day) $\frac{(-5\ \text{nM})}{(5\ \text{m})}$	10
$+S_s$	(by difference)	4
$S_m = -\left(A_z\frac{\partial c}{\partial z}\Big\|_{z_{sm}} - A_z\frac{\partial c}{\partial z}\Big\|_{z_{mb}}\right)$	(opposite of terms above & below)	21
$H\frac{\partial c}{\partial t} =$	(15 m) $\frac{(4\ \text{nM})}{(2\ \text{days})}$	30 =
$-uH\frac{\partial c}{\partial x}$	– (17 cm/s)(15 m) $\frac{(-2\ \text{nM})}{(20\ \text{km})}$	22
$+A_z\frac{\partial c}{\partial z}\Big\|_{z_{mb}}$	– (7 m²/day) $\frac{(8\ \text{nM})}{(5\ \text{m})}$	11
$+S_b$	(by difference)	-3

Figure S5. Subtidal along-channel velocities at M2. (a) Time-mean velocity between 9/13/2013 00:00 UTC and 9/15/2013 02:00 UTC, versus depth of water column. (b) Instantaneous values at six-minute intervals are shown depth-averaged over the surface (upper 10 m, green) and bottom (13-25 m depth, purple) layers. The depth-averaged traces were 25-hour lowpass filtered to produce the thicker lines. Positive is landward. MATLAB was used to determine average surface and bottom velocities of -9 cm/s and 14 cm/s, respectively, between 9/13/2013 00:00 UTC and 9/15/2013 02:00 UTC.

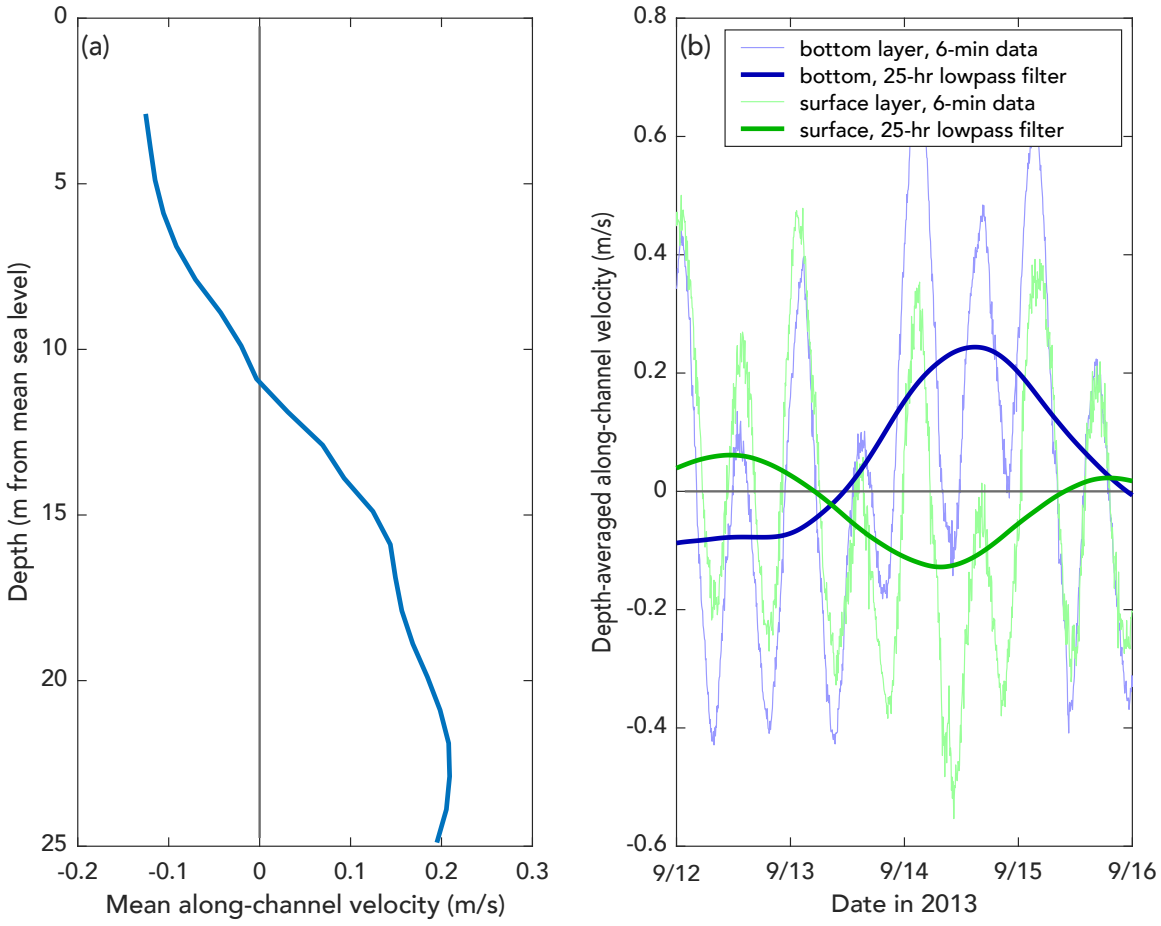

Figure S6. Vertical eddy diffusivity A_z as a function of 3-day prior wind speed. Data derived from separate study as described in the text. Black line shows depth-averaged values over the full 14 m water column. Blue, green, and orange lines aggregate data above, within, and below the pycnocline, respectively. The 0-6 m and 8-14 m aggregations were applied to the surface and bottom layers, respectively, in the N_2O mass balance estimates.

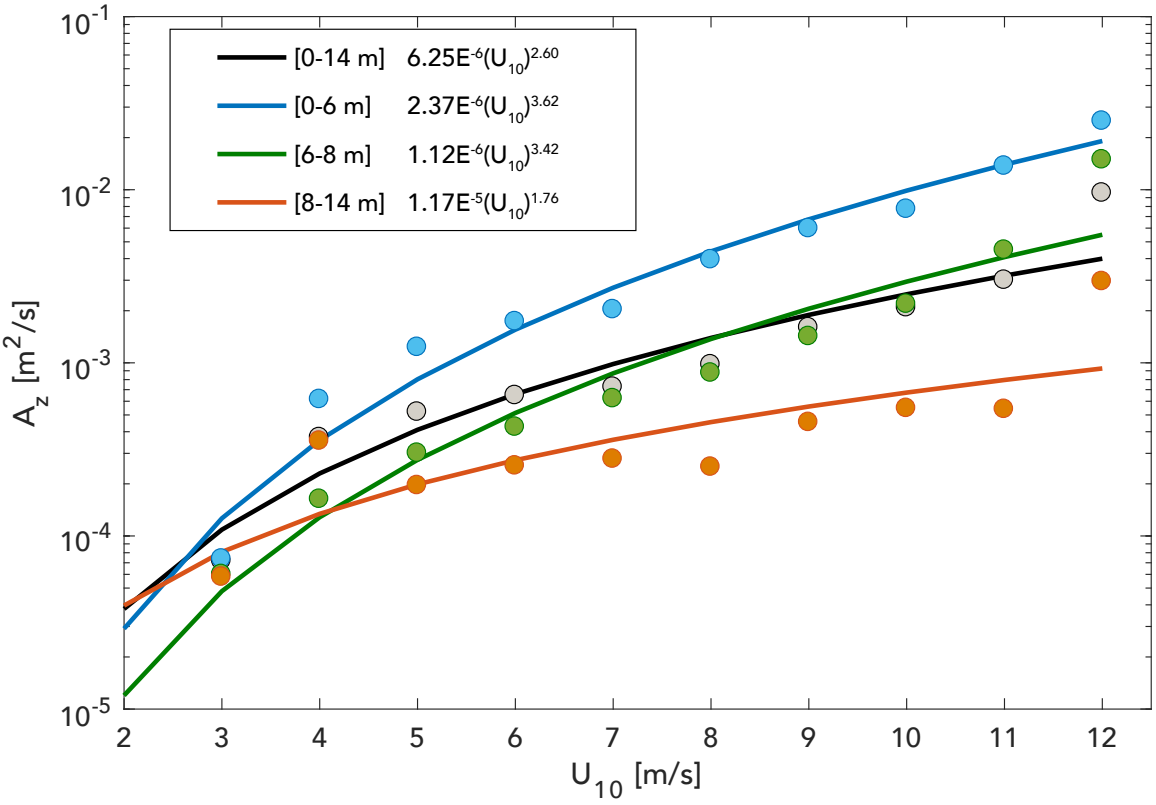

Table S1. Nitrous oxide concentrations (nmol L^{-1}) used to estimate gradients and terms in box model analysis, Fig. S4.

	Station N2		Station M2		Station S2	
	13-Sep	15-Sep	13-Sep	15-Sep	13-Sep	15-Sep
Surface box	8	8	8	9	9	11
Middle box	9	11	14	10	11	14
Bottom box	5	10	6	10	6	13

References

Fisher, Alexander W., Lawrence P. Sanford, and Malcolm E. Scully. 2018. Wind-Wave Effects on Estuarine Turbulence: a comparison of observations and second-moment closure predictions. *Journal of Physical Oceanography* JPO-D-17-0133.1. doi:10.1175/JPO-D-17-0133.1.

Xie, Xiaohui, Ming Li, and William C. Boicourt. 2017. Baroclinic Effects on Wind-Driven Lateral Circulation in Chesapeake Bay. *Journal of Physical Oceanography* 47: 433–445. doi:10.1175/JPO-D-15-0233.1.

C. An intercomparison of oceanic methane and nitrous oxide measurements

Samuel T. Wilson[1*], Hermann W. Bange[2], Damian L. Arévalo-Martínez[2], Jonathan Barnes[3], Alberto V. Borges[4], Ian Brown[5], John L. Bullister[6], Macarena Burgos[1,7], David W. Capelle[8], Michael Casso[9], Mercedes de la Paz[10†], Laura Farías[11], Lindsay Fenwick[8], Sara Ferrón[1], Gerardo Garcia[11], Michael Glockzin[12], David M. Karl[1], Annette Kock[2], Sarah Laperriere[13], Cliff S. Law[14,15], Cara C. Manning[8], Andrew Marriner[14], Jukka-Pekka Myllykangas[16], John W. Pohlman[9], Andrew P. Rees[5], Alyson E. Santoro[13], Philippe D. Tortell[8], Robert C. Upstill-Goddard[3], David P. Wisegarver[6], Guiling L. Zhang[17], Gregor Rehder[12]

[1]University of Hawai'i at Manoa, Daniel K. Inouye Center for Microbial Oceanography: Research and Education (C-MORE), Honolulu, Hawai'i, USA

[2] GEOMAR Helmholtz Centre for Ocean Research Kiel, Düsternbrooker Weg 20 24105 Kiel, Germany

[3]Newcastle University, School of Natural and Environmental Sciences, Newcastle upon Tyne, UK

[4]Université de Liège, Unité d'Océanographie Chimique, Liège, Belgium

[5]Plymouth Marine Laboratory, Plymouth, UK

[6]National Oceanic and Atmospheric Administration, Pacific Marine Environmental Laboratory, Seattle, Washington, USA

[7]Universidad de Cádiz, Instituto de Investigaciones Marinas, Departmento Química-Física Cádiz, Spain

[8]University of British Columbia, Vancouver, Department of Earth, Ocean and Atmospheric Sciences, British Columbia, Canada

[9]U.S. Geological Survey, Woods Hole Coastal and Marine Science Center, Woods Hole, USA

[10]Instituto de Investigaciones Marinas, Vigo, Spain

[11]University of Concepción, Department of Oceanography and Center for climate research and resilience (CR2), Concepción, Chile

[12]Leibniz Institute for Baltic Sea Research Warnemünde, Rostock, Germany

[13]University of California Santa Barbara, Department of Ecology, Evolution, and Marine Biology, Santa Barbara, USA

[14]National Institute of Water and Atmospheric Research (NIWA), Wellington, New Zealand

[15]Department of Chemistry, University of Otago, Dunedin, New Zealand

[16]University of Helsinki, Department of Environmental Sciences, Helsinki, Finland

[17]Ocean University of China, Department of Marine Chemistry, Qingdao, China

[†]Current address: Instituto Español de Oceanografía, Centro Oceanográfico de A Coruña, A Coruña, Spain

Biogeosciences 2018 15, 5891-5907. doi:10.5194/bg-15-5891-2018

Abstract. Large scale climatic forcing is impacting oceanic biogeochemical cycles and is expected to influence the water-column distribution of trace gases including methane and nitrous oxide. Our ability as a scientific community to evaluate changes in the water-column inventories of methane and nitrous oxide depends largely on our capacity to obtain robust and accurate concentration measurements which can be validated across different laboratory groups. This study represents the first formal, international, intercomparison of oceanic methane and nitrous oxide measurements whereby participating laboratories received batches of seawater samples from the subtropical Pacific Ocean and the Baltic Sea. Additionally, compressed gas standards from the same calibration scale were distributed to the majority of participating laboratories to improve the analytical accuracy of the gas measurements. The computations used by each laboratory to derive the dissolved gas concentrations were also evaluated for inconsistencies (*e.g.* pressure and temperature corrections, solubility constants). The results from the intercomparison and intercalibration provided invaluable insights into methane and nitrous oxide measurements. It was observed that analyses of seawater samples with the lowest concentrations of methane and nitrous oxide had the lowest precisions. In comparison, while the analytical precision for samples with the highest concentrations of trace gases was better, the variability between the different laboratories was higher; 36% for methane and 27% for nitrous oxide. In addition, the comparison of different batches of seawater samples with methane and nitrous oxide concentrations that ranged over an order of magnitude revealed the ramifications of different calibration procedures for each trace gas. Overall, this study builds upon the

intercomparison results to develop a framework for improving oceanic methane and nitrous oxide measurements, with the aim of precluding future analytical discrepancies between laboratories.

1. Introduction

The increasing mole fractions of greenhouse gases in the Earth's atmosphere are causing long-term climate change with unknown future consequences. Two greenhouse gases, methane and nitrous oxide, together contribute approximately 23% of total radiative forcing attributed to well-mixed greenhouse gases (Myhre et al., 2013). It is imperative that the monitoring of methane and nitrous oxide in the Earth's atmosphere is accompanied by measurements at the Earth's surface to better inform the sources and sinks of these climatically important trace gases. This includes measurements of dissolved methane and nitrous oxide in the marine environment, which is an overall source of both gases to the overlying atmosphere (Nevison et al., 1995; Anderson et al., 2010; Naqvi et al., 2010; Freing et al., 2012; Ciais et al., 2014).

Oceanic measurements of methane and nitrous oxide are conducted as part of established time-series locations, along hydrographic survey lines, and during disparate oceanographic expeditions. Within low to mid-latitude regions of the open ocean, the surface waters are frequently slightly super-saturated with respect to atmospheric equilibrium for both methane and nitrous oxide. There is typically an order of magnitude range in concentration along a vertical water-column profile at any particular open ocean location (e.g. Wilson et al., 2017). In contrast to the open ocean, near-shore environments, which are subject to river inputs, coastal upwelling, benthic exchange and other processes, have higher concentrations and greater spatial and temporal heterogeneity (e.g. Schmale et al., 2010; Upstill-Goddard and Barnes, 2016).

Methods for quantifying dissolved methane and nitrous oxide have evolved and somewhat diverged since the first measurements were made in the 1960s (Craig and Gordon 1963; Atkinson and Richards 1967). Some laboratories employ purge-and-trap methods for extracting and concentrating the gases prior to their analysis (*e.g*. Zhang et al., 2004; Bullister and Wisegarver, 2008; Capelle et al., 2015; Wilson et al., 2017). Others equilibrate a seawater sample with an overlying headspace gas and inject a fixed volume of the gaseous phase into a gas analyzer (e.g. Upstill-Goddard et al., 1996; Walter et al., 2005; Farias et al., 2009). The purge and trap technique is typically more sensitive by 2-3 orders of magnitude over headspace equilibrium. However, the purge and trap technique requires more time for sample analysis and it is more difficult to automate the injection of samples into the gas analyzer. Headspace equilibrium sampling is most suited for volatile compounds that can be efficiently partitioned into the headspace gas volume from the seawater sample. Its limited sensitivity can be compensated by large volume analysis (*e.g*. Upstill-Goddard et al., 1996). Additional developments for continuous underway surface seawater measurements use equilibrator systems of various designs coupled to a variety of detectors (*e.g*. Weiss et al., 1992; Butler et al., 1989; Gülzow et al., 2011; Arévalo-Martínez et al., 2013). Determining the level of analytical comparability between different laboratories for discrete samples of methane and nitrous oxide is an important step towards improved comprehensive global assessments. Such intercomparison exercises are critical to determining the spatial and temporal variability of methane and nitrous oxide across the world oceans with confidence, since no single laboratory can single-handedly provide all the required measurements at

sufficient resolution. Previous comparative exercises have been conducted for other trace gases *e.g*. carbon dioxide, dimethylsulphide, and sulfur hexafluoride (Dickson et al., 2007; Bullister and Tanhua, 2010; Swan et al., 2014) and for trace elements (Cutter et al., 2013). These exercises confirm the value of the intercomparison concept.

To instigate this process for methane and nitrous oxide, a series of international intercomparison exercises were conducted between 2013 and 2017, under the auspices of Working Group #143 of the Scientific Committee on Oceanic Research (SCOR) (www.scor-int.org). Discrete seawater samples collected from the subtropical Pacific Ocean and the Baltic Sea were distributed to the participating laboratories (Table 1). The samples were selected to cover a representative range of concentrations across marine locations, from the oligotrophic open ocean to highly productive waters, and in some instances sub-oxic, coastal waters. An integral component of the intercomparison exercise was the production and distribution of methane and nitrous oxide gas standards to members of the SCOR Working Group. The intercomparison exercise was conceived and evaluated with the following four questions in mind:

Q1. What is the agreement between the SCOR gas standards and the 'in-house' gas standards used by each laboratory?

Q2. How do measured values of dissolved methane and nitrous oxide compare across laboratories?

Q3. Despite the use of different analytical systems, are there general recommendations to reduce uncertainty in the accuracy and precision of methane and nitrous oxide measurements?

Q4. What are the implications of inter-laboratory differences for determining the spatial and temporal variability of methane and nitrous oxide in the oceans?

2. Methods

2.1 Calibration of nitrous oxide and methane using compressed gas standards

Laboratory-based measurements of oceanic methane and nitrous oxide require separation of the dissolved gas from the aqueous phase, with the analysis conducted on the gaseous phase. Calibration of the analytical instrumentation used to quantify the concentration of methane and nitrous oxide is nearly always conducted using compressed gas standards, the specifics of which vary between each laboratory. Therefore, the reporting of methane and nitrous oxide datasets ought to be accompanied by a description of the standards used, including their methane and nitrous oxide mole fractions, the declared accuracies, and the composition of their balance or 'make-up' gas. For both gases, the highest accuracy commercially available standards have mole fractions close to current day atmospheric values. These standards can be obtained from national agencies including National Oceanic and Atmospheric Administration Global Monitoring Division (NOAA GMD), the National Institute of Metrology China, and the Central Analytical Laboratories of the European Integrated Carbon Observation System Research Infrastructure (ICOS-RI). By comparison,

it is more difficult to obtain highly accurate methane and nitrous oxide gas standards with mole fractions exceeding modern-day atmospheric values. This is particularly problematic for nitrous oxide due to the nonlinearity of the widely used Electron Capture Detector (ECD) (Butler and Elkins, 1991).

The absence of a widely available high mole fraction, high accuracy nitrous oxide gas standard was noted as a primary concern at the outset of the intercomparison exercise. Therefore, a set of high-pressure primary gas standards was prepared for the SCOR Working Group by John Bullister and David Wisegarver at NOAA Pacific Marine and Environmental Laboratory (PMEL). One batch, referred to as Air Ratio Standard (ARS), had methane and nitrous oxide mole fractions similar to modern air and the other batch, referred to as Water Ratio Standard (WRS) had higher methane and nitrous oxide mole fractions for calibration of high concentration water samples. These SCOR primary standards were checked for stability over a 12 month period and assigned mole fractions on the same calibration scale, known as 'SCOR-2016.' A comparison was conducted with NOAA standards prepared on the SIO98 calibration scale for nitrous oxide and the NOAA04 calibration scale for methane. Based on the comparison with NOAA standards, the uncertainty of the methane and nitrous oxide mole fractions in the ARS and the uncertainty of the methane mole fraction in the WRS were all estimated at better than 1%. By contrast, the uncertainty of the nitrous oxide mole fraction in the WRS was estimated at 2-3%. The gas standards were distributed to twelve of the laboratories involved in this study (Table 1). The technical details on the

production of the gas standards and their assigned absolute mole fractions is included in Bullister et al. (2016).

2.2 Collection of discrete samples of nitrous oxide and methane

Dissolved methane and nitrous oxide samples for the intercomparison exercise were collected from the subtropical Pacific Ocean and the Baltic Sea. Pacific samples were obtained on 28 November 2013 and 24 February 2017 from the Hawai'i Ocean Time-series (HOT) long-term monitoring site, Station ALOHA, located at 22.75 N, 158.00 W. The November 2013 samples are included in Figure S1 and S2 in the Supplement, but are not discussed in the main Results or Discussion because fewer laboratories were involved in the initial intercomparison, and the results from these samples support the same conclusions obtained with the more recent sample collections. Seawater was collected using Niskin-like bottles designed by John Bullister (NOAA PMEL), which help minimize contamination of trace gases, in particular chlorofluorocarbons and sulfur hexafluoride (Bullister and Wisegarver, 2008). The bottles were attached to a rosette with a conductivity-temperature-depth (CTD) package. Seawater was collected from two depths: 700 m and 25 m, where the near-maximum and minimum water-column concentrations for methane and nitrous oxide at this location can be found. The 25 m samples were always well within the surface mixed layer, which ranged from 100 to 130 m depth during sampling. Replicate samples were collected from each bottle, with one replicate reserved for analysis at the University of Hawai'i to evaluate variability between sampling bottles. Seawater was dispensed from the

Niskin-like bottles using Tygon® tubing into the bottom of borosilicate glass bottles, allowing overflow of at least two sample volumes and ensuring the absence of bubbles. Most sample bottles were 240 mL in size and were sealed with no headspace using butyl-rubber stoppers and aluminum crimp-seals. A few laboratory groups requested smaller crimp-sealed glass bottles ranging from 20-120 mL in volume and two laboratories used 1 L glass bottles which were closed with a glass stopper and sealed with Apiezon® grease. Seawater samples were collected in quadruplicate for each laboratory. All samples were preserved using saturated mercuric chloride solution (100 μL of saturated mercuric chloride solution per 100 mL of seawater sample) and stored in the dark at room temperature until shipment. The choice of mercuric chloride as the preservative for dissolved methane and nitrous oxide was due to its long history of usage. It is recognized that other preservatives have been proposed (e.g. Magen et al., 2014, Bussmann et al., 2015), however pending a community-wide evaluation of their effectiveness over a range of microbial assemblages and environmental conditions for both methane and nitrous oxide, it is not evident that they are a superior alternative to mercuric chloride.

Samples from the western Baltic Sea were collected during 15-21 October 2016, onboard the R/V *Elisabeth Mann Borgese* (Table 2). Since the Baltic Sea consists of different basins with varying concentrations of oxygen beneath permanent haloclines (Schmale et al., 2010), a larger range of water-column methane and nitrous oxide concentrations were accessible for inter-laboratory comparison compared to Station ALOHA. For all seven Baltic Sea stations, the water-column was sampled into an on-deck

1,000 L water tank that was subsequently subsampled into discrete sample bottles. At three stations (BAL1, BAL3, and BAL6), the water tank was filled from the shipboard high-throughput underway seawater system. For deeper water-column sampling at the stations BAL2, BAL4, and BAL5, the water tank was filled using a pumping CTD system (Strady et al., 2008) with a flow rate of 6 L min^{-1} and a total pumping time of approximately 3 h. For the final deep water-column station, BAL7, the pump that supplied the shipboard underway system was lowered to a depth of 21 m to facilitate a shorter pumping time of approximately 20 mins. Subsampling the water tank for all samples took approximately 1 h in total and the total sampling volume was less than 100 L. To verify the homogeneity of the seawater during the sampling process, the first and last samples collected from the water tank were analyzed by Newcastle University onboard the research vessel. In contrast to the Pacific Ocean sampling, which predominantly used 240 mL glass vials, each laboratory provided their own preferred vials and stoppers for the Baltic Sea samples. Seawater samples were collected in triplicate for each laboratory. All samples were preserved with 100 μL of saturated mercuric chloride solution per 100 ml of seawater sample, with the exception of samples collected by U.S. Geological Survey, who analyzed unpreserved samples onboard the research vessel.

2.3. Sample analysis

Each laboratory measured dissolved methane and nitrous oxide slightly differently. A full description of each laboratory's method can be found in Table S6 and Table S7 in the Supplement for methane and nitrous oxide, respectively.

The majority of laboratories measured methane and nitrous oxide by equilibrating the seawater sample with an overlying headspace and subsequently injecting a portion of the gaseous phase into the gas analyzer. This method has been conducted since the 1960s when gas chromatography was first used to quantify dissolved hydrocarbons (McAuliffe, 1963). The headspace was created using helium, nitrogen, or high-purity air to displace a portion of the seawater sample within the sample bottle. Alternatively, a subsample of the seawater was transferred to a gas-tight syringe and the headspace gas subsequently added. The volume of the vessel used to conduct the headspace equilibration ranged from 20 ml borosilicate glass vials to 1 L glass vials and syringes used by Newcastle University and U.S. Geological Survey, respectively. The dissolved gases equilibrated with the overlying headspace at a controlled temperature for a set period of time that ranged from 20 min to 24 h. The equilibration process was typically enhanced by some initial period of physical agitation. After equilibration, an aliquot of the headspace was transferred into the gas analyzer (GA) by either physical injection, displacement using a brine solution, or injection using a switching valve. Some laboratories incorporated a drying agent and a carbon dioxide scrubber prior to analysis. The gas sample passed through a multi-port injection valve containing a sample loop of known volume, which transferred the gas sample directly

onto the analytical column within the oven of the GA. Calibration of the instrument was achieved by passing the gas standards through the injection valve.

The final gas concentrations using the headspace equilibration method was calculated by:

$$[1] \qquad C_{gas}\ [\text{nmol L}^{-1}] = \left(\beta\ x\ PV_{wp} + \frac{xP}{RT} V_{hs} \right) / V_{wp}$$

where β is the Bunsen solubility of nitrous oxide (Weiss and Price, 1980) or methane (Wiesenburg and Guinasso, 1979) in nmol L^{-1} atm^{-1}, x is the dry gas mole fraction (ppb) measured in the headspace, P is the atmospheric pressure (atm), V_{wp} is the volume of water sample (mL), V_{hs} is the volume (mL) of the created headspace, R is the gas constant (0.08205746 L atm $K^{-1}mol^{-1}$), and T is equilibration temperature in Kelvin (K). An example calculation is provided in Table S8 in the Supplement.

In contrast to the headspace equilibrium method, five laboratories used a purge-and-trap system for methane and/or nitrous oxide analysis (Table S6 and Table S7 in the Supplement). These systems were directly coupled to a Flame Ionization Detector (FID) or ECD, with the exception of University of British Columbia, where a quadrupole mass spectrometer with an electron impact ion source and Faraday cup detector were used (Capelle et al., 2015). The purge-and-trap systems were broadly similar, each transferring the seawater sample to a sparging chamber. Sparging times typically ranged from 5-10 min and the sparge gas was either high purity helium or high purity nitrogen. In addition to

commercially available gas scrubbers, purification of the sparge gas was achieved by passing it through stainless steel tubing packed with Poropak Q and immersed in liquid nitrogen. This is a recommended precaution to consistently achieve a low blank signal of methane. The elutant gas was dried using Nafion or Drierite, and subsequently cryotrapped on a sample loop packed with Porapak Q to aid retention of methane and nitrous oxide. Cryotrapping was achieved for methane using liquid nitrogen (-195^{o}C) and either liquid nitrogen or cooled ethanol (-70^{o}C) for nitrous oxide. Subsequently, the valve was switched to inject mode and the sample loop was rapidly heated to transfer its contents onto the analytical column. Calibration was achieved by injecting standards via sample loops using multi-port injection valves. Injection of standards upstream of the sparge chamber allowed for calibration of the purge-and-trap gas handling system, in addition to the GA. Calculation of the gas concentrations using the purge-and-trap method was achieved by application of the ideal gas law to the standard gas measurements:

[2] $$PV = nRT$$

where P, R, and T are the same as Equation 1, V represents the volume of gas injected (L), and n represents moles of gas injected. Rearranging Equation 2 yields the number of moles of methane or nitrous oxide gas for each sample loop injection of compressed gas standards. These values were used to determine a calibration curve based on the measured peak areas of the injected standards, and thereafter derive the number of moles measured for each unknown sample. To calculate concentrations of methane or nitrous oxide in a water

sample, the number of moles measured were divided by the volume (L) of seawater sample analyzed. An example calculation is provided in Table S8 in the Supplement.

2.4 Data analysis

The final concentrations of methane and nitrous oxide are reported in nmol kg^{-1}. The analytical precision for each batch of samples obtained by each of the individual laboratories was estimated from the analysis of replicate seawater samples and reported as the coefficient of variation (%). The values reported by each laboratory for all the batches of seawater samples are shown in Tables S1 to S4 in the Supplement. Due to the observed inter-laboratory variability, it is likely that the median value of methane and nitrous oxide for each batch of samples does not represent the absolute *in situ* concentration. As this complicates the analytical accuracy for each laboratory, we instead calculated the percentage difference between the median concentration determined for each set of samples and the mean value reported by an individual laboratory. The presence of outliers was established using the Interquartile Range (IQR) and by comparing with one standard deviation applied to the overall median value.

3. Results

3.1 Comparison of methane and nitrous oxide gas standards

Six laboratories compared their existing 'in-house' standards of methane with the SCOR standards. This was done by calibrating in-house standards and deriving a mixing ratio for

the SCOR standards which were treated as unknowns. Four laboratories reported methane values for either the ARS or WRS within 3% of their absolute concentration, whereas two laboratories reported an offset of 6% and 10% between their in-house standards and the SCOR standards (Table S6 in the Supplement). For those laboratories who measured the SCOR standards to within 3% or better accuracy, observed offsets in methane concentrations from the overall median cannot be due to the calibration gas.

Seven laboratories compared their own in-house standards of nitrous oxide with the prepared SCOR standards. Six laboratories reported values of nitrous oxide for the ARS which were within 3% of the absolute concentration, with the remaining laboratory reporting an offset of 10% (Table S7 in the Supplement). The majority of these laboratories (five out of six groups) compared the SCOR ARS with NOAA GMD standards, which have a balance gas of air instead of nitrogen. Some laboratories with analytical systems that incorporated fixed sample loops (*e.g.* 1 or 2 ml loops housed in a 6-port or 10-port injection valve) had difficulty analyzing the WRS, as the peak areas created by the high mole fraction of the standard exceeded the signal typically measured from in-house standards or acquired by sample analysis, by an order of magnitude. The high mole fraction of the WRS was not an issue when multiple sample loops of varying sizes were incorporated into the analytical system, which was the case for purge-and-trap based designs. For the two laboratories with an in-house standard of comparable mole fraction to the WRS, an offset of 3% and a >20% offset was reported.

3.2 Methane concentrations in the intercomparison samples

Overall, median methane concentrations in seawater samples collected from the Pacific Ocean and the Baltic Sea ranged from 0.9 to 60.3 nmol kg^{-1} (Table 2). Out of 101 reported values, 3 outliers were identified using the IQR criterion and were not included in further analysis. The methane data values for each batch of samples analyzed by each laboratory, including the mean and standard deviation, the number of samples analyzed, and the % offset from the overall median value are reported in Table S1 and Table S2 in the Supplement. Analysis conducted by the University of Hawai'i of methane and nitrous oxide from each Niskin-like bottle used in the Pacific Ocean sampling did not reveal any bottle-to-bottle differences. Furthermore, analysis by Newcastle University showed there was no difference between the first and the last set of samples collected from the 1000 L collection used in the Baltic Sea sampling.

The two Pacific Ocean sampling sites had the lowest water-column concentrations of methane (Fig. 1a and 1b). The PAC1 samples collected from within the mesopelagic zone, where methane concentrations have been reported to be less than 1 nmol kg^{-1} (Reeburgh, 2007; Wilson et al., 2017), showed a distribution of reported concentrations skewed towards the higher values. For the PAC1 samples, seven out of twelve laboratories reported values $\leq$1 nmol kg^{-1} and the mean coefficient of variation for all laboratories was 11% (Table 2). In contrast to the mesopelagic samples, the methane concentrations for the near-surface seawater samples (PAC2) were close to atmospheric equilibrium (Fig. 1b). Measured concentrations of methane for PAC2 samples ranged from 1.9 to 3.8 nmol kg^{-1} and the mean

coefficient of variation for all laboratories was 7%. Similar to the PAC1 samples, PAC2 also had a distribution of data skewed towards the higher concentrations.

Three Baltic Sea sampling sites (BAL1, BAL3, and BAL6) had median methane concentrations that ranged from 4.1 to 5.7 nmol kg^{-1} (Fig. 1c). The BAL1 samples also showed a skewed distribution of reported values towards higher concentrations, as seen in PAC1 and PAC2 samples. However, this was not evident in BAL3 or BAL6, which had the closest agreement between the reported methane concentrations. For these three sets of Baltic Sea samples, the mean coefficient of variation for all laboratories ranged from 4% (BAL3) to 9% (BAL1). The next three Baltic Sea samples (BAL4, BAL5, and BAL7) had methane concentrations that ranged from 18.8 to 35.4 nmol kg^{-1} (Fig. 1d). These three sets of samples had a normal distribution of data and the closest agreement between the reported concentrations for all of the Pacific Ocean and Baltic Sea samples. Furthermore, for these three sets of samples, the mean coefficient of variation for all laboratories was 4% (Table 2). The final Baltic Sea sample (BAL2) had the highest concentrations of methane, with a median reported value of 60.3 nmol kg^{-1}, and a large range of values (45.2 to 67.2 nmol kg^{-1}; Fig. 1e). The BAL2 samples had the lowest overall mean coefficient of variation for all laboratories; 2% (Table 2).

Further analysis of the data was conducted to better comprehend the factors that caused the observed inter-laboratory variability in methane measurements. The deviation from median values was calculated for each sample collected from the Baltic Sea (Fig. 2). The Pacific Ocean samples (PAC1 and PAC2) were not included in this analysis due to the

skewed distribution of data. There were also some instances in the Baltic Sea samples, where the median concentration might not have realistically represented the absolute *in situ* methane concentration. This was most likely to have occurred at low concentrations due to the skewed distribution of reported concentrations (*e.g.* BAL1) or at high concentrations where there was a large range in reported values (*e.g.* BAL2). The results revealed that a few laboratories (Datasets D, F, and G) were consistently within or close to 5% of the median value for all batches of seawater samples (Fig. 2). Some laboratories (*e.g*. Datasets B, C, and H) had a higher deviation from the median value at higher methane concentrations. Two laboratories (Datasets J and K) had a higher deviation from the median value at lower methane concentrations. Finally, in some cases it was not possible to determine a trend (Datasets A and E), due to the variability.

The reasons behind the trends for each dataset became more apparent when considering the effect of the inclusion or exclusion of low standards in the calibration curve on the resulting derived concentrations (Fig. 3). The FID has a linear response to methane at nanomolar values and therefore a high level of accuracy across a relatively wide range of *in situ* methane concentrations can be obtained with the correct slope and intercept. To demonstrate this, calibration curves for methane were provided by the University of Hawai'i. These revealed minimal variation in the slope value when calibration points were increased from low mole fractions (Fig. 3a) to higher mole fractions (Fig. 3b). However, the intercept value was sensitive to the range of calibration values used, and this effect was further exacerbated when only the higher calibration points were included (*i.e*. Fig. 3c). The

relevance to final methane concentrations is demonstrated by considering the values reported by the University of Hawai'i for PAC2 samples (Fig. 1b). An almost 30% increase in final methane concentration occurs from the use of the calibration equation in Figure 3c, compared to Figure 3a. This derives from a measured peak area for methane of 62 for a sample with a volume of 0.076 L and a seawater density of 1024 kg m^{-3}, yielding a final methane concentration of 2.1 and 2.8 nmol kg^{-1} using the equations from Figure 3a and 3c, respectively. With this understanding on the effect of FID calibration, we consider it likely that the increased deviation from median values at high methane concentrations (Datasets B, C, and H) results from differences in calibration slope between each laboratory. In contrast, the datasets with a higher offset at low methane concentrations (Datasets J and K) could be due to erroneous low standard values causing a skewed intercept. In addition, there may be other factors including sample contamination, discussed in Section 3.4.

3.3 Nitrous oxide concentrations in the intercomparison samples

Overall, median nitrous oxide concentrations in seawater samples collected from the Pacific Ocean and the Baltic Sea ranged from 3.4 to 42.4 nmol kg^{-1} (Table 2). Of the 113 reported values, ten outliers were identified using the IQR criterion and were not included in further analysis. The nitrous oxide data values for each batch of samples analyzed by each laboratory, including the mean and standard deviation, the number of samples analyzed, and the % offset from the overall median value are reported in Table S3 and Table S4 in the Supplement.

For six sets of seawater samples, BAL1, BAL2, BAL3, BAL6, BAL7, and PAC2, the concentrations of nitrous oxide were close to atmospheric equilibrium. The reported values ranged from 7.7 to 12.7 nmol kg^{-1} in the Baltic Sea (Fig. 4a) and from 5.9 to 7.6 nmol kg^{-1} in the Pacific Ocean (Fig. 4b). For the Pacific Ocean near-surface (mixed layer) sampling site (PAC2), the theoretical value of nitrous oxide concentration in equilibrium with the overlying atmosphere is also shown (Fig. 4b). For these six samples with concentrations close to atmospheric equilibrium, the mean coefficient of variation for all laboratories ranged from 3% (BAL3 and PAC2) to 5% (BAL1) (Table 2).

For the three other sets of samples (BAL4, BAL5, and PAC1), the nitrous oxide concentrations deviated significantly from atmospheric equilibrium (Fig. 4c, 4d, and 4e). At one sampling site, BAL4 (Fig. 4c), nitrous oxide was under-saturated with respect to atmospheric equilibrium and reported concentrations ranged from 2.1–5.5 nmol kg^{-1}. As observed in the low concentration Pacific Ocean methane samples, there was a skewed distribution of the data towards the higher nitrous oxide concentrations. The BAL4 samples also had the highest variability (*i.e*. lowest precision), with a mean coefficient of variation of 8% (Table 2). The two remaining samples (PAC1 and BAL5) had much higher concentrations of nitrous oxide, as expected for low-oxygen regions of the water-column. In contrast to the samples with near atmospheric equilibrium concentrations of nitrous oxide, there was a low overall agreement between the independent laboratories for PAC1 and BAL5 nitrous oxide concentrations (Fig. 4d, 4e). At PAC1 and BAL5, nitrous oxide concentrations ranged from 34.3–45.8 nmol kg^{-1} (Fig. 4d) and 30.1–45.9 nmol kg^{-1},

respectively (Fig. 4e). The mean coefficient of variation for all laboratories was 4% for BAL5 samples compared to 3% for PAC1 samples.

The deviation of individual nitrous oxide concentrations from the median value provides insight into the variability associated with their measurements (Fig. 5). The BAL1 dataset was not included in this analysis due to its skewed data distribution and the high inter-laboratory variability for BAL5 indicated that the median value may differ from the absolute nitrous oxide concentration for this sample. For the low nitrous oxide Baltic Sea and Pacific Ocean samples (Fig. 5a), the majority of data points were within 5% of the median values. Furthermore, for the majority of laboratories, the data points for separate seawater samples clustered together indicating some consistency to the extent they varied from the overall median value. Exceptions to this observation include Datasets E, C, L, and K (Fig. 5a) which demonstrated varying precision and accuracy. At high nitrous oxide concentrations (Fig. 5b), there are fewer data points within 5% of the median value compared to low nitrous oxide concentrations (Fig. 5a). Therefore, for PAC1 and BAL5 samples, 6 and 7 data points fall within 5% of the median value, respectively. Furthermore, only three laboratories (Datasets F, G, and K) had data for both Pacific Ocean and Baltic Sea samples within 5% of the median value. This could have been caused by inconsistent analysis between different batches of samples or by variable sample collection and transportation.

The likely factors that caused these offsets in nitrous oxide concentrations among laboratories include sample analysis and calibration of the gas analyzers. Calibration of the ECD is nontrivial and at least two prior publications have discussed nitrous oxide calibration

issues (Butler and Elkins, 1991; Bange et al., 2001). The laboratories participating in the nitrous oxide intercomparison employed different calibration procedures (Fig. 6). Some used a linear fit and kept their analytical peak areas within a narrow range (Fig. 6a), while others used a step-wise linear fit and therefore used different slopes for low and high nitrous oxide mole fractions (Fig. 6b). Finally, some applied a polynomial curve (Fig. 6c) and sometimes two different polynomial fits, for low and high concentrations. The difficulty in calibrating the ECD was evidenced by the deviation from median values as multiple datasets show good precision but consistent offsets at the lowest (Fig. 5a) and highest (Fig. 5b) final concentrations of nitrous oxide.

3.4 Sample storage and sample bottle size

Because prolonged storage of samples can influence dissolved gas concentrations, including methane and nitrous oxide, the intercomparison dataset was analyzed for sample storage effects (Table S5 in the Supplement). It should, however, be noted that assessing the effect of storage time on sample integrity was not a formal goal of the intercomparison exercise and replicate samples were not analyzed at repeated intervals by independent laboratories, as would normally be required for a thorough analysis. Nonetheless our results did provide some insights into potential storage-related problems. Most notably, there were indications that an increase in storage time caused increased concentrations and increased variability for methane samples with low concentrations, *i.e*. PAC1 and PAC2 samples which had median methane concentrations of 0.9 and 2.3 nmol kg^{-1}, respectively (Fig. 7). In

comparison, for samples of nitrous oxide with low concentrations there was no trend of increasing values as observed for samples with low methane concentrations.

Another variable which differed between laboratories for the intercomparison exercise was the size of samples bottle, which ranged from 25 ml to 1 liter for the different laboratories. There was no observed difference between the methane and nitrous oxide values obtained from the various sampling bottles and it was concluded that sampling bottles were not a controlling factor for the observed differences between laboratories. We note, however, the potential for greater air bubble contamination in smaller bottles.

4. Discussion

The marine methane and nitrous oxide analytical community is growing. This is reflected in the increasing number of corresponding scientific publications and the resulting development of a global database for methane and nitrous oxide (Bange et al., 2009). Like all Earth observation measurements, there is a need for intercomparison exercises of the type reported here, for data quality assurance, and for appropriate reporting practices (National Research Council, 1993). To the best of our knowledge, the work presented here is the first formal intercomparison of dissolved methane and nitrous oxide measurements. Based on our results, we discuss the lessons learned and our recommendations moving forward, by addressing the four questions that were posed in the Introduction.

4.1 What is the agreement between the SCOR gas standards and the 'in-house' gas standards used by each laboratory?

It is typical for laboratories to source some, or all, of their compressed gas standards from commercial suppliers. National agencies, such as NOAA GMD or National Institute of Metrology China, also provide standards to the scientific community. The national agencies typically offer a lower range in concentrations than commercial suppliers, but their standards tend to have a higher level of accuracy. Of the twelve laboratories participating in the intercomparison, eight reported using national agency standards, with seven of them using gases sourced from NOAA GMD. Since the methane and nitrous oxide mole fractions of these national agency standards are equivalent to modern-day atmospheric mixing ratios, they are similar to the SCOR ARS distributed to the majority of laboratories in this study. Laboratories in receipt of the SCOR standards were asked to predict their mole fractions based on those of their own in-house standards. For the majority that conducted this exercise, there was good agreement (<3% difference) between the NOAA GMD and the SCOR ARS for both methane and nitrous oxide. For three laboratories, a larger offset was observed between the NOAA GMD and the SCOR ARS. There was also a good prediction for the higher methane content SCOR WRS, facilitated by the linear response of the FID (Fig. 3). In contrast, the nitrous oxide mole fraction in the SCOR WRS exceeded the typical working range for several laboratories and it was difficult for them to cross-compare with their in-house standards. This reflects an analytical set-up that involves on-column injection via a 6-port or 10-port valve with one or two sample loops, respectively. The sample loops have a fixed volume and their inaccessibility makes it difficult to replace them by a smaller loop size. Therefore either dilution of the standard is required, or smaller loops need to be

incorporated into the calibration protocol. The two laboratories that compared their in-house standards with the SCOR WRS reported an offset of 3% and >20%. This indicates that variability between standards can be an issue for obtaining accurate dissolved concentrations and provides support for the production of a widely available high concentration nitrous oxide standard. We strongly recommend that all commercially obtained standards are cross-checked against primary standards, such as the SCOR ARS and WRS. This should be conducted at least at the beginning and end of their use to detect any drift that may have occurred during their lifetime. With due diligence and care, the SCOR standards provide the capability for cross-checking personal standards for years to decades (Bullister et al., 2016).

4.2 How do measured values of methane and nitrous oxide compare across laboratories? Methane: The methane intercomparison highlighted the variability that exists between measurements conducted by independent laboratories. At low methane concentrations, a skewed distribution of methane data was observed, which was particularly evident in PAC1 (Fig. 1a). Potential causes include calibration procedures (Section 3.2) and/or sample contamination which is more prevalent at low concentrations (Section 3.4). For some laboratories, the low methane concentrations are close to their detection limit, which is determined by the relatively low sensitivity of the FID and the small number of moles of methane in an introduced headspace equilibrated with seawater. An approximate working detection limit for methane analysis via headspace equilibration is 1 nmol kg^{-1},

although some laboratories improve upon this by having a large aqueous: gaseous phase ratio during the equilibration process (*e.g*. Upstill-Goddard et al., 1996). Depending upon the volume of sample analyzed, purge-and-trap analysis can have a detection limit much lower than 1 nmol kg^{-1} (*e.g*. Wilson et al., 2017). Methane measurements in aquatic habitats with methane concentrations near the limit of analytical detection include mesopelagic and high latitude environments distal from coastal or benthic inputs (*e.g*. Rehder et al., 1999; Kitidis et al., 2010; Fenwick et al., 2017). Of additional concern is that the skewed distribution of methane concentrations also occurs in samples collected both from the surface ocean (PAC2; Fig. 1b) and coastal environments (BAL1; Fig. 1c). Methane concentrations between 2–6 nmol kg^{-1} are within the detection limit of all participating laboratories. To address this we recommend that laboratories restrict sample storage to the minimum time required to analyze the samples and incorporate internal controls into their sample analysis (Section 4.4).

There was an improvement in the overall agreement between the laboratories for samples with higher methane concentrations. However, some of the highest variability between the laboratories was observed at the highest concentrations of methane analyzed (BAL2; Fig. 1e). This high degree of variability resulted in significant uncertainty in the absolute *in situ* concentration. Methane concentrations of this magnitude and higher are found in coastal environments (Zhang et al., 2004; Jakobs et al., 2014; Borges et al., 2017) and in the water-column associated with seafloor emissions (*e.g*. Pohlman et al., 2011). These environments are considered vulnerable to climate induced changes and

eutrophication, and therefore it is necessary that independent measurements are conducted to the highest possible accuracy to allow for inter-laboratory and inter-habitat comparisons. To address this we recommend that reference material be produced and distributed between laboratories.

Nitrous oxide: Some of the trends discussed for methane were also evident in the nitrous oxide data. For the samples with the lowest nitrous oxide concentrations a skewed data distribution was observed, as found for methane (Fig. 4c). Such low nitrous oxide concentrations are typical of low-oxygen water-column environments (<10 μmol kg^{-1}). Therefore, the analytical bias towards measuring values higher than the absolute *in situ* concentrations is particularly pertinent to oceanographers measuring nitrous oxide in oxygen minimum zones and other low-oxygen environments (Naqvi et al., 2010; Farías et al., 2015; Ji et al., 2015). The low concentrations of nitrous oxide still exceed detection limits by at least an order of magnitude for even the less-sensitive headspace method due to the high sensitivity of the ECD. Therefore, the bias towards reporting elevated values for low concentrations of nitrous oxide is related less to analytical sensitivity and is more a consequence of calibration issues. During the intercomparison exercise ECD calibration was identified as a nontrivial issue for all participating laboratories and it deserves continuing attention. In particular, the nonlinearity of the ECD means that low and high nitrous oxide concentrations are more vulnerable to error since the values fall outside of the most frequented part of the calibration curve. This is particularly true if a linear fit is used to

calibrate the ECD (Fig. 6a). To circumvent this problem, one laboratory used a step-wise linear function while other laboratories used a quadratic function. The usefulness of multiple calibration curves for low and high nitrous oxide concentrations was highlighted during the intercomparison exercise, although this necessitates some consideration of the threshold for switching between different calibration curves.

The majority of seawater samples analyzed had nitrous oxide concentrations ranging from 7–11 nmol kg^{-1} (Fig. 4a, 4b), which are close to atmospheric equilibrium values, as shown for the Pacific Ocean (Fig. 4b). Collective analysis of these samples gives insight into the precision and accuracy associated with surface water nitrous oxide analysis (Fig 5a). This is discussed further in the context of implementing internal controls for methane and nitrous oxide (Section 4.4). For samples with the highest nitrous oxide concentrations, *i.e.* exceeding 30 nmol kg^{-1}, there was high variability between the concentrations reported by the independent laboratories. This was most evident for the BAL5 samples (Fig. 4e) and similar to the variability observed at the highest methane concentrations analyzed (Fig. 1e). It is difficult to assess how much of this variability was specifically due to the differences in calibration practices between the laboratories and the differences in gas standards with high nitrous oxide mole fractions, but at least some of it can be attributed to this. These results form the basis for a proposed production of reference material for both trace gases.

4.3 Are there general recommendations to reduce uncertainty in the accuracy and precision of methane and nitrous oxide measurements?

There are several analytical recommendations resulting from this study. The use of highly accurate standards and the appropriate calibration fit is an essential requirement for both headspace equilibration and the purge-and-trap technique. It was shown that both analytical approaches can yield comparable values for methane and nitrous oxide, with the main differences observed at low methane concentrations. At sub-nanomolar methane concentrations, four out of the six laboratories that reported methane concentrations <1 nmol kg^{-1} used a purge-and-trap analysis.

This study also revealed that sample storage time can be an important factor. Specifically, the results from this study corroborate the findings of Magen et al. (2014) who showed that samples with low concentrations of methane and more susceptible to increased values as a result of contamination. The contamination was most likely due to the release of methane and other hydrocarbons from the septa (Niemann et al., 2015). Since the release of hydrocarbons occurs over a period of time, it is recommended to keep storage time to a minimum and to store samples in the dark. It should be noted that sample integrity can also be compromised due to other factors including inadequate preservation, outgassing, and adsorption of gases onto septa. For all these reasons, it is recommended to conduct an evaluation of sample storage time for the environment that is being sampled.

One useful item that was not included as part of the intercomparison exercise but can help decrease uncertainty in the accuracy and precision of methane and nitrous oxide measurements are internal control measurements. Internal controls represent a self-assessment quality control check to validate the analytical method and quantify the

magnitude of uncertainty. Appropriate internal controls for methane and nitrous oxide consist of air-equilibrated seawater samples. Their purpose is to provide checks for methane concentrations ranging from 2–3 nmol kg^{-1} and for nitrous oxide concentrations from 5–9 nmol kg^{-1}. The air used in the equilibration process could be sourced from the ambient environment if sufficiently stable or from a compressed gas cylinder after cross-checking the concentration with the appropriate gas standard. Air-equilibrated samples provide reassurance that the analytical system is providing values within the correct range. Air-equilibrated samples also indicate the certainty associated with calculating the saturation state of the ocean with respect to atmospheric equilibrium. This is particularly relevant when the seawater being sampled is within a few percent of saturation. Finally, these air-equilibrated samples provide an estimate of analytical accuracy, which is infrequently reported for methane or nitrous oxide. At present, only a few studies report the analysis of air-equilibrated seawater alongside water-column samples (Bullister and Wisegarver, 2008; Capelle et al., 2015; Bourbonnais et al., 2017; Wilson et al., 2017). It is likely that wider implementation would facilitate internal assessment of the analytical system. Since the main equipment required is a water-bath and an overhead stirrer, the production is not cost-prohibitive. A recommendation of this intercomparison exercise is that laboratories routinely use air-equilibrated seawater samples to provide an estimate of analytical accuracy.

In addition to the self-assessments provided by the analysis of air-equilibrated seawater, this study revealed the need for reference seawater to help assess the accuracy of high

concentration methane and nitrous oxide measurements. Reference seawater in this instance refers to batches of dissolved methane and nitrous oxide samples prepared in the laboratory using an equilibrator set-up, as used for dissolved inorganic carbon (Dickson et al., 2007). In the absence of plans for additional intercomparison exercises, the provision of reference seawater will allow laboratories to continue evaluating their own measurements. Finally, the lessons learned during the intercomparison exercises will be the basis for a forthcoming Good Practice Guide for dissolved methane and nitrous oxide.

4.4 What are the implications of interlaboratory differences for determining the spatial and temporal variability of methane and nitrous oxide in the oceans?

The key outcome of this study was the identification of differences in methane and nitrous oxide concentrations for the same batch of seawater samples measured by several independent laboratories. Emergent from this is the distinct possibility that any given laboratory will incorrectly report data, thereby increasing uncertainty over the saturation states of both gases. The tendency to over-estimate methane concentrations close to atmospheric equilibrium means that marine emissions of methane to the overlying atmosphere will be also overestimated (Bange et al., 1994; Upstill-Goddard and Barnes, 2016). In contrast, for nitrous oxide there does not appear to be either an under-estimation or over-estimation of concentrations. Consequently, there is generally a lower inherent uncertainty in its surface ocean saturation state, as previously proposed (Law and Ling, 2001; Forster et al., 2009).

The inter-laboratory differences highlighted by this study should be viewed in the context of numerous individual efforts to assess temporal and/or spatial trends in methane and nitrous oxide by way of time-series observations (Bange et al., 2010; Farías et al., 2015; Wilson et al., 2017; Fenwick and Tortell, 2018), repeat hydrographic survey lines (de la Paz et al., 2017), and single expeditions. While the value of these in integrating the behaviour of methane and nitrous oxide into the hydrography and biogeochemistry of local-regional ecosystems is beyond question, their value would be enhanced by the rigorous cross-validation of analytical protocols. Without this, perceived small temporal and/or spatial changes in water-column concentrations in any given region are difficult to verify unless the data all originate from a single laboratory. In addition, the value of a global methane and nitrous oxide database (*e.g* Bange et al., 2009) would to some extent be compromised by the uncertainty. Taking due account of the analytical variability between laboratories will clearly be vital to any future assessment of the changing methane and nitrous oxide budgets of the oceans.

5. Conclusions

Overall, the intercomparison exercise was invaluable to the growing community of ocean scientists interested in understanding the dynamics of dissolved methane and nitrous oxide in the water-column. The level of agreement between independent measurements of dissolved concentrations was evaluated in the context of several contributing factors, including sample analysis, standards, calibration procedures, and sample storage time.

Importantly, the intercomparison represents a concerted effort from the scientists involved to critically assess the quality of their data, and to initiate the steps required for further improvements. Recommendations arising from the intercomparison include routine cross-calibration of working gas standards against primary standards, minimizing sample storage time, incorporating internal controls (air-equilibrated seawater) alongside routine sample analysis, and the future production of reference seawater for methane and nitrous oxide measurements. These efforts will help resolve temporal and spatial variability, which is necessary for constraining methane and nitrous oxide emissions from aquatic ecosystems and for evaluating the processes that govern their production and consumption in the water-column.

Acknowledgements:

During the final stages of this work, our coauthor John Bullister passed away. The intercomparison exercise greatly benefited from John's scientific expertise on dissolved gases. He will be greatly missed by the oceanographic community.

The methane and nitrous oxide intercomparison exercise was conducted as a Scientific Committee on Ocean Research (SCOR) Working Group which receives funding from the U.S. National Science Foundation (OCE-1546580). Pacific Ocean seawater samples were collected on HOT cruises which are supported by NSF (including the most recent OCE-1260164 to DMK). Baltic Sea seawater samples were collected during Cruise #142 of the RV *Elisabeth Mann Borgese*, with the ship-time provided by the Leibniz Institute for Baltic Sea Research Warnemünde. We thank Liguo Guo for help with sampling during the Baltic Sea cruise. The methane and nitrous oxide gas standards were produced via a Memorandum of Understanding between the University of Hawai'i and NOAA-PMEL. Funding for the gas standards was provided by for the Center for Microbial Oceanography: Research and Education (C-MORE; EF0424599 to DMK), SCOR, the EU FP7 funded Integrated non-CO_2 Greenhouse gas Observation System (InGOS) (Grant Agreement #284274), and NOAA's Climate Program Office, Climate Observations Division. Additional support was provided by the Gordon and Betty Moore Foundation #3794 (DMK), the Simons Collaboration on Ocean Processes and Ecology (SCOPE; #329108 to DMK), and the Global Research Laboratory Program (# 2013K1A1A2A02078278 to DMK) through the National Research Foundation of Korea (NRF). AVB is a senior research associate at the FRS-FNRS. AES

would like to acknowledge NSF OCE-1437310. MP would like to acknowledge the support of the Spanish Ministry of Economy and Competitiveness (CTM2015-74510-JIN). LF received financial support by FONDAP 1511009 and FONDECYT N°1161138. Any use of trade names is for descriptive purposes and does not imply endorsement by the U.S. government

References

Anderson, B., Bartlett, K., Frolking, S., Hayhoe, K., Jenkins, J., and Salas, W.: Methane and nitrous oxide emissions from natural sources, Office of Atmospheric Programs, US EPA, EPA 430-R-10-001, Washington DC, 2010.

Arévalo-Martínez, D. L., Beyer, M., Krumbholz, M., Piller, I., Kock, A., Steinhoff, T., Körtzinger, A., and Bange, H. W.: A new method for continuous measurements of oceanic and atmospheric N_2O, CO and CO_2: performance of off-axis integrated cavity output spectroscopy (OA-ICOS) coupled to non-dispersive infrared detection (NDIR), Ocean Sci., 9, 1071–1087, 2013.

Atkinson, L. P., and Richards, F. A.: The occurence and distribution of methane in the marine environment, Deep-Sea Res., 14, 673–684, 1967.

Bange, H. W., Bartell, U. H. , Rapsomanikis, S., and Andreae, M. O.: Methane in the Baltic and North Seas and a reassessment of the marine emissions of methane, Global Biogeochem. Cycles, 8, 465–480, doi:10.1029/94GB02181, 1994.

Bange, H. W., Rapsomanikis, S., and Andreae, M. O.: Nitrous oxide cycling in the Arabian Sea, J. Geophys. Res.: Oceans, 106, 1053–1065, 2001.

Bange H.W, Bell, T.G., Cornejo, M., Freing, A., Uher, G., Upstill-Goddard, R.C., and Zhang G. MEMENTO: a proposal to develop a database of marine nitrous oxide and methane measurements. Env. Chem, 6, 195–197, 2009.

Bange, H.W., Bergmann, K., Hansen, H.P., Kock, A., Koppe, R., Malien, F., and Ostrau, C.: Dissolved methane during hypoxic events at the Boknis Eck Time Series Station (Eckernförde Bay, SW Baltic Sea), Biogeosciences., 7, 1279–1284, 2010.

Borges, A.V., Speeckaert, G., Champenois, W., Scranton, M.I., and Gypens, N.: Productivity and temperature as drivers of seasonal and spatial variations of dissolved methane in the Southern Bight of the North Sea, Ecosystems, 1–17, 2017.

Bourbonnais, A., Letscher, R. T., Bange, H. W., Échevin, V., Larkum, J., Mohn, J., N. Yoshida, N., and Altabet, M. A..: N_2O production and consumption from stable isotopic and concentration data in the Peruvian coastal upwelling system, Global Biogeochem. Cycles, 31, 678–698, 2017.doi:10.1002/2016GB005567.

Bullister, J. L., and Wisegarver, D. P.: The shipboard analysis of trace levels of sulfur hexafluoride, chlorofluorocarbon-11 and chlorofluorocarbon-12 in seawater, Deep-Sea Res., 55, 1063–1074, 2008.

Bullister, J. L., and Tanhua, T.: Sampling and measurement of chlorofluorocarbons and sulfur hexafluoride in seawater, IOCCP Report No. 14 ICPO Publication Series No. 134, Version 1, 2010.

Bullister, J. L., Wisegarver, D. P., and Wilson, S. T.: The production of methane and nitrous oxide gas standards for Scientific Committee on Ocean Research (SCOR) Working Group #143, http://udspace.udel.edu/handle/19716/23288, 2016.

Bussmann, I., Matousu, A., Osudar, R. and Mau, S.: Assessment of the radio ^{3}H-CH_4 tracer technique to measure aerobic methane oxidation in the water column, Limnol. Oceanogr.: Methods, 13,.312–327, 2015.

Butler, J. H., Elkins, J. W., Thompson, T. M., and Egan, K. B.: Tropospheric and dissolved N_2O of the west Pacific and east Indian Oceans during the El Niño Southern Oscillation Event of 1987, J. Geophys. Res., 94, 14,865–14,877, 1989.

Butler, J. H., and Elkins, J. W.: An automated technique for the measurement of dissolved N_2O in natural waters, Mar. Chem., 34, 47–61, 1991.

Capelle, D. W., Dacey, J. W., and Tortell, P. D.: An automated, high through-put method for accurate and precise measurements of dissolved nitrous oxide and methane concentrations in natural waters, Limnol. Oceanogr.: Methods, 13, 345–355, 2015.

Ciais, P., Dolman, A.J., Bombelli, A., Duren, R., Peregon, A., Rayner, P.J., Miller, C., Gobron, N., Kinderman, G., Marland, G., and Gruber, N.: Current systematic carbon-cycle observations and the need for implementing a policy-relevant carbon observing system, Biogeosciences, 11, 3547–3602, 2014.

Craig, H. and Gordon, L. I.: Nitrous oxide in the ocean and the marine atmosphere, Geochim. Cosmochim. Acta 27, 949–955, 1963.

Cutter, G. A.: Intercalibration in chemical oceanography - getting the right number. Limnol. Oceanogr.: Methods, 11, 418–424, 2013.

de la Paz, M., García-Ibáñez, M.I., Steinfeldt, R., Ríos, A.F., and Pérez, F.F.: Ventilation versus biology: What is the controlling mechanism of nitrous oxide distribution in the

North Atlantic?, Global Biogeochem. . Cycles, 31, 745–760, doi: 10.1002/2016GB005507, 2017.

Dickson, A. G., Sabine, C. L. and Christian, J. R.: Guide to best practices for ocean CO_2 measurements, PICES Special Publication 3, 2007.

Farías, L., Castro-González, M., Cornejo, M., Charpentier, J., Faúndez, J., Boontanon, N. and Yoshida, N.: Denitrification and nitrous oxide cycling within the upper oxycline of the eastern tropical South Pacific oxygen minimum zone. Limnol. Oceanogr., 54, 132–144, 2009.

Farías, L., Besoain, V., and García-Loyola, S.: Presence of nitrous oxide hotspots in the coastal upwelling area off central Chile: an analysis of temporal variability based on ten years of a biogeochemical time series, Environ. Res. Lett., 10, 044017, 2015.

Fenwick, L., and Tortell, P. D.: Methane and nitrous oxide distributions in coastal and open ocean waters of the Northeast Subarctic Pacific during 2015–2016, Mar. Chem., 200, 45–56, 2018.

Fenwick, L., Capelle, D., Damm, E., Zimmermann, S., Williams, W. J., Vagle, S., and Tortell, P. D.: Methane and nitrous oxide distributions across the North American Arctic Ocean during summer, 2015, J. Geophys. Res.: Oceans, 122, 390–412, doi:10.1002/2016JC012493, 2017.

Forster, G., Upstill-Goddard, R. C., Gist, N., Robinson, C., Uher, G. and Woodward, E. M. S.: Nitrous oxide and methane in the Atlantic Ocean between 50 N and 52 S: latitudinal distribution and sea-to-air flux, Deep-Sea Res., 56, 964–976, 2009.

Freing, A., Wallace, D. W. R., and Bange, H. W.: Global oceanic production of nitrous oxide, Phil. Trans. R. Soc. B, 367, 1245–1255, 2012.

Gülzow, W., Rehder, G., Schneider, B., Schneider, J., Deimling, V., and Sadkowiak, B.: A new method for continuous measurement of methane and carbon dioxide in surface waters using off-axis integrated cavity output spectroscopy (ICOS): An example from the Baltic Sea, Limnol. Oceanogr.: Methods, 9, 176–184, 2011.

Jakobs, G., Holterman, P., Berndmeyer, C., Rehder, G., Blumenberg, M., Jost, G., Nausch, G., and Schmale, O.: Seasonal and spatial methane dynamics in the water column of the central Baltic Sea (GotlandSea), Cont. Shelf Res., 91, 12–25, 2014.

Ji, Q., Babbin, A. R., Jayakumar, A., Oleynik, S., and Ward, B. B.: Nitrous oxide production by nitrification and denitrification in the Eastern Tropical South Pacific oxygen minimum zone, Geophys. Res. Lett., 42, 10,755–10,764, doi:10.1002/2015GL066853, 2015.

Kitidis, A., Upstill-Goddard, R. C., and Anderson, L. G.: Methane and nitrous oxide in surface water along the North-West Passage, Arctic Ocean, Mar. Chem., 121, 80–86, 2010.

Law, C. S., and Ling, R. D.: Nitrous oxide flux and response to increased iron availability in the Antarctic Circumpolar Current, Deep-Sea Res., 48, 2509–2527, 2001.

Magen, C., Lapham, L. L., Pohlman, J. W., Marshall, K., Bosman, S., Casso, M., and Chanton, J. P.: A simple headspace equilibration method for measuring dissolved methane, Limnol. Oceanogr.: Methods, 12, 637–650, 2014.

McAuliffe, C.: Solubility on water of C_1-C_9 hydrocarbons, Nature, 200, 1092–1093, 1963.

Myhre, G., Shindell, D., Bréon, F.-M., Collins, W., Fuglestvedt, J., Huang, J., Koch, D., Lamarque, J.-F., Lee, D., Mendoza, B., Nakajima, T., Robock, A., Stephens, G., Takemura, T., and Zhang, H.: Anthropogenic and Natural Radiative Forcing, In: Climate Change 2013: The Physical Science Basis. Contribution of Working Group I to the Fifth Assessment Report of the Intergovernmental Panel on Climate Change [Stocker, T. F., Qin, D., Plattner, G.-K., Tignor, M., Allen, S. K., Boschung, J., Nauels, A., Xia, Y., Bex, V., and Midgley, P. M. (eds.)]. Cambridge University Press, Cambridge, United Kingdom and New York, NY, USA, 2013.

Naqvi, S. W. A., Bange, H. W., Farías, L., Monteiro, P. M. S., Scranton, M. I., and Zhang, J.: Marine hypoxia/anoxia as a source of CH_4 and N_2O, Biogeosciences, 7, 215–2190, doi: 10.5194/bg-7-2159-2010, 2010.

National Research Council: Applications of analytical chemistry to oceanic carbon cycle studies. Washington DC. National Academy Press, 1993.

Nevison, C. D., Weiss, R. F., and Erickson, D. J.: Global oceanic emissions of nitrous oxide, J. Geophys. Res., 100, 15809–15820, doi: 10.1029/95JC00684, 1995.

Niemann, H., Steinle, L., Blees, J., Bussmann, I., Treude, T., Krause, S., Elvert, M., and Lehmann, M. F.: Toxic effects of lab-grade butyl rubber stoppers on aerobic methane oxidation, Limnol. Oceanogr.: Methods, 13, 40–52, 2015.

Pohlman, J. W., Bauer, J. E., Waite, W. F., Osburn, C. L., and Chapman, N. R.: Methane hydrate-bearing seeps as a source of aged dissolved organic carbon to the oceans, Nature Geosci., 4, 37–41, 2011.

Reeburgh, W. S.: Oceanic methane biogeochemistry, Chem. Rev., 107, 486–513, doi: 10.1021/cr050362v, 2007.

Rehder, G., Keir, R. S., Suess, E., and Rhein, M.: Methane in the northern Atlantic controlled by microbial oxidation and atmospheric history, Geophys. Res. Lett., 26, 587–590, doi: 10.1029/1999GL900049, 1999.

Schmale, O., Schneider von Deimling, J., Gülzow, W., Nausch, G., Waniek, J. J. and Rehder, G.: Distribution of methane in the water column of the Baltic Sea. Geophys. Res. Lett., 37, L12604, doi: 10.1029/2010GL043115, 2010.

Strady, E., Pohl, C., Yakushev, E. V., Krügera, S., and Hennings, U.: PUMP–CTD-System for trace metal sampling with a high vertical resolution. A test in the Gotland Basin, Baltic Sea, Chemosphere, 70, 1309–1319, 2008.

Swan, H. B., Armishaw, P., Iavetz, R., Alamgir, M., Davies, S. R., Bell, T. G., and Jones, G. B.: An interlaboratory comparison for the quantification of aqueous dimethylsulfide. Limnol. Oceanogr.: Methods, 12, 784–794, 2014.

Upstill-Goddard, R. C., Rees, A. P., and Owens, N. J. P.: Simultaneous high-precision measurements of methane and nitrous oxide in water and seawater by single phase equilibration gas chromatography, Deep-Sea Res., 43, 1669–1682, 1996.

Upstill-Goddard, R. C., and Barnes, J.: Methane emissions from UK estuaries: Re-evaluating the estuarine source of tropospheric methane from Europe, Mar. Chem., 180, 14–23, 2016.

Walter, S., Peeken, I., Lochte, K., Webb, A., and Bange, H. W.: Nitrous oxide measurements during EIFEX, the European Iron Fertilization Experiment in the subpolar South Atlantic Ocean, Geophys. Res. Lett., 32, doi:10.1029/2005GL024619, 2005.

Weiss, R. F., and Price, B. A.: Nitrous oxide solubility in water and seawater, Mar. Chem., 8, 347–359, doi: 10.1016/0304-4203(80)90024-9, 1980.

Weiss, R. F., Van Woy, F. A., and Salameh, P. K.: Surface water and atmospheric carbon dioxide and nitrous oxide observation by shipboard automated gas chromatography: Results from expeditions between 1977 and 1990, Scripps Institution of oceanography Reference 92-11. ORNL/CDIAC-59, NDP-044. Carbon Dioxide Information Analysis Center, Oak Ridge National Laboratory, Tennessee, 1992.

Wiesenburg, D. A., and Guinasso, N. L.: Equilibrium solubilities of methane, carbon monoxide and hydrogen in water and seawater, J. Chem. Eng. Data, 24, 354–360, doi: 10.1021/je60083a006, 1979.

Wilson, S. T., Ferrón, S., and Karl, D. M.: Interannual variability of methane and nitrous oxide in the North Pacific Subtropical Gyre, Geophys. Res. Lett., 44, doi: 10.1002/2017GL074458, 2017.

Zhang, G. L., Zhang, J., Kang, Y. B., and Liu, S. M.: Distributions and fluxes of methane in the East China Sea and the Yellow Sea in spring, J. Geophys. Res., 109, C07011, doi:10.1029/2004JC002268, 2004

Table 1. List of laboratories that participated in the intercomparison. All laboratories measured both methane and nitrous oxide except U.S. Geological Survey (methane only), U.C. Santa Barbara (nitrous oxide only), and NOAA PMEL (nitrous oxide from the Pacific Ocean). Also indicated are the twelve laboratories that received the SCOR gas standards of methane and nitrous oxide.

Institution	Lead Scientist	SCOR Standards
University of Hawai'i, USA	Samuel Wilson	Yes
GEOMAR, Germany	Hermann Bange	Yes
Newcastle University, UK	Robert Upstill-Goddard	Yes
Université de Liège, Belgium	Alberto Vieira Borges	No
Plymouth Marine Laboratory, UK	Andrew Rees	Yes
NOAA PMEL, USA	John Bullister	Yes
IIM-CSIC, Spain	Mercedes de la Paz	Yes
CACYTMAR, Spain	Macarena Burgos	No
University of Concepción, Chile	Laura Farías	Yes
IOW, Germany	Gregor Rehder	Yes
University of California Santa Barbara, USA	Alyson Santoro	Yes
National Institute of Water and Atmospheric Research, NZ	Cliff Law	Yes
University British Columbia, Canada	Philippe Tortell	Yes
U.S. Geological Survey, USA	John Pohlman	No
Ocean University of China, China	Guiling Zhang	Yes

Table 2. Pertinent information for each batch of methane and nitrous oxide samples. This includes contextual hydrographic information, median and mean concentrations of methane and nitrous oxide, range, number of outliers, and the overall average coefficient of variation (%).

Sampling parameters									
Sample ID	PAC1	PAC 2	BAL1	BAL2	BAL3	BAL4	BAL5	BAL6	BAL7
Location	22.75N 158.00W	22.75N 158.00W	54.32N 11.55E	54.11N 11.18E	55.25N 15.98E	55.30N 15.80E	55.30N 15.80E	54.47N 12.21E	54.47N 12.21E
Location name	Station ALOHA	Station ALOHA	TF012	TF022	TF213	TF212	TF212	TF046a	TF046a
Sampling date	24.2.17	24.2.17	16.10.16	17.10.16	18.10.16	19.10.16	20.10.16	21.10.16	21.10.16
Sampling depth (m)	25	700	3	22	3	92	71	3	21
Seawater temperature (^{o}C)	23.6	5.1	12.0	13.6	12.2	6.6	6.7	11.8	13.4
Salinity	34.97	34.23	13.85	17.37	7.87	18.40	18.08	8.81	17.65
Density (kg m^{-3})	1024	1027	1010	1013	1006	1014	1014	1006	1013
Nitrous oxide									
Number of datasets	13	13	12	13	12	13	12	13	12
Outliers	0	1	2	1	1	0	1	2	2
Median N_2O conc. (nmol kg^{-1})	42.4	7.0	11.0	9.4	11.1	3.4	40.2	11.0	9.6
Mean N_2O conc. (nmol kg^{-1})	41.3	7.0	11.1	9.2	11.0	3.4	39.0	10.8	9.5
Range	34.3-45.8	5.9-7.6	10.1-12.7	7.7-11.0	9.6-11.6	2.1-5.5	30.1-45.9	9.5-11.5	8.0-10.4
Average coeff. variation (%)	2.8	4.4	4.5	4.2	2.7	7.5	4.0	2.6	4.4

Table 2. Continued

Sampling parameters									
Sample ID	PAC1	PAC 2	BAL1	BAL2	BAL3	BAL4	BAL5	BAL6	BAL7
Methane									
Number of datasets	12	12	11	11	11	11	11	11	11
Outliers	0	1	0	0	0	1	1	0	0
Median CH_4 conc. (nmol kg^{-1})	0.9	2.3	5.7	60.3	4.1	31.3	18.8	5.0	35.2
Mean CH_4 conc. (nmol kg^{-1})	1.8	2.6	5.8	58.6	4.4	31.1	18.8	5.4	35.4
Range	0.6-3.1	1.9-3.8	2.9-8.9	45.2-67.2	2.5-6.5	26.9-35.3	16.5-20.7	3.8-6.8	30.1-42.1
Average coeff. variation (%)	10.9	7.2	8.6	2.1	4.3	3.5	4.2	6.5	3.5

Figures

Figure 1. Concentrations of methane measured in nine separate seawater samples collected from the Pacific Ocean (Fig. 1a, 1b) and the Baltic Sea (Fig. 1c, 1d, 1e). The dashed grey line represents the value of methane at atmospheric equilibrium (Fig. 1b.) Individual data points are plotted sequentially by increasing value. The same color symbol is used for each laboratory in all plots.

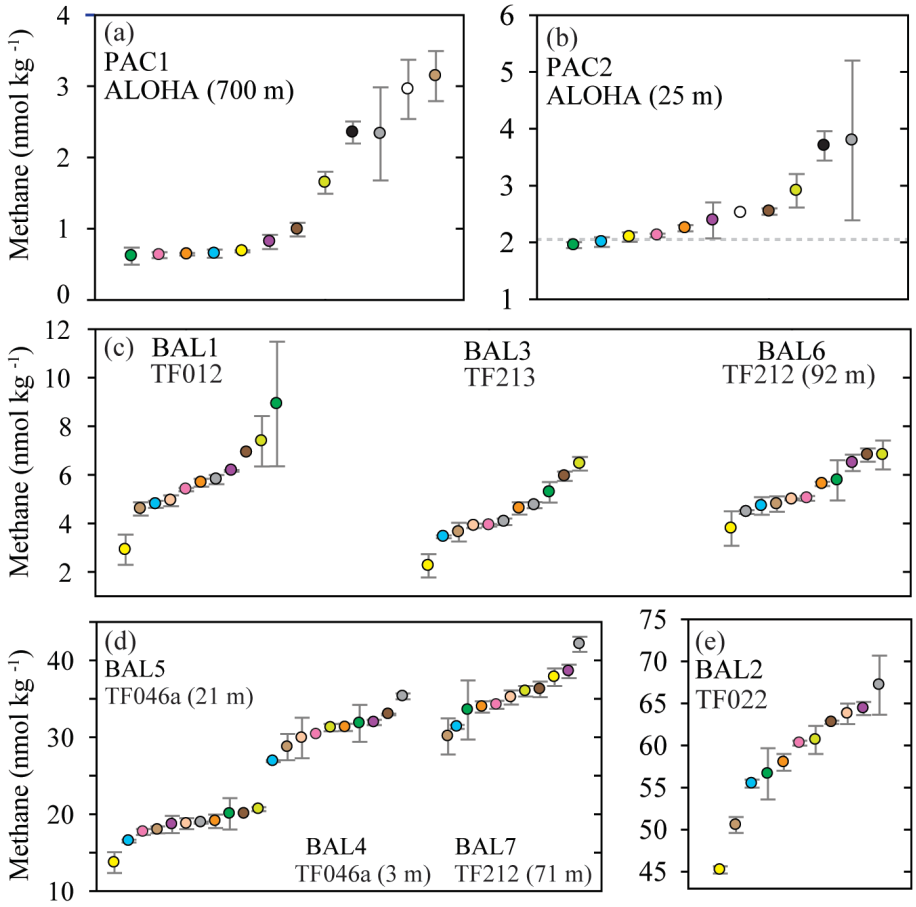

Figure 2. Deviation from the median methane concentration (reported as absolute values in nmol kg^{-1}) for the seven Baltic Sea samples. The batches of seawater samples include BAL1, BAL3, and BAL6 (Fig. 2a), BAL4, BAL5, and BAL7 (Fig. 2b), and BAL2 (Fig. 2c). The shaded grey area indicates values ≤5% of the median concentration. The color scheme for each laboratory dataset is identical to that used in Figure 1 and the letters allocated to each dataset are to facilitate cross-referencing in the text. Note that the y-axis scale varies between the Figures.

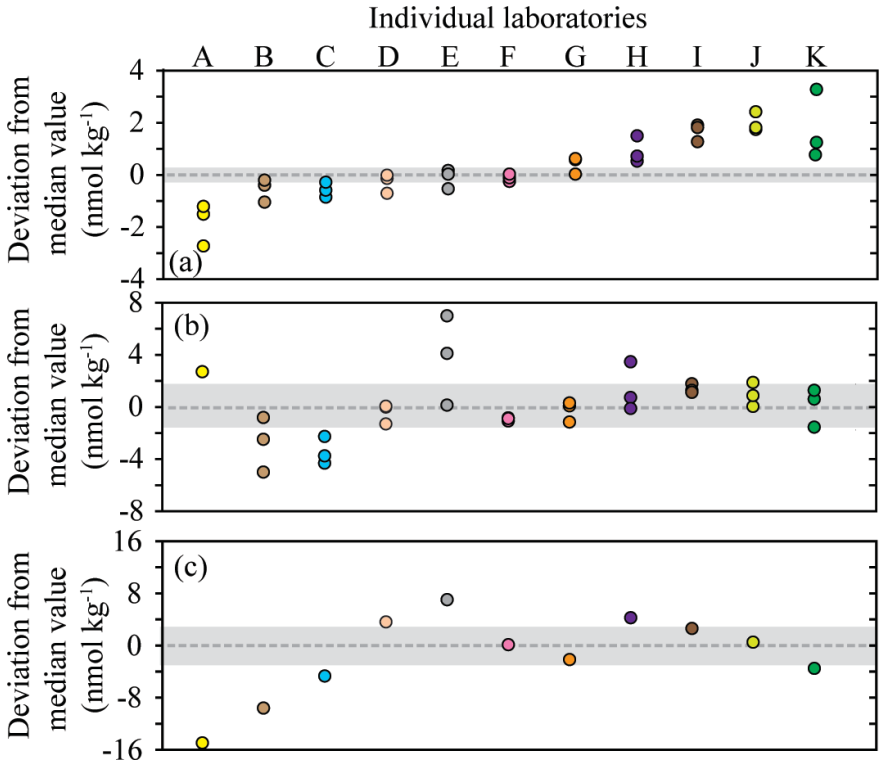

Figure 3. FID response to methane, fitted with a linear regression calibration. The inclusion (Fig. 3a and Fig. 3b) or exclusion (Fig. 3c) of low methane values cause the calibration slope and intercept to vary. However, the observed variation in the calibration slope does not have a significant effect on the final calculated concentrations of methane. In contrast, variation in the intercept does have an effect on the final concentrations of methane.

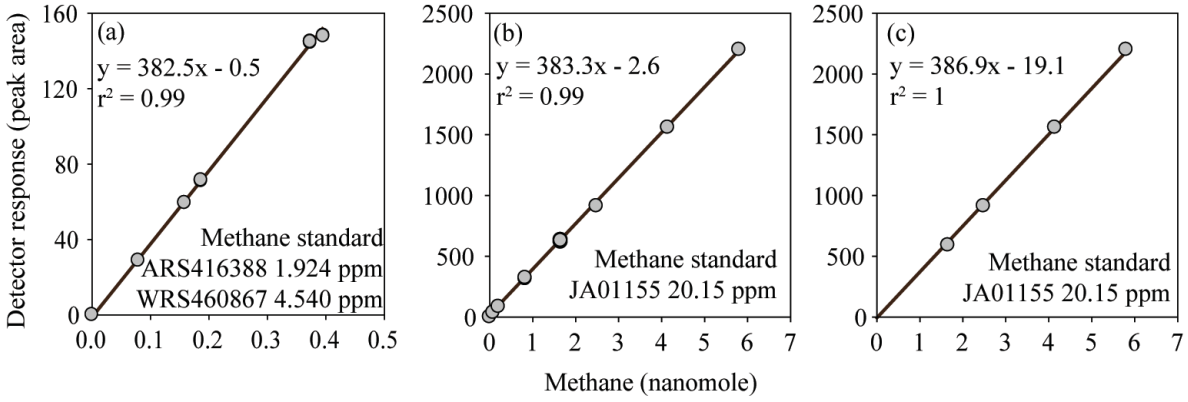

Figure 4. Concentrations of nitrous oxide measured in nine separate samples from the Baltic Sea and the Pacific Ocean. The dashed grey line represents the value of nitrous oxide at atmospheric equilibrium (Fig. 4b). Individual data points are plotted sequentially by increasing value. The same color symbol is used for each laboratory in all plots.

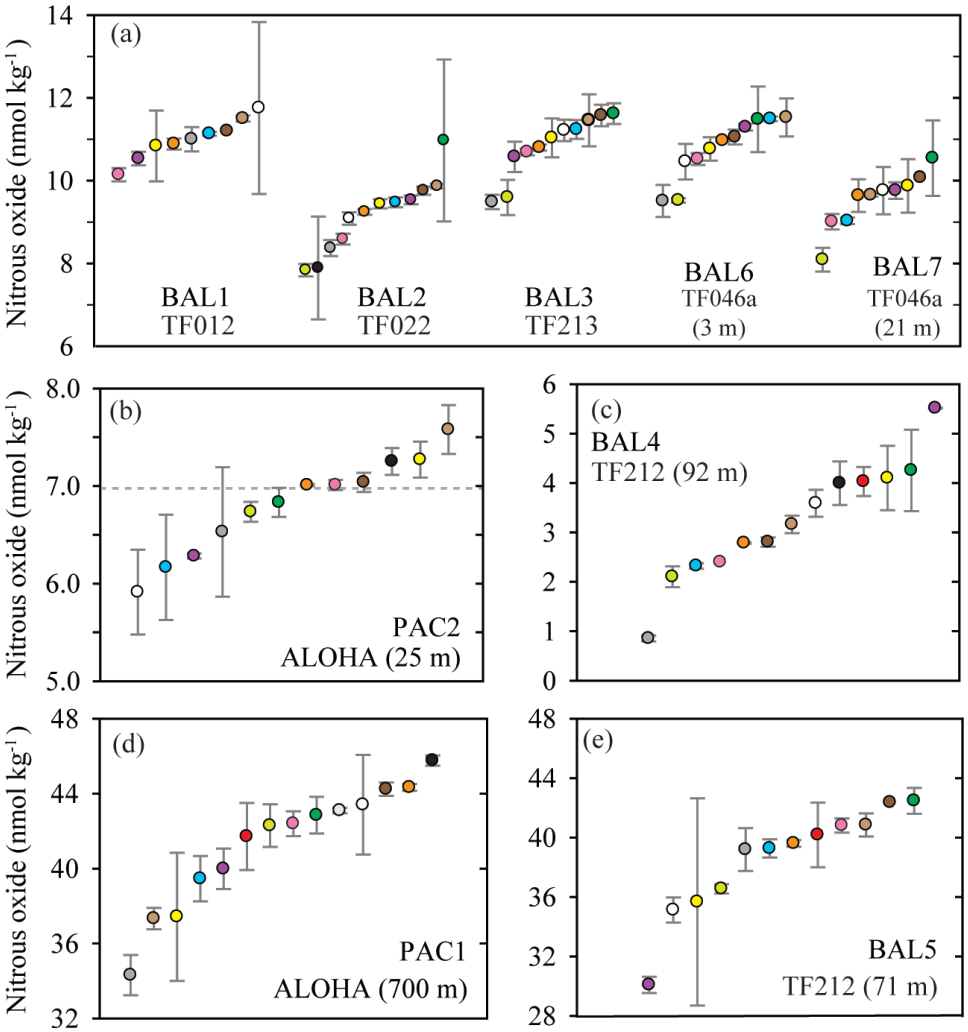

Figure 5. Deviation from the median value (reported in absolute units) for nitrous oxide datasets. The batches of samples include BAL1,2,3,6,7 (Fig. 5a) and PAC2 and BAL5 (Fig. 5b). The Baltic Sea samples are represented by circles and the Pacific Ocean samples are represented by triangles. The shaded area indicates a deviation ≤5% from the median value, based on a water-column concentration of 11 nmol kg^{-1} and 42 nmol kg^{-1} for Fig. 5a and 5b, respectively. The color scheme for each laboratory dataset is identical to that used in Figure 4 and the letters allocated to each dataset are to facilitate cross-referencing in the text. Note the y-axis for Fig 5a and 5b are plotted on a different scale.

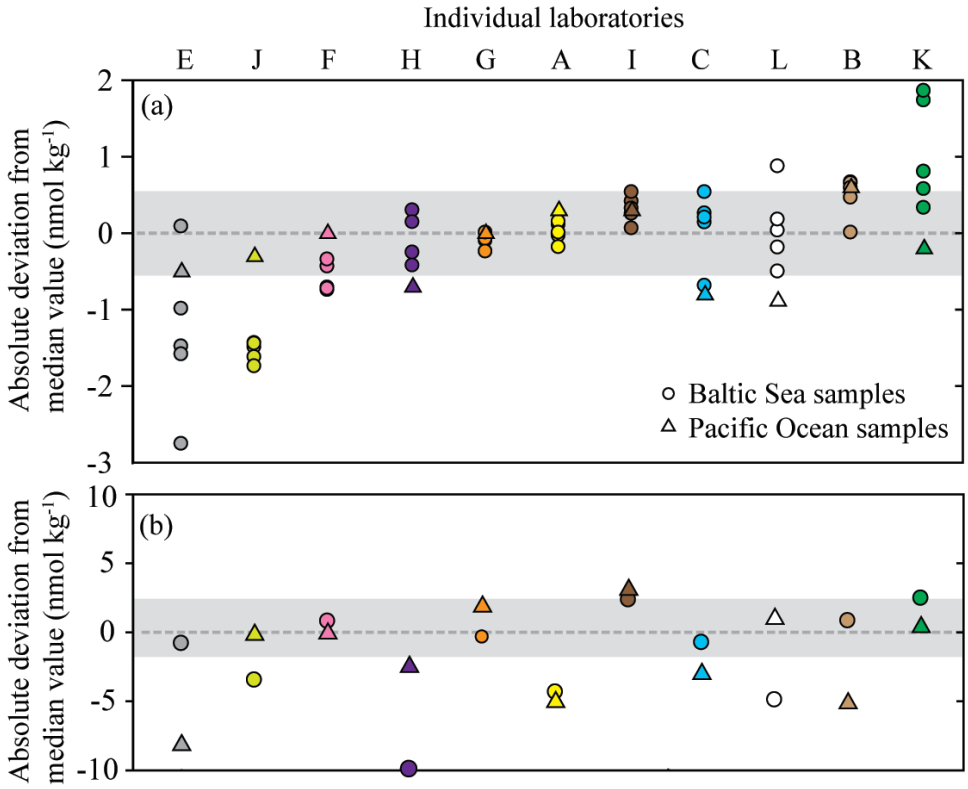

Figure 6. Three calibration curves for nitrous oxide measurements using an ECD including linear (Fig. 6a), multilinear (Fig. 6b), and quadratic (Fig. 6c) fits.

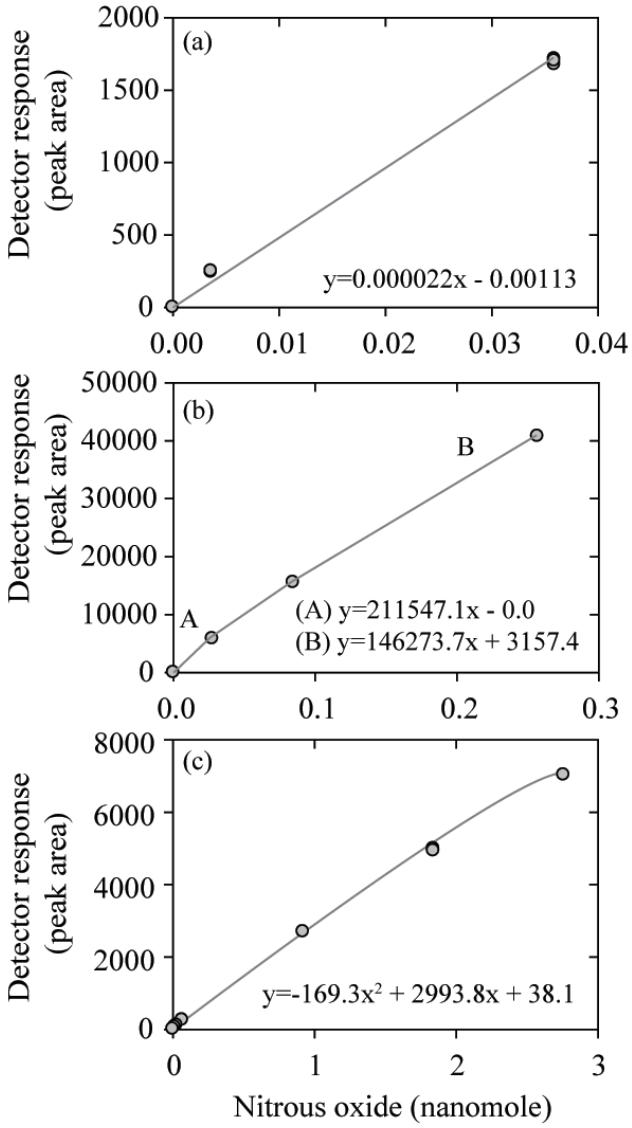

Figure 7. Comparison of sample storage times with measured concentrations of methane (Fig. 7a) and coefficient variation (Fig. 7b) for two sets of seawater samples (PAC1 and PAC2) collected in February 2017. These two sets of seawater samples had the lowest methane concentrations and appear to be influenced by the duration of storage time. The data points enclosed in parentheses were not included in the regression analysis. The PAC1 regression line is black and the PAC2 regression line is grey. All of the storage times are included in the Supplementary Material.